The Study of the Self-Damping Properties of Overhead Transmission Line Conductors Subjected to Wind-Induced Oscillations

By

Ojo Evans Eshiemogie

Student No. 206520793

A Thesis

Submitted in fulfillment of the requirements for the degree

Doctor of Philosophy in Engineering

School of Engineering

College of Agriculture, Engineering, and Science

University of KwaZulu-Natal

Durban, South Africa

Supervisor: Professor Nelson M. Ijumba

October, 2017

Approved by:

Supervisor: Professor Nelson M. Ijumba

"As the candidate's supervisor, I agree/do not agree to the re-submission of this dissertation"

Signed_____ Date _____

Prof. N. M Ijumba (Supervisor)

COLLEGE OF AGRICULTURE, ENGINEERING AND SCIENCE

DECLARATION 1 - PLAGIARISM

I, Ojo Evans Eshiemogie, declare that

1. The research reported in this thesis, except where otherwise indicated, is my original research.
2. This thesis has not been submitted for any degree or examination at any other university.
3. This thesis does not contain other persons' data, pictures, graphs or other information, unless specifically acknowledged as being sourced from other persons.
4. This thesis does not contain other persons' writing, unless specifically acknowledged as being sourced from other researchers. Where other written sources have been quoted, then:

a. Their words have been re-written but the general information attributed to them has been referenced

b. Where their exact words have been used, then their writing has been placed in italics and inside quotation marks, and referenced.

5. This thesis does not contain text, graphics or tables copied and pasted from the Internet, unless specifically acknowledged, and the source being detailed in the thesis and in the References sections.

Signed 

……

COLLEGE OF AGRICULTURE, ENGINEERING AND SCIENCE

DECLARATION 2 - PUBLICATIONS

DETAILS OF CONTRIBUTION TO PUBLICATIONS that form part and/or include research presented in this thesis (include publications in preparation, submitted, *in press* and published and give details of the contributions of each author to the experimental work and writing of each publication)

Publication 1

- E. E. Ojo and N. M. Ijumba *The Implementation of the Developed Finite Element Method used to Analyse the Dynamic Behaviour of Transmission Line Conductors on Matlab"* 8th South African Conference on Computational and Applied Mechanics Johannesburg, 3 - 5 September, 2012.

This presentation, it entails the preliminary investigation of wind induced vibration on power line conductors. The analytical and numerical modelling of wind-induced vibration was presented as well as the analysis of concepts used to achieve these models. Using the analytical modelling, the conductor was modelled as a continuous system and the investigation of its transverse vibration with regards to Aeolian vibration was investigated. The area of numerical modelling, using the finite element model, the conductor was discretized to produce a FEM model. The dynamic responses of the conductor were simulated. The results from both models were compared, this help to identify the modelling parameter used to analyse the dynamic characteristics of overhead transmission line conductors.

Publication 2

- E.E. Ojo and S. Shindin "*Finite Element Analysis of the Dynamic Behaviour of Transmission Line Conductors Using MATLAB"* 11th International Conference on Vibration Problems, Z. Dimitrovová et al. (eds.), Lisbon, Portugal, 9-12, September, 2013

In this paper, the finite element analysis model for the power line conductors were presented. The paper investigated the conductors as a bundle of strands (composite structure). This composite structural modelling approach was used to understand the damping mechanism in stranded conductors. This concept serves as a means of evaluating the hysteresis damping around the inter-strands contact points. The contact points were characterized with friction force acting and based on this characterization, it established that energy dissipation occurs around the contact regions within the conductor. This damping is as a result of the strands flexes and then experiences a stick-slip phenomenon. Identifying the boundary conditions coupled with the displacement between strands was used to generate the hysteresis loop. A computer code was developed and implemented in Matlab to simulate the stick-slip phenomenon. The area of the loop formed was used to evaluate the conductor self-damping. This result from this simulation was compared to that documented by C. Hardy and it showed some degree of agreement.

Publication 3

- E.E. Ojo and S. Shindin "*Finite Element Analysis of the Dynamic Behaviour of Transmission Line Conductors Using MATLAB"* Journal of Mechanics Engineering and Automation 4 (2014) 142-148, Published: February 25, 2014.

This paper presented further analysis on the previous paper. In this paper, the finite method was used to verify the relationship between the axial loading and damping. This established that damping decrease as the axial load was being increased.

Publication 4

- E. E. Ojo and N. M. Ijumba **"***Finite Element Analysis of Mechanical Oscillation of Power Line Conductors"* Southern African Universities Power Engineering Conference (SAUPEC), Vaal University of Technology, Vanderbijlpark, 26 - 28 January, 2016

In this paper the finite element analysis for the conductor was used to evaluate the global parameters for pure bending loading condition. The conductor geometry was discretized using the beam model in 2D. This was used to generate mass, stiffness, damping matrices and load vector. Iso-parametric interpolation was used to generate the system matrix equation. The simulation of this equation helps to obtain the dynamic response for the conductors. This help to identify parameters such as natural frequencies, mode shapes and damping.

Publication 5

- E. E. Ojo and N. M. Ijumba **"***Numerical Method for Evaluating the Dynamic Behaviour of Power Line Conductors: A Global Approach for Pure Bending"* International Journal of Engineering Research & Technology (IJERT), ISSN: 2278-0181, Vol. 5 Issue 03, March, 2016

In this paper, the developed finite element analysis for the power line conductors was used to evaluate the global parameters for pure bending. The conductor geometry was discretized using the beam model in 2D. This was used to generate mass, stiffness, damping matrices and load vector. Iso-parametric interpolation was used to generate the system matrix equation. The solution of this equation helps to obtain the dynamic response of the conductor. These parameters such as natural frequencies, mode shape and damping were evaluated. Also presented were the experimental results from the experiment conducted at the Vibration Research and testing centre VRTC. These experimental results were used to validate the FEM results.

Signed: 

Acknowledgements

I would like to sincerely thank and express my appreciation to my Supervisor Professor Nelson M. Ijumba for his guidance, support, and encouragement throughout my study. I appreciate the opportunity to work with him, and also for his encouragement, trust and untiring support. Professor M. N. Ijumba has been a mentor both academically and morally throughout this work.

I would like to thank Professor Thomas J. Afulllo for playing the fatherly role and offering counselling during my trying period.

I am is indebted to Mr Pravesh Moodley for providing valuable resources, preparation of the electronic instruments and setting up the test span utilized in the experimental study.

I would also like to thank Ms Charlain King, Ms Avenal Jane Finlayson, Ms Fiona Higginson, and Ms Bennedin Mokoena for their support, and encouragement.

It is my pleasure to acknowledge the following individuals who have contributed to, and influenced this work: Dr Alain Cardou, Mr Tom Irvin, Mr Denvre White, Dr Onunka Chimela and Dr Ming Liu, for sharing their expert knowledge and valuable resources.

My thanks go to my friends at the HVDC/VRTC; Tunji, Gilbert, Stacy, Daniel and Larry.

I thank my parents and my siblings, for their tireless and relentless love, continuous support, and the countless sacrifices they have had to make on my behalf. I want to specially thank my elder brother Cyril Etsekhagbor Ojo, thank you for being the shoulder I can always rest on.

Dedication

I dedicate this work to my daughter: Sandra Mamira A. K. Ojo

Abstract

Conductors are flexible, elastic structural components of power lines. The relatively high flexibility of the conductors, coupled with the long spans and the axial tension, makes conductors to be highly prone to dynamic excitation such as wind loading. The problem of the dynamic behavior of overhead power transmission line conductors under the action of wind and other forms of excitations is very important, since it proffers the optimal design of the line in terms of its dynamic characteristics. Thus, mechanical vibration of power lines needs to be mitigated, especially from aeolian vibration as they can lead to damage of the lines causing power interruptions. The dynamic behaviour of conductors can be influenced by its damping. However, available tools for the analysis of this phenomenon is scarce. The objective of this study is to evaluate the conductor self-damping. The goal is to characterize and ascertain the influence of various conductors' parameters on the amount of energy dissipation.

In this study, a numerically based investigation of the response of conductors was carried out i.e. finite element analysis (FEA or FEM). This was used to model the conductor using a new modeling approach, in which the layers of its discrete structure of helical strands were modelled as a composite structure. Due to the helical structure of the conductor strands, this give rise to inter-strands contacts. During bending caused by external loading, the stick-slip phenomenon does occur around the contact region resulting in damping of energy out of the system. Characterizing the damping mechanism as hysteresis phenomenon, this resulted from coulomb's dry-friction with the stick-slip regime at contacts points between the conductor strands. Employing contact mechanics to characterize and the use of FEM to discretize these contact regions, parameters such as the contact forces, strain and stress were established. When the conductor experiences a dynamic excitation in a sinusoidal form, a hysteresis loop is formed. The use of contact region parameters, to evaluate the area of the hysteresis loop and the area of the loop determines the amount of self-damping.

Experimental studies were conducted to validate the FEM model. Two forms of experiment were done. The first was the sweep test, done at a specified axial tension i.e. as a function of its ultimate tensile strength. This was used to determine the resonance frequencies for the conductors. In the second test, using the determined resonance frequencies from the first test were used to vibrate the conductors at these frequencies to establish the hysteresis loop at the same specified axial tension. The experiment was conducted with four different conductors with different number of layers. This was used to establish the relation between the numbers of layer and the amount of damping from the conductor.

The conductors' vibration experimental results obtained at a defined axial tension (as percentage of its UTS) correlate with that of FEM model. The results obtained showed a general increase in the resonance frequencies of vibration and a decrease in damping as the axial tension of the conductor is increased.

The establishment of the hysteretic constitutive behaviour of strands under specific loading conditions as described in the thesis, using this FEM model, an algorithm was developed to evaluate the conductor self-damping. Based on this algorithm, computer programs have been developed to evaluate the conductor's dynamic behaviour and implemented in MATLAB environment. Due to the very close relation between damping and conductor fatigue, this model can also be extended to investigate fatigue failure of conductors.

Table of Contents

List of Figures

List of Tables

Nomenclature

a	: Major half-width of the Hertzian contact
a_i	: Area of a strand in *i*-layer
A_T	: Total area of the conductor cross section
b	: Minor half-width of Hertzian contact
C	: Damping force per unit length
C_S	: Strouhal number
$[C]$	: Damping matrix
d_i	: Diameter of strand in *i*-layer
D_N or D	: Outer diameter of the conductor or the conductor diameter
$D_{i,i+1}$	: Diameter of the path that passes between two strands in different layers
D_i	: Diameter of the path passing through the centres of the strands in *i*-layer
R_i	: Strand location at *i*-layer from the neutral
E_C	: Young modulus for the core strand
E_i	: Young modulus for strands in *i*-layer
E^*	: Equivalent Young's modulus
EI	: Flexural rigidity or bending stiffness for the conductor
$EI_{\max}$	: Maximum bending stiffness
$EI_{\min}$	: Minimum bending stiffness
f_n	: Natural Frequency for a given *n*-mode shape
F_S	: Frictional force
F_N	: Normal contact force per unit length
G	: Shear modulus for strand in given layer
H	: Horizontal component of the static conductor tension
H_i	: Shape functions for the bilinear finite element
i	: Indicating series of successive parameters
I	: Second moment of area of conductor cross section about its neutral axis
J	: Polar moment of area
$[K]$	: Global stiffness matrix
L_C	: Chord length of the conductor
L_D	: Mid-span sag
L_S	: Span length of the Conductor
m_L	: Conductor mass per unit length
m_P	: Strand mass moment about the strand axis
m_S	: Strand mass per unit length

$[M]$: Mass matrix

n : Mode number or mode shape

n_i : Number of strand in a given layer

ncp : Number of contact points between helical layers

N : Number of layers in the conductor

N_i : Shape functions for the beam finite element

$P(i, j)$: Indicating strand position in a conductor cross-section

p : Pressure i.e. the force acting per unit length

$p_{\max}$: Maximum Hertzian pressure

$p(x)$: Normal Hertzian pressure

$P_{L(i)}$: The pitch length for *i*-layer

P_{wind} : The power imparted by the wind on the conductor

P_{cond} : The power dissipated by the self-damping of the conductor,

P_{damp} : The power dissipated by the damper.

$q(x)$: Tangential Hertzian pressure

r_i : The radius of a strand for *i*-layer

R^* : Equivalent radius of contacting cylinders

R_i : Distance from the neutral axis of the section to the centre of the *i*-layer

S : Axial tension

T_i : Axial force acting on individual strands

u_i, v_i, θ_i : Axial, vertical deformations and rotation at node *i*.

w_L : Conductor weight per unit length

x : Longitudinal displacement

$\dot{x}$: Velocity

$\ddot{x}$: Acceleration

$y(x, t)$: Transverse displacement with respect to position x, and time t

α_i : The lay angle for a given *i*-layer

ϕ_j : The incremental helical angle for a given layer

φ_i : The angular position of the strand from the y-axis

ρ_{cur} : Radius of curvature

ρ : The conductor density

κ : Curvature

ρ_i : Strand density

μ : Co-efficient of friction

$\varepsilon_A, \varepsilon_T, \varepsilon_B$: Axial, torsion, and bending strains

List of Acronyms

1D	One Dimensional
2D	Two dimensional
3D	Three dimensional
AAAC	All Aluminium Alloy Conductor
ACAR	Aluminium Conductor Alloy Reinforced
ACSR	Aluminium Conductor Steel Reinforced
FEM	Finite Element Method
FEA	Finite Element Analysis
LabVIEW	Laboratory Virtual Instrument Environmental Workstation
Matlab	Matrix Laboratory
OHTL	Overhead transmission line
RSME	Root mean square error
UTS	Ultimate tensile strength
URS	Ultimate rated strength
VRTC	Vibration Research and Testing Centre

Chapter 1

Introduction

1.1 General Background

The design of a new transmission line and the maintenance of existing ones require the selection of components to meet the performance requirements for the lines. The reason for this is based on the cost of the line, weight of materials, and on the reliability and safety of the transmission lines. Overhead Transmission Line (OHTL) conductors are engineering structure, which are very important in power transmission. The knowledge of the properties of conductors (both electrical and mechanical), are critical parameters in the design and the operation stages of the lines. Often, power line conductors are usually subjected to vortex-induced vibration resulting from wind loading. This phenomenon is a limitation in power line design, because if not adequately taken into consideration, it usually results in damage to conductors and its associated components. This damage ultimately reduce the life span of the lines. This is evident in scenarios as documented reports [1, 2] where conductor damage has been as a result of wind loading phenomenon. Figure (1.1) shows conductor damage from wind loading.

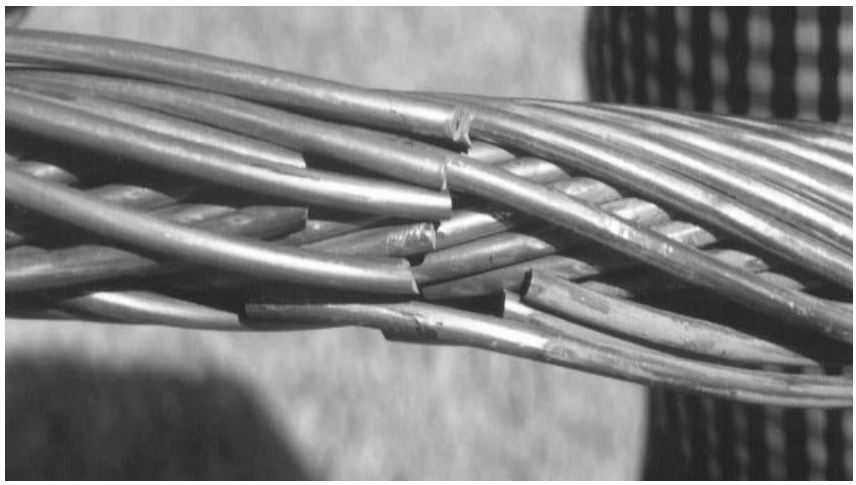

Figure 1.1: Broken strands in a Conductor [1, 2]

Therefore, a thorough understanding of this phenomenon is of interest to power utilities across the globe. The dynamic behaviour of conductors needs adequate understanding in order to guarantee a model which can be a good representation of the problem. Based on this, appropriate solutions can then be obtained. Conversely, adequate understating of the dynamic behaviour of the conductor is essential in order to know the proper tools to counter the effect of wind induced vibration.

The understanding of the dynamic behaviour of power lines has remain a challenge and many researchers in this field have carried out investigation in order to adequately model this phenomenon. Adequate comprehension of the dynamic behaviour of power lines has proven to be very difficult. This is due to factors such as the complex geometry of power line conductors, as well as variables associated with the geometry like inter-strand contacts and strands slippage during bending in these contact areas resulting in variable flexural rigidity. The complexity associated with modelling conductor also has to do with frictional effects around the inter-strand contact regions. The analysis of these areas of contact is of utmost importance to the phenomena that are associated with inter-strand contact such as energy dissipation and fatigue failure of the conductors used in power lines. Modelling the contact mechanics around these areas of contacts is most challenging in the field of conductor dynamics and attempt to model the contacts within conductors is documented in [3, 4].

Conductor manufacturers produce various forms of conductors that come with different number of layers, strands sizes and materials that are applicable to various conditions. The selection of conductors is done not only to meet the power transmission requirement, but also to meet the mechanical properties in order to satisfy the prescribed safety and reliability requirements for the line.

A conductor can be modelled as a distributed system in which the conductor is assumed to be homogeneous, and isotropic material with continuous parameters. Also, the conductor can be modelled as a collection of strands either as a semi-continuous or as a bundle of helical strands. In this study, the latter form of conductor structure, as a bundle will be referred to as "the composite structure" of a conductor. The form of modelling of conductor as a composite structure enables the analysis of the concepts associated with the internal geometry of conductors such as contact and frictional effect around the contact regions. In addition, the analysis of stick-slip behaviour between strands under dynamic condition can be carried out to generate the hysteresis phenomenon in order to evaluate the conductor damping. This can then be used to determine how much the coulomb friction energy dissipation from the helical strands contact regions, exhibiting relative motion has on the dynamic behaviour of the conductor.

This study was focused on the energy dissipation within the conductor (self-damping) and its effects on the dynamic response of conductors when subjected to wind loading. Power line conductors are well known for their inherent low damping characteristics and this has made them prone to vibration with adverse effects. In the past, some researchers have carried out investigation

in order to model the conductor damping. However, in this study numerical modelling has been selected as the option to be used in modelling the phenomena of damping.

1.2 Problem Description

In power engineering, conductors' mechanical behaviour applications require the use of sophisticated design tools that can be used to analyze their dynamic properties. When a conductor is subjected to natural force such as wind loading, it can be loaded beyond its elastic limit resulting in fatigue failure. The conductors have highly complex constructions that require structural analysis beyond using simplified mathematical models such as the taut string or the beam which is a common approach employed by most researchers. The attempt to model the conductor as a composite structure, due to the difficulty in modelling the cylindrical helical strands geometries as a bundle as found in actual conductors, result in the use of these simplified models. These simplified models do not adequately address the problem especially those associated with the conductor geometry. Hence, there was a need to develop a realistic modelling tool specifically to model conductor response when subjected to dynamic forces such as that from wind loading. In the study, such a model was developed to represent the conductor as function of its geometry in order to facilitate rapid and reliable parametric design processes for the construction of power lines. The model can be used in the form of a design and analysis tool for analyzing the power line mechanical properties. This design tool will take advantage of the known symmetric geometrical properties of the conductor. With this advantage, using the numerical tool, such as the creation of finite element can achieve this process of modelling the dynamic behaviour of conductors.

Employing most commercial software to model and simulate conductor vibration, when the conductor structure is characterized as a bundle of strands can in some cases pose a lot of challenges. During the implementation of model codes in most cases, the code fails to converge or produce a numerical solution. In order to obtain the numerical solution, the code needs to be developed within the software library and then simulated. This process is not possible in most commercial software because most of these software libraries are designed to be like a 'black box' in which the user is not given the access to modify the code, but can only implements his code in an input-output process. Due to this constrain for most researchers, the simplified models of beam elements are then used to simulate the conductor dynamic response.

In modelling the conductor using the beam model, the conductors are considered as a continuous, homogeneous solid. This has been employed by numerous researchers [5-7]. In order to get a more realistic model, some researchers have modelled the conductor analytically as a composite

structure, as an assembly of bars, strings or beams as documented in [8-13]. To model numerically the conductor as a composite structure, very few researchers have tried to attempt to model the conductor structure. The finite element model of the twisted conductor's strands and analysis of the assembly, treating the strand as individual entities was the most appropriate means to take care of these complexities of conductors helicoidally assembled composite structures in terms of the concept of energy dissipation.

As mentioned earlier, in most cases the numerical implementation of the geometric model as a composite fails to converge and the simulation will go on for infinite time. Thus, for the analysis of the conductor specifically, this process in the software library lacks the ability to implement parameters like variable bending stiffness, taking into account the frictional effect around the inter-strand contact regions, implementing the stick-slip regime during bending. Based on this inference, there arise the need to numerically develop a model that takes into account the following:

- The geometric and material properties of the conductor as a composite structure
- The deformation of the conductor due to gravity
- The various contact condition within the conductor structure
- The boundary conditions
- The application of stick-slip regime as a function of its variable flexural rigidity
- The energy dissipation process due to periodic bending of the strands caused by the dynamic loading

The above reasons then raise the need for a further study to employ the numerical technique of finite element method (FEM). The finite element method can generate a more realistic representation of the physical model of the conductor. The resultant model can then be translated into a computer code. This code has the capability of characterizing its geometry as well as evaluating the damping. This finite element analysis tool ensures that the developed model uses the physics associated with various phenomena around the contacts regions in the realization of the mechanism responsible for damping. The FEM model is characterized as a function of its geometry, independent of the parameters from the experimental results but in comparison produces good results.

1.3 Purpose of this Study

The proposed research was embarked upon, with the aim to develop a numerical model for the dynamic behaviour of transmission line conductor when subjected to natural forces such as wind.

Firstly, the study was expected to provide an adequate explanation of the current research in this area of conductor mechanical vibration. Secondly, was to advance the current state of research in this field in the aspect of developing a numerical model and analysis tool. As explained in my previous study [14], in which the analysis of the conductor transverse vibration was done using the linear concept of a continuum model to describe the conductor response to wind loading. This linear modelling concept was used to carry out both the analytical and finite element modelling for the conductor in order to determine the conductor dynamic characteristics. The model used was a simplified model of the conductor vibration, a lesser degree of the actual representation of the problem found in the real world which actually exhibits a non-linear response. Consequently, in order to improve on this developed linear model, to some degree, a FEM model, that was of adequate representation of the conductor was developed in this study.

The study presented in this thesis was used to develop a computational model of the conductor as composite structure. The model would be able to adequately represent a vibrating conductor as means of explaining the structural dynamics of what happen in reality. The study was tasked to develop a numerical conductor model as a bundle. Hence, the developed model was used to simulate, with the aim to evaluate the self-damping capability, predict the conductor vibration level and then evaluate the significance of damping on its dynamic response. The research that is presented in this thesis was used to investigate the variation in damping between the various damping mechanisms as the axial tension was being varied. This research was set to accomplish the above task by using the numerical tool of finite element method (FEM). This was then followed by series of experimental studies to evaluate the accuracy of the developed FEM model as well the assessment of damping properties of the conductor.

In accordance with the above modelling approach, the research was used to determine the contributions of the hysteresis damping mechanisms found in the vibrating conductor to the total damping as the stringing tension is being increased. The numerically derived equation for these damping mechanisms and the incorporation of its damping model, the computational model was developed for the conductor. The variation in damping with regards to the hysteresis damping as the axial tensions at both ends was increased was investigated.

Finally, on the basis of all the areas that were investigated, couple with the finite element method, an algorithm was developed that can be used to evaluate the conductor damping. This developed algorithm can be implemented in both the design and the construction stages of the power lines in

order to predict the effect the wind induced oscillation might have on the overhead transmission line conductors.

1.4 Research Hypothesis

"The finite element analysis based model can be developed to predict the self-damping properties and behaviour of overhead power line conductors subjected to wind loading under different axial tensions"

1.5 Aims and Objectives

The aims of this study in relation to the concepts as explained in the previous sections are as follows:

- To carry out a technical review of models used in modelling the conductors' vibration
- To model analytically the transverse vibration of bare conductors
- To develop a finite element method for the vibrating conductors as a composite structure
- To evaluate (analytically and numerically) the self-damping capability of bare conductors
- To carry out experimental study to validate the analytical and finite element models

In line with the above aims, this study seeks to achieve the following objectives:

- To further the understanding of the dynamics of wind-induced vibration that occurs in overhead transmission line conductors
- To analyze the analytical models describing the transverse vibration of conductors
- To develop a finite element model for the conductors
- To further the understanding of conductors' response based on experimental data in order to predict the dynamic action of lines conductors
- To develop an algorithm in assessing the self-damping properties of overhead line conductors

1.6 Scope and Assumptions

Vibration of power line conductor is a problem usually caused by wind loading. The problem cuts across many discipline; rigid body dynamics, strength of materials, mechanics of materials, contact mechanic, aerodynamics, fluid mechanics, and system vibration. The physics involved in these

disciplines is very complex and the analysis tends to be nonlinear in response. Thus, this problem has a wide problem formulation depending on the interest of the area of analysis and the concept employed. The conductor vibration modelling and analysis in terms of power flow can be broadly divided into three problem areas: power input, power dissipated by the conductor itself and the required power dissipation by external dampers. For this study, the finite element analysis that was used will cover the area of rigid body dynamics with regards to vibration analysis and contact mechanics. This will ascertain the power dissipated by the conductor. The areas of fluid mechanic and aerodynamics in relation to conductor excitation will not be covered. Although, these areas are much related but the aspects that were of interest was deduced from literature and then used accordingly.

Also not covered in this study were the fatigue failure and the vibration absorbers placement on the lines. The area of vibration absorbers (dampers) placement on conductor is completely outside the scope of this study. Although, ascertaining the conductor damping capability as the findings of this research will be of great importance in that area of research. This will be beneficial because normally self-damping is ignored when modelling the damper placement on lines. It is approximately determined using the criterion of 80 % of the minimum vibrating loop length.

The following assumptions were made in the course of this study.

1) As earlier indicated, the phenomenon of solid-fluid interaction responsible for the conductor oscillation will not be covered in this thesis. Although, the input power is needed and this was sourced for from literature. The form of input power on a conductor by wind in the actual power lines is the distributed loading. Although, the input power is distributed, an equivalent point loading on the conductor was used to simulate the conductor dynamic response. This was in line with experimental results and also a point loading of its equivalent distributed loading was also used for implementation, in the area of FEM.
2) Displacements and strains were assumed to be small. This assumption was applied when modelling the conductor or its strands, using the Euler-Bernoulli beam theory. The assumption was applied in the modelling the complete conductor structure as a unit especially when the parameter was of global interest i.e. natural frequencies and mode shapes. For the case of the strands, it was developed using the curved thin beam model.
3) The conductor core, and the helical strands was assumed to have a circular cross-section, though due to axial loading the helical strands assume the elliptical cross-section.

4) Effect of Poisson's ratio at the contact areas are considered, but the effect of Poisson's ratio on the material of the strands geometry are neglected.
5) For the contact conditions, the core and helical strands interaction and interaction between helical strands of different layers are considered in the analysis, but those interactions between strands of the same layer are neglected.

1.7 Contribution of this Study to the Body of Knowledge

Since the problem of wind-induced vibrations was first noticed on transmission lines, the field of power line transmission has developed a specific body of knowledge: conductor static and dynamics analysis. This body of knowledge was developed on the basis of exploring the mathematical modelling (analytical and numerical) and extensive experimental studies from both indoor and outdoor test facilities. This has led to the formulation of empirical formulae that are of practical applications. However, these empirical formulae are developed with some assumptions of the physical and mechanical theories governing the understanding and the prediction of the mechanical response of the conductors. Most of the researches in the field of overhead electrical conductor mechanical vibration were compiled and documented in the EPRI's *Transmission Line Reference Book* [1, 2]. The contents of the book were mostly oriented towards the transverse vibration phenomena in the various vibration types and modes.

Most models found in literature, in many cases, fail to account for the phenomenon of damping. This is because, these conductors' models used, describe the conductor structure as distributed parameters, but in reality, the conductors are a composite structure consisting of helically arranged strands. The conductor's composite structure due to the strands arrangement, gives rise to some form of contacts between strands. As documented in the literature [1-19], during bending the frictional effects between strands gives rise to damping and this is dependent on the axial tension, number of layers and the rate of bending during the transverse vibration. However, it is difficult to model the helical strands geometries as a bundle found in actual conductors to account for this damping process analytically.

The above reason then led to the consideration of an alternative approach, by employing the numerical tool of finite element analysis. Thus, as a contribution to the body of knowledge, a finite element method model was developed and the model was used to model, simulate and analyze the dynamic behaviour of overhead transmission line conductors. This model was developed to produce a more realistic representation of the physical structure of the conductor and also enable the characterization of its damping. The model was developed using the physics associated with

various phenomena that have to do with its geometry. The FEM enables the representation of a conductor by discretizing the structure with the creation of its finite element. The successful geometric formulation paved the way for the realization of the model and this enabled the explanation of the mechanism responsible for damping and its evaluation numerically.

This FEM study falls within the context of rigid body dynamics, with the goal to develop a FEM conductor model that can be used for the analysis of its dynamic behaviour. In addition, the model was designed for the determination of the structure parameters by trying to incorporate most of the factors necessary for analysis in order to determine the conductor dynamic response.

1.8 Organization of the Thesis

The thesis was devoted to the development of a finite element analysis model with the main objective of evaluating conductor self-damping. Chapter 1 highlighted and discussed the problem of wind-induced vibration on power line conductors and the reasons for this research. Also, discussed in chapter 1 was the aims and objectives for embarking in this study. This chapter highlights the areas of interest of this study which was to develop an efficient numerical solution technique for the conductors' vibration.

Chapter 2 discusses the literature that relate to conductor vibration. The literature review of the problem of conductor vibration was discussed and the analysis of the problem of the conductor as a bundle, as found in literature were critically examined in this chapter. The historical review of the various models used in representing the conductor vibration was discussed. The analysis of the conductor geometry as a composite was done in terms of the Cartesian coordinates. The various areas of interest associated with its internal geometry were identified. The parameters such as stresses and strains were evaluated in terms of the axial and bending properties. A review of the vibrating conductor modelled as a cylinder immersed in fluid, vortices were generated as the wind flows passed creating pressure differences upstream and downstream. The analysis of wind excitation was also done to understand how and the amount of power imparted on the conductor. Empirical formula formulated for power imparted by the wind as documented in literature with regards to wind tunnel experiments were reviewed to numerically determine the wind power loading on conductors. The energy balance principle was derived by comparing the energy input into the system due to wind loading and to the energy losses (both from self-damping and external dampers) in order to obtain the vibration level of the conductor.

Chapter 3 discussed the analytical modelling of the power conductor. On the basis of comparison, the three forms of modelling are explained. The first was the continuous parameters modelling, in which the conductor was model as a distributed parameters system. This was mostly used to obtain

the global variables like natural frequencies and mode shapes. For this method, the conductor damping was introduced mathematically. This is achieved by using the various damping models in modelling energy dissipation from systems. The second is the semi-continuous model which uses the properties of homogenous properties of the layer, been replaced by the orthotropic properties. The third form of modelling was a more realistic model of conductors as an assembly of strands arranged in layers with alternate lay angle. This was a more adequate representation of the real conductor as a bundle and from the problem formulated the eigenvalues are obtained. The formulation is largely dependent on discrete analysis of strands and the analysis of the physics around the contact regions. This helped to have good analysis of the structure and also in the evaluation by the integration of all energy dissipation as a function of tension, radius of curvature. In this model, the frictional effect at the inter-strand contacting areas determines the hysteretic conductor self-damping.

Chapter 4 was devoted mainly to the analysis of the conductor damping. This chapter presents an in-depth analysis of conductor self-damping and how it occurred on power line conductors. It describes the mechanisms responsible for damping of energy as a function of its inter-strand contact, frictional effect and the inter-strand slippage during bending. The analytical formulation to evaluate damping was done based on the stick-slip model. The stick-slip hysteresis phenomenon was modelled using the Bouc-Wen model [20, 21]. As a result, this chapter thus presents the critical theoretical background and analytical evaluation of energy dissipation within the conductor.

Chapter 5 discussed the formulation and implementation of the finite element method for the power line conductors. This numerical formulation was done for the 2D FEM topology in terms of geometry using the curved beam element for the strand. The FEM formulation procedures for the conductor follow the normal formulation of the basic finite element type and implementation of the solution of the resulting equations in a computer environment. This entails the finite element discretization of the conductor and the FEM modelling; including considerations in selecting the number and types of elements for discretizing the conductor geometric problem. The interpolation process for the formation of the conductor was done in terms of Cartesian and natural coordinate systems, and the nodal variables described by polynomials in terms of the iso-parametric elements interpolation. The derivation of the finite element characteristic equations for the mass and stiffness matrices and load vectors were obtained using the energy approaches. The system matrix was formed by the assembly of these finite element equations in form of matrices and vectors and then the solution for this system equation, including the incorporating of the boundary conditions. The solutions of these finite element equations are obtained in term of the equilibrium, eigenvalue, and propagation (transient or unsteady state) problems, with the computer implementation. Also

in this chapter, due to computational cost, the FEM model formulated was done to characterize the contact area as a two-dimensional (2D) problem. This was used to evaluate damping. The damping matrix formulation was obtained and the implementation by the use of Lagrange multiplier for the damping matrix.

The experimental studies were presented in Chapter 6, in which the laboratory tests that were conducted at the Vibration Research and Testing Centre (VRTC) are discussed. Two forms of tests were carried out. The first test that was conducted was the sweep test. This test was used to resonate the conductor at its natural frequencies. This was done primarily to determine the various natural frequencies and the vibrating modes. The second test, a LabVIEW program was developed and it was designed to send signals to drive the shaker via the function generator and then the conductor. Also, the program was designed to receive signals from the accelerometers placed on the conductor. The natural (resonance) frequencies from the first test serve as the input frequencies in the second test to vibrate the conductor at a constant amplitude. The main aim of designing the program was to generate a hysteresis loop from the signal received from the conductor as a function of frequency.

Analysis and discussion of results was done in Chapter 7. This includes results obtained from analytical, finite element method and experimentation. Comparisons of the different results are done critically; for the purpose of determining their correlation in term of damping obtained from the analytical, the experimental and the FEM. From the FEM, an algorithm was then developed to evaluate damping.

In Chapter 8, the conclusion on the study are made and the future recommendations on possible areas of further research are highlighted.

1.9 Publications

- E. E. Ojo and N. M. Ijumba *The Implementation of the Developed Finite Element Method used to Analyse the Dynamic Behaviour of Transmission Line Conductors on Matlab"* 8th South African Conference on Computational and Applied Mechanics Johannesburg, 3 - 5 September, 2012
- E. E. Ojo and S. Shindin "*Finite Element Analysis of the Dynamic Behaviour of Transmission Line Conductors Using MATLAB"* 11th International Conference on Vibration Problems Z. Dimitrovová et al. (eds.), Lisbon, Portugal, 9-12, September, 2013
- E.E. Ojo and S. Shindin "*Finite Element Analysis of the Dynamic Behaviour of Transmission Line Conductors Using MATLAB"* Journal of Mechanics Engineering and Automation 4 (2014) 142-148, Published: February 25, 2014.

- E. E. Ojo and N. M. Ijumba "Finite Element Analysis of Mechanical Oscillation of Power Line Conductors" Southern African Universities Power Engineering Conference (SAUPEC), Vaal University of Technology, Vanderbijlpark, 26 - 28 January, 2016.

- E. E. Ojo and N. M. Ijumba **"***Numerical Method for Evaluating the Dynamic Behaviour of Power Line Conductors: A Global Approach for Pure Bending"* International Journal of Engineering Research & Technology (IJERT), ISSN: 2278-0181, Vol. 5 Issue 03, March, 2016.

Chapter 2

Literature Review

2.1 Introduction

Power lines play an indispensable role in the activities of our everyday lives and these include homes, hospitals, industries, where the application of electrical power is required. This power is transferred by conductors. A typical power line is shown in figure (2.1). This chapter presents and discusses the various concepts which are relevant when dealing with the problems of both the static and the dynamic behaviour of overhead transmission line conductors. Adequate analysis of the

dynamic properties of power line conductors is vital as a design and analysis tool in determining its reliability and safety.

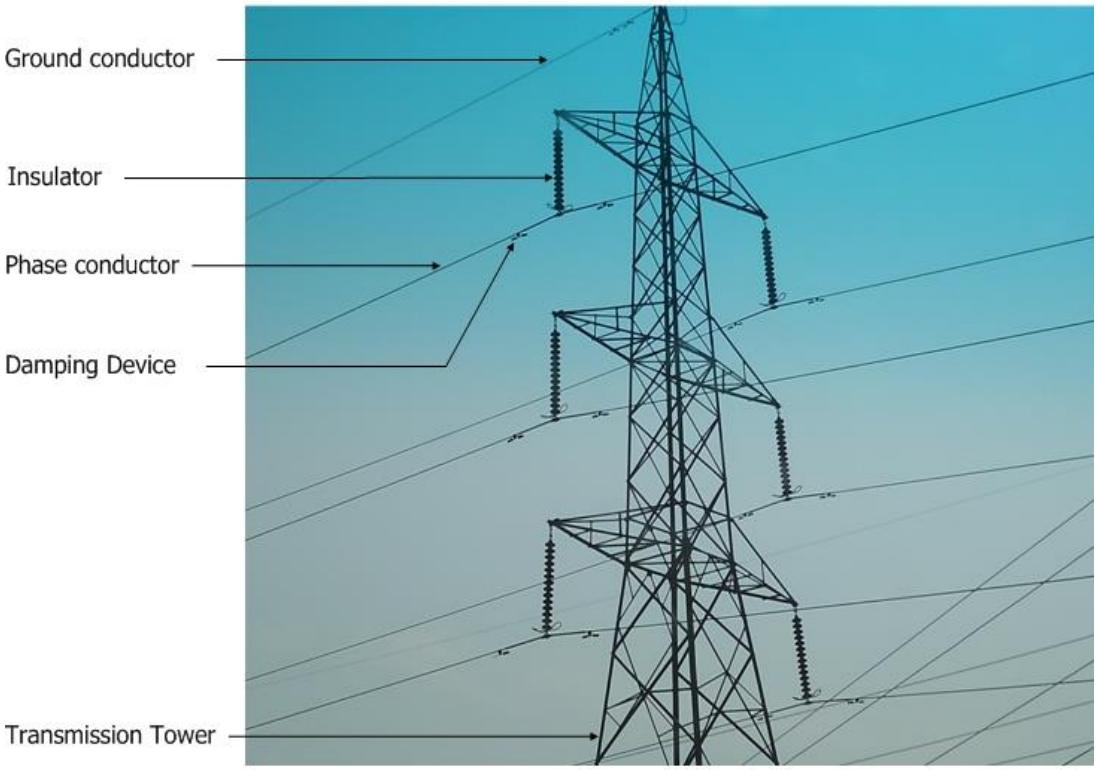

Figure 2.1: Overhead Transmission Line [22]

In the 1920s, the phenomenon of conductor vibration was observed on overhead power lines which were mainly caused by wind loading. The excitation mechanism was the formation of vortices, at the top and bottom of leeward side of the conductor due to pressure differences caused as the wind flow passed the conductor as shown in figure (2.2). These vortices induce an aerodynamic instability on the conductor and the conductor then oscillates tangentially to the direction of the prevailing wind. There are many forms of motion that result from this aerodynamic effect [1, 2], but the main concern of this study has to do with the vortex-induced vibration also known as aeolian vibration. When the conductor is subjected to the wind excitation, as it undergoes the aeolian vibrations, with a transverse small amplitude and this displacement corresponds to the conductor bending. In such a motion, in its inception, the individual strands relative slip is restricted, up to a certain limit, by the friction forces, beyond a critical curvature, the conductor strands slip in relative to other strands in the adjacent layer.

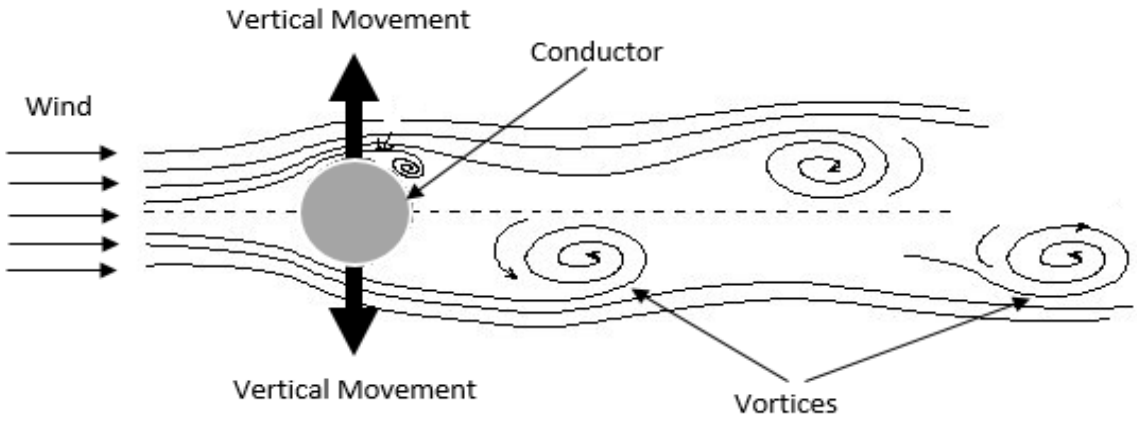

Figure 2.2: Vortex wake shedding from a conductor

For the aeolian vibration, the amplitude of vibration is relatively small with maximum amplitude in the order of one diameter of the conductor. The frequency of vibration ranges from 5 Hz as the minimum vibration frequency of a large conductor and 150 Hz as the maximum vibration frequency of a small conductor or shield wire. Although, the main focus of this study was on the vortex-induced vibration, the findings of this study can be extended to cover the area of wake-induced vibration which also occurs on power lines.

In the past various models have been developed to describe the mechanical vibration of power line conductors. These developed models have brought into the fore various important concepts that are associated with the conductors in the aspect of both the static and the dynamic analysis. These concepts were developed by bringing into play the principles and laws from different disciplines of science and engineering. These disciplines that were explored in developing these models include such fields as differential geometry, contact, solid, and analytical mechanics (linear or nonlinear), fluid-solid interaction and fluid dynamics as well as aerodynamics in relative to both the vortex and wake-induced vibrations. There have been numerous attempts at solving the problem of conductor vibration analytically and experimentally. The modelling of the dynamic behaviour of overhead power conductors is still an on-going investigation, this is because the conductors' geometry is quite difficult to mathematically model, especially with respect to their mechanical behaviour due to wind loading.

To be able to improve on these existing mechanical vibration models numerically, various concepts emanating from these previous models used in modelling the wind-induced vibration have to be well reviewed. This is important; on the basis of understanding these previous models, which can then be used to ascertain how well these models have represented the real problem. Therefore, this chapter is poised in achieving this task.

To achieve the task of this chapter, the next section was used to discuss the historical review of previous analytical models. This was followed by the descriptions of a typical conductor geometric structure. This was then followed by the description of the conductor geometry in terms of the analysis of the internal contacts between strands. The conductor reaction to tensile and bending loading was then explored with the discussions of conductor responses in terms of internal contacts, tension-induced torque and rotation as well as the developed strains and stresses. The chapter is concluded with the discussion in the area of wind excitation and the power imparted by the wind on the conductor, this help in indicating the onset of the power flow, and then the conductor damping that is of relevance to this study.

2.2 Review of Previous Analytical Models

This section is used to preview some of the already developed analytical models, describing the conductor response to axial, or bending load or combination of both. However, some of the models presented here also have its wide applications in wire ropes, mooring cables, and cables used in bridges and cable-guide structures, but also applicable to the power line conductor configurations. Transmission line conductors' susceptibility to mechanical vibration has been an area of research for a long time ever since the phenomenon was first discovered. Due to the complexity of the dynamic motion of the transmission line conductors, the accurate modelling of this phenomenon has proven to be very difficult. This has led to many researches all over the world trying to provide, with some degree of simplification, an accurate model that can be used to describe the mechanical oscillation of conductors [1, 2]. To predict the conductor response, to some degree of accuracy, several theoretical models for the conductor vibration have been proposed by several researchers [1-7].

When the phenomenon of wind-induced vibration was first noticed, over the years, attracted the attention of researchers with the purpose of understanding the dynamics involved in the conductor motions from which a solution can be inferred. The early investigations in this area of mechanical vibration of transmission line conductors was carried out and documented by T. Varney [23]. He conducted several experimental investigations, coupled with the analytical evaluation to determine the conductor response. His analysis led to the determination of the flexural rigidity for the conductors. He calculated the maximum value, considering the conductor as a solid unit and the minimum value for the conductor as the groups of strands with complete slip between each strand. On the basis of calculating the bending stiffness (maximum and minimum), he indicated that the true value for the bending stiffness lies between these two values. This led to the concept of the determination of the actual value for bending stiffness for a conductor experiencing bending and this value was expected to be between the two extreme conditions i.e. maximum and minimum

bending stiffness. The authors [24] investigated the conductor dynamic behaviour using the experimental study similar to that of T. Varney's work. This study determined the stresses imposed on the conductor. R. G. Sturm [25] carried out investigation by embarking on the analytical analysis of the conductor. The equation of motion for the conductor system was derived using the modal synthesis method with the structural formulation. Free and forced vibrations of the conductor system were analysed in order to determine the various stresses imposed on the conductor structure. The results from this investigation showed that the conductor structure has different stresses being impose at different positions but a higher stress level is imposed in areas where motion is constrained. Also, the later paper by R. G. Sturm [26] shows that the author was among the earliest investigators who tried to determine the hysteretic damping of the vibration absorbers. The calculation for this damping was done by using the cyclic hysteresis loop to determine the structural damping. He indicated that greater damping can be obtained if the inter-strand motion between the strands in the damper is at greater amplitude. He also derived the mathematical model describing the conductor response with the placement of vibration absorbers on the line. The work documented by Tompkins et al [27], gave the analysis of the conductor vibration using the impedance to quantitatively determine the conductor self-damping. The method authors used was based on the principle of electrical-mechanical equivalence. The method entails a process where the conductor mechanical parameters are converted into their electrical equivalence for analysis. Based on this analogy of electrical-mechanical equivalent the conductor self-damping was evaluated. T. Slethei and J. Huse [28], the authors used both the analytical and experimental studies to determine properties of conductors in relation to the wind input data and the damping devices on the line. This process was used to determine the condition at which input loading on the conductor balance the power dissipation from the conductor. Their investigation developed a method for measuring the conductors' input force. In their work, the determination of the conductor stiffness and damping coefficient was based on the direct measurements of force, displacement, and phase angle and these values were obtained from the experiments conducted in the laboratory. R. Claren and G. Diana [5] developed an analytical model using the concept of principal modes. The developed analytical model and the experimental study conducted on transmission conductor were used to develop the equation for the conductor strains in relation to the external exciting force. Also, their study provided the basis of using the hysteresis loop test method to accurately determine the conductor damping.

To understand the mechanism of the conductor excitation and wind input power, series of investigations have been conducted using both static and dynamic model of the conductor in the field of fluid-solid interaction. This has led to various models been developed to describe this fluid

excitation mechanism on power line conductors. Most investigations were carried out in order to determine how much power is imparted by the wind loading on the conductor that causes its excitation. F.B Faquharon and R.E McHugh [29], G. Diana and M. Falco [30] and C. B. Rawlins [31], all used the phenomenon of fluid-solid dynamic excitation and carried out experimental investigations in the wind tunnel. These investigations were carried out to explain the aerodynamic phenomenon that occurs on power lines causing it excitation. These investigations that were conducted, entails using both the theoretical concepts of fluid-solid interaction and the actual experiments carried out in wind tunnels to determine the input energy on the conductor. These models were developed by using the cylindrical model to represent the conductor in the wind tunnel experiments and exposed it to wind flow. The analysis of conductor excitation is very complex because exploring the spatial flow around a conductor structure in the form of formation of vortices had been a difficult task. The analysis of excitation process involves the formation of the vortex pattern due to pressure difference producing resultant aerodynamic forces acting at different longitudinal locations on the conductor and this induces the spatial correlation of these distributed forces with the aim to determine the amount of the tangential components responsible for its oscillation. Thus, the experiments they carried out in the wind tunnels were used to investigate the vibration of conductor with the aim of determining the amount of input power and how wind loading on the conductors causes it to oscillate. From these wind tunnels experiments, empirical formulae were formulated to estimate the power input on the vibrating conductor.

M. Lutchansky [32], developed a model for the armor cable. When the cable is subjected to bending, this model was used to determine axial stresses induced in the helically wound armor strands of a submarine cable bent over a drum. He investigated the effect of shear interaction in a single layer helically wound cable, considering the outer layer of the strand slipping over the strands of an adjacent inner layer. The expression for the stresses was used to account for the stress induced at a rigid region such as a clamp. This shows the effects of the entire range of interaction of stiffness from frictionless slip to infinite interaction shear stiffness of the cables.

J. W. Phillips and G. A. Costello [33] presented a more detailed derivation for a wire rope based on the equations for the equilibrium of a curved rod by A. E. H. Love [34]. The model considered the wore rope as a bundle by discretizing the cable or wire rope into thin rods (strands) and solving the general nonlinear equations for the bending and twisting of a thin rod subjected to axial loads. In the initial unloaded configuration of the cable, the strands are just touching each other. The model assumed that the cable strand was loaded by an axial force and an axial twisting moment and that there are no frictional forces between the strands. The model was used to determine the axial stiffness and strain on the cables due to the axial loading.

S. Machida and A.J. Durelli [35] presented a more detailed derivation of equations for the cable, however their derivation was also based on A. E. H. love's equations for the equilibrium of a curved rod [34]. The model added the strands bending moment and twisting to the curved rod model. In this model, the cable strands were subjected to axial force and an axial twisting moment and also there are no frictional forces between the strands. In a similar vein to that in [33], the imposed stresses and strain on the cable were determined due to the axial loading.

R. Knapp [36] improved on earlier work of pure axial loading model of the cables developed by A. F. Hruska [37] to include in this case, a compressible core and large strand strains. He developed a new stiffness matrix for cables, consisting of layers of helical armouring wires wrapped around a central elastic core. This model considered the effects of both tension and torsion in predicting the structural behaviour of the cables.

K. G. McConnell and W.P. Zemke [38], showed based on their investigation that the mechanical properties of conductors have a strong coupling effect between the axial and the torsional behaviour. The model formulation was based on assumption that the strand can be treated as a single curved line element wrapped on a frictionless cylinder. The axial and the torsional coupling mechanism for both the ACSR and ACAR electrical conductors were analysed mathematically and verified experimentally.

J. Lanteigne and A. Akhtar [39] developed a model to predict the minimum load that can cause a failure of cable. This model was developed with the assumption that there is no frictional force between the strands. This work was extended by the experiments carried out by A. Akhtar and J. Lanteigne [40]. The model was validated by the experimental data showing a good agreement with the predictions for the multi-strand conductors made of aluminium alloy strands and for the measured values of true tensile stress for all cables. However, this model failed to predict the torsion values for cables containing galvanized steel strands as the predicted value deviate substantially from those measured experimentally.

X. Huang and O. G. Vinogradov [41], developed analytical model to analyse the frictional damping in cables which was assumed to be caused mainly by the dry friction between strands. In the model the damping occurs due to twisting and bending deformations resulting to slip between alternate strands in a wire rope, cable or conductor. It was this slipping between strands that allows energy to be dissipated due to dry friction. The model also accounts for small amount of energy dissipated through individual strands losses due to the relatively small material viscosity of the individual strands.

W. Jiang [42] has proposed a general formulation for the linear and nonlinear analysis of wire ropes. In this formulation, wires/conductors, and wire ropes are all considered as a kind of identical

structure characterized by seven stiffness and deformation constants, and as such they can be considered as a similar structure, as component elements of strands formed in layers, in a particular twisted axis to produce the general structure arrangement. Based on such arrangement, the general formulation thus developed can be used to analyse wire ropes of various sections: simple and complex cross-sections. The model can be used to analyse wire strands including all the aspects of loading on the single strands cables, and this can also be extended to more complex situations, such as the multi-strand ropes.

H. Ramsey [43] developed a model for the individual strands in a multi-layered cable, treating the stands as a helical rod. The model was used to account for inter-strand frictional forces which were derived from the equilibrium conditions and kinematic constraints imposed by the uniform extension and twisting of the cable. This model established that, the coupling effect can only occur due to the strands couples or moments which oppose the change of the lay angles.

S. Sathikh and N.S. Parthasarathy [44] developed a new discrete pre-slip bending response of a cable of helical strands having strand-to-core contacts under the constant curvature bending. Contacts were considered only for those between the core and the layer strands with coulomb friction acting. Small bending was assumed and the difference between the final and initial curvatures, twist and the strains were small and their second order effects are negligible. The core is assumed to be radially rigid. The Poisson effect on the strand and core were neglected. Elongation, shear, bending, and twist of a bent strand are considered together. This formulation was used to develop a model that can be used to analyse the conductor response taking into consideration the coupling effect.

The effect of strand deformation on the strand curvatures and twist due to the strand bending was discussed by Labrosse et al [45]. The authors investigated the frictional damping properties of axially loaded metallic cables consisting of one central core and one layer of helically wrapped strands. The damping properties of the cable due to friction was caused by the contact between the internal strands and the geometry of the individual strands. Tests were conducted so that the outside strands were assumed to be in contact between the strands and also with the central core. Their results proved that the total pivoting friction is a much smaller source of dissipation than the total slip friction. Therefore, whenever inter-strand sliding and inter-strand pivoting or both present; the friction associated with the pivoting can be neglected with respect to cable damping effects [45].

In the paper by F. Foti and L. Martinelli [46], also based on the concept of curved thin rod theory by A. E. Love [34], under the hypothesis of small displacements and rotations, the mechanical behaviour of each rope constituent, irrespective of its hierarchical level, can be described by the generalized stress and strain variables. This was used by the authors to propose a procedure to

evaluate the mechanical response of wire rope as a function of its geometry of the internal structure and for possible internal sliding due to the biaxial bending.

The investigation conducted by A. Yu [47] was used to determine the stranded cable damping. His study, both the static and dynamic experimental tests were performed on the cable, from which the deformation and energy relationships were developed. From his investigation, he proposed that the damping mechanism of a stranded cable was primarily due to inter-strand friction. The inter-strand friction depends on the contact forces, which is a function of the amplitude and the axial tension. In the past years, some researches in the field of conductor oscillation have been carried out with the goal to come up with a model that can be used to determine the conductor self-damping. The studies by E. E. Ojo [14], and C. Hardy [16], investigated the various damping mechanisms found in a vibrating conductor that give rise to conductor self–damping. It was ascertained that the conductors can damp out energy imposed on it using three means. First means is by internal friction at the molecular level i.e. material hysteresis that is, in any case negligible. The second means, is when a conductor flexes, it strands slip against each other, and this relative motion generates frictional forces that provide damping. The third is the aerodynamic damping through which a small amount of energy is returned to the wind. Additional damping can be provided by transference of the vibration to clamps, dampers, spacer dampers and suspension assembles, as well as by transference to adjoining sub-conductors (in case of bundled conductors). The authors [48] proposed a new approach to evaluate the conductor self-damping. This new approach was developed based on experimental work developed by A. Godinas and G. Fonder [49]. The new approach was the development of an analytical formula that can be used to determine the power dissipation within the conductor as a function of the conductor parameters. The approach resulted in the introduction of a new parameter which has the same dimension as energy (Joules). In the publication by C. Rawlins [19], where he gave an analytical description, coupled with the mathematical derivations of the various damping mechanisms found in a vibrating conductor. This publication gave good mathematical equations to determine damping, resulting from the various damping mechanisms in a conductor. In addition, in relation to self-damping, both the analytical and the field investigations have since been embarked upon by various researchers [6, 15, 50, 51]. They all came up with models to determine the conductor damping and also models to determine the position, type and the number of vibration absorbers (dampers) that are needed on the line to curtail the effect of mechanical oscillation on the line conductors.

The field of conductor transverse vibration that have received attention specifically is the determination of bending stiffness. Although, T. Varney [22] indicated that the actual bending stiffness of conductor lies between the two extreme values, due to the difficulty of characterizing

the conductor geometry in terms of contacts/friction in relation to stick/slip, he could not determine the actual value. To determine the true value, many investigations have been carried out. A model to determine the bending stiffness as function of deformation, radius of curvature was developed by K.O. Papuilliou [52]. The model established the fact that flexural rigidity of the conductor is not constant, it varies along the conductor due to curvature. Hong et al [13], extended the work of K.O. Papuilliou and proposed the frictional bending model. The proposed model considered the cable as a one-dimensional continuum with varying flexural rigidity, to estimate damping due to internal friction. This study also showed that the variation of the conductor flexural rigidity along the path of the deformation of the conductor.

In some other aspect of mechanical vibration of conductor modelling, some investigations have been done using numerical methods especially the use of finite element analysis. The investigation by Ghoreishi et al [53] was used to analyse, compare and established some developed closed-form analytical models, describing the mechanical behaviour of cables when subjected to axial loading. In this paper, various already developed models that can be used to analyse the cables for axial loading were compered in terms of the stiffness matrix as a function of its lay angle, in order to determine the strain. The validation of these models as a function of extension and rotation was determined by the use of the 3D FE model for the cable structure. Jiang et al [54], the authors proposed a concise finite element model for cables using three-dimensional solid brick elements, and the FEM took advantage of the benefit symmetries both for the structural arrangement and loading. This model was developed to decrease the computational cost when using a 3D approach in FE modelling of the cable geometry. This model takes into account the combined effects of tension, shear, bending, torsion, contact, friction and local plastic yielding in axially loaded simple straight strands but the model cannot be generalized to the case of bending or more complex loadings. A. Nawrocki and M. Labrosse [55] developed a finite element model for a simple straight wire. The model allowed the analysis of all the possible inter-strand motions. This allowed the analysis of mechanics around the contact areas in relation to energy dissipation. In the model, the role of the contact conditions for pure axial loading and for the axial loading combined with bending was investigated. To determine the energy dissipation due to the dynamic condition was evaluated using the Langrage multiplier to impose constrains at the area of contacts.

2.3 The Power Line Bare Conductors

Power lines conductors are usually in the form of ‘bare conductors’ used either as a single or as bundled (e.g. twin, triple, quadruple.) configuration. The conductors consist of a central core surrounded by one or more layers of helically laid strands. Stranded bare conductors mostly formed to consist of round strands that are helically laid in a particular helical axis with reference to the

central core axis. The term “stranded” applies to a flexible structure of the conductor used to transmit a tensile load and has sufficient flexibility to accommodate repeated bending during dynamic loading. Due to their flexibility, this is the main reason why stranded conductors are used in power transmission line. Stranded conductors allow more flexing movement before breaking, compared with solid conductor of the same diameter. For this reason, it is common for manufacturing specification, the requirements for bare conductor structure to consist of concentric-lay strands, in order guarantee or obtain the needed conductor flexibility.

Stranded conductors can be manufactured in the following ways: From only pure aluminium strands (AAC); from aluminium alloy strands (AAAC); from a combination of the two materials (ACAR) or from steel and aluminium strands (ACSR). In ACSR conductors the steel strands are used to provide reinforcement against the imposed tensile load. Sizes, number of strands, and the strand diameter found in various classes of the concentric-lay-stranded conductors conformed to the prescribed requirements based on the mechanical and electrical specifications for which the conductor is to be used. The diameters, areas, and the mass of concentric-lay-stranded aluminium and steel if present in the conductors conform to the prescribed requirements.

Bare conductors’ classification can be done on the following basis:

- Materials: The conductor can be homogenous like the All Aluminium Conductor (AAC), in which all including the core consists of identical strand. The conductor can be heterogeneous like the Aluminium Conductor Steel Reinforced (ACSR), in which the centre strand or the first few layers are made of steel strands, to protect the conductor, by providing reinforcement against the tensile stress resulting from tensioning and the dynamic loading due to bending.
- Strands Sizes: Strands in the same layer normally have the same size which may be the same or different from that of successive layers.
- Number of layers: This indicates whether the conductor is a single or multi-strand conductor.

Figure (2.3) shows the conductors with a homogenous and a heterogeneous cross-section.

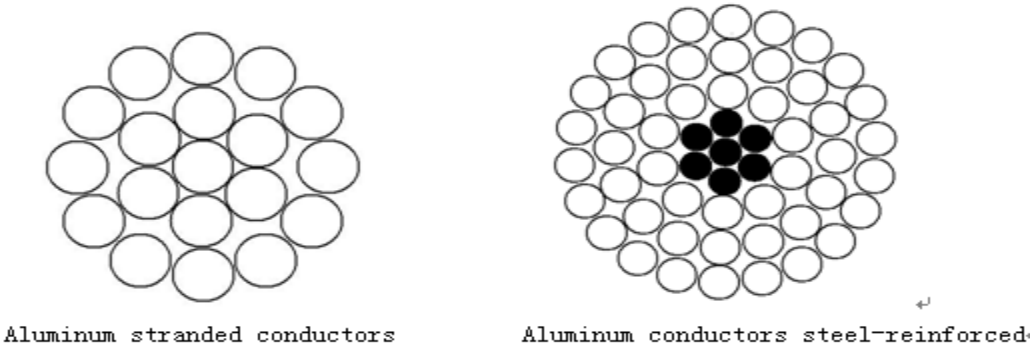

Figure 2.3: Cross-sectional views of circular strand conductors

There are some forms of conductors that are being manufactured to improve the current carrying capacity, weight to length ratio, resistance to mechanical vibration, the strands resistance to corrosion and improved self-damping capability. Figure (2.4) shows the cross-sectional views of some of these types of conductors that are used in power lines.

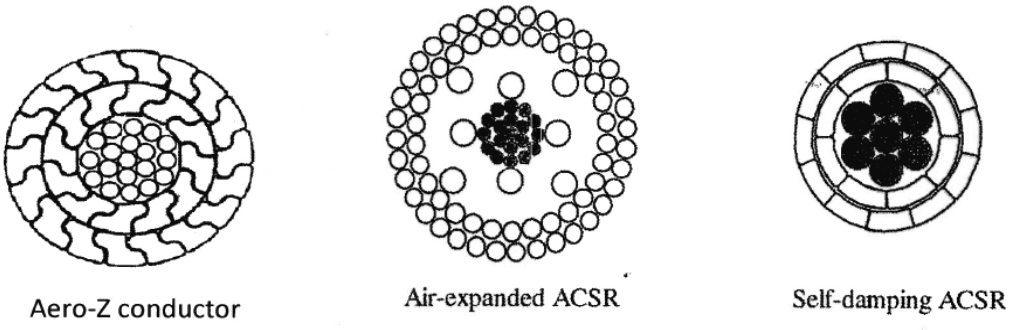

Figure 2.4: Cross-sectional views of some non-circular strand conductors [2]

These forms of conductors cannot be described by the convectional circular cross-section of a strand, whose geometric description will be given in the subsequent subsection (2.4.3). Thus, for these form of conductors in which some of the strands are not round in cross-section, the concepts that will be used for analysis in this study will not be applicable i.e. the analysis of these form of conductors will not be considered in this study.

2.4 Power Line Conductors Geometric Analysis

2.4.1 The Conductor Geometry

A transmission line conductor structure can be formed either as single layer or multiple layers of strands. The conductor is produced in the form of a stranded structure, produced by the assembly of substructure known as the strand. The strand is the basic structure for the formation of the conductor and the arrangements which comprises of the central core and the helically curved strands in various layer(s). Therefore, the stranded conductor can be treated as composite structure of the assemblies of strands, arranged in layers and each layer is constituted by a helically wound

profile of a number of strands with a lay angle and the helical strands lay arrangement is alternated in successive layers with opposite lay angle direction. This means that, the stranding is done in the right and left lay direction in the arrangement of alternating layers.

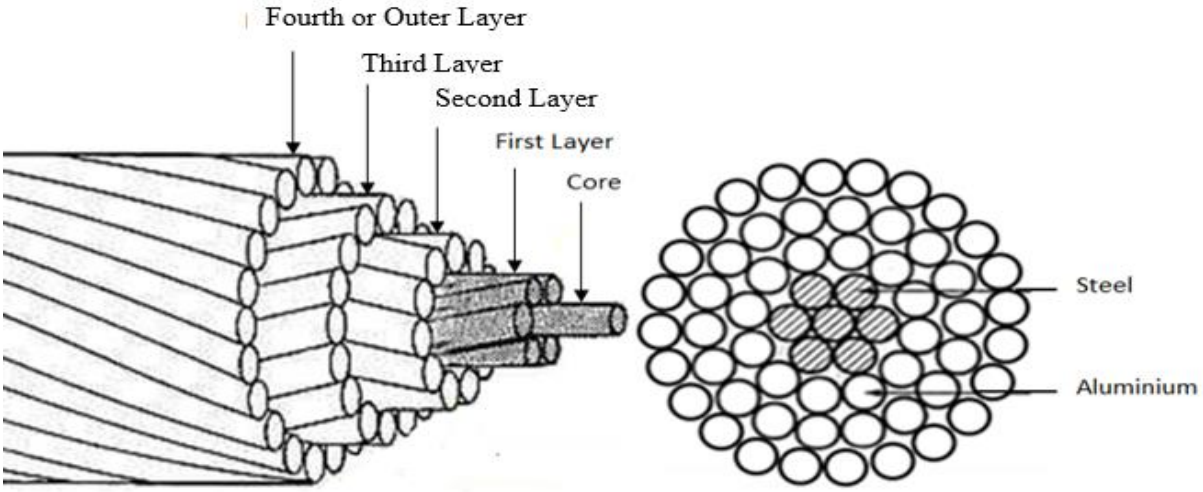

Figure 2.5: The four-layered conductors

For a four-layered conductor as shown in figure (2.5), comprise of a centre core strand, a first layer of 6-strand with left hand lay direction and the second layer of 12-strand in the right-hand layer direction. The normal arrangement indicated that the next successive layers has an addition of 6 strands with an opposite lay angle and so on till the fourth or the outer layer is reached.

2.4.2 Lay lengths and Lay angles

The geometric arrangement of the helical strands of conductors is done in a particular layer with specific lay values. The arrangement of strands in a given layer is a function of its lay length and the lay angle, either in right or left lay direction. The right hand lay arrangement is taken as positive and the left hand lay negative. Figure (2.6), illustrates the helical length (pitch length) and the layer angle and these parameters are very vital in defining the path the strands takes in the conductor geometric formulation.

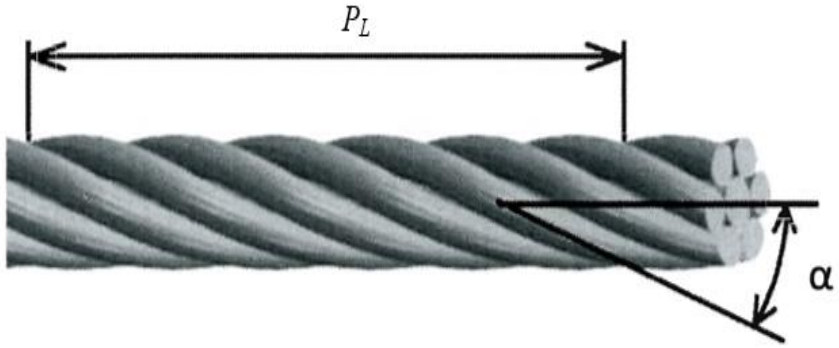

Figure 2.6: The pitch length and lay angle

The length of lay or pitch length is the path of the helix formed by a strand in a layer, which is the distance along the conductor for one complete turn of the strand along the axis of the helical path defined with respect to the conductor neutral axis.

For given layer, *i*, the pitch length $P_{L\,(i)}$, and the lay angle α_i, can be calculated by using the following equations:

$$P_{L(i)} = \frac{2\pi R_i}{\tan\alpha_i} \qquad \text{..... (2.1)}$$

$$\tan\alpha_i = \frac{\pi\left(D_{i,i+1} - d_i\right)}{P_{L(i)}} \qquad \text{..... (2.2)}$$

Usually the manufacturers may provide these parameters and where provided, the geometric formulation of the conductor will be found using these equations. In the absence of some of these parameters, in this study, these values were obtained based on theoretical evaluation as documented in [56]. The evaluation of these parameters was done using the ratio of the length of lay of a given layer to the diameter of that layer enveloping the strands. This ratio is known as the "theoretical layer ratio" of the layer. When the concentric lay rule is observed, there is a certain value of lay ratio that results in perfect packing of the strands of the layer such that there are neither gaps nor interference between strands. The value for the "theoretical lay ratio" can be obtained as indicated by C. Rawlins [56]:

$$\frac{P_{L(i)}}{D_{i,i+1}} = \frac{1}{1+{}^{3}\!/_{n_i}} \frac{\pi}{\sqrt{\left(\frac{n_i^2}{9}-1\right)\tan^2\left(\frac{\pi}{n_i}\right)-1}} \qquad \text{..... (2.3)}$$

In case the number of strands in the first layer; just above the core strand, if it is a 6-strands layer, equation (2.3) will fail to give a real value for the lay ratio. This is because with 6 strands at first layer the solution to this equation is undefined. For this layer, the lay ratio is determined using

figure (2.7). The graph is obtained by plotting the fill ratio and lay ratio against the number of strands in a given layer. The fill ratio is obtained as the ratio of diameter strand in a given layer to the diameter of strand in the next layer. The interpolation of the graph using the number of strand and the fill ratio gives a layer ratio for a particular strand distribution. In most cases, the size of the central strand and that on the first layer is assumed to be equal, thus the fill ratio for that layer equal to one, the trace along the graph using these two variables is used to determine the lay ratio.

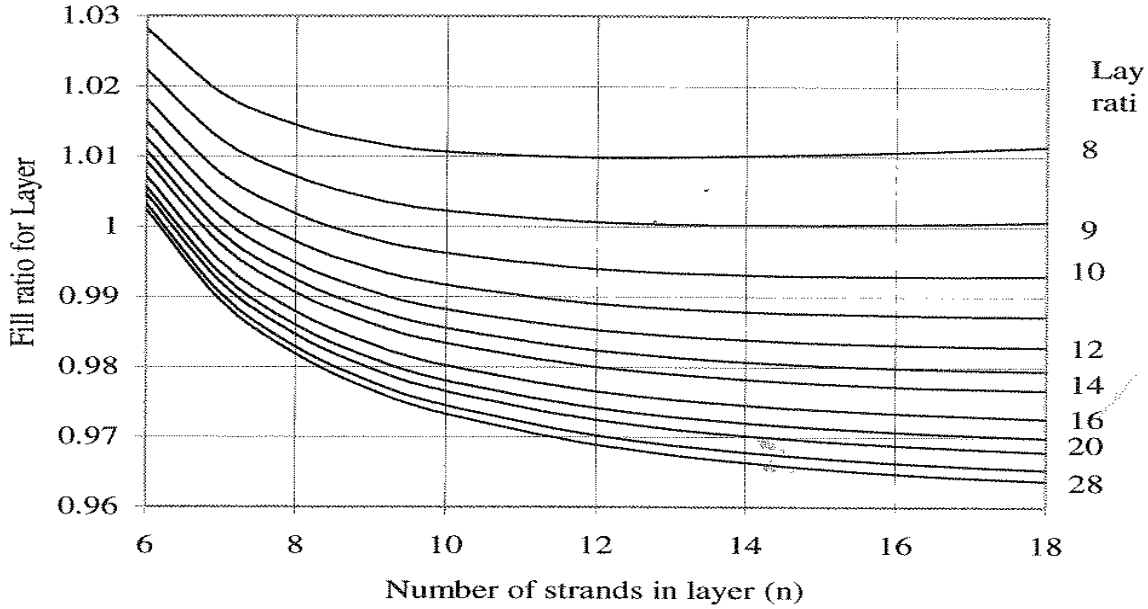

Figure 2.7: Lay fill ratio as function of lay ratio and number of strands [56]

2.4.3 Geometric Description of a Conductor Cross-Section

The conductor, the centreline of generic strands in a given layer can be described as a circular helix path, with radius *R*, and lay angle α. A typical cross-section of the conductor is made of strands, arranged as represented in figure (2.8). In the top corner of figure (2.8), define the coordinate system used as a reference for the geometric description of the conductor. This Cartesian coordinate system is the right-handed system and positive x-direction determine path of formation of the conductor, the y- and z-axis determine the transverse and normal directions respectively. This global coordinate system was used throughout this study.

Cross-sections of the strands are usually round shaped. Consider figure (2.8), which is a cross-section of a conductor, made up of strands of circular cross-section. The stranded bare conductor cross-section with a total cross-section area A_T, consisting of *i*-layers ($i = 0, 1, 2, \ldots, N$), of strands of radius r_i ($d_i = 2r_i$) with lay angle α_i, wrapped over the centrally located core strand, of radius r_0 ($d_0 = 2r_0$).

Each particular layer consists of *n* number of strands. Using the compact arrangement, the number of strands in each layer will be defined as n_i = 1, 6, 12, 24, … This may not necessary be the case, as other number of strands can be formed, in the case of Tern conductor, n_i = 1, 6, 9,15, and 24. The position of each strand in a given layer is defined as P (i, j), where (j = 0, 1, 2, …, n_i). Therefore, P (0, 0) defines the position of the core strand and others positions of strands in each layer are defined on yz-plane in figure (2.8) in the anti-clockwise direction along the x-axis. The positions of each strands as located at its cross-section can be determined by:

$$P(i, j) = R_i \cos \varphi_i \qquad \text{..... (2.4)}$$

where $\varphi_i = 0 : \frac{360^o}{n_i} : 360^o$

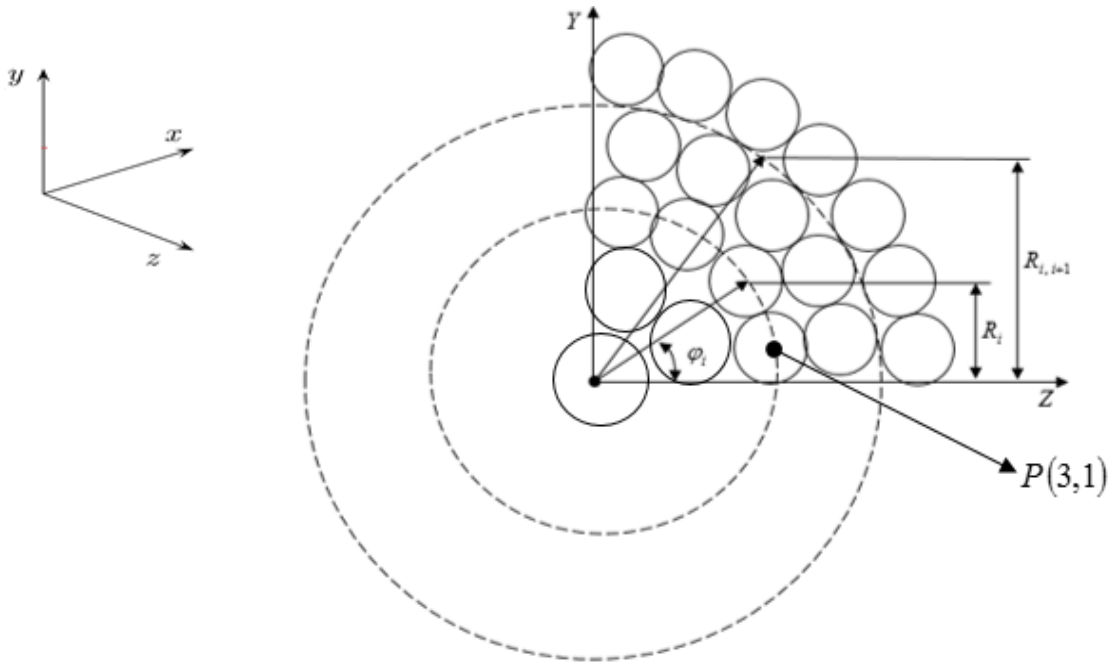

Figure. 2.8: The conductor cross-section

The outer radius and the conductor cross-section can be calculated respectively by

$$r_N = \frac{d_N}{2} + \sum_{i=1}^{N-1} d_i + \frac{d_0}{2} \qquad \text{..... (2.5)}$$

$$A_T = \pi (r_N)^2 \qquad \text{..... (2.6)}$$

The radius between layers and the radius of the circular path that passes through the centre of strands located at *i*-layer (excluding single layer conductor) from the origin, are calculated by

$$R_{i,i+1} = r_0 + \sum_{i=0}^{N-1} d_i \text{ and } R_{i,} = r_0 + \sum_{i=0}^{N-1} d_i + r_{i+1} \qquad \text{..... (2.7)}$$

In the case of a single layer conductor, these values are obtained as:

$R_{0,1} = r_0$ and $R_1 = r_0 + r_1$ ..... (2.8)

For the strands arrangement in various layers, parallel to the x-axis, where the distance for the strand centre are defined from the centre of the core. The position of the centre line of each strand in a given layer and the distance along these centres along the curvilinear axis of helix from the conductor neutral axis which is located in the same direction to the *x*-axis are given as:

$$R_{i,i+1} = r_{i,i+1}\sin(\varphi_i) \text{ and } R_i(x) = r_i \sin\left(\frac{2\pi x}{P_{L(i)}} \pm \varphi_i\right) \quad \text{..... (2.9)}$$

Where φ_i incremental helix angle (wrap angle), which is the angular position of strand from the *z*-axis in the anti-clockwise direction.

This form of descriptions given above is applicable to any conductor with strands of circular cross-section.

2.5 Parameters Associated with the Conductor Geometry

The application of conductor in power transfer requires a quantitative evaluation of the relevant mechanical parameters in order to determine its dynamic response in the advent of external power loading. The helical arrangement of strands is responsible for its flexibility and one of the major advantages of such structures like a conductor is their capacity to support large axial loads with comparatively small bending or torsional stiffness.

Most analysis of the internal geometry of conductor as a composite structure, can be done by applying differential geometry of helical strands, due to the complexity of the problem. This entails the use of the constitutive equation for the strand either using the thin curved rod or the deformed beams in the space, with or without frictional effect between strands. A system of nonlinear, differentials equations are set up, under suitable hypotheses, these equations can be reduced to linearized equations for the system. This form of analysis is based on the famous general theory of thin curved rod [34].

Conductor response is usually influenced by its geometry. As far as the conductor static, bending, fatigue, and energy dissipation are concerned, the dynamic response is influenced by phenomena and parameters that are related to its internal geometry, such as:

- The strands tensile force
- The relative movements, in the contact points between the strands of the same layer and between the strands of two adjacent layers of the conductor.
- The stresses variations around the contact points.
- The stresses due to the variation of curvature of the conductor when it is deformed.

The analyses of the strands in terms of stresses generated internally and the energy dissipated requires the knowledge of the inter-strand contacts. The factor of inter-strand contact requires a much more complex theory in order to model and analyse the elastic contact surface and in the presence of friction forces.

2.5.1 The Analysis of Conductor Inter-Strand Contacts

The closely packed arrangement of strands, coupled with the conductor being subjected to tensile force give rise to some form of contacts between strands. The conductor dynamic behaviour and the fatigue characteristics are both dependent on the inter-strand contacts and this is due to the operation of the frictional effects between the strands around these areas of contact. This makes it imperative to have an adequate knowledge of the inter-strand contacts mechanics and forces resulting from such inter-strand contacts. In a conductor, contacts is as a result of the conductor helical geometric arrangement and the axial loading applied at its ends.

In the analysis of the conductor geometry starting from the core strand outward, the first form of contact is the core to strand or the inter-strand contact between strands of adjacent layer. This type of contact occurs due to strands resisting the inwards radial force which tends to lengthen the strands due to the applied axial loads. To model the conductor using this form of contact, it is assumed that the strands in the same layer do not touch each other, and are in contact only with those in adjacent layers either above or below. This form of contact is referred to as the radial contact. The second form of contact within the conductor is due to the closely compact arrangement of the conductor. This results in a strand to strand packed contact, in which strands in the same layer are in contact, and inter-strand contact with adjacent layers are neglected. This form of contact is referred to as lateral or circumficial contact.

The combination of the two forms of contacts above described, is the third type of contact in the conductor. In modelling, this form of contacts is the combination of the radial and the lateral contacts. This form of contact combines the interlayer-strand and alternate layer strand-strand contact i.e. in which lateral contacts occur between strands of the same layer and the radial contacts occurs between strands of different layers. In most models, one form of these contacts has to be selected as the primary aim in order to avoid a statically indeterminate solution, which is mathematically difficult to solve. Under actual loading conditions, a strand may have both contacts.

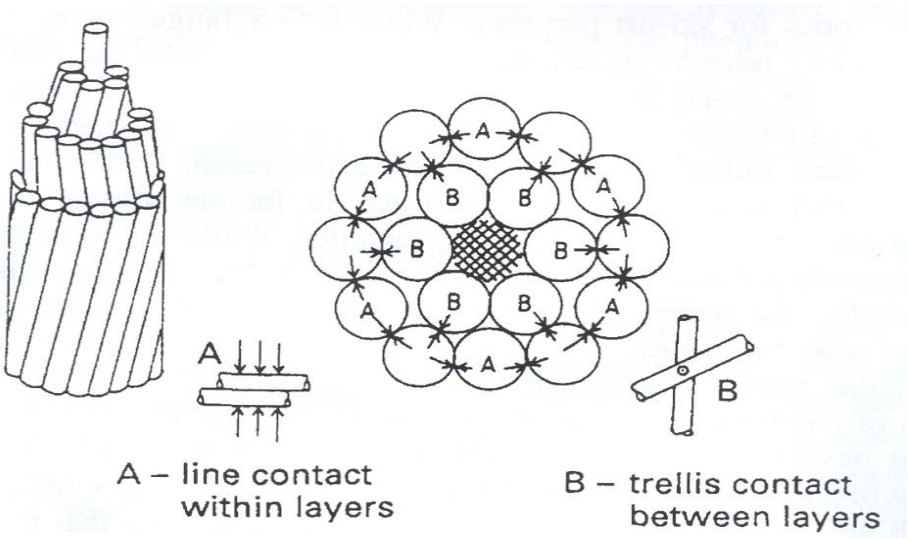

Figure 2.9: Inter-strand contacts in helical stands [12]

Various explanations have been given for the phenomena associated with various types of contacts within conductors, as can be found in many literature [11, 18, 19]. A general characteristic of the contacts between the strands depends on the helix angle. The description of the contacts within the cables also applicable to conductors is documented in the paper by T. Hobbs and M. Raoof [12], the authors identified two forms of contacts. They are the line and the point contacts. The diagram in Figure (2.9) shows where these types of contacts occur in a multilayer conductor. As shown in this diagram, the points mark A is used to indicate the areas that experience line contact, while the points mark B, indicates the areas of point or trellis contact.

The line contact occurs between the parallel layered helical strands of the same layer and it also exists between the first layer and the core. The line contact is a form of strand-strand contact i.e., lateral contacts. For the point or trellis contact, this form of contact occurs due to the helical arrangement of strands. This arises due to the opposite lay angle arrangement, strands in alternate layer crosses each other producing a point or trellis contact: inter-layer contact i.e. radial contacts. In this form of contact, the strands in the one layer touches only those in alternate layers each at a point either below or above depending on the number of layers in the conductor.

The knowledge of any form of deformation and motion in the area contact is very important because of the action of friction, which causes energy dissipation to occur. In [16] it was stated that for stranded conductors, it may be assumed that virtually all of the internal damping energy originates from the mutual dry coulomb friction between the different layers of conductor including the core. In his model, the author used the analyses of the line contacts between the strands under sinusoidal conditions to determine the energy dissipation from the conductor. In a similar process, C. B. Rawlins [19] also used the analysis of line contacts in their models to determine the contact stress, interlayer shear stress, and slip condition under both the axial and

bending loads. These models use the equivalent of line contacts for the point contacts. Although most authors use the line contact for their analysis, actually the contacts between alternate strands are point contact. To reduce the complexity of numerically when implementing the point contact, in the area of finite element analysis, this study will implement the equivalent of line contact capable of representing the effect of the point contact. The line contact and the equivalent of the line contact for the point contact was used to characterize various contact regions and then used to determine the energy dissipation from a conductor.

2.5.2 Number of Contacting Points

As explained earlier, the helical arrangement of strand gives rise to some form of inter-strand contacts. The shear force that tends to resist the unwinding of strands occurs at inter-strand contacts (line and point) between layers. The shear forces are applied to a strand at the lines or discrete points along its length, where it lay parallel or crosses the strands of the layer above or below. For analysis of the contact areas, it is necessary to determine this array of these line and discrete tractions within a conductor. For point contact, the number of contacts within a lay length determine the number of traction point and compliance function for analysis. For this it becomes imperative to know how many contact points lies along the pitch length.

Consider a point contact between strands, which occurs with the layer above and beneath, and this arrangement produces a number of the contact patches between the layers. The number of contact point can be determined for two contacting layers over a lay length of a strands along the path of the helical strands with opposite lay angles. Reference [57], gives the equation to determine the number of contacts between strands of different layers. The number of contact points between two layers can be defined as the number of contact points between layer, *i*, and layer, *i +1*, i.e. contact between a given strand and the strand above it. Hence, the number of contact points per lay length of a strands of layer, *i* with layer, *i+1*, as given in [58] is:

$$ncp_{i,\,i+1} = n_{i+1}\left(\frac{R_i \tan\alpha_{i+1}}{R_{i+1}\tan\alpha_i} + 1\right) \qquad \text{..... (2.10)}$$

Conversely, on the other hand, the point contact between a given layer, *i*, and layer, *i*-1, i.e. for contact between a given strand and the strand below it.

$$ncp_{i,\,i-1} = n_{i-1}\left(\frac{R_i \tan\alpha_{i+1}}{R_{i+1}\tan\alpha_i} - 1\right) \qquad \text{..... (2.11)}$$

The number of contact points on interface, *i*, over a conductor unit length is analysed in [58] as:

$$ncp_i = n_i\left[(1+n_{i+1})\left(\frac{\tan\alpha_i}{2\pi R_i}+n_{i+1}\frac{\tan\alpha_{i+1}}{2\pi R_i}\right)\right] \quad \text{..... (2.12)}$$

Substituting the pitch length as defined by equation (2.1), into equation (2.11):

$$ncp_i = n_i \times \left[n_{i+1}\left(\frac{1}{P_{L(i)}}+\frac{1}{P_{L(i+1)}}\right)+\frac{1}{P_{L(i)}}\right] \quad \text{..... (2.13)}$$

The number of point contacts in a conductor can be determined by the approximation made by C.B. Rawlins [19], where the number of contacts between layers was given as:

$$ncp_i = n_{i+1}\left(1+\frac{P_{L(i)}}{P_{L(i+1)}}\right) \quad \text{..... (2.14)}$$

For a given conductor, the actual distance of contact points, measured on the strand centre line can be evaluated [58]:

$$d_{ci} = \frac{1}{n_{i+1}}\frac{1}{\cos\alpha_i}\frac{2\pi R_i R_{i+1}}{R_i\tan\alpha_{i+1}+R_{i+1}\tan\alpha_i} \quad \text{..... (2.15)}$$

To find the normal contact force due to the axial load on conductor using the number of the normal point force at the interface contact points between *i*-layers and *i+1*-layer can be found [58].

2.6 Contact Mechanics

Contact mechanics with friction is concerned with a large range of different aspect of investigation. The deformation field in the solids including contact areas can be determined by minimizing the elastic deformation energy. In this case of conductor inter-strand contact, the investigation will be at the macroscopic scale, and this was used for the investigation of the motion between the contacting strands. Here, the resultant force versus lateral displacement is of main concern and this will be explored in chapter 5.

The value of the tensile force acting on each strand will be determined in later section of this chapter. This tensile force acting on each strand gives raise to normal force at the contact areas. In this study, the concept of a Hertzian contact was used to model the area of contact between strands, as function of the type of contact. The description of the mechanic of the contact surfaces between two elastic cylindrical bodies (parallel or inclined at an angle) are given in [59]. The cylinders are squeezed together by the normal force, F_N. Due to the fact that both line and point contacts are both present in the conductor structure, the contact mechanics for both are presented as documented in [59, 60].

Generally, the effective radius of curvature is defined by the radii of curvature of the two contacting bodies and effective radius:

$$\frac{1}{R^*} = \frac{1}{r_1} + \frac{1}{r_2} \qquad \text{……...… (2.16)}$$

Also, the effective modulus of elasticity for the contacting bodies can be evaluated and the contact modulus given as:

$$\frac{1}{E^*} = \frac{1-\upsilon_1^2}{E_1} + \frac{1-\upsilon_2^2}{E_2} \qquad \text{……...… (2.17)}$$

Where E_1 and E_2 are the elastic modulus of the solids and ν_1 and ν_2 are their corresponding Poisson ratios.

2.6.1 Point Contact Mechanics

For the case of point contacts which can be depicted as two cylinders in contact and both are subjected to tensile force T_i, as indicated by figure (2.10). The analysis of two cylinders that crosses each other can be used to analyse the contact that occur between two strands due to the lay angle between them. The contact between these two cylinders produces a contact patches which has an elliptical contact area.

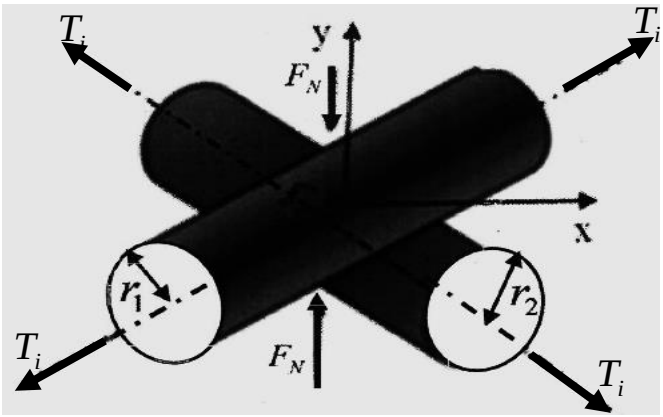

Figure 2.10: Point contact

Two cylinders with contact radius and the Hertz equations for elliptical contact:

Relative Radii

$$r = \sqrt{r_1 r_2} \qquad \text{……...… (2.18)}$$

where

$$r_1 = \frac{1}{(A+B)-(B-A)} \quad r_2 = \frac{1}{(A+B)+(B-A)} \quad A+B = \frac{1}{2}\left(\frac{1}{r_{1xx}} + \frac{1}{r_{2yy}} + \frac{1}{r_{2xx}} + \frac{1}{r_{1yy}}\right)$$

$$B-A=\frac{1}{2}\left\{\left(\frac{1}{r_{1xx}}-\frac{1}{r_{1yy}}\right)^2+\left(\frac{1}{r_{2xx}}-\frac{1}{r_{2yy}}\right)^2+2\left(\frac{1}{r_{1xx}}-\frac{1}{r_{1yy}}\right)\left(\frac{1}{r_{2xx}}-\frac{1}{r_{2yy}}\right)\cos(2\alpha)\right\}^{\frac{1}{2}}$$

Eccentricity of contact ellipse:

$$e^2=1-\left(\frac{b}{a}\right)^2\cong 1-\left(\frac{r_b}{r_a}\right)^{\frac{4}{3}} \qquad \text{.....................…. (2.19)}$$

Equivalent radius of contact:

$$c=\sqrt{ab}=\left(\frac{3F_N R^*}{4E^*}\right)^{\frac{1}{3}} \qquad \text{.....................…. (2.20)}$$

Major and minor contact radii:

$$a=c\left(1-e^2\right)^{-1/4} \quad b=c\left(1-e^2\right)^{1/4} \qquad \text{.....................…. (2.21)}$$

Maximum Pressure for point contact:

$$p_{\max}=\frac{3F_N}{2\pi c^2}=\frac{3F_N}{2\pi ab} \qquad \text{.....................…. (2.22)}$$

2.6.2 Line Contact Mechanics

The line contact is illustrated by figure (2.11), the contact modulus expresses the elastic properties of strands. For line contact, the following equations are applicable:

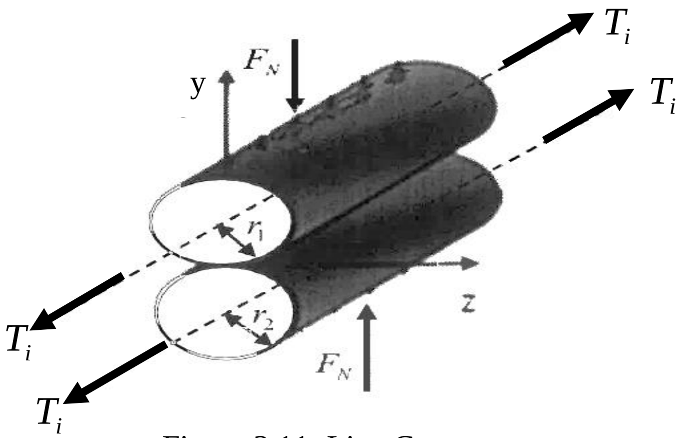

Figure 2.11: Line Contact

Half width of contact:

$$a=\left(\frac{4F_N R^*}{\pi E^*}\right)^{1/2} \qquad \text{.....................…. (2.23)}$$

Maximum pressure for the line contact:

$$p_{\max} = \frac{2F_N}{\pi b} = \left(\frac{F_N E^*}{\pi R^*} \right)^{\frac{1}{2}} \quad \text{……...…} \quad (2.24)$$

As it can be deduced from figure (2.9), the stresses from point contacts can only be applicable to multi-layered conductors. It is worthy to note, the formulations of the stresses along the contacts areas between strands (excluding that between the core and the first layer), occur at the point contact but an equivalent line contact have been used in most analytical model [19, 58]. This have been employed for the evaluation of the conductor flexural rigidity as only the stresses from the equivalent line contacts was employed due to the cumbersome of using the analysis of stresses from the point contacts. This concept was adopted in later chapter in the FEM formulation, where the form of line contact stresses of an equivalent point contact stress was used and its implementation was done taking into consideration bending due to the sinusoidal forcing function.

2.7 Pressure between Strands of Different Layers

The strands of the conductor are subjected to tensile force due to the conductor under axial tensions exerted at points of support at the towers. This axial force imposed on the strands tends to straighten the strand which causes a decrease of the radius of the lay cylinder. This force which tends to lengthen the strands then give rise to resistive forces between layers, i.e. forces are exerted at the contacts between strands. This inward radial elongation action on a layer will be countered by the reaction of the layer below, thus leading to an interlayer pressure. The pressure between two strands of different layers was calculated as documented in [37, 58]. It is shown that the radius of curvature can be obtained by:

$$\rho_{cur} = \frac{R_i}{\sin^2 \alpha_i} \quad \text{……..……} \quad (2.25)$$

where the curvature is obtained from equation $\kappa = \frac{1}{\rho_{cur}} = \frac{\sin^2 \alpha_i}{R_i}$

The strand is subjected to tensile force T_i, the equivalent force per length for the line contact is obtained as:

$$p = \frac{T_i}{\rho_{cur}} = T_i . \kappa = T_i . \frac{\sin^2 \alpha_i}{R_i} \quad \text{…..……..……} \quad (2.26)$$

2.8 Evaluation of Inter-Strand Contact Force

This section takes a discrete analysis approach in examining the contacts within the conductor with a view of identifying the various forces acting. For a single layer conductor as shown in figure (2.12), the contact between the only layer and the core are line contact and the stresses are analysed along the line contact as a form of pressure distribution, shown in figure (2.13). For a multilayer conductor as shown in figure (2.14), while, apart from the contact between the first layer and the core, other forms of contact between layers are actually point contacts. It is well known that most stresses are located in the area of point contacts. Though, most inter-strand contacts are point contacts, in most studies, a line contact of an equivalent point is normally used. Similarly, also used here, concepts associated with the already well-established line contact stresses were used to deduce the various forces that acts within the conductor [13, 52, 57].

Presented as follows is the combined summarized derivations, as documented in [13, 52, 57]. For the derivation, a single layer conductor as shown in figure (2.12) was considered first and later extended to the multilayer conductor.

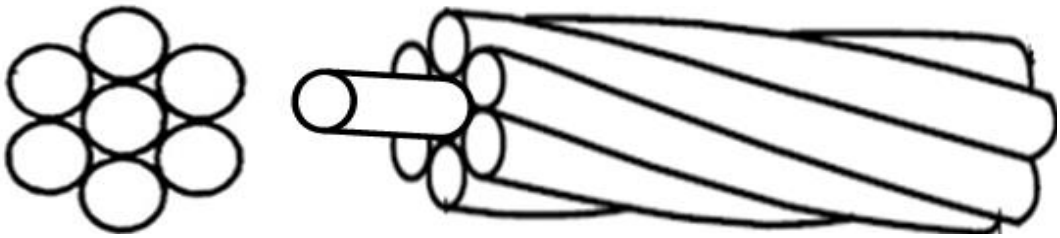

Figure 2.12: Single-layered conductor

To evaluate the various internal forces acting within the conductor, the analysis starts when the conductor is assumed to be in the stick condition and only the axial force acting on each strand is considered. Under the stick condition there is no relative displacement between strands. This is made possible because the friction force at the contacting regions is greater than the shearing forces tending to pull the strands apart. It is assumed that both strands exert equal and opposite force at these regions of contacts. Also, the only internal loads acting on a conductor cross-section is assumed to be the normal force (tension) and the small bending moment arising from the strand curvature.

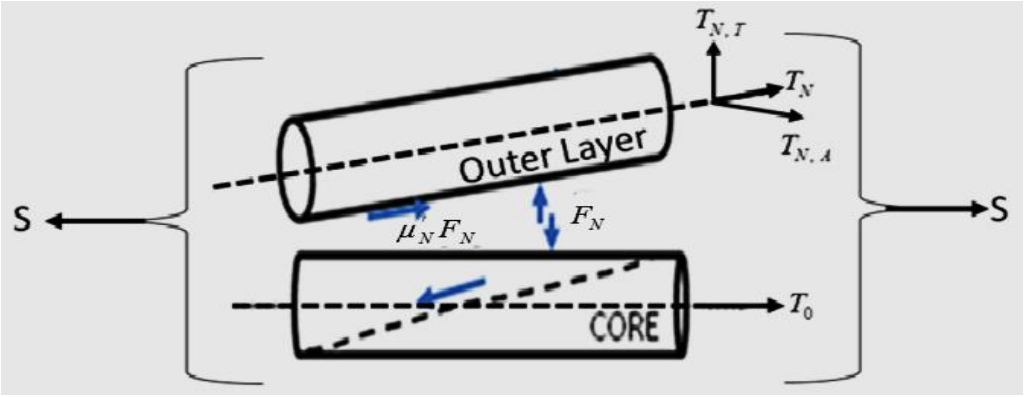

Figure 2.13: The normal and frictional forces in a single-layered conductor

In line with the above, considering the outer layer forces of the single layer conductor ($i = 1$ or N = 1) as shown in figure (2.13), with the conductor cross-section subjected to axial loads, S due to tensioning acting at both ends. The axial load induces tension on individual strands T_i and this tension has two components due to the helical arrangement: axial $T_{i,A}$ and tangential $T_{i,T}$ components. Neglecting the tangential components, the tensioning force on each individual strand in given layer of the conductor is therefore calculated as:

$$T_i = \frac{T_{i,A}}{\cos\alpha_i} \qquad \text{…….……..……. (2.27)}$$

Under this static condition with the presence of the conductor's axial tension S, each individual strand can be assumed to be subject to the same tensile force as given by [57]

$$T_i = \frac{E_i A_i \cos^2\alpha_i}{\sum EA\cos^3\alpha_i}\cdot S \qquad \text{……..……. (2.28)}$$

The axial load S, acting on the conductor cross-section tends to straighten the strands, thereby inducing pressure on the core below. For the single layer conductor shown in figure (2.13), the layer exerts a pressure on the core and this can be evaluated as:

$$p = \frac{2T_{i,S}\sin(d\beta/2)}{\rho d\beta} = \frac{T_{i,S}}{\rho} \qquad \text{…… (2.29)}$$

where ρ is the radius of curvature and β is the wrap angle

Considering a curve differential element of the strand of an arc length, given as

$$ds = \rho d\alpha = \frac{r d\varphi}{\sin\alpha} \qquad \text{. ……..……. (2.30)}$$

The exerted pressure gives rise to the radial force along the arc length of the differential element. Hence, this radial force is calculated as

$$F_N = \rho\cdot ds = T_{i,S}\sin\alpha_i d\varphi \qquad \text{……..……. (2.31)}$$

The surface along the line contact gives rise to the component of normal force. Mathematically, at the surface for a two contacting strands:

$$dF_{S(i)} = \mu F_N \quad \text{..... (2.32)}$$

Substituting equations (2.30) and (2.31) into equation (2.32), the radial force that acts on the individual strand under tension is obtained as:

$$dF_{S(i)} = \mu T_{i,S} \sin\alpha_i \, d\varphi \quad \text{..... (2.33)}$$

If the frictional effects is said to be greater than the shear force that is tending to pull the strands apart and assuming the sliding is just about to occur, which implies that friction force is maximum. The reaction force $dT_{i,S}$ on an individual strand due to friction can be calculated as:

$$dT_{i,S} = dF_{S(i)} = \mu dF_N = \mu T_{i,S} \sin\alpha_i \, d\varphi \quad \text{..... (2.34)}$$

The summation of all the normal forces for the entire cross sections is obtained by integrating the above first order differential equation and the solution is given as:

$$T_{i,S}(\varphi) = C_i e^{\mu \sin\alpha \varphi} \quad \text{..... (2.35)}$$

The constant C_i is evaluated with the above equation satisfying the boundary condition: where $\varphi = 0 \quad and \quad T_{i,S}(0) = C_i e^{\mu \sin\alpha \varphi}$. Thus

$$C_i = T_i = \frac{E_i A_i \cos^2 \alpha_i}{\sum EA \cos^3 \alpha_i}.S \quad \text{..... (2.36)}$$

Therefore, the normal force acting, is given as: $T_{i,S}(0) = T_i$

In the no-slip condition, the force exerted due to bending can be calculated according to the usual Bernoulli-Euler beam bending theory. Hence, the total force $T_{i,S}$ for the stick state is calculated and this will yield the function:

$$T_{stick}(\varphi) = T_i \, e^{\mu \sin\alpha_i \, \varphi} \quad \text{..... (2.37)}$$

The above equation gives the value for the normal force that acts just before bending i.e. when the strand is just about to slip. During bending under dynamic loading, the frictional force is overcome resulting in relative sliding between the strands in point contact. Sliding occurs when reaction force is greater than friction force assuming that the tensile force is constant along the strand. Thus, beyond a given bending amplitude, micro-slip occurs at the inter-layer contact points. During slippage, the normal force is reduced and this can be calculated as

$$T_{slip}(\varphi) = T_{stick}(\varphi) - T_i = T_i(e^{\mu \sin\alpha_i \varphi} - 1) \quad \text{..... (2.38)}$$

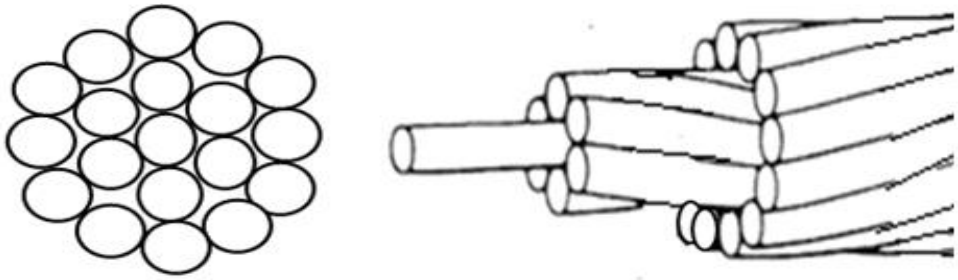

Figure 2.14: Double-layered conductor

Next, was to extend the above procedure used to determine the normal force acting on a single layer to a multilayer conductor. Starting with double layer conductor shown in figure (2.14). In analysing a multilayer conductor, the above derivation done for the single layer above the core is applicable to the outer most layer of the multilayer conductor.

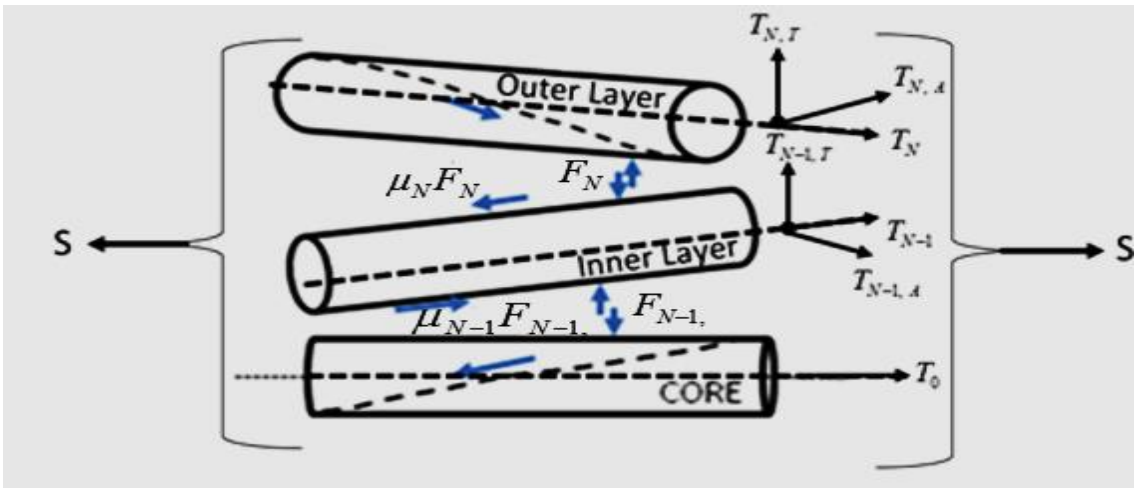

Figure 2.15: The normal and frictional forces in a double-layered conductor

Considering each layer of a multilayer conductor, shown in figure (2.14) which is a doubled-layered conductor subjected to axial tension, S. Firstly, consider the double layer conductor shown in figure (2.15), the number of layer *i =1, 2 or N=2.* In this case, extending already derived equations for a single layer conductor as applicable to the outer layer where *N = 2*.

Now considering the derivation for the penultimate layer, *i =1 or N-1* i.e. layer just below the outer layer. The normal forces acting on the outer part of the strand with the outer strand can be determined as:

$$dF_{N(i,\,outer)} = dF_{N,\,N-1} = T_{N-1} \sin\alpha_i d\varphi_{N-1} \quad \text{..... (2.39)}$$

Also, the normal forces acting on inner part of the strand with the inner strand can be determined as:

$$dF_{N(i.\,inner)} = dF_{N-1,\,N-2} = T_{N-1}\sin\alpha_{N-1}d\varphi_{N-1} \quad \ldots\ldots\ldots\ldots\ldots\ldots\ldots (2.40)$$

Therefore, the imbalance force acting on the strands in this layer is by the summation of equations (2.39) and (2.40), then multiply by its coefficient of frictions.

$$dT_{N-1} = (\mu_{N,N-1}dF_{N(i,outer)} + \mu_{N-1,\,N-2}dF_{N(i,inner)}) \quad \ldots\ldots\ldots\ldots\ldots\ldots\ldots (2.41)$$

The substitution of equations (2.39 and 2.40) into equation (2.41) result to

$$d\,T_{N-1}(\varphi) = \mu_{N-1}T_{N-1}\sin\alpha_{N-1}d\varphi_{N-1} + (\mu_{N-1} + \mu_N)T_N\sin\alpha_N d\varphi_{N-1} \quad \ldots\ldots\ldots\ldots\ldots\ldots\ldots (2.42)$$

The solution to the above differential equation comprise of the homogeneous and the particular solutions given as

$$T_{N-1}(\varphi_{N-1}) = T_{N-1}e^{\mu_{N-1}\varphi_{N-1}\sin\alpha_{N-1}} + T_N e^{(\mu_{N-1}+\mu_N)\varphi_{N-1}\sin\alpha_N} \quad \ldots\ldots\ldots\ldots\ldots\ldots\ldots (2.43)$$

The evaluation of the above equation is by satisfying the boundary conditions as the same for single layer conductor, but in this case the constants T_{N-1} *and* T_N must be determined. Because in this study, the conductors used for analysis is ACSR, thus a constant co-efficient of friction is not assumed. Applying similar boundary condition for the multilayer conductor:

Where $\varphi = 0, \quad T_{N-1,\,S}(0) = T_{N-1}e^{\mu_{N-1}\sin\alpha_{N-1}\varphi_{N-1}}$ *and* $\quad T_{N,S}(0) = C_N e^{(\mu_{N-1}+\mu_N)\sin\alpha_N\varphi_{N-1}}$.

The normal force for the stick condition is calculated by

$$T_{stick}(\varphi) = \left(T_{N-1}e^{\mu_{N-1}\sin\alpha_{N-1}\varphi_{N-1}} + 2T_N e^{(\mu_{N-1}+\mu_N)\sin\alpha_N\varphi_{N-1}}\right) - (T_{N-1} + T_N) \quad \ldots\ldots\ldots\ldots\ldots\ldots (2.44)$$

For the slip condition, this force becomes an exponential function whose exact form depends on the selected slip state. Taking this into account, the force is given by

$$T_{slip}(\varphi) = \left(T_{N-1}e^{\mu_{N-1}\sin\alpha_{N-1}\varphi_{N-1}} + 2T_N e^{(\mu_{N-1}+\mu_N)\sin\alpha_N\varphi_{N-1}}\right) - (T_{N-1} + T_N) - 1 \quad \ldots\ldots\ldots\ldots\ldots\ldots (2.45)$$

The above derivations can now be extended to the case of various normal forces between each strand, for any given layer for the general case of the conductor geometry, with an arbitrary number of layers in the conductor.

Generally, the normal force acting in the stick condition for any arbitrary number of multilayer conductor can be calculated by

$$T_{stick}(\varphi) = \left(T_i + \sum_{i+1}^{N} 2T_{i+1}\right)e^{(\mu_{i-1}+\mu_i)\sin\alpha_i\,\varphi_{i-1}} - \sum_{i+1}^{N}(T_i + T_{i+1}) \quad \ldots\ldots\ldots\ldots\ldots\ldots\ldots (2.46)$$

For the slip condition

$$T_{slip}(\varphi) = \left(T_i + \sum_{i+1}^{N} 2T_{i+1}\right)\left(e^{(\mu_{i-1}+\mu_i)\sin\alpha_i\,\varphi_{i-1}} - 1\right) \quad \ldots\ldots\ldots\ldots\ldots\ldots\ldots (2.47)$$

2.9 Characterization of the Conductor Cross-Sectional Parameters

2.9.1 Description of the Conductor Cross-Section

This section describes the operational parameters of the conductors in terms of its static and dynamic behaviour that is a function of its geometry. Conductors have a high tensile strength, which is responsible for their ability to withstand high tensile stress under the mean static load and the superimposed cyclic bending loading. The tensile strength is a function of the material, number and cross section of strands. When imposed, the axial and bending loads induces parameters on each strand such as extension, rotation, forces, moments, and stiffnesses in terms of axial, torsion and bending. In most operations, these are parameters used to analyse the conductors' responses under static and dynamic conditions. These parameters are a function of the geometric arrangement of strands and they can be evaluated at the conductor cross-section, this means, analysing the properties of each strand and their contribution to the overall conductor behaviour in both static and dynamic conditions. This analysis is complicated by the fact that the conductor strand materials have nonlinear stress versus strain characteristics when subjected to bending. This is because of the conductor's geometry and the exhibiting variable bending stiffness during bending.

A power line conductor is a composite structure and the exact calculation of the inner stresses within a conductor is a difficult process. The analysis of conductor variables associated with its geometry has proven to be a very complex exercise. This is because, to evaluate these parameters used to evaluate the stresses, the inter-strand contact, frictional effect around the contact regions and the phenomenon of stick and slip regime during bending have to be taken into account. For the simplified model, the considerations of these parameters that are function of the conductor geometry are usually neglected when a continuous linear model is used. But to model the conductor as a bundle of strands, considering the parameters poses a challenge and there are no possibilities to implement the composite model without a lot of substantial complications. Hence, some level of simplified assumptions is required.

The helical strands components are subjected to the static axial load and the dynamic bending load. The base component strands, its geometric arrangement, plus the conductor stiffness give rise to some form of strain and stress. Analytical models [1, 2, 5] have been developed to predict the mechanical behaviour of conductor structures when subjected to different forms of loads. Most of these models were developed based on knowledge of the component material behaviour in terms of geometry of the structure. Some of these analytical approaches incorporate effects associated with tension, the bending and torsion stiffness of the strands. Such analyses have been performed by F. H. Hruska [37, 61, 62] for the conductor as continues system. More recent and complex

analytical models are based on beam theory assumptions where the behaviour of strands is described using the Love's curved beam model [34].

A strand is normally subjected to the tensile force in the axial direction, the bending moment in the normal and bi-normal direction, and the twisting moment. Under the stress due to bending, every contact location of the conductor is directly related to the change of local bending of the strands. The strands are usually characterized by an initial curvature when it is assumed straight due to their helical shape and then assume a new curvature when it is deformed due to its weight. From the local curvature of the strands based on the two aforementioned situations it is possible to find the net variation in curvature and the stresses generated inside the strands by the bending when the initial condition on the strands is considered as pre-loaded. Consequently, the analysis of the strands response can then be expressed as the mechanics of a helical beam in terms of the strands' axial strain, the change in curvatures and the twist expressions. It can be noted that these expressions are defined, as per the generalized strain theories for a beam, applied accordingly and to conform to the linear concept where a small deformation is assumed. This makes it possible to use the Hook's law and this can be expressed for the following situations:

- ✓ Tensile analysis of the conductor
  - ➢ Only strands axial displacement
  - ➢ Strands coupling of axial displacement and rotation
- ✓ Bending analysis for only flexural or transverse displacement
- ✓ Combined effect of axial and bending loads

2.9.2 Tensile Analysis of the Conductor

In every conductor, the axial load generates inner axial stresses, shear, and torsional moments which give rise to coupling effects. The reaction of the conductor to the pure axial loading applied at its ends, assumes that the conductor is in a static condition. The strands are subjected to tensile force producing an axial displacement. This tension-induced elongation on strands generates two components due to coupling; the elongation and rotation. The magnitude of either of these components is likely to be strain rate dependent. It is usually desirable for a conductor to have good torque balance so that it produces little torque when loaded with both ends constrained. However, an optimum combination of helix angles for the various strength member layers allow each strength member to maintain good stress and torque balance regardless of the magnitude of the tension-induced changes.

The analysis of the tensile response of the conductors can be done either for only axial displacement of strands neglecting the coupling effect, or for displacement and rotation of strands where the coupling effect is considered.

2.9.2.1 Tensile Analysis of Conductor for only Strands Axial Displacement

The modelling for pure axial load for the helical structure also applicable to power line conductors can be credited to the pioneer work of F.H. Hruska [37, 61, 62], in which he developed the simple axial model for cables. His formulation assumed that the strands are subjected to only tensile forces. He assumed no moments, friction, no radial contraction of strands is not considered but only radial contact is considered. The global strand strain is considered small. This model was used to calculate for the strand interlayer pressure, unwinding torque, and the strand stress and strain.
As the tension is applied to such cables, the strengthened members exert a radial pressure on the strands below. For the case of single layer strand, the strand layer presses against the core. This pressure produces deformations of the core elements and the strands due to both material elongation and the elimination of space within the conductor structure. There may also be slight contact deformations at the interface between the strands and the core. All of these factors contribute to a reduction in overall conductor diameter and a corresponding increase in conductor length. Detailed explanation for this case as the conductors is assumed to experience pure axial displacement can be found in [58], and the extract of this work that are of relevance to this study are reproduced in this section as stated below.
Figure (2.16) shows the strands along the helical path, subjected to loads, and this causes the conductor individual helical strands to experience a tensile force. Due to the helical angle, tensile force, T, gives rise to two components i.e. the tangential and normal forces. These components of the radial tensile force are the axial component, T_A, which is parallel to the neutral axis and the tangential component, T_T, which is perpendicular to the neutral axis.

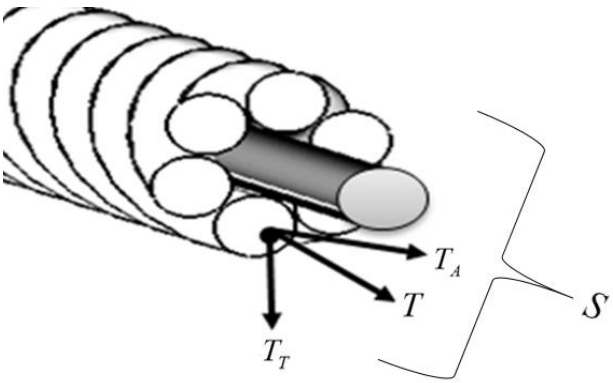

Figure 2.16: Axial forces action on the conductor cross-section

Neglecting bending and torsional effects, the total tensile stress acting across the cross-section of the conductor can be evaluated as:

$$\sigma_x = \frac{S}{A_T} \qquad \text{..... (2.48)}$$

Where A_T is the conductor cross section area and can be calculated by using equation (2.6). The only internal force being considered in the equations is the axial force component or tensile force on a strands cross-section. Each individual strand is assumed to be subject to the same tensile force, this can be calculated for using equation (2.28). The tensile stress acting on the individual strands:

$$\sigma_{ij} = \frac{T_{ij}}{A_{ij}} \qquad \text{..... (2.49)}$$

Neglecting the effect of Poisson ratio, the strain acting along the line contact between the strand and the core is given by [15]:

$$\varepsilon_{ij} = -R_i \frac{d^2Y}{dX^2} = E_i \sigma_{i,j} \qquad \text{..... (2.50)}$$

The axial strain due to the axial loading along the line contacts as function curve helical path can be determine as

$$\varepsilon_A = \frac{T(s)}{EA_i} = \int_0^s \mu(\xi) \cdot q \, \mathrm{d}\xi \qquad \text{..... (2.51)}$$

Expressing the axial strain along the x-axis for a given strand:

$$\varepsilon_x = \varepsilon_c = \varepsilon_{xi} \qquad \text{..... (2.52)}$$

$$\varepsilon_i = \varepsilon_{xi} \cos^2 \alpha_i \qquad \text{..... (2.53a)}$$

$$\varepsilon_c = \frac{\varepsilon_i}{\cos^2 \alpha_i} \qquad \text{..... (2.53a)}$$

The strain for the core and the strain for each strand in a given layer, the corresponding axial unit strain is:

$$\varepsilon_c = \frac{T_c}{A_c E_C} \qquad \text{..... (2.54a)}$$

$$\varepsilon_i = \frac{T_i}{A_i E_i \cos^2 \alpha_i} \qquad \text{..... (2.54b)}$$

The total applied force on the conductor in terms of forces acting on each strand including the core can be evaluated as:

$$S = T_c + \sum_{i=1}^{N} n_i T_i \cos\alpha_i \qquad \text{…….. (2.55)}$$

Substituting equations (2.54) into (2.55) will results in

$$S = \frac{T_c}{E_c A_c}\left(E_c A_c + \sum_{i=1}^{N} n_i E_i A_i \cos^3\alpha_i \right) \qquad \text{..…….. (2.56)}$$

The component in the bracket in the above equation is known as the axial stiffness of the conductor:

$$AE = E_c A_c + \sum_{i=1}^{N} n_i E_i A_i \cos^3\alpha_i \qquad \text{....…….. (2.57)}$$

The equation (2.57) can then be used to calculate the conductor's axial stiffness *AE*, with the knowledge of conductor geometry and material parameters. Once the axial stiffness is known, strands forces, strain and stresses can be calculated for a given axial load S, on the conductor for each layer, including the core. This can be calculated for as follows:

The forces can be expressed as:

$$\left.\begin{aligned} T_c &= \frac{A_c E_c}{(AE)}.\ S \\ T_i &= \frac{A_i E_i \cos^2\alpha_i}{(AE)}.\ S \end{aligned}\right\} \qquad \text{..…….. (2.58)}$$

The corresponding stresses are:

$$\left.\begin{aligned} \sigma_c &= \frac{E_c}{(AE)}.\ S \\ \sigma_i &= \frac{E_i \cos^2\alpha_i}{(AE)}.\ S \end{aligned}\right\} \qquad \text{…….. (2.59)}$$

2.9.2.2 Tensile Analysis of Conductor for Strands Axial Extension and Rotation

In section (2.9.2.1), only the strand extension was considered, neglecting the strand rotation as well as the coupling effect of strand extension and rotation. But actually, in the static condition for the axial loading, axial displacement produces extension and rotation and the coupling effect of extension and rotation. In a conductor, the helical strands generally produce both elongation and rotation of strands simultaneously. The helical strand construction exhibits a geometric symmetric characteristic and due to this helical design of the strands, the overall axial behaviour exhibits a coupling between tensile and torsion strains. This coupling effect has been investigated in [63]

Tangential components of the radial force, T_T yield a non-zero moment with respect to the x axis. When it is not balanced, it leads to a possible rotation of the layer. Such rotation can be minimized

by having alternate left and right lay layers (reverse-lay). If the balance is not perfect, and depending on the end conditions, there may be a small rotation due to the axial force, S.

The balance of forces and moments in the strands gives the equilibrium equations similar to the helical spring. This governing equation describing the coupling relation between the extension and rotation that is induced on the individual strand can be expressed using the following equation

$$\begin{bmatrix} F \\ M \end{bmatrix} = \begin{bmatrix} K_{11} & K_{12} \\ K_{21} & K_{22} \end{bmatrix} \begin{bmatrix} \varepsilon_A \\ \varepsilon_T \end{bmatrix} \quad \text{…..……..…… (2.60)}$$

Where ε_A denotes the overall axial strain, ε_T the twist angle per unit length, F, the axial force and M, the torque. The four stiffness matrix components ($K_{11}\ K_{12}\ K_{21}\ K_{22}$) which are for pure tensile (extensional stiffness), coupling of tensile and torsion (extensional-torsion stiffness), coupling of torsion and tensile (torsion-extensional stiffness) and pure torsion (torsion stiffness) respectively. For there to be a close-form solution, the stiffness matrix should be symmetric and using Betti's reciprocal theorem $K_{12} = K_{21}$. The value for each of the stiffnesses will be determined later in chapter 3.

2.9.3 Flexural Analysis of the Stranded Conductor

The conductor reaction to bending can be described by only its transverse vibration. This includes the associated stresses and motions experienced by the conductor components defined with regards to the radius of curvature. The effects of bending on the conductor can be identified by strands breakage from the conductor cyclic amplitudes especially at the clamp resulting to fatigue. The following equations are presented for estimating the bending characteristics of stranded conductors.

The magnitude of bending and twist on the conductor are given as:

$$\kappa = \frac{\sin^2 \alpha}{R_i} \quad \text{…….…… (2.61)}$$

$$\tau = \frac{\sin \alpha \cos \alpha}{R_i} \quad \text{…….…… (2.62)}$$

The strain (bending and torsional) can be the obtained by the product of bending and twist respectively with the distance from the neutral axis. Therefore, the stains can be evaluated as:

$$\varepsilon_b = \kappa \cdot y = \frac{\sin^2 \alpha}{R_i} .r.\sin\theta \quad \text{…….…… (2.63)}$$

$$\varepsilon_t = \tau \cdot r = \frac{\sin \alpha \cos \alpha}{R_i} .r \quad \text{…...…… (2.64)}$$

For elastic material of strands, the stresses can be obtained as:

$$\sigma_b = E.\varepsilon_b \quad \text{..... (2.65)}$$

$$\sigma_t = E.\varepsilon_t \quad \text{..... (2.66)}$$

The bending moment M and twisting H on the strands are given as [56]

$$M = M_e + M_p = \int\int_{Ae} \sigma_b.y_i.dA_e + \int\int_{Ap} \sigma_p.y_i.dA_p \quad \text{..... (2.67)}$$

$$H = H_e + H_p = \int\int_{Ae} \sigma_t.r_i.dA_e + \int\int_{Ap} \sigma_p.r_i.dA_p \quad \text{..... (2.68)}$$

2.9.3.1 Pure Bending Action for Individual Strand

In a similar analogy, the form of nomenclatures used for the geometric description of the strands as given in section (2.4.2) also applied to the description of the parameters for the bending imposed on each strand. For the sake of clarity, for example, the stress on a strand in a given layer is defined as $\sigma(i,j)$, this implies the stress on *j*-strand in an *i*-layer. When a *j*-strand in a given *i*-layer is bent with a constant curvature, κ (curvature of the conductor from neutral axis), the resultant bending stress imposed on the strand consists of two terms [57]. The first part is the stress arising from the bending of the strand around in its own neutral axis. It should be noted that this stress component is always present and it is a function of the actual curvature, κ, independent of the history of deformation. To evaluate this minimum stress for a given layer i, this stress is the same for all strands and varies linearly over the conductor section from negative minimum stress to positive minimum stress in the opposite side of the neutral axis $(-\sigma(i)_{min}\ to + \sigma(i)_{min})$ and it is zero at the strands neutral axis. This form of stress can be obtained as:

$$\sigma(i)_{\min} = E_i R_i.\kappa \quad \text{..... (2.69)}$$

The second part of the stress is due to the state of friction between the strands and those in the alternate layers. It is assumed that the inter-strand friction forces between strands in the same layer are negligible. The friction forces between the alternate layers exist due to the tension in the conductor and the helical construction, which causes the radial forces. At the beginning of bending, these radial forces are high enough to prevent relative slipping between the strands in a given layer and the strands in alternate layers. In this state, the stands stick together as a solid structure. This stress arising from this so called stick stress and it is denoted here as $\sigma(i,j)_{stick}$ for the *i*-strand in j-layer. This stress is a function of the distance of the strands from the neutral axis of the conductor.

This strand distance from the neutral can be evaluated by equation (2.9). When the strand is first bent from an initial zero curvature, the stick stress is given as [57]:

$$\sigma(i,j)_{stick} = E_i R_i \left(\cos^2 \alpha_i\right) \kappa \qquad \ldots\ldots\ldots\ldots\ldots\ldots\ldots\ldots (2.70)$$

This stress component is constant over the wire cross section and is equal and opposite in directions for strand at the same distance above and under the conductor neutral axis (tension and compression). For strands on the conductor neutral axis of bending, the stress is zero since the distance, R_i is zero. Therefore, strands neutral axis corresponds to the conductor neutral axis that passes through the core axis.

As the curvature increases, a point is reached where the friction forces acting on the strands are no longer high enough to prevent slipping between strands. At this point, the stress component reaches its maximum value reached and this initiate the onset of slipping. At this condition, the slip stress component take effect, this denoted here $\sigma(i,j)_{slip}$. If the curvature change proceeds in the same direction long enough, with the decrease to a minimum slip stress value. The stress will remain for an arbitrary increase in curvature until there is a reversal in the sign of the rate of curvature change. At this point, the strands stick again and the sticking stress will again be obtained. Thus, the strands then remain in this stick state value until another reversal in the sign of the rate of curvature change. The bending process from sticking to slipping for this stress component as function of is bending stiffness is illustrated in figure (2.17).

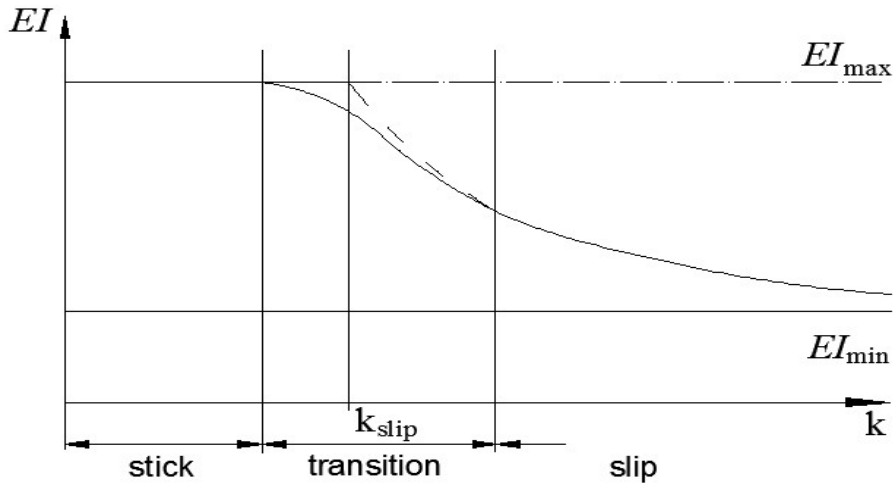

Figure 2.17: A plot of bending stiffness versus curvature [57]

For an arbitrary variation of the strands position from the neutral-axis, initiated at zero curvature and proceeding in the direction along the conductor.

This figure illustrates the similarity of the variation in the sticking or slipping stress to the behaviour of an elastic-plastic material. It is observed that there are two stress regimes. The first is the elastic regime represented by the slopes where the stress increases or decreases linearly

around a reference value. The second is the plastic regime represented by the horizontal lines when the wire is slipping. As observed, the value of the elastic or sticking stress can be computed according to the history of deformation and equation (2.70) therefore becomes:

$$\sigma(i,j)_{stick} = E_i.R_i.\cos^2\alpha_i\left(\kappa - \kappa(i,j)_{ref}\right) \quad \text{..... (2.71)}$$

Where $\kappa(i,j)_{ref}$ is the reference curvature obtained when the stick stress equal to zero, from the point of reversal in the sign of the rate of change of curvature in the plastic regime. The absolute difference between the curvature at the point of reversal and the reference curvature is denoted $\Delta\kappa_{slip}$. This value is the required for change of curvature from the state of zero stress to reach the slipping state in either direction in the elastic regime. Therefore, for there to be a complete cycle, the required change in curvature passes from one plastic state to the other when the reversal in the plastic regime is $2\Delta\kappa_{slip}$ .Thus, this implies when the sign of the rate of change of curvature changes and the strands sticks, its stress first decreases to zero and then increases again in the opposite direction until slipping is attained again.

2.9.3.2 Conductor Bending Stresses and Moments

As explained in the last section, under bending, the conductor is subjected to two forms of stress (minimum and stick) as defined as:

$$\sigma_{Cond} = \sigma_{\min} + \sigma_{add} \quad \text{..... (2.72)}$$

The σ_{add} stress value is determined based on the condition which is a function of curvature, depending on its states produces the stick or slip states. In [57] it was stated that for a small value for lateral deflection/span ratio the stands undergo plane-section bending to a certain value in which beyond this limit of this ratio, the plane section does not remain plane. Then, depending on the level of axial tension and the imposed radius of curvature, interlayer slippage occurs. The slip starts from the outer layer and continues towards the centre of the strands.

These stresses are defined as follows:

For the stick condition:

$$\sigma_{add} = \sigma_{stick} = E_i R_i \sin(\phi)\cos^2(\alpha_i)\cdot\kappa \quad \text{..... (2.73)}$$

For slip condition

$$\sigma_{add} = \sigma_{slip} = \frac{T_{slip}}{A_i} = \sigma_T\left(y^{\mu\sin\alpha_i\varphi} - 1\right) \quad \text{..... (2.74)}$$

The bending moment acting on a conductor as a function of the curvature can be obtain as:

$$M_{stick} = \int \sigma_{\min} \cos\alpha \cdot ydA + r\int \sigma_{stick} \cos\alpha \, dA \quad \text{..... (2.75)}$$

$$M_{slip} = \int \sigma_{\min} \cos\alpha \cdot ydA + r\int \sigma_{slip} \cos\alpha \, dA \quad \text{..... (2.76)}$$

Generally, the bending moment acting on the conductor cross-section as a function of its bending stiffness and curvature can be evaluated as:

$$M = \sum_{i=1}^{N} M = EI(\kappa) \cdot \kappa \quad \text{..... (2.77)}$$

2.9.3.3 Conductor Flexural Rigidity

The determination of the exact value of the bending stiffness for the conductor is still a contentious issue and an on-going investigation. For conductor experiencing transverse vibration, the knowledge of its flexural rigidity is very important but still the exact value based on analytical modelling is still impossible. The reason is because of its geometry in which the stranded conductors bending stiffness can vary with tension, curvature and deformation. Several investigations have been carried out in this area to try and find an analytical solution.

From analytical analysis, it has been established that the actual flexural rigidity for a conductor experiencing bending lies between two extreme conditions: full stick and full slip [1, 2, 13, 52, 57]. For the stick conditions, a conductor is assumed to have a solid cross section with the strands sticking together and the individual strands are completely restricted with no relative displacement. The value for the bending stiffness under this condition is the maximum value and can be obtained as:

$$EI_{\max} = \frac{\pi}{8}\sum_{i=1}^{N} E_i n_i d_i^2 \left(\frac{d_i^2}{8} + R_i^2 \right) \cos\alpha_i \quad \text{..... (2.78)}$$

The second condition is the full slip. This condition assumes the conductor individual strands are completely allowed to move freely with a complete independent of other stands. The value for the bending stiffness is a minimum value and is given as

$$EI_{\min} = \frac{\pi}{64}\sum_{i=1}^{N} E_i d_i^2 \cos\alpha_i \quad \text{..... (2.79)}$$

Thus, the actual value for conductor bending stiffness lies between these two conditions as defined by equations (2.78) and (2.79).

In the paper by M. Rooaf and T. J. Davis [64], using experimental results, a novel experimental method was reported for obtaining a reliable measurement of the effective bending stiffness of axially loaded spiral strands. This simple and relatively inexpensive method can be use in practice,

for even a very large diameter spiral strands. The effective bending stiffness measurements, based on the experimental approach, were reported with the detailed theoretical analysis in justification for use as a proposed method for determining effective bending stiffness for cables and ropes which can also applied to the power line conductors. This approach can be used in the experimental studies as documented in chapter 6, but because the emphasis of this study was not to determining bending stiffness, thus, this was not explored. Consideration will be given to this approach in future experimental study.

In [65], the authors used the experimental techniques to determine the effective bending stiffness of helically steel cable. From the experimental results, the authors were able to draw the inference that the cable bending stiffness is dependent on the applied tension and can vary between two limiting conditions, corresponding to either full or zero interlayer shear interaction of the strands in a helically wound cable.

The K. O. Papailiou [52, 57] presented a novel and more realistic model to determine bending stiffness of a conductor under both axial and bending loads. He developed the secant bending stiffness model that can be used to determine the variable bending stiffness under the conditions of inter-layer friction and slip as a function of displacement and curvature. This model established the fact that the bending stiffness value at any point along the conductor varies non-linearly with the curvature. Also, the model postulated that the value of flexural rigidity of the conductor is maximum at certain bending curvature and decreases to the minimum value as the curvature increase. The variable bending stiffness concept was later expanded upon by the authors in reference [66] using the tangent stiffness method.

Based on the derivation in [57], the stiffness at various states can be calculated as follows:

$$EI_{\min} = E_i \frac{\pi \cdot d_i^2}{64} \cos\alpha \qquad \text{..... (2.80)}$$

$$EI_{stick} = EA(R_i \sin\phi)^2 \cos^3\alpha \qquad \text{..... (2.81)}$$

$$EI_{slip} = \sigma_T A\left(y^{\mu \sin\beta\varphi} - 1\right) R_i \sin\varphi \cos\alpha / \kappa \qquad \text{..... (2.82)}$$

The bending stiffness for a conductor based on the formulation in terms of the two conditions for stiffness is as follows

For stick condition

$$EI_{\max} = EI_{\min} + EI_{stick} = \text{Constant} \qquad \text{..... (2.83)}$$

For the slip state

$$EI = EI_{\min} + EI_{slip} = function \ \ (\kappa, T) \qquad \text{..... (2.84)}$$

2.9.4 Analysis of Conductor for Combined Effect of Axial and Bending Loads

In the application of conductor in the real world, the conductor is actually subjected to high tension load at both ends combined with the bending load from the wind loading. The wind loading usually causes the superposition of bending stress on the mean axial stress already present caused by the tensioning. In most models, the loading conditions are decoupled, where analysis is done either for pure tensile stress or pure bending as explained in the last previous two subsections. The analysis of the combined effect can be found in [67], in which the bending moment of strands due to transverse loading was taking into consideration in conjunction with the axial load.

The helical configuration model provides the best protection analysis for the conductors; it is designed to provide high strength, good torque balance, and good tensile and cycle bending load performance for the complete analysis of the conductor. The use of this form of model is the only option to analyse completely the combine effect of axial and bending loads on the conductor.

The local mechanical properties of the conductor strands are often modelled by a uniform elastic potential energy of rod model, dependent on extension and twist in the static condition plus bending under the dynamic condition. This implies that for dynamic condition the alternating stress is imposed on the axial stress.

The total internal forces, torsion and moments acting on the strands due to these conditions can be evaluated with the following equations.

$$F = \sum_{n-1}^{N}\sum_{i=1}^{n} T_A \cos\alpha_i \qquad \text{..... (2.85a)}$$

$$m = \sum_{n-1}^{N}\sum_{i=1}^{n} R_i T_A \sin\alpha_i \qquad \text{..... (2.85b)}$$

$$M = \sum_{n-1}^{N}\sum_{i=1}^{n} R_i T_A \cos\theta_i \sin\alpha_i \qquad \text{..... (2.85c)}$$

Under the dynamic loading, the three component exhibit a coupling effect as defined in the matrix below, with regards to the axial, torsional and bending strains:

$$\begin{pmatrix} F \\ m \\ M \end{pmatrix} = \begin{pmatrix} K_{11} & K_{12} & K_{13} \\ K_{21} & K_{22} & K_{23} \\ K_{31} & K_{32} & K_{33} \end{pmatrix} \begin{pmatrix} \varepsilon_A \\ \varepsilon_T \\ \varepsilon_B \end{pmatrix} \qquad \text{..... (2.86)}$$

Where the matrix defined above with K-values is called the stiffness matrix. Some of the components of the stiffness matrix are already define with regards to equation (2.60). Others are defined as follows, K_{13} is tensile-bending stiffness, K_{31} is bending-tensile stiffness, K_{23} is torsion-bending stiffness and K_{32} is bending-torsion stiffness.

Strength balance implies that all strands in the layers have equal strength. The maximum stress on a strand is influenced by the stresses induced on the strand by its axial elongation, bending deformations and twisting effects, during loading. The strand stress can be effectively evaluated if all the possible modes of deformations are considered. Hence, if the strand axial, bending and twisting stresses, when considered together simultaneously, then the maximum stress on the conductor can be adequately determined.

2.10 Fluid-Solid Interaction

2.10.1 Vibration of a Cylinder in a Fluid

This concept of fluid-solid interaction has ever since been a very important area of investigation in terms of the oscillation of flexible structures. Numerous researches have been carried out to gain more understanding into the structural vibration of systems due to wind loading. The bare conductors of an overhead transmission lines are usually subjected to the dynamic forces of wind resulting in it exhibiting various modes of mechanical oscillations. Conductor excitation is a very complex phenomenon. This is most probably due to the fact that the observed conductor vibrations are as a result of varying excitation mechanisms, which is due to the complex mechanism of fluid-solid interaction. The mechanism responsible for vibration of power line conductors is due to phenomenon of vortex shedding. This occurs as results of flow separation, generating alternating pressure at the leeward side as the wind flow passed the conductor. This vortex formation phenomenon for the conductor is usually modelled as a cylinder immersed in a fluid stream [29-31].

The three primary variables involved in vortex shedding for a circular cylinder are the cylinder diameter, the fluid velocity, and the kinematics viscosity of the particular fluid.

The wind excites the conductors as it flows pass, causing the vortex-shedding which causes the vortex-induced vibration also known as the aeolian Vibration. Another form of excitation by wind is associated with the bundle configuration of the power line; the wake-induced vibrations. A third excitation mode exists, due to the accumulation of ice on the conductors and modifies the conductors' aerodynamic profile to the point of making them aerodynamically and aero-elastically unstable causing it to vibrate. This form of conductor oscillation is known as the conductor galloping. In this case of vibration mode, very high amplitude vibrations have been observed [1, 2].

2.10.2 Vortex Induced Vibration

The investigation of the phenomenon of fluid-solid interaction of the flow fluid as it flows past a cylinder, Von Kármán [68] in 1911 published the vortex theory. He used this concept of vortex generation to explain the vibration that occurs when a fluid flow past a cylinder i.e. fluid-solid interaction. In his investigation, he found out that the cylinder is set into vibration by the fluctuating lift force generated by alternating vortices created behind the cylinder by the air stream.

Further investigation of this phenomenon by Lord Rayleigh [69] established the fact that though the wind flows is in plane with cylinder but the component causing the oscillation is perpendicular to the plane of the air stream. As the wind flows past the cylinder two components of forces are generated by vortices: the vertical lift force and the horizontal drag force. The vertical vibration does occur due to the vertical component of force induced by the air stream as it flows past the cylinder is responsible for the transverse vibration with small amplitude i.e. aeolian vibration.

2.11 Conductor Wind-Induced Vibration

2.11.1 The Aeolian Vibration

Wind induced vibration can be explained by the vortex formation that occur due to fluid-solid structure interaction. This theory attributes that the aerodynamic excitation of the structure is due to the action of periodic forces induced on it. In the case of the conductor, the wind loading imposed as a form of periodic force generated by the pressure difference, will induce a certain degree of resonance with a natural mode of vibration of the conductor. Vortices, which are formed around the trailing edge of the conductor, are shed on alternating sides, giving rise to periodic forces and the oscillations transverse perpendicularly to the direction of the wind.

The aerodynamic forces that wind imparts on a conductor depend on the wind velocity and direction, and on the size, and the shape of the conductor. Whether resonance will occur under wind forces depends on these parameters. The amplitude of oscillation that may build up depends on the strength of the wind forces, the energy damping capacity of the structure i.e. the structural damping, and the duration of the wind capable of exciting the conductor.

Wind excitation causes a transverse displacement and this transverse vibration that can be self-sustaining due to the phenomenon of lock-in effect as explained later in subsection (2.11.3). This condition occurs when the frequency of input loading by the wind coincides with one of the natural frequencies of the conductors. It becomes catastrophic if the vertical motions take place at the same coupled frequencies of the conductor over long period, generating stresses, especially in areas in which the motion is constrained.

Several models have been developed for mathematical analysis of the wind excitation mechanism with the aim to develop a good understanding of the process of wind excitation.

The tensioning of the conductor and the tightening of the keeper of the suspension clamp induces stresses on the conductor strands at the points of support. The damage caused by wind-induced vibration to conductors seems to be noticed at the attachment position (suspension clamps, spacers, spacer-dampers, etc.) and this can be attributed to the dynamic stress resulting from wind loading being imposed on the static stress. This occurs because at this position, the motion of the conductor is constrained and the travelling waves will be reflected producing bending amplitude which will result in the bending strain and stress. The aeolian vibrations induces an alternating bending load at this area where motion is constrained, causing slip at specific contact points. This process usually results in the failure of conductors. The failures of conductors can be considered as a fretting fatigue problem [58].

2.11.2 Conductor Excitation

This concept of fluid-solid interaction (vortex induced vibration) has been used as a means of explaining wind-induced vibration on overhead lines conductor since the early 1920s when this phenomenon was first noticed. As the conductor experiences a transverse vibration caused by the wind input force, this form of oscillation is periodic in nature as shown in figure (2.18). This form of vibration usually occurs when one of the natural frequencies of the conductor is equal to the frequency of the vortex shedding of the Von Karman vortices caused by the imposed dynamic forces of the wind.

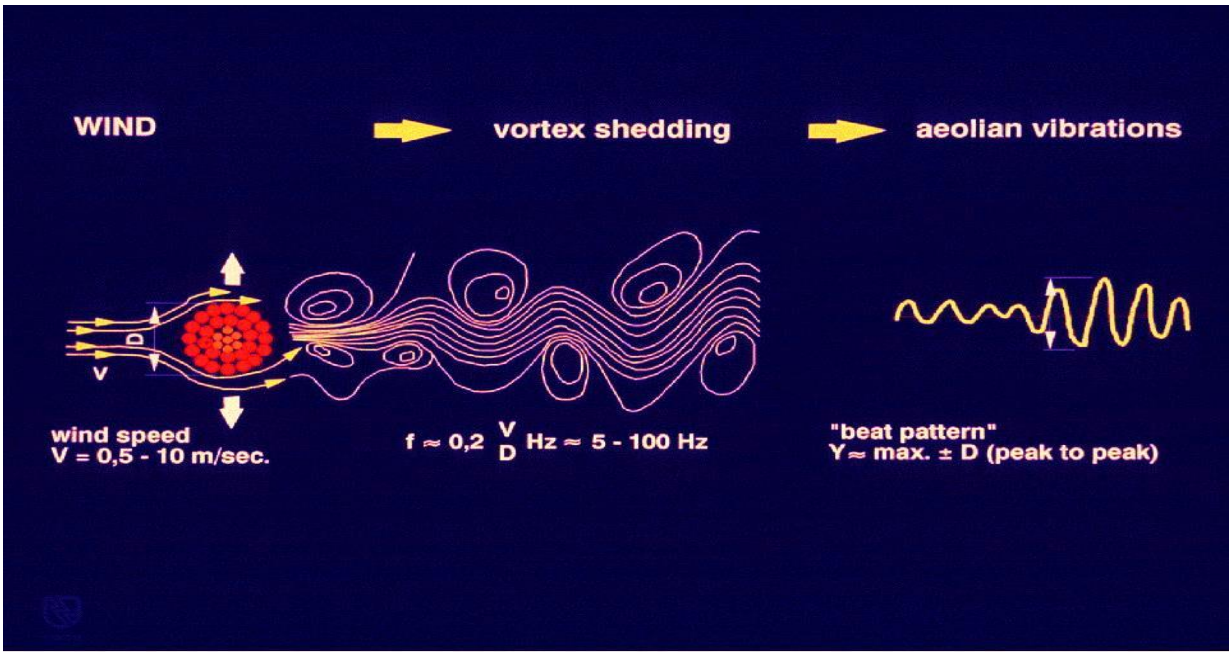

Figure 2.18: Vortex wake shedding from a conductor

This happens due to the occurrence of resonance when the natural frequency of the cylinder coincides with the Strouhal frequency [1, 2]. The Strouhal number is a dimensionless number, defined as a function of the velocity of the airstream, the diameter of the conductor, and the frequency of vortex shedding. This vortex shedding frequency can be calculated by

$$f = \frac{C_S V}{D} \qquad \text{…..……..……. (2.87)}$$

Where C_S is the Strouhal number ($C_S \approx 0.18 - 0.22$), D is the conductor diameter, and v is the air flow velocity in the direction perpendicular to the conductor's longitudinal axis.

2.11.3 Resonance and Lock-in Effect

As the wind flow passes the conductor, the Von Kármán vortex shedding induces an onset instability, corresponding to the wind speed. If the frequency generated by the vortex shedding approaches one of the natural frequencies of the conductor, when the Strouhal frequency generated by the wind as it flows past the conductor approaches the natural frequency of the conductor, there will be a superposition of this frequencies, initially producing beats as shown in figure (2.19)

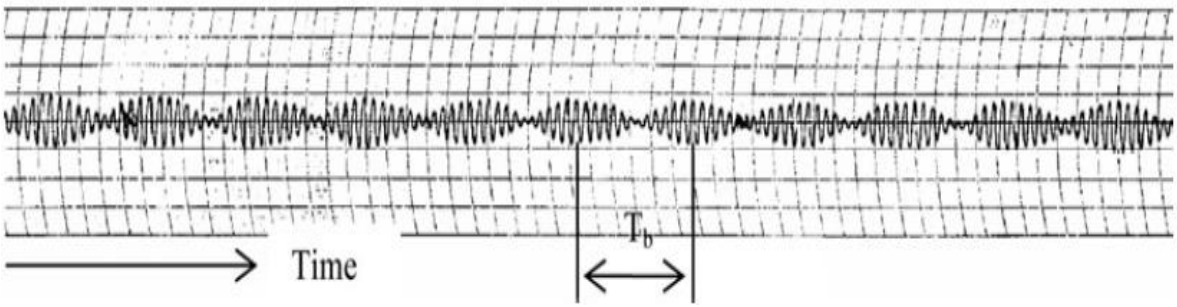

Figure 2.19: Beating phenomenon in an oscillating conductor [1]

With a further approach, the beats frequency decreases at a value of the difference between the imposed of the excitation frequency and the natural frequency, ($\omega - \omega_0$). A further decrease, the beats phenomenon will suddenly disappear and also the natural frequency, remaining the Strouhal frequency or the exciting frequency as shown in figure (2.20).

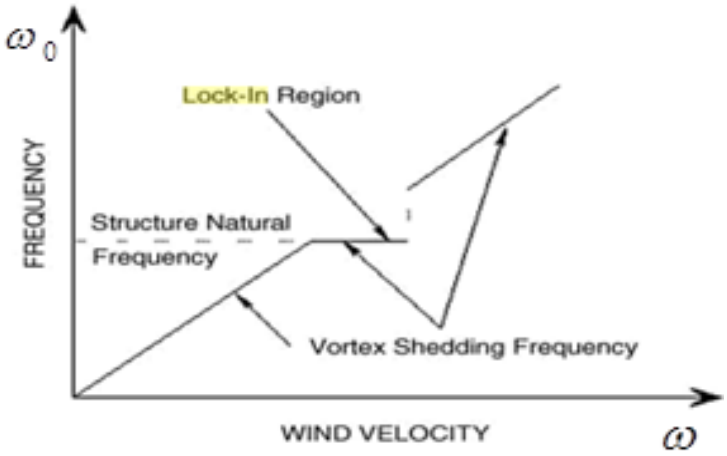

Figure 2.20: The graph illustrating Lock-in Effects [70]

At this point the conductor is said to experience resonance or set into resonance. This produces a sensation that the natural frequency, w_0 is being influenced by the external frequency w. It is assumed that there is a range of wind speeds over which the vortex shedding frequency and the conductor's natural frequency will lock-in and this will result in large conductor vibration [70]. This occurrence indicates that the frequency of the exciting force due to the wind loading and any of the natural frequencies of the conductor are approximately equal. When this occurs, the frequency of vortex shedding envelops any of the natural frequencies of the conductor that coincide with, thus the amplitude of vibrations increases. This leads to a condition known as "Lock-in effect".

The lock-in effect is a concept from nonlinear mechanics, it is also known as the synchronization effect. It occurs as a result of fluid-solid interaction. When the lock-in phenomenon occurs, in the case of power line conductor vibration, severe vibration can persist long enough to cause structural failure. The difficulty with lock-in phenomenon arises from finding the range of natural frequency of the structure, for each mode shape, over which lock-in can occur. To determine the frequency of wind that has the tendency of vortex shedding that can cause the vibration of conductor, with regards to lock-in effect can be computed as a range of frequencies around the shedding frequency as a comparison to modal vibration frequencies of the conductor.

The phenomenon of lock-in effect explains why during the conductor excitation by wind loading, the occurrence of lock-in means that changes in the wind speed at or near the resonant response frequency do not cause the vortex shedding frequency to change, but instead the response frequency will remain constant. After the initiation of resonance, the lock-in effect at resonance can stay for wind speed as large as 90 to 130% of the onset velocity [2]. Flow visualization as shown in figure (2.18) demonstrates the vortex-shedding as the formation of pressure fluctuation producing lifting force which equal to the Strouhal frequency, which can be sustained for a long period by the lock-in effect.

2.12 Analytical Evaluation of Wind Loading

To determine the conductor response, it is of very great importance to know the magnitude of aerodynamic forces that is being imparted on the conductor. The laminar air flow tends to produce a perpendicular displacement on the conductor. The issue becomes even more complex if the conductor vibration amplitudes are large (up to one conductor diameter) in the case of Aeolian vibration. Also of concern is if the fluid flow is not perpendicular to the conductor, or the fluid flow is turbulent.

The investigation of the motions of a dynamic conductor's model is usually done in the proper scaled wind tunnel test. This wind tunnel tests is capable of duplicating reliably the motions of a convenient length of the conductors usually modelled as a cylinder. The wind forces and the rate at which they can build up energy of oscillation respond to the changing amplitude of the motion. The rate of energy change can be measured as a function of its amplitude. Thus, the section-model test measures the one unknown factor, which can then be applied in the calculation of the variable amplitude of motion along the conductor to predict the full behaviour of the structure under the specific wind conditions of the test.

The maximum power brought into the system by aerodynamic forces as the stationary laminar air flow perpendicular to the conductor, can be determined using empirically derived equations. This empirical formula was formulated based on wind tunnel experiments.

The mechanical power transferred from the wind to a vibrating conductor may be expressed in the general form [1, 2]:

$$P = Lf^3 D^4 \, fnc(A/D) \qquad \text{……..…….…… (2.88)}$$

Where *fnc* (*A/D*) is the power function (function of relative vibration amplitude *A/D*), *L* is the span length, D, is the conductor diameter and *f* is the vibration frequency.

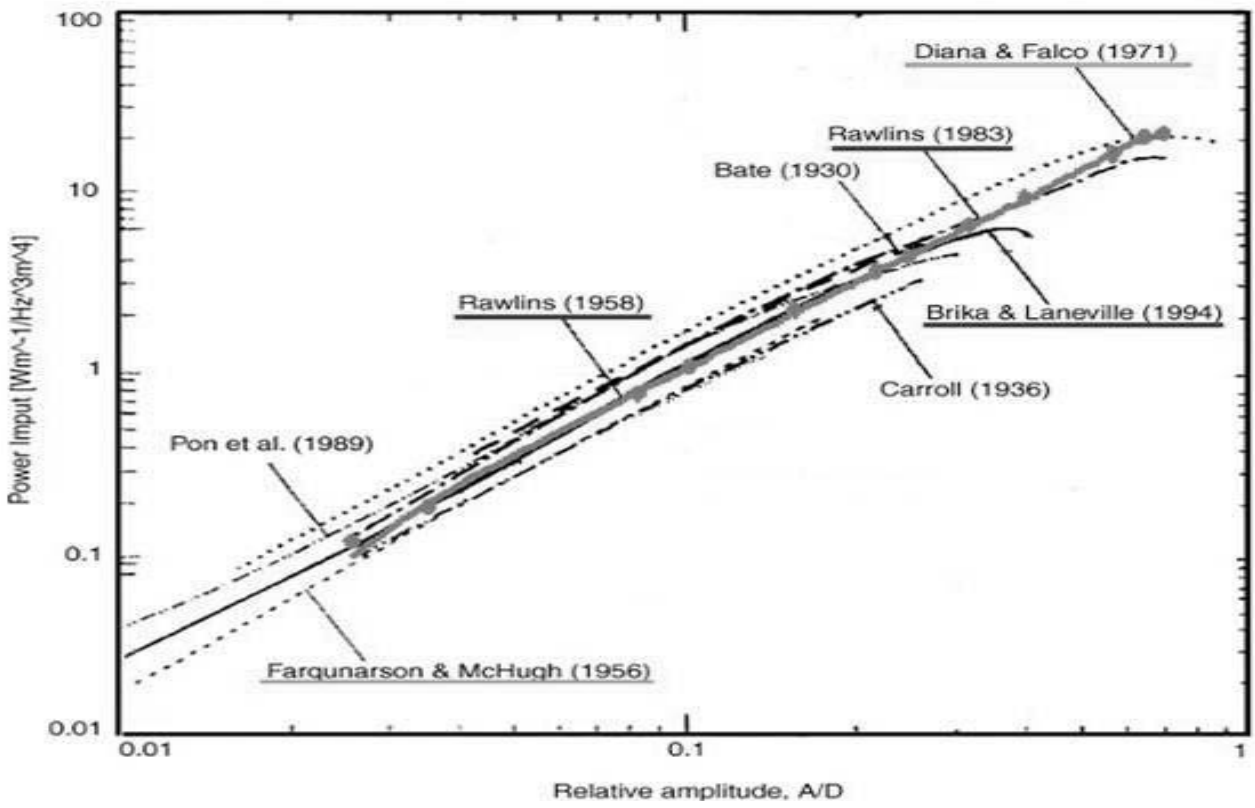

Figure 2.21: The Graph to determine empirically the input power on a conductor [1, 2]

The rate of power imparted on the conductor can be measured and plotted against amplitude. Figure (2.21) shows the graph of the power that is plotted against the relative amplitude (*A/D*) as obtained based on the research conducted in a wind tunnel by some investigators as documented in [1, 2]. As it can be seen on the graph, the power functions vary significantly from researcher to researcher. This is because the different results obtained by the researchers are due to the different characteristics of wind tunnels and different test methods. The form measurements from these experiments are of small energy levels (fractions of a watt per meter of conductor) which are very sensitive to disturbances. Thus, the turbulence of the incoming flow is another parameter which will influence the value of the power imparted by wind to a vibrating conductor. The lower the turbulence, the higher the wind power that can be imparted. This factor in the form of the level of turbulence was investigated and documented in [31, 71]. This turbulence parameter, as related to a wind power input, is a function of reduced velocity, Vr, dimensionless amplitude [Y_{max}/D], and reduced decrement δ_r. The reduced decrement can be used to convert input power into reduced wind power as given below.

$$\frac{P_{Wind}}{f^3 D^4} = \rho \delta_r \frac{\pi^2}{4}\left[\frac{Y_{\max}}{D}\right]^2 \qquad \left[W.s^3/m^5\right] \qquad \text{..... (2.89)}$$

Where ρ = mass density of the fluid medium; 1.2 kg/m^3

δ_r = reduced decrement

The reduced wind power as a function of relative amplitude has been drawn for different level of turbulence. Increasing the turbulence level decreases the wind power input. An example of wind power curves for different turbulence levels is shown on figure (2.22). This graph illustrates how increase in turbulence decreases the energy imparted by wind on the conductor.

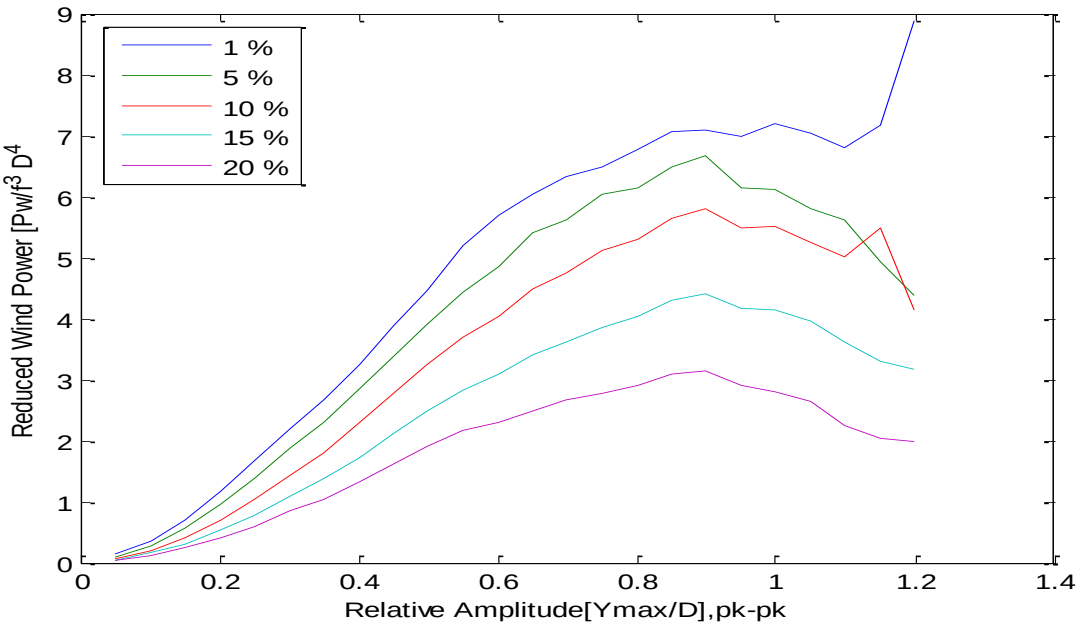

Figure 2.22: The graph used to determine the reduced input power on a conductor [71]

2.12.1 Energy Balance Principle

The analysis of dynamic behaviour of conductor follows an energy flow pattern in terms of input power and the various energy dissipation mechanism i.e. self-damping and vibration absorbers. But the analysis of the phenomenon of vortex shedding caused by wind loading and energy dissipation can be done by the simplified approach known as 'Energy Balance Principle' (EBP). This method is based on some simplifications that give useful estimates of the maximum vibration levels [1, 2]. This means that the principle is used when the conductor undergoes maximum vibration amplitude due to Aeolian vibrations. The steady state amplitude of vibration for a single or bundle conductor due to Aeolian vibration is that for which the energy dissipated by the conductor and other devices used for its support and protection, equals the energy input from the wind. The vibration amplitude is determined by a power balance between what is provided by the wind and what is dissipated by the conductor self-damping and by any dampers. This can be mathematically formulated as [1, 2]

$$P_{wind} = P_{cond} + P_{damp} \qquad \text{..... (2.90)}$$

This means, the power imparted by the wind equals the power dissipated by the conductor self-damping, and the power dissipated by the damper. The EBP as document in [72] has been used to develop an algorithm for analysing Aeolian vibration of a span of a single conductor with multiple dampers. Each of these terms in equation (2.90) is a function of the frequency and amplitude of the conductor oscillations. In chapter 4, the empirical formulae for evaluating power dissipated

will be presented for the power line conductors. Most analysis are done by the use of the power law according to Noiseux's exponents [50] to calculate the self-damping power for conductor.
The conductor vibration level (anti-node displacement) can be evaluated as function of frequency or the wind speed and this can be estimated by using this principle. This is based on presumed knowledge of energy:

(a) Imparted to the conductor by the wind
(b) Dissipated by the transmission line conductor (conductor self-damping)
(c) Dissipated by the vibration absorbers (dampers)

The energy balance method has been used for studying the energy balance among the input power, the internal damping and the influence the section of dampers as a means for optimizing its placements on the span. The vibration level is determined by calculating the complex eigenvalues and eigenfunctions. These values are used to determine the amplitudes of vibrations at each resonance frequency. In case of laboratory experiments for fatigue failure, bending strains are estimated at the critical points, usually 89 mm from the suspension clamp.

Chapter 3

Analytical Modelling

3.1 Conductor Modelling

This chapter is devoted to deriving and analysing analytically the appropriate governing equations that can be used to describe the transverse vibration of power line conductors. Mathematical modelling can be either analytical or numerical; the aspect of numerical modelling of the dynamic behaviour of conductors will be done later in chapter 5. Analytical modelling entails the process of representing a physical problem with mathematical equation(s). Some of the physical phenomena are very difficult to formulate and translate into mathematical equations. This makes it necessary for simplifying assumptions to be made in order to reduce the system to an idealized version of the system. This simplified model, to some level of accuracy, can approximate the behaviour of the real system. The process by which a physical system is analysed, the parameters are identified with simplifications and then translated to obtain a mathematical equation is called modelling. The analytical modelling of power line conductors is done to obtain a simplified version that can approximate the real system. To date, no known analytical model can completely model the dynamic behaviour of power line conductors.

Despite the fact that there is no known model that can fully model the conductor dynamics, important accomplishments have been made in recent years in the development of mathematical models use in the design and analysis of structures such as wire ropes, cables and power line conductors [9, 19]. For power line conductors, modelling of these structures can be used to assess their designs prior to their usage in power lines. This has been done for the purpose of predicting their performance in both tensile and bending conditions. These analytical models not only minimize the requirement for prototype fabrication and time consuming and expensive testing, but they also provide the insight into their failure mechanisms. This provides a means of improving the overall structural performance.

The dynamic behaviour of power line conductors has generated much research interest both in the fields of academics and power utilities. Several authors have developed analytical models for the conductors in order to predict the conductor behaviour for different loads [12, 32]. The main goal of the analytical analysis of conductors is the prediction of its static and dynamic behaviours. Since the real conductor system has complex geometry, an exact analysis of its response and the evaluation of its energy dissipation are often not completely possible analytically. The analytical modelling of the vibration of overhead power lines has proved to be very difficult. The difficulty

is based on the established facts that conductor vibration exhibits non-linear characteristics. In most developed model some simplifications are made, in which the linearized concepts are employed in modelling the conductor system.

This non-linearity was as a result of the following. Firstly, it is a well-known fact that conductors have complex geometry and exhibits a relative large deformation. Because of this form of geometry, during bending, the conductors exhibit a variable bending stiffness [13, 57]. Till date, a method to determine the exact value for bending stiffness has not yet been established. To obtain an analytical solution, an approximate approach of continuous distributed model is normally used. Also, its geometric non-linearity for large deformation is linearized by the use of small deformation during bending.

Secondly, the dynamic behaviour of overhead line conductors is characterized by non-linear damping. The distributed parameters model when used, depending on the area of research, and to achieve this model some researchers in this area of conductor vibration have adopted the analytical model of solid beam [5] or the taut string [73]. The conductor equation of motion that describes the transverse behaviour is derived from its equilibrium state using Newton second law of motion. These forms of models are used to obtain the conductor natural frequencies, and mode shapes. The conductor material damping is non-linear, which give rise to an equation that is difficult to find a closed-form solution. The equivalent linear damping model is normally incorporated mathematically to formulate the damped equation for the conductor. This approach indicates that damping is obtained as a mathematical parameter not as a function of its structure.

The third is the characterization of its geometry. Using these simplified models i.e. beam and taut string, has had its flaws in the sense that on the contrary, a conductor is not a solid body but a composite body. It is made up of strands arranged in layers along the helical path, in opposite lay direction in alternate layer and over the central strand of conductor. In chapter 2, the complex nature of the conductor geometry was explained. Based on this explanation, instead of regarding a conductor as a solid system, a more realistic approach would be to consider a conductor as a composite, consisting of an assembly of a number of helical strands arranged in alternate layers. In this regard, treating the conductor as a composite structure will help to explain why the dynamics of conductors tends to exhibits a non-linearity. The conductor dynamics is a function of parameters that have to do with its geometry and this proffers the reason why it is impossible to obtain exact analytical solution. Therefore, the approach of modelling the conductor as a single, homogenous continuous system is incapable of addressing local phenomenon within the conductor. These include strands contact, inter-strand slippage and frictional effects when under the influence of tension and bending.

The fourth problem has to done with boundary conditions. Since the geometry is complex, attention is drawn to determining two auxiliary equations. This involves how to relate curvature changes and strains due to displacements and rotations at its ends as a function of its axial loading. For now, there is no established equation for the boundary conditions, but some investigators have used the simply supported [14], while others have used the fixed support [7] at both ends. In line with this concept, the derivation of the equation analytically is completely done in terms of geometry of continuous beam or taut string not as the function of the insulator suspension, which is neither fixed nor simply supported. This area of end conditions for power line conductors needs further investigation.

Analytical modelling takes into consideration the equilibrium equation of the linear/nonlinear stress versus strain behaviour of various conductors' materials. The accuracy of the mathematical models is usually validated through extensive laboratory testing which will be done in chapter 6.

3.2 Conductor Static Profile

In this section, the analysis is done for the conductor static profile in the form of the deformed shape of a completely flexible conductor structure suspended between two towers and defined as a catenary. This catenary configuration of power line conductors when strung on towers can be treated as the deformation of slender structures. This analysis is imperative because the Sag-tension calculations predict the behaviour of conductors based on recommended tension limits under varying loading conditions. These tension limits specify at a certain percentages of the conductor's rated breaking strength that are not to be exceeded during installation in order to guarantee long life for the line and also conform to regulations. To accurately determine the sag limits for stringing the power line is very essential during the line design process. The sag of conductors is used to select support point heights and span lengths so that the minimum clearances will be maintained over the life of the line.

As explained in [14], because the conductor is the most expensive component of any power line, from an economic perspective, it is disadvantageous to employ low conductor tensions. Based on specification, a minimum clearance is required between the ground and the lowest point of an overhead conductor. Therefore, if the span length is fixed, the height required for a transmission-line tower increases as the conductor tension decreases. Alternatively, if the amount of conductor sag is fixed, the span length required decreases as the conductor tension decreases; in this case, the more number of towers required, not the tower height, must increase to transmit electricity over a specified distance. Both scenarios result in greater transmission-line costs. It has been shown that significant cost reduction is possible if higher conductor tensions could be used safely.

The conductor's size, tension, and span length, together, primarily affect a line's susceptibility to Aeolian vibration [2]. The amount of energy imparted on a conductor varies directly with the span length. The longer the span, the more wind-induced energy is absorbed. Conductors tend to vibrate more readily at higher tensions because of their low self-damping capability (the frictional interaction between strands) to reduce the imparted energy. In order to identify the axial tension limit to employ, the condition at which the conductor damping capability balances the energy imparted on it by wind loading is of importance in this study. The analysis of various sags and the conductor slack is used as the bases of ascertaining the cost benefit of stringing a line using the span length as the reference with regards to percentage of its ultimate braking point. This can be used to determine the cost saved by power utilities in terms of cost contributed by the conductor in constructing the power line.

The single span of a transmission line conductor static profile as shown in figure (3.1), is considered as a continuous structure and can be described by a set of parabolic or hyperbolic functions i.e. parabola or catenary curve. This deformed shape curves under the static condition, the conductor deforms due to gravity. It assumes a catenary profile by sagging along the span.

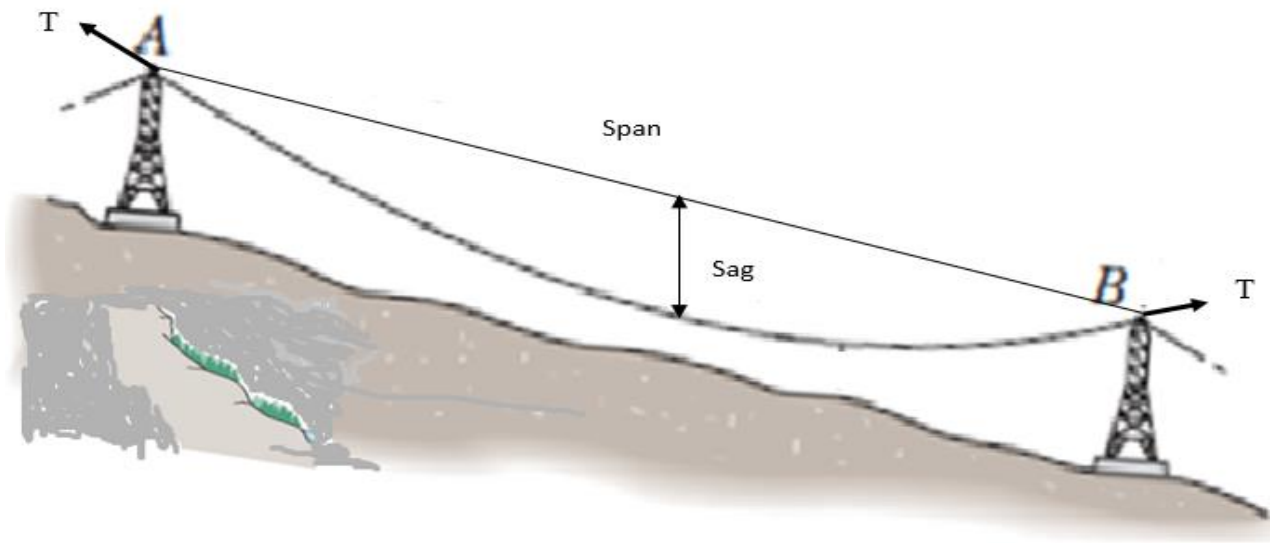

Figure 3.1: The conductor static profile

In the analysis, a parabolic curve is the shape that is formed by a conductor supporting an evenly distributed horizontal weight, whereas a catenary is the shape that is formed by hanging the conductor whose weight is constant per unit of the arc length.

Though the hyperbolic or the catenary curve equations are more accurate, the mathematical formulae which are used for the derivations of conductor as a parabola are much simpler with very good results in comparison. Detail derivation of equations for both hyperbolic and parabolic

equation can be found in [74]. The equations for the power line curves for cases were the power line passes non-level and mountainous terrain can be found in [75].

Consider a conductor attached to two fixed points A and B, supporting it weight as shown in figure (3.2). Assume the conductor between AB carries its weight that is uniformly distributed along the horizontal. If w_L denote the weight per unit length.

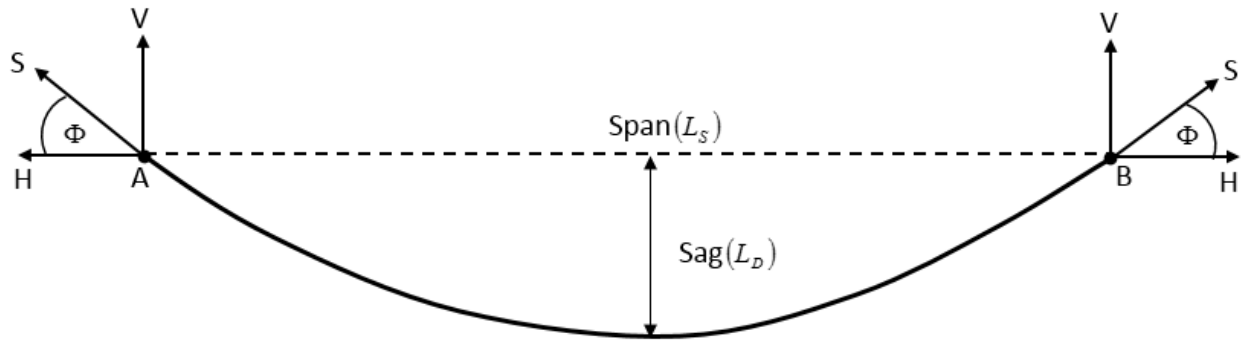

Figure 3.2: The Conductor parabola or catenary curve.

For the conductor with a span-length L_C, weight w_L, and horizontal tension H, the maximum sag distance L_D (the vertical distance between the point of attachment and the cable, at the lowest point in the span) is described by the parabolic function. Apply the equation of a parabola to a span of the same elevation, with a vertical axis and its vertex are at the origin of coordinates located at point A.

$$\tan\Phi = \frac{w_L x}{H} \qquad \text{…….. (3.1)}$$

The equations of the parabola for this curve are given as:

$$y(x) = \frac{w_L x^2}{2H} \qquad \text{…….. (3.2a)}$$

$$L_D = \frac{w_L L_S^2}{8H} \qquad \text{…….. (3.2b)}$$

$$L_C = L_S\left(1 + \frac{L_S^2 w_L^2}{24H^2}\right) \qquad \text{…….. (3.2c)}$$

Where L_D = mid-span sag (m), w_L = conductor weight (N/m), L_C = horizontal span length (AB), (m), H = conductor tension (N).

For the case in which the single span of the transmission line is represented by a set of hyperbolic functions which is similar to the description of catenary curve. The equations describing the conductor as a hyperbolic function curve are given as:

$$y(x) = \frac{H}{w}\left[\cosh\left(\frac{w_L x}{H}\right) - 1\right] \quad \text{……..…….} \quad (3.3a)$$

$$L_D = \frac{H}{w}\left[\cosh\left(\frac{w_L L_C^2}{2H}\right) - 1\right] \quad \text{……..…….} \quad (3.3b)$$

$$L_C = \frac{2H}{w}\sinh\left(\frac{wL_S}{2H}\right) \quad \text{……..…….} \quad (3.3c)$$

The slack which is the difference between the conductor length and the span length can be evaluated by

$$\Delta L = L_C - L_S \cong \frac{w_L^2 L_S^3}{24H^2} \quad \text{……..…….} \quad (3.4)$$

It is pertinent to note, the main motivation for this study has to do with determining conductor damping, but the overall aim was to determine at least the sag that can effectively damped out the imposed energy on the conductor. This directly determines minimum conductor chord length required for a particular span length. If this length is adequately determined and effectively implemented, on a long distance stretch of a power line, it saves the power utilities huge savings as the cost of the conductor is the most expensive component of any power line. Analysis of the sag as a function of different stringing tensions for single span is done in appendix B

3.3 Analytical Modelling Approach

Over the years, considerable progress has been made in the formulation of analytical models to predict the mechanical characteristic of power line conductors. These analytical models can be broadly classified into three forms. The first is the analytical models that treat the conductor as a continuous distributed parameters system. The second consider the conductor as a discrete set of concentric orthotropic cylinders i.e. the individual layer of strands is replaced by an equivalent cylindrical orthotropic sheet. The third is when the conductor is regarded as an arrangement of helically curved rods, assembled to form a bundle. Analytical modelling is done with different assumptions about the conductor geometry or the inter-strands contacts, depending on any of the three forms of modelling the researcher adopt.

In the analytical modelling of power lines, the parameters of interest usually determine the modelling approach used. Also, the degree of accuracy and the ease of linearizing the equations in order to achieve the set objectives also influences the approach adopted. The possible approaches that can be used for conductor analytical modelling are:

a. The Global Approach

b. The Local Approach

3.3.1 The Global Approach

Several researchers have adopted this approach for modelling the conductors [1, 5, 14]. The global approach which has proven to be sufficiently accurate for cases where the conductors' parameters are assumed to be distributed under relatively high stress and small displacement. In this condition, the solution of the equation is of global interest. The global phenomena that are of interest are the natural frequencies, mode shapes, damper placements, loop lengths, wave speed etc. This approach is achieved by employing either a straight or catenary profile to model the geometry of conductor. The solid beam or the taut string model is usually used for the analytical modelling of the conductor.

3.3.2 The Local Approach

The local approach is implemented, when the conductor is model as a bundle made up of an assembly of discrete element of strands. The approach treats the conductor as a composite structure rather than a continuous distributed structure. This entails considering the conductor as a composite structure formed by the assembly of helical strands in various layers over the core. This approach is required when the analysis of the inter-strand contact areas, the effects of friction and the stick-slip regimes are of importance during the periodic motion. This approach gives a more accurate representation of the conductor structure and results for the conductor. Since the formulation of equation for strands element yields complex expressions, it is used when more accurate results are required.

3.4 Forms of Analytical Modelling

Based on the two already explained approaches used for the analytical modelling, as used to determine the parameters of interest based on the problem formulation. Depending on either of the approach used, the concept used in modelling is categorized into a particular form of analytical modelling. The conductor modelling, depending on the approach used for the analytical modelling can be broadly categorized into three forms of analytical modelling:

The Continuous Structure Model
The Semi-Continuous Structure Model
The Composite Structure Model:

As already explained in chapter 2, these forms of analytical modelling can be done for the condition such as:

Pure tensile loading, pure bending or combination of both and the parameter for the problem formulation can be for any of the following:

- Axial loading using only the axial displacement
- Axial loading using coupling effect of axial displacement and rotation
- Pure Bending loading for only the transverse displacement
- Combination of tensile and bending loads using the axial, and transverse displacements and rotation.

3.5 The Analytical Continuous Structure Model

The continuous structure model is where the conductor is treated as a continuous system with distributed properties. This form of modelling uses the global approach in which the modelling goal is primarily concerned with the evaluation of global parameters. The conductor is model using a partial differential equation of beam or taut string. Using the form of modelling, the analytical study of a transmission line conductor is done using the global structural configuration. The modelling of the damping of the conductor is done mathematically, by independently incorporating the damping model into the partial differential equation for the conductor.

This form of modelling has been used in [5-7], to investigate

- The dynamic characteristics of the conductors with sufficient prediction of dynamic response for the structural system for global parameters such as natural frequencies and mode shapes.
- The frictional bending model, where the conductor was modelled as a one-dimensional continuum structure with varying flexural rigidity to estimate damping due to internal friction.
- The propagation of wave speed, loop length and vibration modes of conductor that is completely dependent on the global scale of its geometry.
- The determination of the optimal placement of vibration absorber on the power line.

To model the conductor as continuous distributed parameters can be further broadly classified into:

- Linear Analytical Modelling
- Non-Linear Analytical Modelling

3.5.1 Linear Analytical Modelling of Conductor Vibration

This approach if used, the parameters of interest are those related to the global phenomena and these are analyzed globally as a function of the span length, rather than those parameters associated with the composite structure. The slender conductor structure of the power line deforms and sags due to gravity. This deformation can be described analytically by the elastic continuous distributed

parameter theory. This form of structural engineering applications can be adequately modelled either by taut spring or beam. The Euler- Bernoulli beam theory is mostly employed if only small deformations need to be considered.

Mathematically, in the form of modelling, the conductor is modelled as a curve in space mostly described as a one-dimensional structure, with effective mechanical properties such as axial, bending and torsional stiffness's.

In the case of using the beam model, the partial differential equation is formulated as continuous solid with circular cross-section subjected to axial loading (tensioned at both end) as documented in [5, 23, 24, 25]. The equation of motion for the transverse displacement is given as:

$$EI\frac{\partial^4 y(x,t)}{\partial x^4} - S\frac{\partial^2 y(x,t)}{\partial x^2} + \rho A\frac{\partial^2 y(x,t)}{\partial t^2} = f(x,t) \qquad \text{..... (3.5)}$$

for $x\epsilon(0,l)$, t > 0 , with the boundary conditions at

$$y(0,t) = \frac{\partial^2 (0,t)}{\partial x^2} = 0 \quad \text{x = 0}$$

$$y(l,t) = \frac{\partial^2 (l,t)}{\partial x^2} = 0 \quad \text{x = } l$$

Initial conditions:

$$y(x,0) = y_0(x) \quad \text{at } t = 0$$

$$\dot{y}(x,0) = \dot{y}_0(x) \quad \text{at } t = 0$$

Where ρ = the conductor density

$y\,(x, t)$ = transverse displacement position x, time t

A = the cross-sectional area

$f\,(x, t)$ = the external force

Substituting the conductor mass per unit length, $m_L = \rho A$

$$EI\frac{\partial^4 y(x,t)}{\partial x^4} - S\frac{\partial^2 y(x,t)}{\partial x^2} + m_L\frac{\partial^2 y(x,t)}{\partial t^2} = f(x,t)$$

Using separation of variables

$$Y(x,t) = X(x)T(t) \qquad \text{..... (3.6)}$$

The natural frequencies for the conductor is obtained as

$$\omega_n^2 = \left(\frac{n\pi}{l}\right)^2 \frac{S}{A\rho} + \left(\frac{n\pi}{l}\right)^4 \frac{EI}{A\rho}$$

$$\omega_n = \sqrt{\left(\frac{n\pi}{l}\right)^2 \frac{S}{m_L}\left[1 + \left(\frac{n\pi}{l}\right)^2 \frac{EI}{S}\right]} \quad \text{in rad/s} \qquad \ldots\ldots\ldots\ldots\ldots\ldots\ldots\ldots (3.7)$$

If $F_n = \frac{\omega}{2\pi}$

$$f_n = \frac{1}{2\pi}\sqrt{\left(\frac{n\pi}{l}\right)^2 \frac{S}{m_L}\left[1 + \left(\frac{n\pi}{l}\right)^2 \frac{EI}{S}\right]} \quad \text{in Hz} \qquad \ldots\ldots\ldots\ldots\ldots\ldots\ldots\ldots (3.8)$$

For the conductor response for both free and force vibration, see [14] for further details.

3.5.2 Non-Linear Analytical Modelling of Conductor Vibration

In some other applications of conductor structural mechanics, the deformations may be large; this means that nonlinear geometric effects have to be taken into account. Also, the dynamic behaviour of conductor can be characterized by non-linearity due to damping. Therefore, the problem of conductor in the case of non-linearity may be due to geometry or damping.

For the case of aeolian vibration, because of small displacement, the non-linearity is mostly as a result of the damping mechanism. This damping due to friction at contact region tends to have a significant effect on the conductor parameters especially at low axial tensions. In [14], it was suggested that to improve on the linear conductor model some form of non-linear concepts can be introduced, which in this case is for damping.

This form of modelling can be achieved by considering the conductor as visco-elastic beam with the two forms of damping as explained in [16]. If the conductor obeys the stress-strain relationship as given below:

$$\sigma = E\varepsilon + \beta E \frac{\partial \varepsilon}{\partial t} \qquad \ldots\ldots\ldots\ldots\ldots\ldots\ldots\ldots (3.9)$$

Incorporating the relation defined by equation (3.9) and other form of damping as a viscous damping into equation (3.5), the equation describing the transverse vibration of the conductor will be in the form:

$$\frac{\partial^2}{\partial x^2}\left(EI(x)\frac{\partial^2 y}{\partial x^2}\right) - T\frac{\partial^2 y}{\partial x^2} + \beta I \frac{\partial^5 y}{\partial t \partial x^4} + C\frac{\partial y}{\partial t} + \rho A \frac{\partial^2 y}{\partial x^2} = f(x,t) \qquad \ldots\ldots\ldots\ldots\ldots\ldots\ldots\ldots (3.10)$$

In chapter 2, it was highlighted that the bending stiffness *EI*, of a conductor is a function of curvature i.e. variable bending stiffness. To model the non-linearity for damping with variable bending stiffness, is to consider the classical beam equation in terms of various energies associated with the kinetic, potential and the energy dissipation.

The kinetic energy for the transverse vibration is defined by its transversal displacement and this is given as:

$$T = \frac{1}{2}\int_0^l \rho A(x)\left(\frac{\partial y}{\partial t}\right)^2 dx \qquad \text{..... (3.11)}$$

The potential energy of the system is defined in terms of bending energy and this is given as:

$$U = \frac{1}{2}\int_0^l \left[EI(x)\left(\frac{\partial^2 y}{\partial x^2}\right)^2 + S\left(\frac{\partial y}{\partial x}\right)^2 \right] dx \qquad \text{..... (3.12)}$$

To determine the energy dissipation by the conductor in line with the various forms of damping as documented in [16], in which the internal damping is assumed to be proportional to the rate of strain in the conductor. Also, the conductor inter-strand motion and fluid damping (both form the external damping) of the conductor is proportional to its velocity and it is represented by viscous damping model. The above concepts will be defined with respect to the beam transversal damping energy as dissipated by the conductor.

The damping energy by the conductor as defined by the Rayleigh energy dissipation function in terms of both viscous damping and rate of strain is given as:

$$D_{conductor} = \frac{1}{2}\int_0^l \left[\beta EI(x)\left(\frac{\partial}{\partial t}\frac{\partial^2 y}{\partial x^2}\right)^2 + C\left(\frac{\partial y}{\partial t}\right)^2 \right] dx \qquad \text{..... (3.13)}$$

Using the developed above equations, the equation for the transverse vibration for the conductor can then be derived using the Lagrange equation which is defined as:

$$\frac{d}{dt}\left(\frac{T}{\partial \dot{q}_i}\right) - \frac{\partial T}{\partial q_i} + \frac{\partial U}{\partial q_i} + \frac{\partial D}{\partial \dot{q}_i} = Q_{i,} \quad i = 1, 2, 3, \ldots, n \qquad \text{..... (3.14)}$$

Hence, the transmission line conductor as mechanical system with distributed parameter has an infinite number of distributed-parameter (continuous or infinite-dimensional) systems. That is, the mass, and stiffness of the system is considered to be distributed throughout the structure as a series of infinitely small elements.

Deriving the differential equation for the conductor using the above Lagrange equation as a continuous system, the transverse displacement is defined as:

$$Y(x,t) = \int_{n=1}^{\infty} X_n(x) T_n(t) \qquad \text{..... (3.15)}$$

where $X_n(x)$ is the space-dependent function known as the eigenfunction and $T_n(t)$ is the time-dependent function. Transforming the conductor infinite natural frequencies into finite natural frequencies, equation (3.15) becomes:

$$Y_n(x,t) = \sin\frac{n\pi x}{l}\cos\omega_n t \qquad \text{where } n = 1, 2\ 3, \ldots \qquad \ldots\ldots\ldots\ldots\ldots\ldots\ldots\ldots (3.16)$$

The boundary conditions are defined as:

$$y(0,t) = \frac{\partial^2(0,t)}{\partial x^2} = 0 \quad , \text{x} = 0$$

$$y(l,t) = \frac{\partial^2(l,t)}{\partial x^2} = 0 \quad , \text{x} = l$$

The solution to the resultant equation for the transverse vibration can be obtained by using the techniques of the separation of variables:

$$Y(x,t) = X(x)T(t) \qquad \ldots\ldots\ldots\ldots\ldots\ldots\ldots\ldots (3.17)$$

Substituting, equation (3.17), into equation (3.11), the kinetic equation for the conductor is obtain as:

$$T = \frac{1}{2}\int_0^l \rho A(x)\left(\frac{\partial y}{\partial t}\right)^2 dx = \frac{1}{2}\int_0^l \rho A(x)\left(\sum_{n=1}^{\infty} X_n(x)\dot{T}_n(t)\right)^2 dx \qquad \ldots\ldots\ldots\ldots\ldots\ldots\ldots\ldots (3.18)$$

Utilizing the orthogonality condition, the kinetic energy equation becomes

$$T = \frac{1}{2}\sum_{n=1}^{\infty}\int_0^l \rho A(x)X_n^2(x)dx\left(\dot{T}_n(t)\right)^2 \qquad \ldots\ldots\ldots\ldots\ldots\ldots\ldots\ldots (3.19)$$

Also, the potential energy equation for the conductor is obtained by substituting, equation (3.17), into equation (3.12):

$$U = \frac{1}{2}\int_0^l \left[EI(x)\left(\frac{\partial^2 y}{\partial x^2}\right)^2 + C\left(\frac{\partial y}{\partial x}\right)^2 \right] dx$$

$$= \frac{1}{2}\int_0^l \left[EI(x)\left(\sum_{n=1}^{\infty} X_n''(x)T_n(t)\right)^2 + C\left(\sum_{n=1}^{\infty} X_n'(x)T_n(t)\right)^2 \right] dx \qquad \ldots\ldots\ldots\ldots\ldots\ldots\ldots\ldots (3.20)$$

Also utilizing the orthogonality condition, the potential energy equation becomes

$$U = \frac{1}{2}\sum_{n=1}^{\infty}\int_0^l \left[EI(x)\left(X_n''(x)\right)^2 dx T_n^2(t) + S\left(X_n'(x)\right)^2 dx T_n^2(t) \right] \qquad \ldots\ldots\ldots\ldots\ldots\ldots\ldots\ldots (3.21)$$

The energy dissipation equation of the conductor was obtained as:

$$D = \frac{1}{2}\int_0^l \left[\beta EI(x)\left(\frac{\partial}{\partial t}\frac{\partial^2 y}{\partial x^2}\right)^2 + C\left(\frac{\partial y}{\partial t}\right)^2 \right] dx$$

$$= \frac{\beta}{2}\int_0^l EI(x)\left(\sum_{n=1}^{\infty} X_n''(x)\dot{T}_n(t)\right)^2 dx + C\int_0^l \sum_{n=1}^{\infty}\left(X_n'(x)\dot{T}_n(t)\right)^2 dx \qquad \ldots\ldots\ldots\ldots\ldots\ldots\ldots\ldots (3.22)$$

Also, taking into consideration the orthogonality condition, the damping energy equation becomes

$$D = \frac{\beta}{2}\sum_{n=1}^{\infty}\int_0^l EI(x)\left(X_n''(x)\right)^2 dx\dot{T}_n^2 + C\sum_{n=1}^{\infty}\int_0^l \left(X_n(x)\right)dx\dot{T}_n^2(t) \quad \text{..... (3.23)}$$

Substituting the equations for kinetic, potential and the energy dissipation into the Lagrange equation above and the following is obtained

$$\int_0^l \left(\rho A(x) X_n^2(x)dx\right)\ddot{T}_n(t) + \int_0^l \left(EI(x)\left[X_n''(x)\right]^2 dx + S\left[X_n'(x)\right]^2\right)T_n(t) + \int_0^l \left(\beta EI(x)\left[X_n''(x)\right]^2 dx + CX_n^2(x)dx\right)\dot{T}_n(t) = 0 \quad \text{..... (3.24)}$$

The equation can be compared with the *n-th* mode of vibration equation given as

$$\ddot{T}_n + 2\xi\dot{T}_n + \omega^2 T_n = 0 \quad \text{..... (3.25)}$$

Using the Rayleigh Method, the natural frequencies for the conductor is obtained as

$$\omega_n^2 = \frac{\int_0^l \left(EI(x)\left[X_n''(x)\right]^2 dx + S\left[X_n'(x)\right]^2 dx\right)}{\int_0^l \rho A(x) X_n^2(x)dx} \quad \text{..... (3.26)}$$

The damping coefficient is obtained as

$$\zeta = \frac{\int_0^l \left(\beta EI(x)\left[X_n''(x)\right]^2 dx + C\left[X_n^2(x)\right]^2 dx\right)}{2\int_0^l \rho A(x) X_n^2(x)dx} \quad \text{..... (3.27)}$$

3.6 The Semi-Continuous Model

The semi-continuous structure model entails developing homogeneity parameters for each layer of the conductor using orthographic concepts. This form of analytical modelling employs the homogenization of material in a given layer using the 'orthotropic sheet theory', in the continuum modelling of a discrete system that composed of many identical repetitive elements. This form of modelling was first developed by T. Hobbs and M. Raoof [76] for the modelling of the steel cables. Using the 'semi-continuous' model, each layer of wires/strands is mathematically represented by an orthotropic circular cylinder with the use of the 'averaged' mechanical properties. The individual layer of strands is modelled as an equivalent cylindrical thin orthotropic sheet; with each sheet having the 'averaged' elastic properties. Thus, the whole cable is treated as continuous but discrete concentric orthotropic cylinders.

Using the semi-continuos model, modelling the conductor is based on the homogenization of the conductor layers into orthotropic cylindrical sheets. This concept was used in most of the

investigation for the conductor fatigue analysis. The ‘semi-continuous’ model was developed by F. Blouin and A. Cardou [77], and later extended by C. Jolicoeur and A. Cardou [78], and also by C. Jolicoeur and A. Cardou [63]. In these models, the strand layers are replaced with a cylinder of orthotropic, isotropic material. In these studies, using the form of modelling, a great deal of attention has been given to the inter-strands contact phenomena and friction between the layers. For fatigue analysis, in all, the proposed ‘orthotropic sheets theory’ gives a good prediction of cable/conductor characteristics for fatigue analysis, as the accuracy increases with the increase in the number of layers.

Though, this form of model produces good results for fatigue analysis, it is not an appropriate method for a general analysis of the conductor. Base on this, the analytical description, formulation and analysis for the conductors using this method will not be done for the conductors in this study. For details regarding semi-continuous for cables or conductors, consult the references mentioned in this section.

3.7 The Composite Structure Model

3.7.1 Curved Beam Theory

The composite structure modelling for the conductor is where the conductor is treated as a bundle of the helical assemblies of beam, rod or spring. For the conventional conductor structure, the geometric description of the circular cross-section is that of the arranged helical strands in layers. This form of conductor structure, applying the exact analytical solution as a solid continuous structure is virtually impossible. This is because the conductor exact geometry cannot be determined mathematically; thus, it is neither classified as continuous body nor a body of completely independent strands.

To achieve a more realistic model for the conductor, is by using the helical rod model. This model treats the conductor as a composite structure of helical strands rather than a continuous body of distributed parameters i.e., the conductor is represented as an assembly of helical strands. This form of conductor modelling considers the equilibrium equation of the individual strands in the stranded assembly under the influence of both internally and externally applied loads. Each strand is treated as a curved rod with analysis in terms of the effects of strand axial elongation, bending and twisting either considered separately by decoupling or with the coupling effect. The equations of A. E. H. Love [34] are used as the basic equations for the individual strand. The modelling is done for the strand depending on the conditions for friction and slips initiation at the inter-strands contact locations between the helical strands. The complex stiffness is derived with the material characteristics in relation with uncoupling or coupling effects among the forces and the moments.

Before the kinematic analysis for the thin rod model for the strand is done, it is imperative to firstly carry out analysis of the mechanics of helical curve rod.

3.7.2 Mechanics of Helical Curve Rod

The concept of composite structure of a conductor, consisting of helical strands can be formulated and analysed using the mechanics of cylindrical helices. Consider a helical elastic strand as shown in figure (3.3), the position of the helical strand in the composite conductor is considered in terms of the arc-length. The arc-length is defined along the curvilinear axis of the strand in line with the axis of the helix path. Its position is defined by a distance, R_i from the parallel x-axis of the Cartesian coordinates or from the centre core in case if it is in the deformed state.

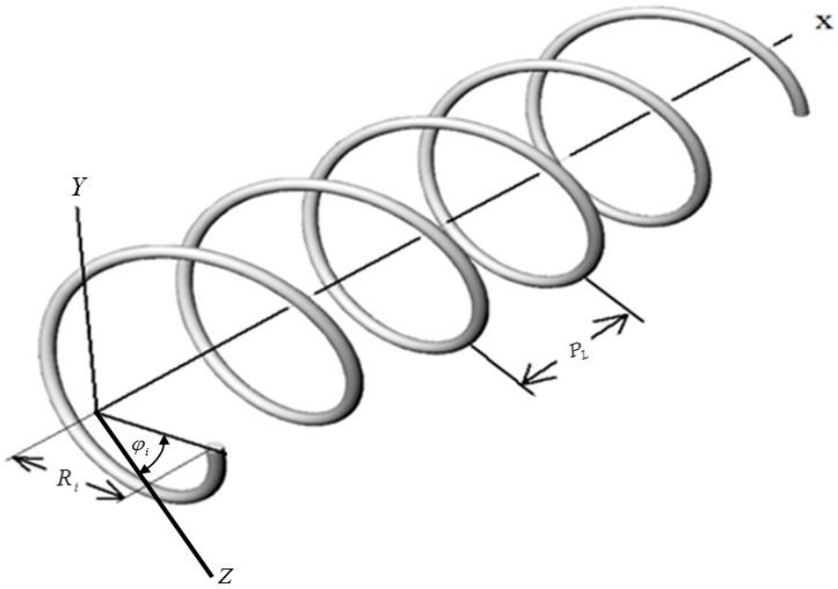

Figure 3.3: A helical strand

The geometrical properties of the cylindrical helix can be obtained as function of the wrapped φ and the pitch p_L:

$$\left.\begin{aligned} x &= p_L(\varphi)\varphi \\ y &= R_i(\varphi)\cos(\alpha) \\ z &= R_i(\varphi)\sin(\alpha) \end{aligned}\right\} \qquad \text{..... (3.28)}$$

Where $p_L(\varphi) = R_i(\varphi)\tan(\alpha)$, α denotes the lay angle, $R_i(\varphi)$ is the centreline radius as the step value of angle of the helix as a function of the horizontal angle φ, respectively.

In the Cartesian coordinate system, the position vector of any point on a helix can be expressed in the directions of X, Y and Z axes, respectively. In the Frenet coordinate system, the units Frenet vectors differentially depend also on the position vector, R, in terms of $(\tau, n \text{ and } b)$ which are the unit vectors for tangent, normal and bi-normal respectively. The parameters associated with this

coordinated system are as follows: κ is the curvature, τ is the torsion of the curve and P_L is the pitch length of the helix.

The helical strand shown above can be described using the orthogonal Frenet triad:

$$\tau = R' \qquad \text{..... (3.29a)}$$

$$\tau' = \kappa n \quad \kappa = \frac{\sin^2 \alpha}{R_i} \qquad \text{..... (3.29b)}$$

$$n' = -\kappa \tau + t b \quad \tau = \frac{\sin \alpha \ \cos \alpha}{R_i} \qquad \text{..... (3.29c)}$$

$$b' = -\tau n \quad and \quad P_L = 2\pi R_i \cot \alpha \qquad \text{..... (3.28d)}$$

For the strand helical configuration, in the pre-stress state, the curvature and torsion are defined as follows

$$\kappa_o = 0 \qquad \text{..... (3.30a)}$$

$$k_0' = \frac{\cos^2 \alpha}{R_i} \qquad \text{..... (3.30b)}$$

$$\tau_o = \frac{\sin \alpha \cos \alpha}{R_i} \qquad \text{..... (3.30c)}$$

When subject to axial load, the curvature and torsion are now defined as:

$$\kappa_1 = 0 \qquad \text{..... (3.31a)}$$

$$k_1' = \frac{\cos^2 \alpha}{R_i} \qquad \text{..... (3.31b)}$$

$$\tau_1 = \frac{\sin \alpha \cos \alpha}{R_i} \qquad \text{..... (3.31c)}$$

3.7.3 Thin Rod Kinematic Analysis

In this section, the formulation of kinematic equation for the cylindrical helical rods subjected to forces and moments. A typical helical strand property is the coupling which appears between the extension and torsion responses. Under axial loading, the helical strands exhibit a coupling effect of elongation with torsional responses. Under the static conductor where the strands are subjected to pure axial loading, an axial force and twisting moment are imposed on the strand. Explicit forms of four constitutive coefficients of the helix are derived for the coupling effects of extensional, and torsion, as already indicated in equation (2.60). The strands are rod-like, their corresponding constitutive relations governing the moments and torque due to bending and twist are more

complicated. The local bending moment is, at least in principle, a function of curvature along the entire strands length.

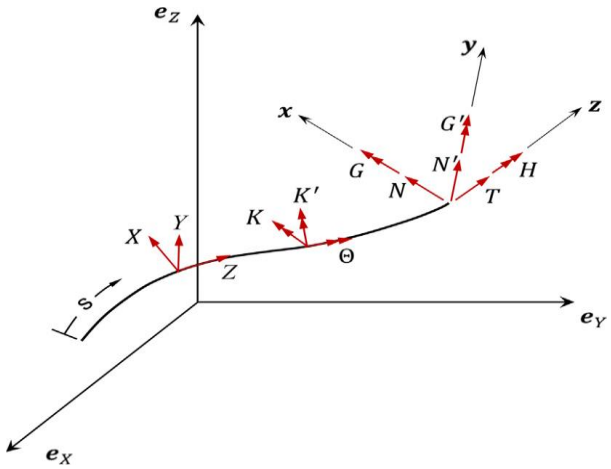

Figure 3.4: Forces and moment distribution in a strand [9]

The material properties are that of viscoelastic response of the helix and its constitutive differential equations are derived for the viscoelastic models for the material at the micro level. Solutions to these constitutive differential equations are expressed for the dynamic behaviour of the helix. In such a case, all the strands in a given layer are assumed to carry exactly the same loads. The various forms of forces and moments acting on a single strand are indicated on figure (3.4).

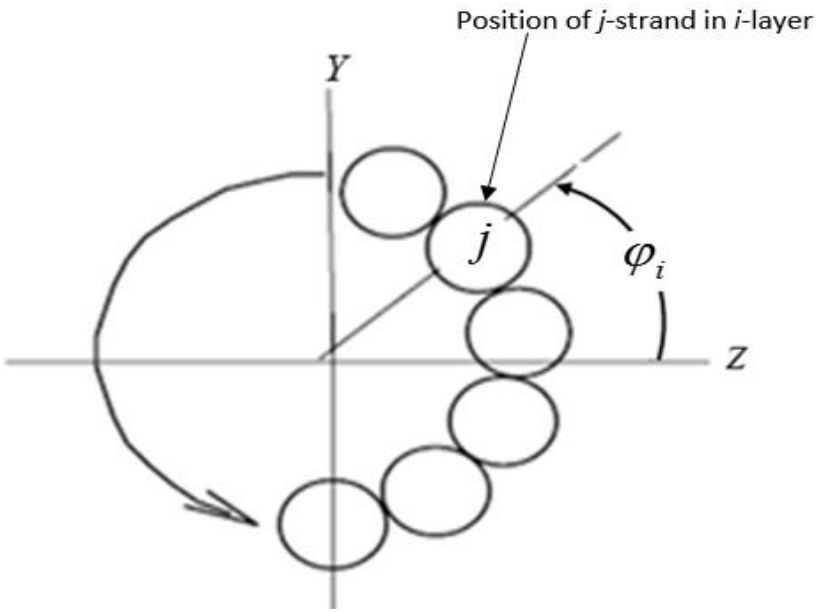

Figure 3.5: The strands arrangement

Consider figure (3.5), using thin curved rod model with various internal forces and moments and the equilibrium equations for the rod as given by A. E. H love [34]:

$$\frac{dN_z}{ds} - N_y\tau + T\kappa_y + Z = 0 \qquad \text{..... (3.32a)}$$

$$\frac{dN_y}{ds} + N_z\tau + T\kappa_z + Y = 0 \quad \text{..... (3.32b)}$$

$$\frac{dM_z}{ds} + M_y\tau + H\kappa_y - N_y + K_y = 0 \quad \text{..... (3.32c)}$$

$$\frac{dM_y}{ds} + M_z\tau - H\kappa_z + N_z + K_z = 0 \quad \text{..... (3.32d)}$$

$$\frac{dT}{ds} - N_z\kappa_z - N_y\kappa_y + Z = 0 \quad \text{..... (3.32e)}$$

$$\frac{dH}{ds} - M_z\kappa_y - M_y\kappa_z + \Theta = 0 \quad \text{..... (3.32f)}$$

N_y, N_Z, T are forces acting at the ends of the segment and M_y, M_Z, T are moments or torques. $x\ y\ y$ are distributed external loads and K_y, K_Z, Θ are distributed external moments. κ_y, κ_z are curvatures in the planes of bending normal to the axes identified by their subscripts. τ is the twist of the segment, defined as the rate of rotation of its principal bending axes with respect to longitudinal position s.

Solution of Love's equations for any particular case requires the assumption of suitable constitutive relations connecting the bending moments and torque in a rod element with its curvature and twist. The axial strains and torsion are defined as:

$$\varepsilon_A = \varepsilon\cos^2\alpha_i + \tau R_i\cos\alpha_i\sin\alpha_i \quad \text{..... (3.33)}$$

$$\tau_A = \varepsilon\frac{\cos\alpha_i\sin^3\alpha_i}{R_i} + \tau\cos^4\alpha_i \quad \text{..... (3.34)}$$

Assuming the strand material to be elastic and obey the Hook's law, the expression for the internal force is given as:

$$T = AE\varepsilon \quad \text{..... (3.35)}$$

The internal bending moment is expressed as:

$$M = EI_x\left(\kappa - \kappa_0\right) \quad \text{..... (3.36)}$$

The torsional moment is expressed as:

$$M_t = GJ_x\left(\tau - \tau_0\right) \quad \text{..... (3.37)}$$

Where I_x is the moment of inertia $I_x = \frac{\pi d^4}{4}$, G is the shear modulus of the rod material and J_x is the polar moment of inertia $J_x = \frac{\pi d^4}{2}$

In [45] the authors presented an analytical approach to predict the global response for cables also applicable to conductors subjected to bending, tension and torsion. Using the constitutive equations described in terms of the stresses over the cable cross-section and the inter-strand effect as a function of the generalized strains of the cable can be used for the derivation of conductor's stiffnesses. For the axial loads the stiffness matrix components become [45]:

$$K_{11} = (AE)_0 + \sum_{i=1}^{N} n_i (AE)_i \cos^3 \alpha_i \quad \text{..... (3.38a)}$$

$$K_{12} = K_{21} = \sum_{i=1}^{N} n_i (AE)_i R_i \sin \alpha_i \cos^2 \alpha_i \quad \text{..... (3.38b)}$$

$$K_{22} = (GJ)_0 + \sum_{i=1}^{N} n_i (AE)_i R_i^2 \sin^2 \alpha_i \cos \alpha_i + (GJ)_i \cos^5 \alpha_i + (EI)_i \sin^2 \alpha_i \cos \alpha_i (1 + \cos^2 \alpha_i) \text{..... (3.38c)}$$

3.7.4 The Conductor Composite Structure Model

To model analytically, the conductor as a bundle, this is achieved by discrete assemblies of continuous solid of the helical strands in various layers. The helical strand is the basic structural element of the conductor. The analysis of the local mechanical properties of the conductor's strands are often modelled by a uniform elastic potential energy of the rod model, dependent on extension and twist in the static condition plus bending under the dynamic condition. For the axial static condition, the strands exhibit a coupling of axial and torsional responses. The said coupling is expressed by the constitutive equations as defined by equation (2.60). Global strand strains are designated by the strand axial strain, ε_A and the strand axial twist radians per unit length, ε_T. Using the force-strain relationships, with each parameter as defined, where *F* is the tensile force and *M* is the torque, while $\varepsilon_A = \partial u/\partial x$ is axial strain and $\varepsilon_T = \partial \emptyset/\partial x$ is the angle of twist per unit length. The parameter *x* is the measure of length parallel to the axis of a helix for the strand. Furthermore, the values $(K_{11} - K_{22})$ are the constitutive constants and these constants depend on both the conductor material and the geometric construction of the strands as defined by equations (3.34 and 3.35).

The equations of motion of a helix, referred to the unstressed conductor length, and in the absence of body forces, become [79]:

$$\frac{\partial F}{\partial x} = m \frac{\partial^2 u}{\partial t^2}$$
$$\frac{\partial M}{\partial x} = J \frac{\partial^2 u}{\partial t^2} \quad \text{..... (3.39)}$$

The helical analysis of the strands demonstrates that for the uniform helical equilibrium, the balance constitutive equations are equivalent to the conditions for the constrained strand condition in the presence of body force. The strand helical equation becomes:

$$\begin{aligned} K_{11}\frac{\partial^2 u}{\partial x^2}+K_{12}\frac{\partial^2 \phi}{\partial x^2}&=m_S\frac{\partial^2 u}{\partial x^2}\\ K_{21}\frac{\partial^2 u}{\partial x^2}+K_{22}\frac{\partial^2 \phi}{\partial x^2}&=m_P\frac{\partial^2 u}{\partial x^2}\end{aligned} \qquad \text{..... (3.40)}$$

Where $m_S = a_i\rho_i$ and neglecting the contribution from the core strand, then

$$m_P = 2\rho_i\sum_{i=1}^{N}\left(\frac{\pi^2}{256}\left[(2R_i+2r_i)^4-(2R_i-d_i)^4\right]\right)$$

Using the method defined in [79] where the Laplace transform for displacement and rotation are given as follows:

$$u(x)=\bar{u}(x)=\ell[u(s)]=\int_0^\infty e^{-sx}u(x)dx$$

$$\theta(x,t)=\bar{\theta}(x,s)=\ell[\theta](x,s)=\int_0^\infty e^{-st}\theta(x,t)dt$$

$$L[u_t](x,s)=\int_0^\infty e^{-st}u_t(x,t)dt$$

$$=e^{-st}u(x,t)\Big|_0^\infty+s\int_0^\infty e^{-st}u_t(x,t)dt=u_0(x)+s\bar{u}(x,t)$$

A similar transformation was also done for rotation and substituted into equation (3.36) to obtain:

$$\left.\begin{aligned} K_{11}\frac{\partial^2 \bar{u}}{\partial x^2}+K_{12}\frac{\partial^2 \bar{\theta}}{\partial x^2}-m_S\,s^2\,\bar{u}&=m_S\,u_0(x)\\ K_{21}\frac{\partial^2 \bar{u}}{\partial x^2}+K_{22}\frac{\partial^2 \bar{\theta}}{\partial x^2}-m_P\,s^2\,\bar{\theta}&=m_P\theta_0(x)\end{aligned}\right\} \qquad \text{..... (3.41)}$$

Defining the stiffness in a matrix form

$$K=\begin{bmatrix}K_{11} & K_{12}\\ K_{21} & K_{22}\end{bmatrix} \quad\Rightarrow\quad K^{-1}=\frac{1}{\det}\begin{bmatrix}K_{22} & -K_{21}\\ -K_{11} & K_{11}\end{bmatrix}$$

Therefore equation (3.37) becomes

$$\begin{bmatrix}\frac{\partial^2 \bar{u}}{\partial x^2}\\ \frac{\partial^2 \theta}{\partial x^2}\end{bmatrix}-\frac{1}{\det K}\begin{bmatrix}K_{22} & -K_{12}\\ -K_{21} & K_{11}\end{bmatrix}\begin{bmatrix}m_S & 0\\ 0 & m_P\end{bmatrix}\begin{bmatrix}\bar{u}\\ \bar{\theta}\end{bmatrix}=-\frac{1}{\det K}\begin{bmatrix}K_{22} & -K_{12}\\ -K_{21} & K_{11}\end{bmatrix}\begin{bmatrix}m_S & 0\\ 0 & m_P\end{bmatrix}\begin{bmatrix}u_0\\ \theta_0\end{bmatrix} \text{.... (3.42)}$$

Transforming the above equation

$$\begin{bmatrix} \frac{\partial^2 \bar{u}}{\partial x^2} \\ \frac{\partial^2 \theta}{\partial x^2} \end{bmatrix} = A \begin{bmatrix} \bar{u} \\ \bar{\theta} \end{bmatrix} + F(x)$$

Therefore

$$A = -\frac{1}{\det K} \begin{bmatrix} K_{22} & -K_{12} \\ -K_{21} & K_{11} \end{bmatrix} \begin{bmatrix} m_S & 0 \\ 0 & m_P \end{bmatrix} = \frac{1}{\det K} \begin{bmatrix} m_S K_{22} & -m_P K_{12} \\ -m_S K_{21} & m_P K_{11} \end{bmatrix}$$

The transforming the above equation into an eigenvalue equation

$$(m_P K_{22} - \lambda)(m_S K_{11} - \lambda) - m_P m_S K_{12} K_{21} = 0$$

$$\lambda^2 - \lambda(m_S K_{11} + K_{22}) - m_S m_P K_{12} K_{21} = 0 \qquad \text{..... (3.43)}$$

$$\lambda_{1,2} = \frac{(m_S K_{11} + m_P K_{22}) \pm \sqrt{(m_S K_{11} + m_P K_{22})^2 - 4 m_S m_P K_{12} K_{21}}}{2} \qquad \text{..... (3.44)}$$

$$\omega_{1,2} = \frac{(m_S K_{11} + m_P K_{22}) \pm \sqrt{(m_S K_{11} + m_P K_{22})^2 - 4 m_S m_P K_{12} K_{21}}}{2(K_{11} K_{22} - K_{12} K_{21})} \qquad \text{..... (3.45)}$$

To obtain the stiffness matrix that is developed with the relation for coupling of axial, torsional, and flexural rigidities as well as the coupling parameters as indicated in equation (2.86). For small curvatures, the flexural rigidity is comparable to the upper limit accepted in current practice by ACSR users. As the curvature increases, however, frictional forces develop between the outer layers and sliding of strands may occur, with the result that the flexural rigidity decreases. The tension level also influences the flexural rigidity of the conductor. Actually, this form of model does not consider the flexural rigidity of the conductor as a fixed entity but as directly influenced by local compressive forces and internal radial and tensile forces.

To introduce bending response of the conductor to the coupling equation for axial and torsion response is based on the formulation by J. Lanteigne [80]. This formulation is used to analyse the conductor under dynamic loading with all three responses present. The stiffnesses obtained are for the three coupling components as the conductor exhibits a coupling effect as defined in the matrix in equation (2.86). Consider a conductor cross-section as shown in figure (3.6). Following the path of a typical strand, and keeping in mind that frictional forces contribute to maintain the cross-section plane after bending, the strands undergo an axial elongation component due to the curvature.

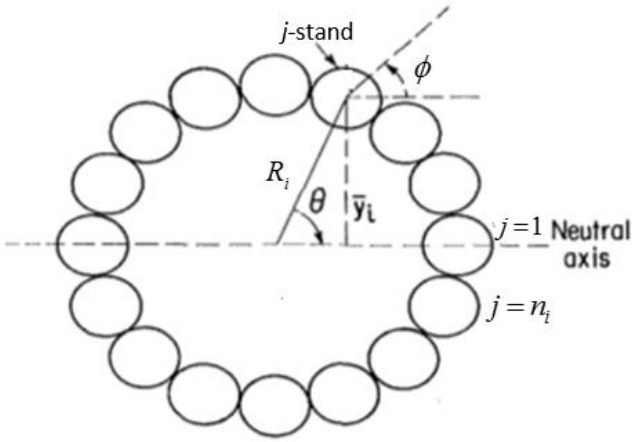

Figure 3.6: Strands arrangement in given layer with respect to the neutral axis.

The stiffness value for $(K_{11}-K_{22})$ have been defined by equations (3.37, a-c). The strain on the conductor due to bending with its coupling effect can be introduced into the analysis, with the axial strain on the conductor strands as:

$$\varepsilon_i = \cos^2\alpha_i\left(\frac{\partial u}{\partial x}+y_i\frac{\partial \psi}{\partial x}\right)+R_i\sin\alpha_i\cos\alpha_i\left(\frac{\partial \phi}{\partial x}\right) \quad \text{..... (3.46)}$$

The bending strain and the distance from the neutral axis can be evaluated as

$$y_i = R_i\sin\left(\frac{2\pi i}{n_i}\right) \qquad i=1,\,2,\,.....,\,N \quad \text{..... (3.47)}$$

The value varies with distance x along the centriodal axis by

$$y_{i,x} = R_i\sin\left(\frac{2\pi i}{n_i}+\frac{2\pi x}{P_{L(i)}}\right) \quad \text{..... (3.48)}$$

With the introduction of the bending strain for each strand, this results to the combined strain on the conductor strands given as:

$$\varepsilon_i = \cos^2\alpha_i\left(\frac{\partial u}{\partial x}\right)+R_i\sin\alpha_i\cos\alpha_i\left(\frac{\partial \phi}{\partial x}\right)+\left[R_i\sin\left(\frac{2\pi i}{n_i}+\frac{x\tan\alpha_i}{R_i}\right)+\rho_i\sin\varphi_i\right]\cos^2\alpha_i\left(\frac{\partial \psi}{\partial x}\right). \quad \text{(3.49)}$$

Where the bending coupling stiffnesses and bending stiffness are obtained as:

$$K_{13}=K_{31}=\sum_{i=1}^{N} n_i A_i E_i A_X \quad \text{..... (3.50a)}$$

$$K_{23}=K_{32}=\sum_{i=1}^{N} n_i A_i E_i R_i \tan\alpha_i A_X \quad \text{..... (3.50b)}$$

$$K_{33}=(EI)_0+\sum_{i=1}^{N} n_i (AE)_i\left(\frac{r_i^2+R_i^2}{2}\right)\cos^3\alpha_i+\sum_{i=1}^{N}\sum_{i=1}^{n_i} A_i E_i B_X \quad \text{..... (3.50c)}$$

Where

$$A_X = \frac{R_i^2 \cos^3 \alpha_i}{L_C \tan \alpha_i}\left[\cos\left(\frac{2\pi i}{n_i}\right) - \cos\left(\frac{2\pi i}{n_i} + \frac{L_C \tan \alpha_i}{R_i}\right)\right]$$

$$B_X = \frac{R_i^3 \cos^3 \alpha_i}{4L_C \tan \alpha_i}\left[\sin\left(\frac{4\pi i}{n_i}\right) - \sin\left(\frac{4\pi i}{n_i} + \frac{2L_C \tan \alpha_i}{R_i}\right)\right]$$

3.8 Analytical Evaluation of Conductor Self-Damping as a Composite Structure

Due to the complexity of characterizing damping in the composite conductor structure, the proportional damping is the most common approach used to model dissipative forces. This method was introduced by Lord Rayleigh. In order to apply proportional damping to damped systems, it is common to assume the proportional damping, that expresses the damping matrix as a linear combination of the mass and stiffness matrices, that is,

$$C = \alpha[M] + \beta[K] \qquad \text{..... (3.51)}$$

The problem of using this model is that the mass and stiffness proportional damping approximation comes from the fact that the arbitrary variation of damping factors with respect to vibration frequency cannot be modelled accurately by using this approach.

The evaluation of energy from a conductor as a bundle has to do mainly with the modelling of the inter-strand contact problems of the helical strand of conductors' structures. The interacting forces at the contact points between strands play an important role in energy dissipation within the conductors. As will be explained later in chapter 4, the cyclic bending of strands results in energy dissipation. However, these analyses are restricted to the model of the strands as rods in contact at discrete points. The analytical analysis of conductor self-damping, where a flexural rigidity-curvature relationship exists, result in energy being removed from the system. This showed that the variation of conductor flexural rigidity during bending with helical strand cyclic slip causes the friction energy dissipation in the conductor. Also, the energy dissipation is defined with a critical value of curvature that causes the inception of traction force to overcome the frictional force at contact points. The magnitude of the damping depends on the axial displacement which is a function of its axial tension. The stick-slip phenomenon is the mechanism mainly responsible for damping in the discretized conductor structure. The evaluation of this for the conductor is documented in [16, 81] and this form of damping will be explained in details in chapter 4.

Chapter 4

Conductor Self-Damping

4.1 Conductor Damping

Damping is the term used to define the non-conservative force acting on or within a system that dissipates the imposed energy. In the field of structural engineering, it is well known that the apparent performance of structures is highly sensitive to damping. Many suspended cables like structures such as power line conductors are highly susceptible to vibrations mainly caused by power imparted on the conductors by wind. This makes the transmission lines conductors to be subjected frequently to significant vibration problems, especially from those caused by vortex shedding, and wake-induced oscillation. This problem, if not mitigated tends to produce catastrophic consequences. Therefore, the mitigation of conductor vibration is necessary in order to minimize the negative impact it might have on power transfer.

Conductors are flexible structure with low inherent damping, this makes it highly susceptible to vibration. Although, at the normal working tension, the conductors have low inherent damping characteristics, they have the ability to mitigate the vibration levels within safety limits when strung at low tension. The ability of the conductor to damp out the imposed energy is a function of the axial loading, the number of strand layers and the vibration absorbers if present on the line. Many criteria have been developed by various bodies like IEEE, Cigre, IEC etc., to set the limit for the axial loading that can be used to string the line, in order to militate against the occurrence of high level of vibration.

The phenomenon of self-damping is mostly due to frictional effect as a function of its geometry and the helical geometry result in inter-strand contacts. The axial load gives rise to normal forces at the contact between strands. The product of coefficient of friction and the normal force determines the friction acting at these contact points. During bending loads, the reciprocating sliding between the strands; generate considerable wear and energy dissipation. The later mechanism was of interest in this study because it characterizes the self-damping capability of the conductor. To explain this phenomenon using analytical approach was extremely difficult. This is because the analysing of these areas of contacts, taking into consideration the complexity of phenomena like friction and stresses at the strands contact is very difficult.

The self-damping capability of power line conductors is an important parameter used to determine its dynamic response. This parameter is the main factor that determines the conductor response to the dynamic forces in the absence of external dampers. The parameter is generally not specified

by the manufacturer and can be determined through, mathematical models, and by the measurements performed in a laboratory test span of a range of 30-100 m long. Because this parameter is core in this study, therein, this chapter was specifically used to deal with concepts associated with the conductor self-damping. The chapter elaborates on the comprehensive concepts describing damping as a function of its inter-strand contact as well as the stick and slip phenomenon within the conductor as a composite structure.

4.2 Damping Models

Modelling damping in vibrating structures is a challenging task. Before analysing the conductor damping specifically, it will be imperative to have a general overview of the various damping models that can be used to represent the different damping mechanisms in different structures. Most often, damping in a many mechanical systems can be modelled by one of the following damping models. This includes viscous damping, proportional damping, material damping, structural damping and fluid damping. All but some of these categories of damping are present in a conductor. An overview explanation of these damping models is imperative as a means of identifying which will be applicable in modelling the various mechanisms responsible for the conductor damping. The following subsections gives an overview description of these damping models:

4.2.1 Viscous damping

This damping model is the most commonly used and the simplest way to represent damping in systems. For a system descripted by figure (4.1), with the following variable; *x* the vector of generalized coordinates, *K* the stiffness matrix of the system, M its mass matrix and *f (t)* the forcing function vector.

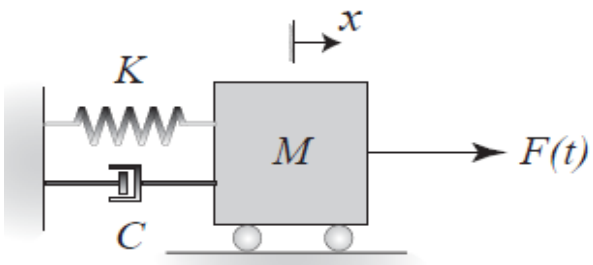

Figure 4.1: Viscous damping model

The idea contained in the damping concept as applied to this system is to represent the damping capacity of the system by the so called equivalent viscous damping. The damping, which is a function of only acceleration, can be used to characterize the same amount of damping per cycle as compared to the real system. This linear viscous damping model can be introduced into the

equation for the system by means of the damping matrix C, so that the damped equation of motion becomes:

$$M\ddot{x} + C\dot{x} + Kx = f(x) \qquad \text{.....} \quad (4.1)$$

4.2.2 Proportional Damping

Mentioned already in chapter 3, is the proportional damping and this form of model used in modelling damping was formulated by Lord Rayleigh [69]. Using this damping model for a system, the damping is developed as a function of its systems' mass and stiffness. Incorporating this damping model into equation (4.1), if proportional damping is used, the damping matrix C will be a linear combination of the mass and stiffness, defined in the form:

$$C = \alpha M + \beta K \qquad \text{.....} \quad (4.2)$$

where α and β are the proportionality constants

Thus, the proportional damping is a special form of viscous damping.

4.2.3 Material Damping

The behaviour of systems on the basis of the so-called material damping or hysteric damping model is based on the formation of the stress-strain curve, as a tilted ellipse with average slope equal to Young's modulus. The material damping represents the energy dissipation that takes place within the micro-structure of the system. As explained latter, the energy dissipated over a cycle is given by the area covered by the stress-strain curve. This form of damping can be further classified into viscoelastic and hysteretic damping.

4.2.3.1 Viscoelastic damping

This damping is normally formulated by the relationship between stress and strain with respect to time. The viscoelastic form of damping is usually model by the "Kelvin-Voigt" model for viscoelastic materials. For this model, the damping capacity of the material is frequency dependent. The linear differential equation for this form of damping is expressed as:

$$\sigma = \varepsilon E + E\left(\frac{d\varepsilon}{dt}\right) \qquad \text{.....} \quad (4.3)$$

4.2.3.2 Hysteretic damping

The second form of material damping is the hysteretic damping. This damping model represents the energy dissipated in a structure over a cycle of deformation. The amount of energy dissipation is independent on the frequency, and also proportional to the square of the amplitude of vibration.

In fact, all types of internal damping exhibiting hysteretic damping that produces a hysteresis loop, which will be used later in this chapter to evaluate energy dissipation within the conductor. The hysteretic damping as a function of the stress-strain relationship satisfies the equation:

$$\sigma = \varepsilon E + \frac{E}{\omega}\left(\frac{d\varepsilon}{dt}\right) \qquad \text{..... (4.4)}$$

4.2.4 Structural damping

The structural damping is the energy dissipation mechanism which involves rubbing between components with friction acting at the areas of contacts in the mechanical system. The Coulomb friction model is the most commonly used model to represent this form of energy dissipation by rubbing or sliding i.e. Coulomb damping is shown in figure (4.2).

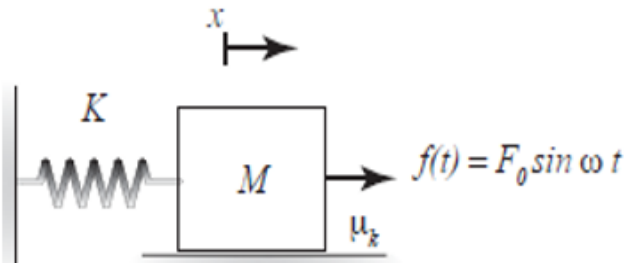

Figure 4.2: Coulomb friction model

This damping mechanism occurrence in the system are caused by sliding friction or dry friction and it is commonly modelled using the Coulomb damping model. The damping can be characterized by the relation:

$$f = \mu_k * \mathrm{sgn}(\dot{x}) \qquad \text{..... (4.5)}$$

Where f is the damping force, x is the relative displacement at the contact and μ_k is the friction parameter.

4.2.5 Fluid damping

The fluid damping is the last form of damping model. Fluid damping is produced when a body is immersed in a fluid and exhibits a relative motion with respect to the fluid flow. For a cylindrical system immersed in fluid, the drag force can be evaluated by:

$$f_d = \frac{1}{2} C_D \rho d \dot{x}^2 \,\mathrm{sgn}(\dot{x}) \qquad \text{..... (4.6)}$$

where $\dot{x}$ is the relative velocity [m/s], C_D the drag coefficient [L], ρ the fluid density [kg/m^3] and d the cylinder diameter [m].

From these models explained above, in the case of a vibrating power line conductor three form of damping exist. The first is the material damping which occurs within the material of any strand.

This corresponds to the energy dissipation that takes place in the micro-structure. The second is the structural damping which involves the rubbing friction between component strands of the conductor system, at contacts both at the clamp and along the entire conductor structure. Structural damping in conjunction with hysteretic forms of damping (material damping) occurs at the contact between two strands. The sliding at these contact points tends to exhibits the hysteretic phenomenon, because it is periodic. The form of damping mainly accounts for energy dissipation by the conductor. Finally, is the fluid damping which occurs due to the interactions between the vibrating conductor and the fluid in which it is immersed.

4.3 Mechanisms Responsible for Conductor Self-Damping

Damping is of great importance in curtailing the adverse effect of wind loading on conductors. In this section, the mechanisms responsible for conductor damping in power line conductors are discussed. The mechanisms responsible for the conductor energy dissipation are very complex. The self-damping of a conductor has been identified to be generated by three main mechanisms when subjected to transverse motion under the influence of the dynamics forces of nature.

The first damping mechanism is as a result of the inter-strand motion between strands of the conductor. Due to frictional effect, the inter-strand motion in the form of reciprocating sliding at the contact points results in energy dissipation. This form of damping is known as structural damping. The explanations of how this mechanism causes damping processes to occur can be found in literature [1, 2]. In references [16] and [19], the authors gave a comprehensive and extensive explanation of this form of damping with various analytical and mathematical derivations of the various parameters associated with this form of conductor damping. For this form of structural damping within the conductor, at the inter-strands contacts due to the geometry as shown in figure (4.3). The assembly of helical strands constitutes the conductor as bundle structure. When exposed to bending caused by wind loading, around the contact points, there will be sliding with frictional effect resulting in energy dissipation.

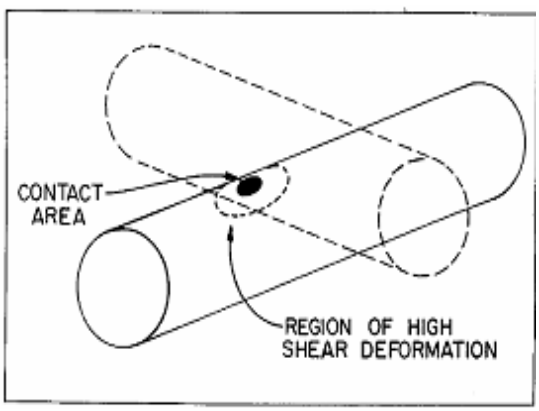

Figure 4.3: Contact between two cylinder bodies with elliptical contact surface [2]

This damping mechanism exhibits a hysteresis effects, the activities of friction between the individual strands act as the memory of the system and the output is the conductor strands displacement as it undergoes the bending deformation.

This process is mainly responsible for dissipation of energy imparted on the vibrating conductor by the excitation forces. The second form of conductor damping is that which occurs in the micro-molecular level within the strands in the conductor's structure. In this second form of energy dissipation, part of the external energy is transformed into molecular energy and this form of damping is known as material damping. The material damping corresponds to the energy dissipation that takes place in the micro-structure; in the case of a conductor, this takes place within the strand. The conductor strand is assumed to be a continuous system along the helical path. Thus, this form of damping takes place throughout the entire length of the conductor and the distributed element damping model can be used for its evaluation.

The third form of energy dissipation is the fluid-dynamic (aerodynamic) damping resulting from the interactions between the conductor and the fluid in which it was immersed. This occurs as part of the frictional effect in which the energy was dissipated as heat and then transmitted to surrounding objects or the atmosphere by the fluid flow. The aerodynamic in a conductor is due to the conduction of heat from the material damping and also from the elastic hysteresis of friction at the inter-strand contacts, transferred to the atmosphere due to air resistance and then absorbed by the surrounding bodies.

4.4 Analytical Determination of Conductor Self-Damping

Conductor damping as a complex engineering problem has attracted attention from numerous researchers [1, 2]. The complex nature of the problem is based on the fact that the mechanical behaviour of overhead line conductors is characterized by non-linear response due to damping [5]. Some of the models used to evaluate damping, have evaluated energy dissipation by using the non-conservative mathematical equation and then incorporate it into the conductor equation of motion. Others models have focused on quantifying the energy dissipated through friction due to the motion between strands when the conductor is experiencing bending load.

The power dissipated by a conductor is often deduced from laboratory tests. This has resulted in the formulation of an empirical equation expressed using the power law to evaluate the power dissipated per unit length of the conductor.

The power dissipated due to the conductor self-damping using the empirical formulation can be estimated based on CIGRE recommendation [1, 2]:

$$P_C = LK\frac{(A/D)^l f^m}{T^n} \quad \text{……..……..…… (4.7)}$$

Where *K* is the so-called proportionality factor that characterizes the self-damping properties of each conductor, and *l, m* and *n* are the exponents of the amplitude, frequency and conductor tension, which can be obtained as documented [1, 2], and this is applicable and equal for all conductors.

For a particular conductor, the value for K is a special function involving the diameter, the rated strength, and the mass per unit length of a conductor. This is expressed as:

$$K = \frac{D}{\sqrt{UTS \times m_L}} \quad \text{……..……..…… (4.8)}$$

Where UTS is the rated tensile strength [kN], and m_L is mass per unit length [kg/m].

Table 4.1 [2] shows the comparison of some of the values of the exponents' *l, m* and *n* obtained through experimental research of some authors [1, 2, 50]. The differences are the result of high sensitivity of the equipment used, as well as some characteristics of the experimental procedures; this includes parameters and conditions such as the span lengths, conductor fixtures on the span ends, and the methods used.

Table 4.1[2]: Comparison of conductor self-damping rules

Investigators	*l*	*m*	*n*	*Span length*	Method
Tompkins et al.	2,3	5.0	1.9	36	ISWR
Claren & Diana	2,0	4.0	2.5	46	PT
Seppä	2.5	5.75	2.8	36	ISWR
Kraus & Hagedorn	2.47	5.38	2.80	30	PT
Noiseux	2.44	5.63	2.76	63	ISWR
Möcks & Schmidt	2.45	5.38	2.4	30	PT
Mech. Lab Politecnico di Milano	2.43	5.5	2	46	ISWR
Rawlins	2.2	5.4	1	36	ISWR

ISWR: Inverse standing wave method,

PT: Power method

Employing equation (4.7), once accurate information on the self-damping capacity of the conductors were obtained, it became possible to relate all these data and to assess a method of estimating the maximum vibration amplitudes that could occur on a line. Consequently, how much energy can be dissipated by conductor is of importance when considering dynamic behaviour of

conductors. This process helps to device a method than can then be put in place to curtail the adverse effect of conductor vibration.

4.5 Stick-Slip Model

The interactions of contact forces between internal structures play an important role in many mechanical systems such as conductors. In most models used to analyse transmission line conductor's oscillation treats, the conductor as a continuous homogenous system [5-7]. These models completely neglect internal phenomenon such as slippage at contacts point. The modelling of contact problems of helical strand of the conductors' structures have been considered by some authors in terms of using the conductor discrete geometry [9-13]. However, these analyses are restricted to modelling the strands as rods in contact at discrete points as shown in figure (4.3). The rod theory was based on the concept of modelling the helical strand as a long, slender object, which are then regarded as substructures of the conductor. This method has been used by many researchers to investigate many phenomena that are linked with the internal structure.

As explained in earlier section, one of the damping mechanisms is characterized by energy dissipation due to frictional effect brought about by the relative motion between strands at the points of contact. This type of frictional sliding at contacts, the vibration exhibits a stick-slip regime during the harmonic oscillation and the contact-friction model can be used to model and simulate this stick-slip vibration. Stick-slip vibration is characterized by a displacement-time history. The history of the vibration, function as a memory stored in the conductor and this can be characterized by four phases of the vibration history. These are clearly defined as; the stick, the transition from stick to slip, the slip phases and finally the transition from slip to stick. The vibration is governed by a static friction force in the stick phase and a velocity dependent kinetic friction force in the slip phase.

The wind input energy, due to lock-in effect produces a harmonic induced vibration that has a nearly sinusoidal displacement-time pattern. As the motion is initiated the conductor operates from stick to the slip phase in a cyclical manner. As the conductor undergoing the alternating bending between the stick and slip regime, it thus exhibits flexural hysteresis phenomenon. The term hysteresis implies that the relation between the curvature that causes the bending and the bending moment is not unique and the bending moments do not depend on the absolute value of curvature but only on its sign. Therefore, for any given motion the bending moment depends not only on the actual value of curvature but also on sign of the curvature; more generally, the moment depends on the history of the deformation due to the imposed curvature.

During the bending, the conductor experiences damping due to internal friction and this form of damping exhibits significant flexural hysteresis, resulting from inter-strand friction slip. The

flexural hysteresis is due to continual changes between the maximum and minimum bending stiffness. The evaluation of this type of hysteresis damping of mechanical vibrations such as the conductor is very difficult. The damping mechanism in the conductor due to hysteresis resulting from this regime is mostly modelled, using the coulomb dry friction model. This model was applied between the individual strands accounting for inter-strand friction during bending deformation.

The adequate model this stick-slip phenomenon in conductors was achieved by evaluating all possible phases of the hysteresis history and incorporated them into one conditional equation. This follows that during the stick-slip motion two different mechanisms take place, the first is the static friction mechanism and the second is the kinetic friction mechanism. The major problem of the formation of stick-slip for the hysteresis process is the determination of the transition between these two states.

For this sinusoidal motion, the equation for this motion requires a periodic solution with the combination of conditions to describe the periodic stick-slip regime solutions. This phenomenon is an example of nonlinear dynamic system that can be represented by the equation of the contact friction model:

$$F(v_{rel}\ x)=\begin{cases} F(x)=\min\left(\left|F_{stick}(x)\right|,F_s\right)\operatorname{sgn} F_{stick} & \textit{stick condition with } v_{rel}=0 \\ F(v_{rel})=-\dfrac{F_{slip}\operatorname{sgn} v_{rel}}{1+\delta\left|v_{rel}\right|} & \textit{slip condition with } v_{rel}\neq 0 \end{cases} \quad \ldots\ldots\ldots (4.9)$$

This equation can describe the motion of the hysteresis phenomenon of the conductor system as a four different sets of ordinary differential equations: the first is for the stick, the second is for the transition from stick to slip, the third for the slip phase and the fourth back from slip to stick phase. Using quasi-static analysis, this process starts from an initial state which after a certain time step, then due to slippage the conductor goes into slip mode and thus there will be transitions from stick to slip with intermediate process. This process is similar to switching operation. Having then evaluated the first switching point, a new process is then initiated with a modification to the set of differential equations. In this state, the conductor initial condition is identical to the state at the switching point or transition point. At end of slippage there is the second switching as the transition from slip to stick. This process continues as a 'to and fro' motion for the periodic motion.

The periodic solution of the hysteresis time-dependent with contact friction model was then formed. The conditions for changing from the stick mode to the slip mode and vise-vasa are operated as switches between the systems equation as described by sets of condition equations as applied to equation (4.9) are given by the following condition equations.

If $F_{stck} > F$ then

$$\dot{x} = f(x) = [\textit{The equation of solid beam is used}] \qquad \textit{stick} \quad \ldots\ldots\ldots\ldots\ldots\ldots \text{(4.10a)}$$

Else if $F_s > F$

$$\dot{x} = f(x) = [\textit{The equation of composite beam is used}] \qquad \textit{stick to slip} \quad \ldots\ldots \text{(4.10b)}$$

Else $F_s = F$

$$\dot{x} = f(x) = \begin{bmatrix} \textit{The equation of composite beam is used in} \\ \textit{which the strands are completely free to move} \end{bmatrix} \qquad \textit{slip} \quad \ldots\ldots\ldots\ldots \text{(4.10c)}$$

Else if $F_s > F$

$$\dot{x} = f(x) = [\textit{The equation of composite beam is used}] \quad \textit{slip to stick} \quad \ldots\ldots\ldots \text{(4.10d)}$$

Firstly, the stick states where the system was considered to be at equilibrium. In imposing bending, during the sticking, the friction force rises until a maximum value is reached and this is the static friction force also known as breakaway friction force. The time-dependent static friction model, considers the static friction force to be dependent on the stick time. The static and kinetic friction forces can be evaluated by equations (2.46) and (2.47) and now expressed as:

$$F_{stick} = T_{stick}(\varphi) \qquad \ldots\ldots\ldots\ldots\ldots\ldots\ldots\ldots \text{(4.11a)}$$

$$F_{slip} = T_{slip}(\varphi) \qquad \ldots\ldots\ldots\ldots\ldots\ldots\ldots\ldots \text{(4.11b)}$$

The externally applied force on the conductor system, is then transferred to the strands causing its displacement. If the conductor state lies within the stick regime the conductor assumes a solid mass. If the imposed deformation on the strand which is a function of the force applied forces on the conductor structure exceeds the breakaway friction force acting at the contacts area, the system is considered to be experiencing a transition from stick to slip. The system is considered to be in the slip mode if there is relative velocity as a result of inter-strand motion. When in the slip mode, the slippage is defined by a sliding velocity which is defined by the wave speed across the conductor.

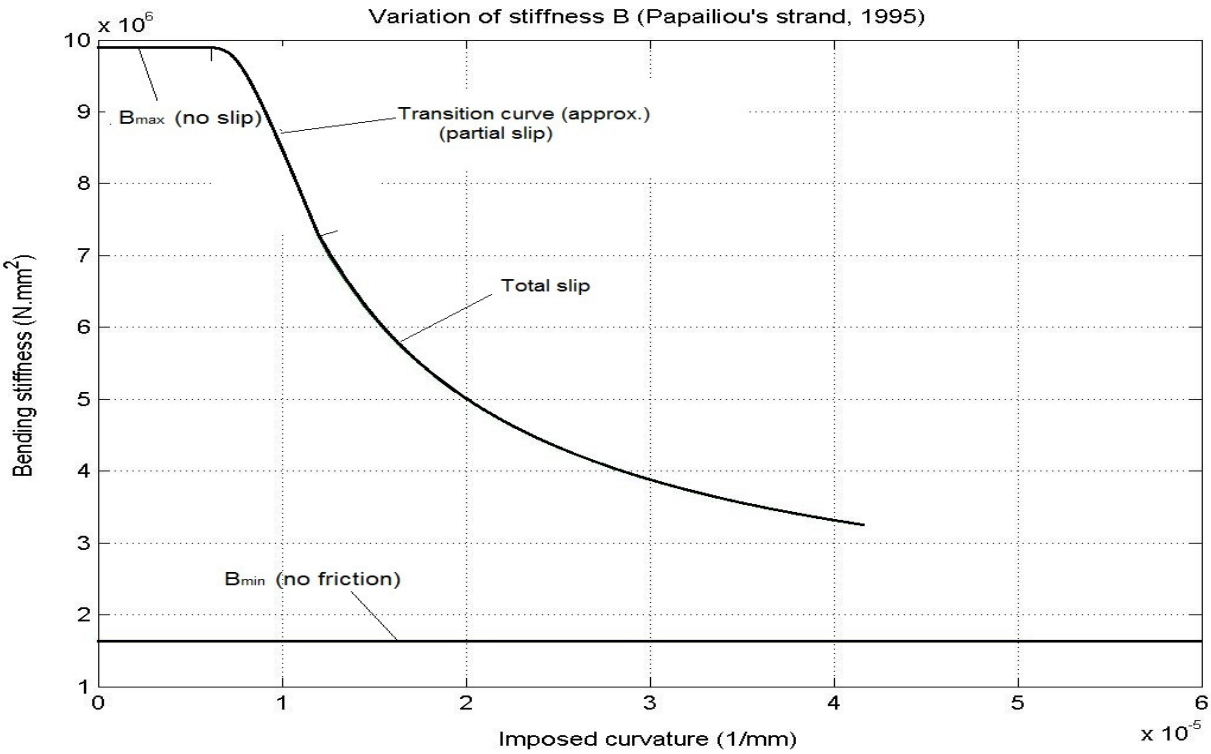

Figure 4.4: The graph of bending stiffness and curvature [57]

The motion was necessary for the computation of the strand displacement and the subsequent evolution of energy dissipation as the conductor goes from stick to slip and from slip back to stick. Figure (4.4) shows the transition from stick to total slip as a function of the bending stiffness and the imposed curvature. The switch mode alternating between the stick and slip regime gives rise to the hysteresis phenomenon as explained in the next section.

4.6 Hysteresis Damping

A system with hysteresis can be described as a system that may be in any number of states, independent of the inputs into the system. Generally, a viscoelastic material in terms of damping has the properties to generate the hysteresis loop as represented by the stress-strain curve shown in figure (4.5). Viscoelastic material is a material that behaves elastically, but also has damping ability when stress is applied and removed. The Kelvin-Voigt model, also known as the Voigt model, can be used to model the viscoelastic behaviour of materials in relation to the energy dissipation.

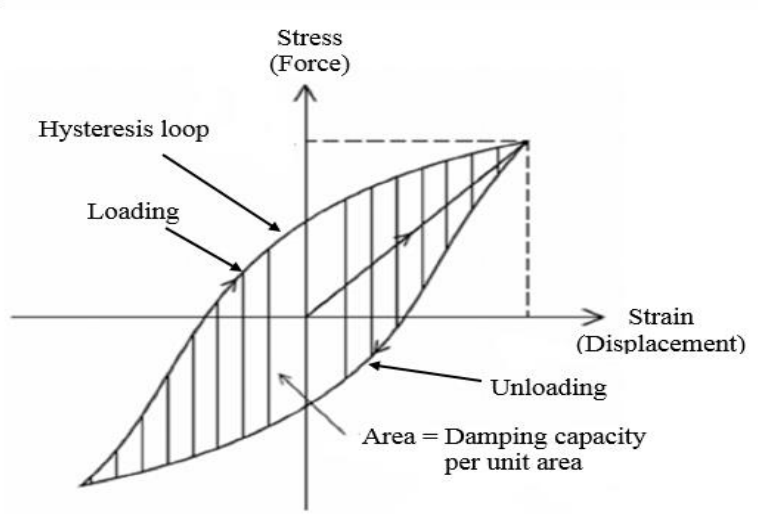

Figure 4.5: The formation of hysteresis Loop under periodic loading

The model constitutive relation is expressed as a linear first-order differential equation:

$$\sigma(t) = E\varepsilon(t) + \eta \frac{d\varepsilon(t)}{dt} \qquad \text{..... (4.12)}$$

The hysteresis phenomenon in viscoelastic materials, if cyclic loading was applied, hysteresis (a phase lag) occurs between the load and the displacement to form a loop. In comparison, the conductor exhibits a similar response to that of viscoelastic material. Therefore, the conductors can be considered as viscoelastic material that exhibits both viscous and elastic characteristics. This implies that the stick-slip model of a conductor, also exhibits the phenomenon of hysteresis loop as shown in figure (4.5). The area covered by the hysteresis loop represents the energy dissipation from the system. The phenomenon of hysteresis was discussed in the previous section as alternating processes between the maximum and the minimum bending stiffness leading to a dissipation of mechanical energy. The bending stiffness on the conductor at a particular point depends on the rate of application of the bending load. This process represents conductor undergoing reversible, viscoelastic strain. Upon application of a constant stress, the material deforms at a decreasing rate, asymptotically approaching the steady-state strain. When the stress is released, the material gradually relaxes to its un-deformed state. For the periodic stress, the stick-slip model is quite the realistic model for the conductor as the predicted strain tends to the ratio of the stress to Young's modulus as time continues to infinity. Due to the repeated cyclic displacement of strands, a hysteresis loop is formed.

The explanation of the formation of the hysteresis loop with regards to strands displacement, due to bending, as a sinusoidal deflection is imposed on the strands including core. The imposed bending causes the shearing force between strand to increase until the shear forces between strands succession in different layers and core reaches the maximum admissible friction force;

subsequently, strands slide over. The process causes the strands to displace away from other strands. This produces the behaviour of a strand with a uniform state of axial pressures by imposing the continuity of displacement at contacts regions in a form of slip. Considering this slip in these regions under the imposed constant radius and sinusoidal bending, using the Coulomb friction law gives some form of energy conversion, with stress being generated. However, the sinusoidal bending yields discontinuous stress and strain both as a function of axial tension, and this process imposes constrain on the transition points between stick and slip regions. In summary, the energy dissipation is consequently due to the stick-slip process and this occurs due to the continuous gross sliding of the strands as periodic process takes place as a transition between the stick and slip conditions.

4.7 The hysteretic behaviour of Conductors

The composite structure of the conductor when subjected to external force, this induces shearing force, with impending slip and ultimately the gross slipping at the interlayer strand contact interfaces. The sinusoidal nature of the force causes a form of a to and fro harmonic motion (oscillation). This oscillatory motion makes the conductor to be considered as stick-slip system as explained in the previous section. During the bending, the traction force at the point of contact between the strands, at a critical point is overcome by the bending. The continuous sliding around the contact regions against friction leads to energy dissipation. This is due to friction as the conductor flexes with relative displacements between strands.

This form of motion with the presence of the frictional forces at the surface of contacts cause shears strains, resulting in structural damping. A single conductor strand is shown figure (4.6). This static configuration of the strand is a function of the axial load and gravity, thus assume deformed state.

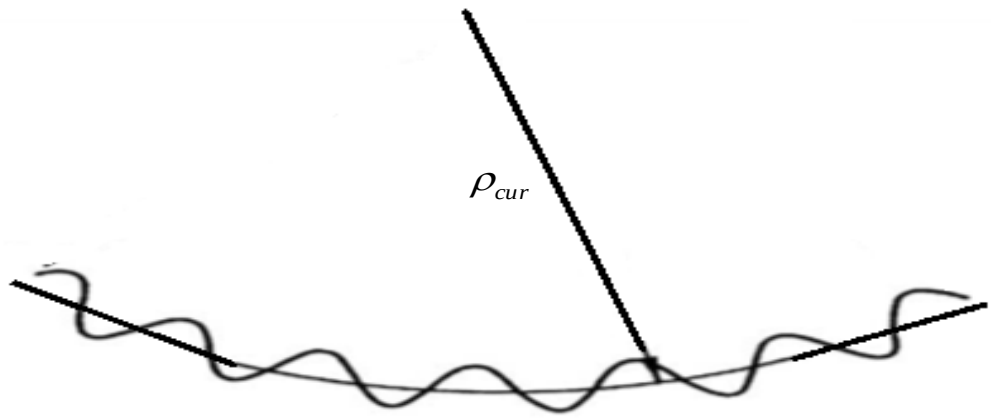

Figure 4.6: A single strand in bending

The resultant deformation, due to curvature, every point on the strand of the conductor was bent as a form of rectilinear helical strand. The strand is assumed to have a variation of curvature that

equal that of the central strand or core. This assumption is sufficiently correct if the radius of curvature is much greater than the radius of the conductor. Otherwise, the calculated stress is that of the average. This is because the radius of curvature of every strand as a beam depends on its position with respect to the origin of the strand axis to the radius of curvature.

The figure (4.6) shows the values of the radius of curvature, ρ of a single stand. It is necessary to know the radius of curvature and that the axis of the conductor assumes a deformed state when it is strung on the towers. Because this will help to evaluate the imposed bending moments on the strand. By setting up the equation for a deformed thin beam in space also using this equation for the strand as it is being subjected to only bending moment.

The radius of curvature was already defined by equation (2.25). The change in curvature expressed a reciprocal of the radius of curvature, it is obtained as:

$$\Delta\kappa = \frac{1}{\rho} = \frac{\sin^2 \alpha}{r} \qquad \text{..... (4.13)}$$

The equation for the bending moments of the strands can be expressed as:

$$m_b = EI\ \Delta\kappa \qquad \text{..... (4.14)}$$

Hence, referring to the bending loading on a single strand as shown in figure (4.6), a typical cross-sectional moment-curvature relation for the strand is comprised of two linear regions, with tangent stiffness, the maximum $EI_{\max}$ and the minimum $EI_{\min,}$ which are related through a smooth non-linear curve as shown in figure (2.7). This non-linear transition is physically related to the evolution of the inter-strand relative displacement. When the sign of the bending load reversed at the completion of the half cycle as in the case of cyclic bending loading, the moment-curvature relation shows symmetric hysteretic cycles. This leads to the formation of a cycle due to the inter-strands relative displacements which is related to the power dissipated, see [16] for a more detailed discussion on the topic.

4.8 The Bending Moment-Curvature Relations

Generally, the bending moment-curvature analysis is a means to accurately determine the load-deformation behaviour of a structure using nonlinear material stress-strain relationships. For a given axial load for a conductor there exists an extreme axial strain and a section curvature at which the nonlinear stress distribution is in equilibrium with the applied axial load. The extreme strain and section curvature can vary for a range of moment-curvature values. A conductor is considered as a composite structure with a peculiar internal sub-structure (the strands) that directly affects its overall mechanical response. This form of structural arrangement of strands makes the analysis of moment-curvature very difficult.

The analysis of the moment-curvature relations, starting with the single layer conductor. Starting with a single layer conductor has the advantage of extending the concepts derived for the single layer conductors to the multilayer conductors. When a curvature is imposed on the conductor, the lay cylinder is deformed as shown in figure (4.6) and the curvature varies along the strand path over a pitch length. The axial load on a conductor generates a normal contact force at the contact region, see details in chapter 2. As the curvature is imposed, slip between core and helical strands are prevented by friction force, generated by the normal contact forces. According to Coulomb's law, the no-slip condition implies that at each point on the contact lines, imposed shear force is less than the friction force. Hence, the conductor is assumed to behave like a solid continuous beam. This is the stick state and the classical Bernoulli-Euler beam theory can be applied. Using the Bernoulli-Euler hypothesis, one gets the bending moments as the strands moments are proportional to the distance from the conductor section neutral axis. A unique bending moment can be calculated at this section curvature for the stress distribution.

Also discussed in chapter 2, due to the imposed stress, the bending moment on a conductor strand has two components: the normal and secondary moments. The combined moments can be expressed as:

$$M = M_{normal} + M_{secondary} \qquad \text{..... (4.15)}$$

Using the Bernoulli-Euler hypothesis the conductor bending stiffness takes its maximum value $EI_{\max}$. The corresponding bending moment is given by the usual expression and for the stick condition:

$$M = EI_{\max}\kappa = EI_{\min}\kappa + EI_{comp}\ \kappa \qquad \text{..... (4.16)}$$

The total bending stiffness of the conductor before any slippage occurs must also include the strands own bending stiffness $EI_{\min}$. Thus the conductor maximum bending stiffness is:

$$EI_{\max} = EI_{\min} + EI_{comp} \qquad \text{..... (4.17)}$$

Expressing the above equation in terms of the bending stiffness and curvature:

$$M = EI_{\max}\kappa = EI_{\min}\cdot\kappa + EI_{\sec}\cdot\kappa \qquad \text{..... (4.18)}$$

When the strand is bent, strands tend to slip relatively over each other, as a consequence of the axial force gradient generated along their length. Relative displacements are contrasted by the friction forces, which are developed at the contact surfaces as a function of the internal geometry of the strand, the material properties of its components and the inter-layer contact pressures.

When the forces which tend to initiate the sliding are greater than the friction force, then strands undergoes relative displacements with respect to their neighbouring strands. If, at a certain location

in given layer, *i*, strand (i) is in the slip regime, then its normal force F_i contributes a moment with respect to the neutral axis which is given by:

$$M(i,j) = F_T\left(e^{\mu\theta(i,j)\sin\alpha} - 1\right)R\sin\theta(i,j)\cos\alpha \qquad \text{..... (4.19)}$$

$$M_{Comp} = 2RF_T\cos\alpha\sum_{i=1}^{3}\left(e^{\mu\theta(i,j)\sin} - 1\right)\sin\theta(i,j) \qquad \text{..... (4.20)}$$

For the slip condition

$$EI\cdot\kappa = EI_{\min}\cdot\kappa + M_{\sec} \qquad \text{..... (4.21)}$$

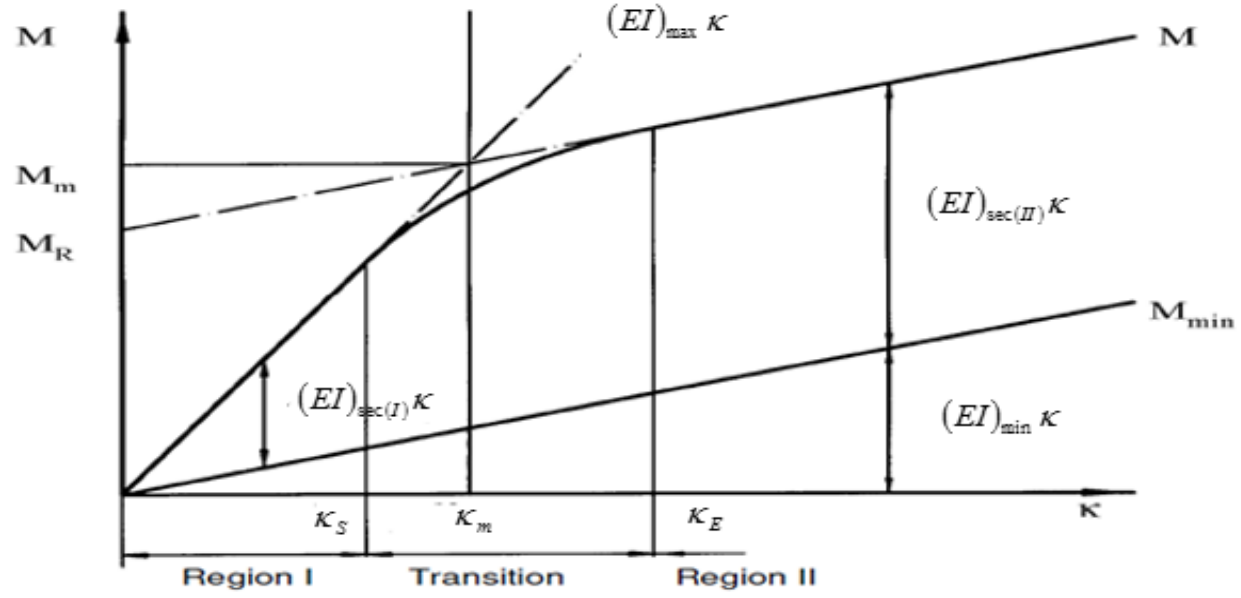

Figure 4.7: The graph of bending moment versus curvature [57]

The diagram for bending moments against curvature for the single conductor is shown in figure (4.7). The slope of a straight line corresponds to the residual bending stiffness EI_i: *EI* corresponds to $EI_{\max}$, EI_{1I} corresponds to the (n-1) sticking layers plus the layer, *i*, minimum bending stiffness when total slip has been reached.

As illustrated in the diagram, as long as $k < k_S$, there is no slip, and the conductor is assumed to behave as a solid beam and indicated in diagram, region I illustrates the behaviour of the conductor in this state.

When the conductor experiences slip, it goes through a transition from region I to region II. At this stage moment-curvature (M vs k) relationship is indicated by region II. Beyond complete slip curvature, the total moment on the section can be obtained as:

$$M_{II} = EI_{\min}\cdot\kappa + M_{\sec} \qquad \text{..... (4.22)}$$

In figure (4.4), it will be imperative to determine the curvature for two limit cases of bending. The first correspond to a full *stick state*, in which friction forces are high enough to prevent any relative sliding among strands all along the strand. In this case, the cross sections of the strand remain plane and their bending stiffness takes the upper bound value, $EI_{\max}$, close to that of a solid circular beam with the same diameter as that of a similar conductor. The second limit case, instead, is attained when the friction forces are no longer able to contrast any relative displacement between stands, which as a consequence behave independently. In this case the plane section hypothesis is no longer valid and the cross section bending stiffness takes the lower bound value, $EI_{\min}$. The expressions to evaluate the bending stiffness limit values [52]:

$$EI_{\max} = EI_0 + \sum_{i=1}^{N} n_i \cdot \cos\alpha_i \cdot EI_i + \sum_{i=1}^{N} \frac{n_i}{2} \cdot \cos^3\alpha_i \cdot R_i^2 \cdot EA_i \qquad \text{..... (4.23)}$$

$$EI_{\min} = EI_0 + \sum_{i=1}^{N} n_i \cdot \cos\alpha_i \cdot EI_i \qquad \text{..... (4.24)}$$

The next step is to determine limit curvatures which have to be imposed on the conductor strands in order to attain these bending moments or bending stiffnesses. Based on work as documented in [57], the curvature imposed on a strand as the starting and end curvatures from start and completion of the strand displacement were determined for a conductor cross-section, based on the balance of forces on the individual affected strand elements. The imposed dynamic loading resulting in a change of curvature, and when a critical curvature is exceeded ($k > k_S$), slip occurs over a bounded domain of each contact line. Because of the imposed curvature, normal force on a conductor cross section is a function of cross sectional angle $[-\pi/2 \le \theta \ge \pi/2]$ from the neutral axis.

The starting and end curvature can be evaluated as [58]:

$$\kappa_S = \sigma_i \frac{\mu \sin\alpha_i}{E_i R_i \cos^2\alpha_i} \qquad \text{..... (4.25)}$$

$$\kappa_E = \sigma_i \frac{\left(e^{\mu \sin\alpha_i \frac{\pi}{2}} - 1\right)}{E_i R_i \cos^2\alpha_i} \qquad \text{..... (4.26)}$$

To extend the bending moment-curvature relation developed for single layer conductors to multi-layer conductors, will pose some challenges. This is because, how to determine the curvature necessary to initiates slip in different layers. This poses the question, how will slip be initiated in various layer in the multiple layer conductor. The problem encountered in this regard is how the slipping pattern from one layer to the other is. There are two hypotheses in this regard. The first is the notions that slip in a given layer start and stop, before being imposed on the next layer [58].

This assumes that there is no overlap of the slip phases, meaning total slip is achieved in one layer before the next slip starts in that next layer. The second hypothesis is that slip in a given layer will come to an end after another slip has been initiated in the next layer as documented in the paper by K. Hong [13]. This slipping process will make it difficult to define the boundary conditions between stick and slip zones as a complete slip is never reached in any layer.

The first hypothesis will be used in this study which assumes slip occurs sequentially and indicate that slip will only starts in layer, *i*, only after it has been completed in layer, *i* -1,. The reason for this sipping process is that the slip always starts on the conductor layer where strand stress at those two locations keeps its initial at zero curvature. Because the inter-layer pressure is higher between inner layers, and also because the maximum tensile force on the strands (due to bending) is smaller due to their closeness to the neutral axis, slip phases start sequentially, from the outer layer to the inner ones.

As explained in [57] moment the curvature relationship for multiple layered conductors

$$M = EI_{\max}\kappa + M_i \qquad \kappa_N \le \kappa \le \kappa_{N-1} \cdots \kappa_1 \qquad \text{..... (4.27)}$$

Where the residual moment of friction is

$$M_i = \sum_{i=N}^{1} M_{rf,i}$$

The expression for the total slip state for a given layer, *i*, when reached, the friction residual moments between layers, *i*, and *i* +1, is given as

$$M_{rf,i} = 2R_i F_{A,i} \cos\alpha_i \sum_{i=1}^{n_i/2} \left(e^{\mu\theta_i \sin\alpha_i} - 1\right)\sin\theta_i \qquad \text{..... (4.28)}$$

This condition is the same as the one obtained for the single layer conductor. This yields the same equations for the limit curvatures, but the parameters are those pertaining to each layer, *i*.

Thus, for layer, *i*, the incipient slip curvature is given by the modified equations (4.25) and (4.26) respectively:

$$\kappa_{S(i)} = \sigma_i \frac{\mu_i \sin\alpha_i}{E_i R_i \cos^2\alpha_i} \qquad \text{..... (4.29)}$$

$$\kappa_{E(i)} = \frac{\sigma_i}{E_i R_i \cos^2\alpha_i}\left(e^{\mu_i(\pi/2)\sin\alpha_i} - 1\right) \qquad \text{..... (4.30)}$$

The above two equations was used to determine the inception and completion of the slip in various layer as the slip start from the outer layer and propagate through various layer to the inner layer,

thus the curvatures takes the form $\kappa_N \leq \kappa_{N-1} \leq ... \leq \kappa_2 \leq \kappa_1$. The plot of the bending moment against the curvature is shown in figure (4.8).

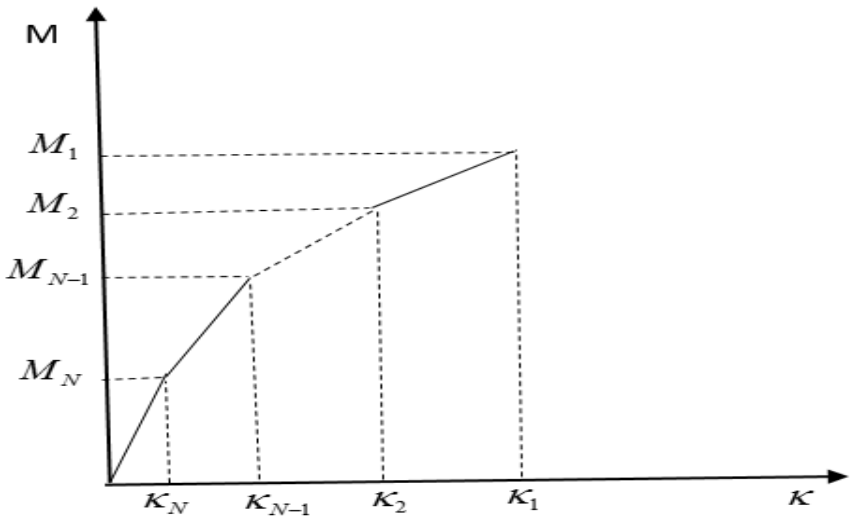

Figure 4.8: The plot of bending moment versus curvature for multi-layer conductor

4.9 The Formation of the Hysteresis Loop

With regards to the transverse displacements, referring to the bending loading for a typical cross-section, the moment-curvature relation of the strands can be described by two regions, with maximum tangent stiffness and with minimum tangent stiffness, which are related through a smooth non-linear curve. This non-linear transition between these regions is physically related to the evolution of energy at the inter-strand contact due to relative displacement.

As the conductor experiences cyclic bending loading, as the sign of the bending load is reversed, the moment-curvature relation will exhibit a symmetric hysteretic cycles. The area of the cycle can be related to the power dissipated through the inter-strand relative slip.

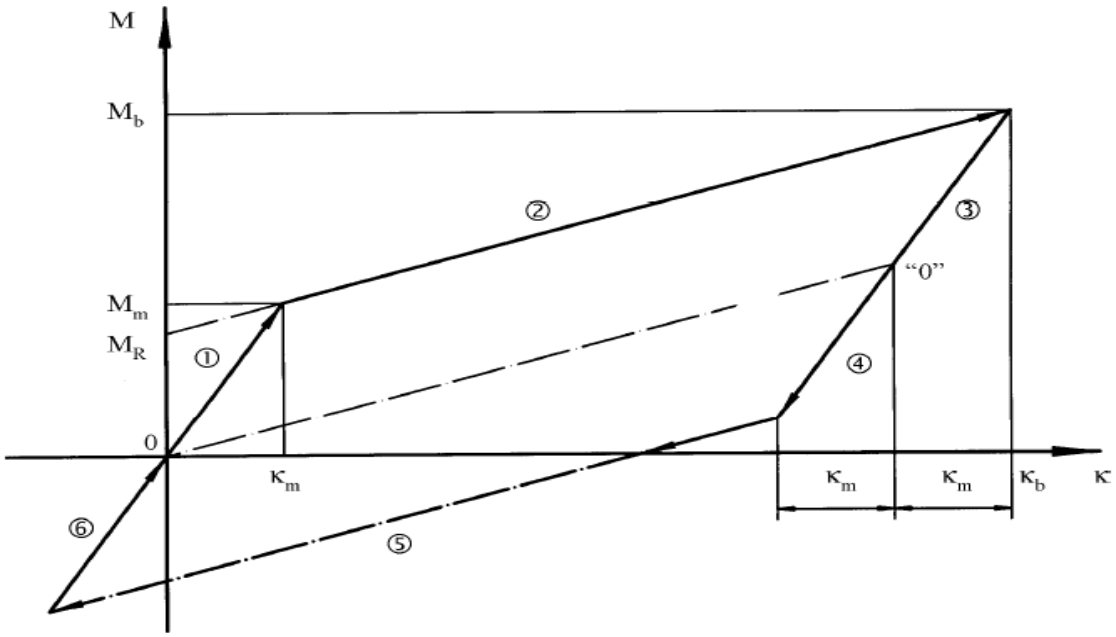

Figure 4.9: Phases for the formation of the hysteresis loop [57]

To develop the hysteresis loop as the function of the bending moment, in [57] the relationship between the bending moment and the curvature was used to generate the hysteresis loop, illustrated using the diagram shown in figure (4.9). The formation of the hysteresis loop as shown involves six phases.

In phase 1, as the imposed curvature exceed the limit curvature, slip occurs in the strands and the bending moment can be obtained as:

$$m_s = M_m = EI_{\max}\,\kappa_b \qquad \text{..... (4.31)}$$

The strand then enters the next mode which is phase 2 and the bending moment in the phase can obtained as:

$$m_s = M_b = EI_{\max}\kappa_b + EI_{nim}\kappa_m \qquad \text{..... (4.32)}$$

In phase 3, for there to be reversal, the bending moment will have a slope as that of phase 1. As indicated in chapter 2, for a complete reverse process equal twice the curvature. The next phase is 4 which has equal curvature as that of phase 3. After phase 4, the strand enters the slip mode again parallel to the phase 2, this is phase 5. The loop is completed with phase 6, which is when the transitions moves back to the origin. To represent this hysteresis loop, a smooth hysteresis model is required, in this study the Bouc-Wen model was used.

4.10 The Bouc-Wen Hysteresis Model

Generally, hysteresis phenomenon that occurs in dynamic systems is due to dependence of the input-output parameters on the time history. The relation between the output and the input variables

forms a loop and such loop occurs due the dynamic lag between input and output parameters. This phenomenon can be represented using the phenomenological model and with a resultant loop formation as shown in figure (4.11). This phenomenological behaviour can be represented by a means of the classic hysteretic models. The smooth hysteretic model presented herein is a variation of the model originally proposed by Bouc [20] and modified by Wen [21]. Documented in [82, 83] were the application of the Bouc-Wen hysteresis models in different areas of structural dynamics. The Bouc–Wen model as used for the smooth hysteresis representation has received an increasing interest in the last few years. This is due to the ease of its numerical implementation and its ability to represent a wide range of hysteresis loop shapes. The Bouc-Wen Hysteretic model is capable of simulating stiffness degradation, strength deterioration.

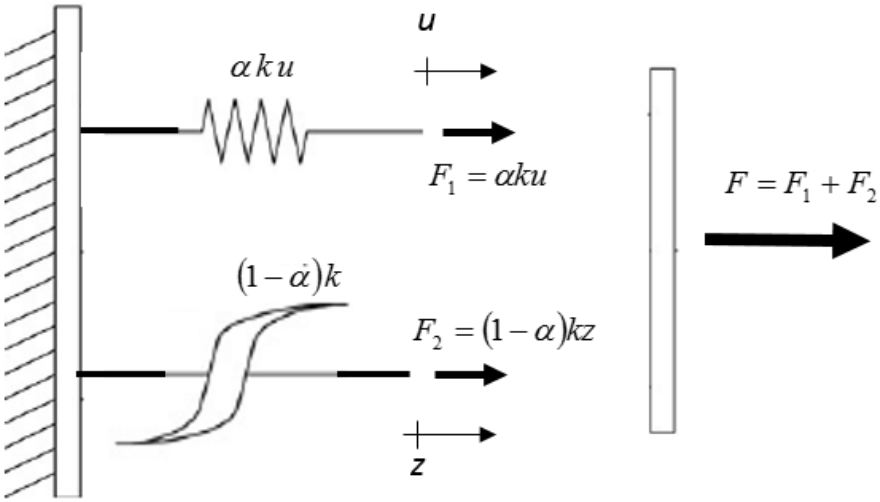

Figure 4.10: The Bouc-Wen Model

Generally, this model consists of a first-order nonlinear differential equation that contains some parameters that can be chosen, using identification procedures, to approximate the behaviour of given physical hysteretic system. By implementing the Bouc-Wen model to the dynamic systems as shown in figure (4.10), one obtains a single non-linear first order equation which can describe the evolution of the damping force developed by a device for almost any loading pattern (periodic, aperiodic or random). The Bouc-Wen model is defined as:

$$F = \alpha K u + (1-\alpha) K z \qquad \text{..... (4.33)}$$

Where $F = F_1 + F_2$ and z is a displacement parameter that controls the response of the non-linear of restoring for and it is governed by the differential equation:

$$\dot{z} = A\dot{u} - \beta|\dot{u}||z|^{n-1} z - \gamma\dot{u}|z|^n \qquad \text{..... (4.34)}$$

$$\frac{dz}{du} = A - \beta \frac{|\dot{u}|}{\dot{u}} |z|^{n-1} z - \gamma |z|^{n} \quad \text{..…….…….} (4.35)$$

Where A, n, β and γ are the set of parameters that controls the hysteretic response of the nonlinear element.

In the formulation of the smooth hysteresis loop, the hysteretic characteristic is a symmetric loop formed between the restoring force ($-F_{\max} \leq F(u) \leq F_{max}$,) obtained for a periodic motion between the displacement ($-u_{max}(t) \leq u(t) \leq u_{max}(t)$), and the displacement is a function of the excitation. Most often, the force-displacement characteristic of most systems is of hysteretic type is shown in figure (4.11).

The hysteresis behaviour of the conductor is a time-dependent process where the output variable is a function of the past inputs.

.

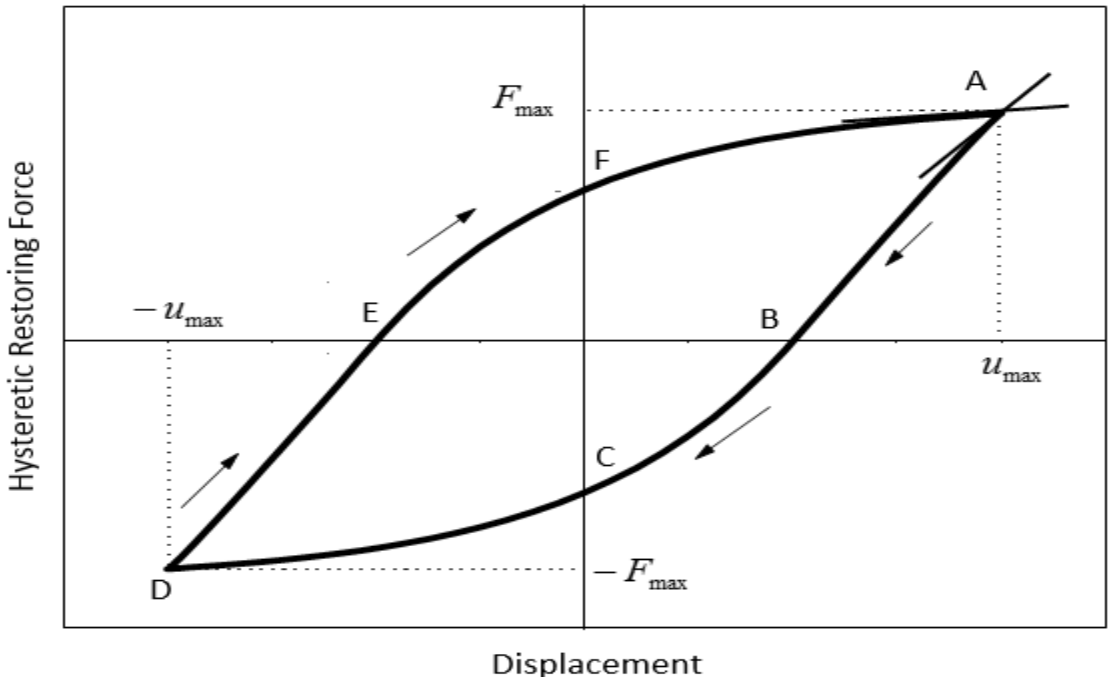

Figure 4.11: Bouc-Wen hysteresis loop

To implement this model for the conductors, under the excitation process, the vortex shedding induces a periodic oscillation resulting in the restoring force at the inter-strand interfaces which causes it to displaying the hysteresis phenomenon. This time-rate dependent phenomenon results in the restoring forces trying to counter the strands movements and that leads to dissipation of energy. The incremental constitutive relation of moment-curvature conforms to the hysteretic behaviour which can be modelled using the Bouc-Wen model.

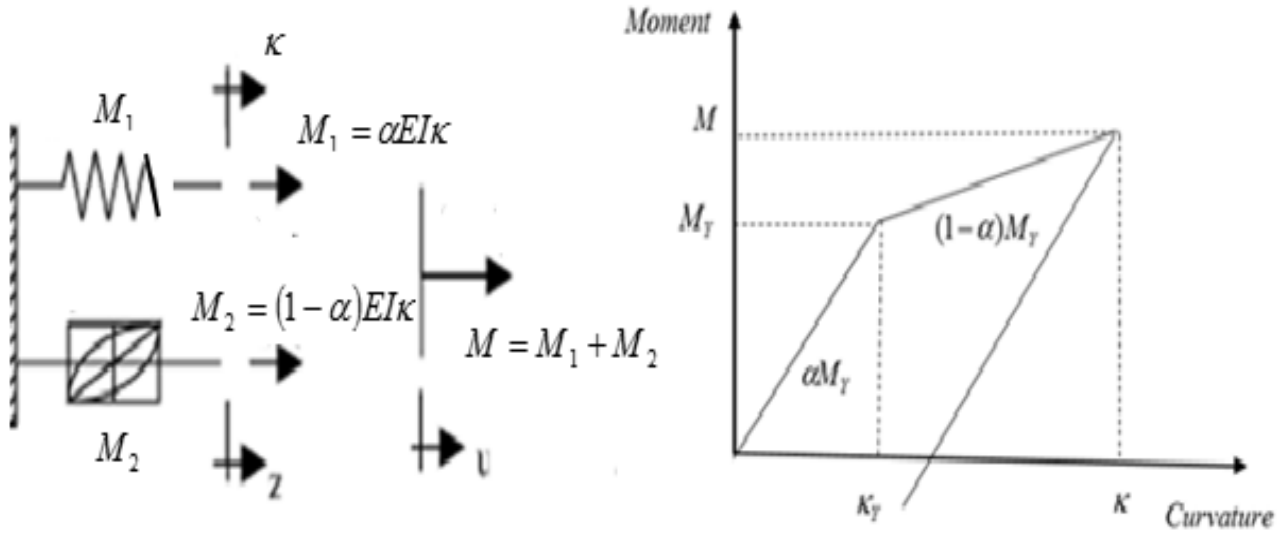

Figure 4.12: The hysteresis Model in terms of bending moment-curvature relation

To achieve the hysteretic modelling, the use of such a hysteretic constitutive law is necessary for the effective representation of the behaviour of the conductor under cyclic loading, since as the conductor structures undergo inelastic deformations, this cyclic behaviour weaken the conductor structure and so there is a loss in stiffness and strength.

The application of Bouc-Wen model to model hysteresis behaviour of conductor as related to the energy dissipation was done as function of the bending moment and the curvature, denoted *M* and *κ* respectively. The form of the Bouc-Wen model as related to the moment-curvature relation, and the model was considered as the coupling of a linear and non-linear element in parallel as shown in figure (4.12).

The relation between bending moments and curvatures can be expressed as:

$$M(\kappa) = M_Y\left[\alpha\frac{\kappa}{\kappa_Y} + (1-\alpha)z\right] \qquad \text{..... (4.36)}$$

Where M_Y is the yield moment; κ is the yield curvature; α is the ratio of the post-yield to the initial elastic stiffness and z is the hysteretic component defined as:

$$M(\kappa) = M_Y\left[\alpha u + (1-\alpha)z\right] \qquad \text{..... (4.37)}$$

The yield moment can be evaluated by:

$$M_Y = EI_{\max}\kappa = EI_{\min}\cdot\kappa + EI_{\sec}\kappa \qquad \text{..... (4.38)}$$

To model the hysteretic behaviour of conductor with the two parallel springs; one linearly elastic and one elasto-plastic spring with changing stiffness upon yielding. The combined stiffness is given as:

$$EI = EI_{elastic} + EI_{hysteresis} \qquad \text{..... (4.39)}$$

In relation to equation (4.33), where the post-yielding stiffness of the linear elastic spring and the stiffness of the hysteretic spring can now be expressed as:

$$\frac{dF}{du} = \alpha K + (1-\alpha)K\frac{dz}{du} \qquad \text{..... (4.40)}$$

$$\frac{dF}{du} = k_0\left\{1-(1-\alpha)\left[\operatorname{sgn}(du)\operatorname{sgn}(z)\beta+\gamma\right]|z|^n\right\} \qquad \text{..... (4.41)}$$

The bending moment-curvature relation in terms of the Bouc-Wen model for the conductor can be obtain by comparing the F and u in the force-displacement in equation (4.33) as exactly as M and κ in the moment-curvature relation. This can then be used to model the hysteretic response of the conductor and upon the substitution this yields:

$$\frac{dM}{d\kappa} = EI_{\max}\left\{1-(1-\alpha)\left[\operatorname{sgn}(d\kappa)\operatorname{sgn}(z)\beta+\gamma\right]|z|^n\right\} \qquad \text{..... (4.42)}$$

$$\dot{z} = A\dot{\kappa} - \beta|\dot{\kappa}||z|^{n-1}z - \gamma\dot{\kappa}|z|^n \qquad \text{..... (4.43)}$$

In this context of evaluating damping, the energy liberated is frequency dependent and the hysteretic behavior of the conductor exhibits stiffness degradation. The stiffness degradation occurs as the conductor moves from stick to slip states.

The analytical expressions for the dissipated energy, taking into account the frequency of vibration can be achieved with respect to the steady-state response under symmetric wave periodic input. This input can be expressed by the sine waves. Thus, the bending moment as a function of the periodic excitation frequency is defined as:

$$M = EI\kappa\sin\omega t \qquad \text{..... (4.44)}$$

Where ω, is the frequency of excitation.

Under this periodic excitation, the response varies asymptotically with periodic input and the hysteretic loop is traced repeatedly. The characterization of the hysteresis loop boundary conditions was done using the initial and final curvature as define by equations (4.25) and (4.26) for the single layer conductors and equation (4.29) and (4.30) for the multiple layer conductors. Thus, the energy dissipation as a function of friction at the contact points, defined in relation to the bending moment and curvature generates the loop as shown in figure (4.13).

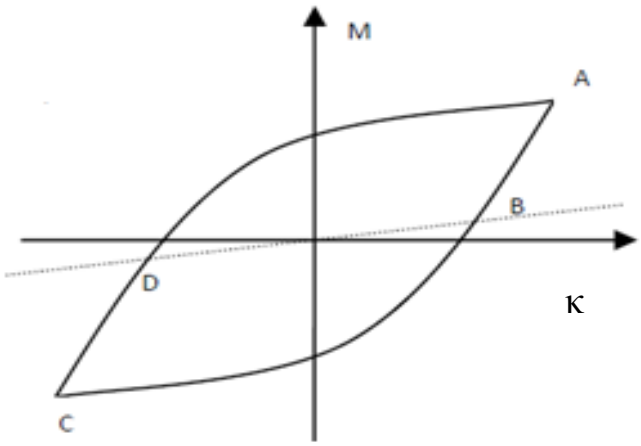

Figure 4.13: The Bouc-Wen hysteresis loop (M vs *k*)

To implement the Bouc-Wen model, the hysteresis parameters in equation (4.43) has to be defined. A developed matlab code was used to implement various combinations of these hysteretic response parameters. Based on various curves that were developed as compared with the optimized Bouc-Wen model parameters the following parameters, A = 1, β = 0.75, n = 0.75, and ɣ = 0.25, were used to implement the hysteresis model in this study

Chapter 5

The Finite Element Analysis

5.1 Introduction

Most dynamic problems in engineering are modelled using the mathematical equations which in many cases are in the form of partial differential equations. These partial differential equations are usually formulated from physical phenomenon with some assumptions. Analytically, some of these mathematical models sometimes cannot adequately model these physical phenomena or in some worse cases these phenomena cannot be described using any form of mathematical equation. In some situations, where these analytical equations are used to describe a physical problem, this might result in an indeterminate solution. These types of physical problems that do not have closed form solutions; the numerical modelling becomes an option. Numerical modelling techniques give an approximate solution to the problem. The most commonly used numerical tool is the finite element analysis or the finite element method [FEA or FEM]. Though, employing this technique can be complex, but its implementation allows in providing an approximate solution to problems that cannot be solved analytically. Thus, a numerical solution is employed to problems where no closed form solution exists.

Over the years, in many areas of science and engineering especially in structural engineering, the structural modelling and analysis are often done using the concept of finite element analysis. This numerical tool has evolved over the past decades to be the most commonly used form of computational mechanics for most structural modelling, simulation and design analysis of systems. This numerical tool requires the structure to be discretized into smaller components known as the finite element. These finite elements are then analysed as they are subjected to the predicted loads or flux and then assembled into the global structure of the system. The finite element analysis can be used to predict the structure deflections, bending, and torsion in order to determine the induced stresses, strains and the possible structural failure. This tool gives the advantage to the designer to analyse the structure for both the static condition and the dynamic response in order to evaluate the design and operating parameters for the structure. This process helps in both design and modelling stages of the structure in both the static or dynamic conditions and the simulation of all possible structural responses. This can help to redesign or optimize the structure and also help to identify the possible associated risks and failure modes. This process helps to reduce design defects or prevent failure of structure when put in operation.

The use of finite element analysis tool follows well-defined procedures which are documented in several textbooks [84, 85, 86]. The basic technique of the finite element method is the discretization of a structure into its substructure i.e. breaking a complex structure into its finite elements. These finite elements are then defined by the shape functions at the nodes of the discretized finite elements. This is then followed by formulation of the finite element equation for the elements. The finite element equations are then assembled to form the system equation. Taking into consideration the boundary conditions, then the system equation is solved for the field or load or flux of interest.

One of such physical phenomenon that cannot be model adequately by analytical model is the mechanical vibration of transmission line conductors. In chapter 3, the developed analytical equations used to model conductor vibration were explained and the limitations of these models were discussed in terms of the geometric representation. Due to the failure of the analytical models to adequately represent the phenomenon of conductor vibration, the numerical modelling becomes a more acceptable alternative. The concept of using FEM to investigate the vibration of power line conductor was done in this chapter in terms of formulation, simulation and analyses. The FEM for the conductor was used to determine parameters such as natural frequencies, mode shapes, and the amplitude of vibration. Also, the FEM was also used to characterize damping around the inter-strand contacts which was used to evaluate the conductor damping.

5.2 Conductor Finite Element Analysis

Chapter 3 considered the vibration of distributed parameter system for the conductor, to obtain variables such as natural frequencies, mode shapes, stresses and strains. Many engineering problems are solved by analyses based on ideal models of an actual system. For the transverse vibration of the conductors, the ideal models such as taut string and beams are usually employed. In the case of power line vibration, because it is a bundle structure using an equivalent model gives solutions that are useful though not adequate. In terms of the geometric profile, however, the equivalent beam-like elements do not adequately represent the real-world scenario.

Employing the finite element method can be used to obtain an approximate solution for complex engineering problems such as the conductor mechanical vibration. The basic concept for implementing this method is the discretization of the structure and replacing the structure by the assembly of it simpler substructures. This approach gives an approximate solution rather than the exact solution.

Over the years, considerable efforts have been made in the formulation of models to predict the mechanical characteristics of power line conductors experiencing transverse vibration. In this study, focus is given to the understanding and gaining more insight into the nature and mechanisms

of conductor mechanical vibration. This was done with regards to the geometric formulation with the goal to characterize energy dissipation. Consequently, this was achieved with the aid of the mathematical-analytical tools used to model the conductor as described in chapter 3. This helps to derive the explicit formulae and expressions that was used for the conductor FEM. This mathematical (analytical) tool provides an insight into the concepts that was used in the formulation and implementation of the finite element method (FEM) for the power line conductors. Generally, in solving mechanics problem numerically, the FEM is usually developed for the structure as a boundary value problem. For the case of the conductor dynamic problem, the expression for the problem was developed as a function of both space and time. The conductor dynamics as a boundary value problem, the aspect of interest for analysis can be categorized into three problem areas.

- Firstly, has to do with the aspect of analysing the conductor behaviour, as a static or bending condition experiencing a sinusoidal displacement. This condition can be analysed as an equilibrium or steady-state or time-independent problem. In this case the analysis of the conductor can be done as a function of displacement or stress distribution of the strands.
- Secondly, this is when the conductor is considered as an eigenvalue problem. The area of interest of analysis is that of its resonance characteristics, finding the natural frequencies and mode shapes of the conductor. Also, the wave speed and the loop length may be parameters of interest.
- Thirdly, is when the analysis of the conductor is done in terms of the phenomena that are propagating through the structure either in a steady state, as a periodic function or as a transient problem resulting from decaying amplitude. These cases are time-dependent. The area of interest of analyses has to do with amplitude of vibration and the structural damping.

In modelling the conductor dynamic characteristics using the FEM, the last scenario was used. Thus, presented in this chapter, the conductor systems were analysed as idealized discretised rigid masses of subdomain that are assembled to form the global domain for the conductor as a bundle. The conductor composite structure as a bundle of strands is set into vibration with amplitude that is a function of the input wind loading, the axial tension and damping. The bending of the strands gives rise to the stick-slip phenomenon as explained in the chapter 4 and the process is time dependent. This process produces fretting or energy dissipation. For the case of energy dissipation, finding the response of the conductor strands under the time-varying force with displacement produces hysteresis. This hysteresis phenomenon exhibited by the conductor strands was used to determine the energy dissipation due to the effect of friction.

5.3 FEA Solution Concepts

Generally, the successful formulation, simulation and analysis of the FEM largely depend on the choice of topology, element type, size of element, and node location. The choice for the topology establishes the dimension in which field will be developed, which can be in one-dimension (1D), two-dimension (2D) or three-dimension (3D).

For the FEM formulation for the conductor, the element type used was the curved truss beam or the curved frame element with three degrees of freedom per node. The element size determines the convergence rate, and they also determine the computational cost. The frame element used, which is a 2D model, this means that there is a less computational cost as compared to the 3D formulation. The advantage in implementing this model was based on the fact that the conductor geometry exhibits symmetry which allows the use of relatively large element and solution was expected to be accurate. Also, the conductor strands normally do not have abrupt changes in geometry, material properties, and also external conditions on the body can be divided into equal subdivisions as distributed load or as point load. Hence, the spacing of the nodes can be uniform and relatively large. Thus, in discretizing the conductor domain into the sub-domain, the curved truss beam element was used to model each strand.

The FEA for the conductor starts with the geometric discretization. The geometric model plays key part in application of the finite element method. The geometric formulation for FEM is in line with Cartesian coordinate system described in chapter 2. The accurate geometric formulation for the conductor helps in implementing the FEM process in terms of mesh generation and in the assembly of the finite element. For the geometric formulation, the three-dimensional curve paths of the helixes are used. The defined mathematical geometric equations for helix are formulated around the neutral axis of the core or the central strand depending on the lay direction, either right or left hand lay. This was used to build the composite model of the conductor. All the constructional aspects for the single helix configuration for individual strands in the conductor are specified using the curvilinear path of the helix.

To successfully formulate and implement the finite element conductor model, the following steps will be employed. Firstly, is the generation of the geometric strand model. Secondly, generation of mesh for the strand using the shape functions. Thirdly, was the formulation of the FE equation and the assembly of these equations to obtain the equation for the system in the matrix form. Finally, the formulated conductor FEM and then the analysis of the conductor response under the required loading condition. This is implemented taking into consideration the boundary conditions and the material proprieties of the strand.

5.4 The Conductor 3D Geometric Formulation

The geometric formulation of strands within the conductor plays a key part in the aspect of static configuration for the conductor that can be extended to the dynamic condition. The successful geometric description of conductor in terms of coordinates system was a very useful tool to generate the mesh for the conductor. For the conductor bundle structure, the three-dimensional mathematical equations for the helix were used to produce the strand geometric model. This help to presents the geometric models that fully consider the helix configuration for the individual strand in the conductor. This implies that, the helices formation of strands in layers around the neutral axis; the right hand lay strands are laid in the formation of helices having a right-hand pitch. Also, the left hand lay strands are laid as helices having left hand pitch. By means of the parametric coordinate systems, the determination of the centreline of strands path which are used to helically arrange the strands in various layer of the conductor. The mathematical representation of the helix in the form of the parametric equations with input parameters which is defined in reference to the centreline of the circular cross-section of strands. Thus, the right hand lay and left hand lay direction was used to produce the lay construction in various layers of the conductor.

The generation of the conductor meshes start with defining the geometric path that will later help during the assembly of the finite element. This help in defining the values for the element field variables such as displacement, strain and stress as a function of spatial coordinates. For conductor dynamic behaviour, the element field variables are defined as a function of both the spatial coordinates (x, y, z) and time (t). The geometry (domain or solution region) of the conductor strands was achieved by using the helical symmetry. To obtain the conductor composite geometric, let start with the geometric formulation for the straight/deformed centre core and then extended the formulation to the strands in various layers.

5.4.1 The Cylindrical Core Strand

In chapter 2, the description of a conductor cross section with circular strands was discussed. Also, in chapter 3, the centenary analysis of the static profile of the conductor span was done. The combine descriptions serve as the bases in formulating the geometric model for the conductor as a composite structure. The geometric formulation, the core strand whose centreline is made to coincide with the centreline of the conductor, the coordinates of this centreline is defined by the discretized parametric equations expressed for the straight conductor configurations:

$$\left.\begin{aligned} x(k) &= L_k \\ y(k) &= 0 \\ z(k) &= 0 \end{aligned}\right\} \qquad \text{..... (5.1)}$$

Where $k = 1, 2, 3, ..., m$

m is defined as the number of evenly spaced distance of the core strands along the span

$L_k = L_0 + (k-1)d$ with L_o the initial length of the core, if placed at the origin, $L_k = (k-1)d$

and $d = L/m$

For the deformed configuration with a sag (L)

$$\left.\begin{aligned} x(k) &= L_k \\ y(k) &= \begin{cases} L_{D(k)} = (k-1)d_D & For\ increa\sin g\ sag \\ L_{D(k)} = (k-1) - d_D & For\ decrea\sin g\ sag \end{cases} \\ z(k) &= 0 \end{aligned}\right\} \qquad \text{..... (5.2)}$$

and $d_D = L_D / m / 2$

The core strand is sweep along the centre line part in the form of circular cylinder, whose centreline is identical with equation (5.1). The size of the core circular cross-section was swept along the path defined as:

$$\left.\begin{aligned} x(k) &= L_k \\ y(k) &= R_k \cos\theta_{ij} \\ z(k) &= R_k \sin\theta_{ij} \end{aligned}\right\} \qquad \text{..... (5.3)}$$

Where $0^0 \le \theta_{ij} \le 360^0$

5.4.2 The Cylindrical Helical Strands

The discretization of the conductor's geometric domain for the strands in various layers was defined by the distance from neutral axis of the core strand. The position of the strands in a given layer of the conductor will be governed by the concentric-lay rule. These position of each strand at the origin of the cross-section, in the anticlockwise direction is determined by

$$\left.\begin{aligned} x(i) &= 0 \\ y(i) &= R_i \cos\psi_{ij} \\ z(i) &= R_i \sin\psi_{ij} \end{aligned}\right\} \qquad \text{..... (5.4)}$$

Where $\psi_{ij} = (i-1)\dfrac{360^0}{n_j}$ and $i = 1, 2, 3, ..., n_j$

The parametric equations for each strand centreline along the helical path are obtained as

$$x(k) = \varphi \frac{R_i}{L\alpha}$$
$$y(k) = R_i \cos(\psi_{ij} + \varphi) \quad \text{……..……. (5.5)}$$
$$z(k) = R_i \sin(\psi_{ij} + \varphi)$$

The coordinate's values that determine the size of each strands in cylindrical form as it is being sweep along centreline helical path are defined as

$$x(k) = \varphi_i \frac{R_i}{L\alpha}$$
$$y(k) = R_i \cos(\psi_{ij} + \varphi) + r_i \cos\theta_l \quad \text{……..……. (5.6)}$$
$$z(k) = R_i \sin(\psi_{ij} + \varphi) + r_i \sin\theta_l$$

These parametric equations defined for the conductor geometry were used to model the strands by providing the coordinates for mapping the reference 2D curved beam model. As will be done later, this was used to generate the finite element mesh for the conductor as a composite structure.

5.5 Finite Element Modelling

5.5.1 FEM Modelling Concept

The geometric modelling of the conductor with the coordinates system defined in section (5.4) provides a geometric approach for implementing the finite element analysis for the structure when subjected to dynamic loads. Modelling the conductor as composite structure which considered the conductor as the assemblies of either thin beams or rods having distributed mass and elasticity for which the governing equations of motion for such structures are described by partial differential equations. To find the FEM solution in a closed form for this complicated bundle structure is very difficult and almost impossible. This is due to the fact that the integration of these equations as a bundle is generally more complicated than the FEM solution of a single ordinary partial differential equation, as a governing equation for an equivalent single continuous beam. The single beam FEM model is a simplified model which may be used to represent the conductor. Due to the mathematical simplicity, the FEM dynamic analysis of conductor structure as a solid continuous system has limited use in practice. Nevertheless, the analysis of conductor systems with the beam or taut string as a generic model can provide very useful information on the overall dynamic behaviour of conductor structures.

Contrary to the use of equivalent FEM beam model, in this study because the parameters of interest are related to the conductor internal geometry, the composite model of the assemblies of strands was used. The method of FEM analysis for the conductor is very complex because each conductor strand was subjected to the coupling effect of axial, torsional, and bending. This FEM composite structure concept for the conductor was achieved by the iso-parametric interpolation of the curve 2D beam for each individual strand along the defined geometric path.

5.5.2 The Curved Beams Model

Most FEM formulation for the conductor found in literature were mostly done with the straight beam model. This has restricted the classical beam theory formulation for the conductors to initially straight beams of constant cross-section. This model has been extensively used and has been implemented by several researches investigating conductor dynamics [8, 14]. This simplified model can be accepted in modelling the conductor to some degree of accuracy, but in real problems, where the curvature becomes significant, this model becomes inadequate. In this case for the conductor, the linear variation of strain over the cross section is no longer valid, and the use of curved beam becomes appropriate. Furthermore, curved beams are known to be more efficient in transfer of loads than straight beams, because the load transfer is affected by bending, shear, and axial action. Thus, conductor strands as the form of the sub-structure was modelled by the curve truss beam or the curved frame element.

In this study, the Euler-Bernoulli curved beam theory was used, though there was still the assumption of plane cross sections remaining plane after deformation is valid. The *xy*- longitudinal plane has been assumed to be the plane of symmetry, with the bending load being applied in this plane. The conductor strands deformations are symmetric; this is why the helical strand can be regarded as an example of a curved beam with body force and restrained sections at the ends. From the conditions of symmetry, the distribution of stress in one quadrant of the helical strands can be balanced by the same continuous strand in the opposite quadrant.

5.5.3 The Beam Constitutive Equation

Before the FEM formulation for the conductor using the curved beam, it is imperative to formulate the constitutive equations for the curved beam. Consider figure (5.1), illustrates the Euler-Bernoulli curved beam, with an axial and transverse displacements, and subjected to rotation. The deflection, y is on the single plane perpendicular to the axis of the beam. The cross-section will have constant density, p, constant modulus, E, constant cross-section, A, and inertia, 1. The

deflection, y, and the slope, θ, vary along the cross-section, x, and with time, t. The horizontal displacement at the beginning of the beam cross-section is denoted by *u*.

The forces and moments acting on the beam, these include the vertical forces, *V,* acting at each end of the segment in the same direction as the vertical deflection, and a moment, *M,* at each end as shown figure (5.1). There are also the axial forces, *T*, acting along the beam centreline. Finally, there is the body force per unit length, *pgA*, which represents the weight of the beam. The equations of motion from the forces and deflection can be determine by summing forces along the *x* and y directions and taking moments about the left end. This produces equation for tensile, moment and inertia mass respectively:

$$\frac{\partial T}{\partial x} = \rho g A \qquad \text{..... (5.7)}$$

$$\frac{\partial M}{\partial x} + V = \rho g A \qquad \text{..... (5.8)}$$

$$\rho A \frac{\partial^2 w}{\partial t^2} = \frac{\partial V}{\partial x} + \frac{\partial}{\partial x}\left(T \frac{\partial w}{\partial x} \right) \qquad \text{..... (5.9)}$$

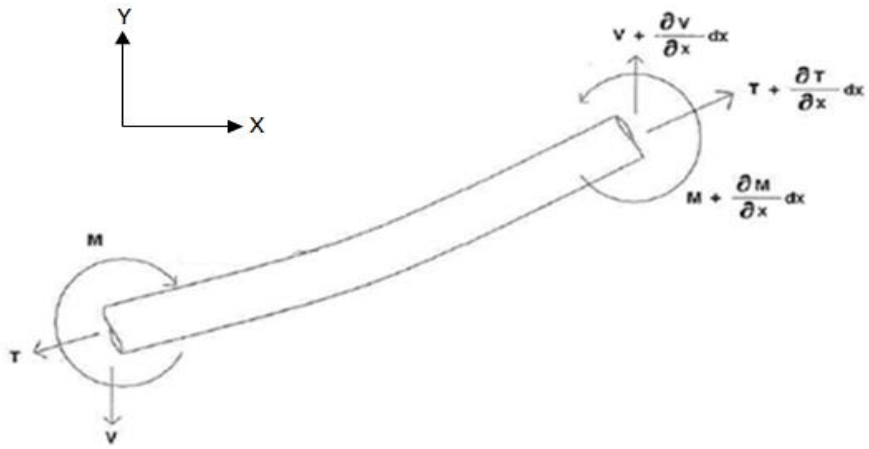

Figure 5.1: Forces and moments acting on the beam

5.5.4 Curved Beam Strain–Displacement Relationships

Consider figure (5.2), let any point on the cross-section of the beam be displaced from its unstrained position through small components of displacements *v* and *u* representing the tangential and radial displacements of points on the cross section, and *y* represent the transverse displacement in a direction normal to the plane of the beam.

The axial displacement at any point (x, y) may be expressed directly in terms of *θ(x)* which is the rotation of the normal to the centroidal axis due to flexural effect, and u(x) which is the axial displacement due to the axial effect and the curvature. The axial displacement for the curved beam is given as:

$$u(x,y) = u_0(x) + \frac{v}{R} - y\left(\theta_x + \frac{u(x)}{R}\right) \qquad \text{..... (5.10)}$$

The ***y*** distance from the centroidal axis of the cross section to the point (x, z) and equals to the lateral displacement at the centroidal axis. The normal rotation θ(x) is equal to the slope of the centroidal axis minus a rotation, which is due to the transverse shear deformation:

$$\theta_x = \frac{\partial v(x,y)}{\partial x} \qquad \text{..... (5.11)}$$

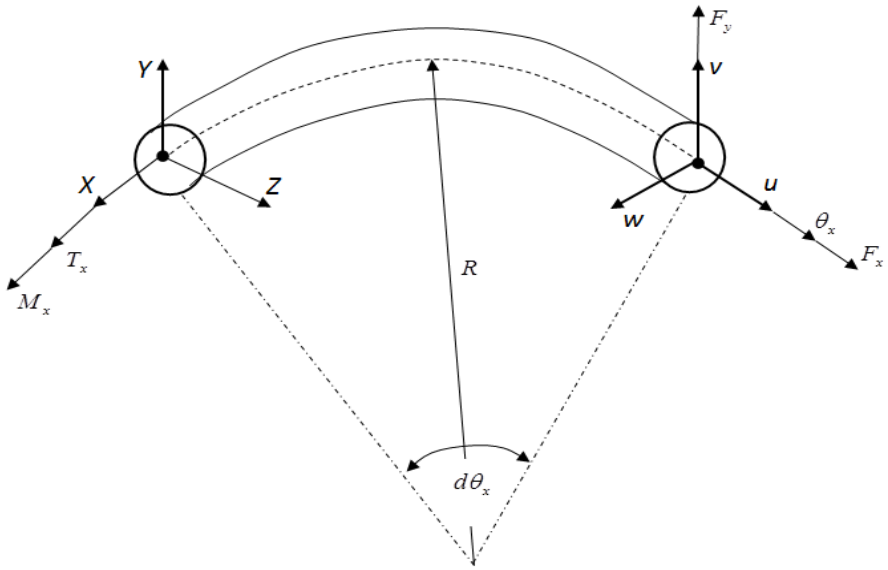

Figure 5.2: The curved beam

The axial strain equation is given as:

$$\varepsilon = \frac{\partial u}{\partial x} \qquad \text{..... (5.12)}$$

If the curved beam obeys Hook law, the stress-strain relation was obtained by multiplying the strain by Young's Modulus which yields the stress as:

$$\sigma = E\frac{\partial u}{\partial x} \qquad \text{..... (5.13)}$$

The balance of equation for the curved beam element in terms of forces and moments:

$$\frac{dT_x}{dx} + F_x = 0$$
$$\frac{d^2M_x}{dx^2} + F_y + \frac{d}{dx}\left(T_x\frac{\partial w}{\partial x}\right) = 0 \qquad \text{..... (5.14a, b)}$$

The axial force and moment can be formulated using the following equations:

The axial tension becomes:

$$T_x = \int_A \sigma \, dA = \int_A E \frac{\partial u}{\partial s} \qquad \text{..... (5.15)}$$

The moment becomes:

$$M_x = -\int_A z\sigma \, dA = EI \frac{\partial^2 v}{\partial s^2} \qquad \text{..... (5.16)}$$

Where $I = \int_A z^2 dA$, is the cross-section moment of inertia, A is the area of the cross-section.

Substituting equations (5.9) and (5.13) into (5.13) to obtain

$$\rho A \frac{\partial^2 u}{\partial t^2} = \frac{\partial}{\partial x}\left(EA \frac{\partial u}{\partial s} - \frac{v}{R} \right) \qquad \text{..... (5.17)}$$

$$\rho A \frac{\partial^2 v}{\partial t^2} = \frac{\partial^2}{\partial x^2}\left(EI \frac{\partial^2 v}{\partial s^2} - \frac{u}{R} \right) + \frac{\partial}{\partial x}\left(T \frac{\partial}{\partial s} - \frac{u}{R} \right) \qquad \text{..... (5.18)}$$

Using the Euler-Bernoulli curved beam, the shear strain is neglected. Therefore, since the beam was assumed to be elastic, the relevant strains in this case are the axial strain and the bending strain, where the bending strain now depends only on the radial displacement, *u*.

The strain-displacement equations describing the deformation of a curved beam neglecting the shear force is obtained, therefore, the axial and bending strains are given as:

$$T - \frac{M}{R} = EA\left(\frac{du}{\partial s} - \frac{v}{R} \right) = EA\varepsilon_A \qquad \text{..... (5.19)}$$

$$\varepsilon_A = \frac{du}{ds} - \frac{v}{R} \qquad \text{..... (5.20)}$$

$$M = EI\left(\frac{d^2 v}{\partial s^2} - \frac{du}{Rds} \right) + T\left(\frac{dv}{ds} - \frac{u}{Rds} \right) = EI\varepsilon_{B,\,EI} + T\varepsilon_{B,T} \qquad \text{..... (5.21)}$$

$$\varepsilon_B = \left(-\frac{d^2 v}{ds^2} - \frac{du}{Rds} \right) + \left(-\frac{dv}{ds} - \frac{u}{Rds} \right) \qquad \text{..... (5.22)}$$

5.6 Finite Element Formulation

The formulation of the FEM equation for the conductor was done as functions of its potential strains, kinetic energies, the energy dissipation function and the virtual work done by the applied loads. The derivations are based upon the linear theory of elasticity. This means that both the stress-strain and the strain-displacement relations are linear. To take advantage of the iso-parametric interpolation, using the geometric formulation that was already done, the strand formulation was done using the natural coordinate system. This concept will help later in the assembly of strands, in which the relationship between the natural and the global coordinates will be used to produce the conductor FEM model.

The mathematical expression for Hamilton's principle is given as:

$$\int_{t_1}^{t_2}\left(\delta\left(T-U\right)+\delta W_{nc}\right)dt=0 \qquad \text{…….…… (5.23)}$$

The strain energy can be evaluated by:

$$U=\frac{1}{2}\int_{-1}^{1}\sigma_x\varepsilon_x A dx \qquad \text{…….…… (5.24)}$$

Using the relation defined in equations (5.20 and 5.22), the following strain energies are obtained.

The axial strain energy stored in the element is given as:

$$U_A=\frac{1}{2}\int_{-1}^{1}EA\left(\frac{du}{ds}-\frac{v}{R}\right)Adx \qquad \text{…….…… (5.25)}$$

The bending strain energy stored in the element is given as:

$$U_B=\frac{1}{2}\int_{-1}^{1}z\sigma\left(\frac{du}{ds}-\frac{v}{R}\right)Adx \qquad \text{…….…… (5.26)}$$

Using the relation defined in equation (5.22):

$$U_B=\frac{1}{2}\int_{-1}^{1}EI\left(-\frac{d^2v}{ds^2}-\frac{du}{Rds}\right)+T\left(-\frac{dv}{ds}-\frac{u}{R}\right)Adx \qquad \text{…….…… (5.27)}$$

The kinetic energy of the beam element is given as:

$$T=\frac{1}{2}\int_{-1}^{1}\rho A\left(\dot{u}^2+\dot{v}^2\right)dx \qquad \text{…….…… (5.28)}$$

The virtual work for the element is express as:

$$\delta W=\frac{1}{2}\int_{-1}^{1}F_y\delta u dx \qquad \text{…….…… (5.29)}$$

The total energy and work for the curved beam element equations was therefore obtained by substituting equations (5.25 -5.29) into equation (5.23). The total energy and work is obtained as:

$$\int_{t_1}^{t_2}\left[\int_{-a}^{a}\rho A\frac{dv}{dt}\left(\delta\frac{dv}{dt}\right)dx-\int_{-a}^{a}Ed\varepsilon\left(\delta\varepsilon\right)dx+\int_{-a}^{a}F_y\delta v dx\right]dt=0 \qquad \text{…….…… (5.30)}$$

5.7 Discretization using Shape and Trial Functions

The discretization of the conductor structure entails converting its continuous body containing infinite number of points i.e. infinite degree of freedom into a discrete model with a defined number of nodes at the ends of the sun-domain. The discretization of structure was modeled using

the shape functions. The approximating function also known as the basis function was defined in terms of the values of the field variables at the nodes, for the beam, thus a polynomial is used.

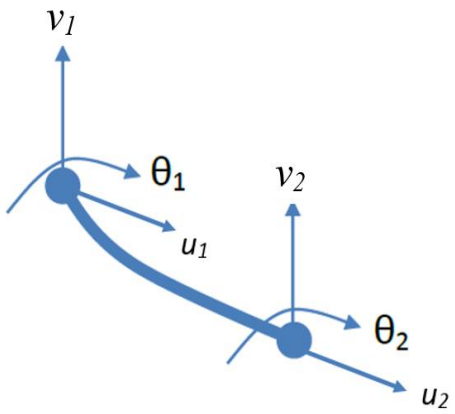

Figure 5.3: The curved beam finite element

For the curved beam shown in figure (5.3), there are three variables *per node* that are used to define the element behaviour. At a typical node is defined by displacements and rotation $\left[u_i \; v_i \; \theta_i\right]$where i = 1, 2 defines the axial, rotation and bending components.

The shape function that was defined for the axial, transverse and rotation at the nodes are expressed as follows:

$$\begin{aligned} u(s) &= b_0 + b_1 s \\ v(s) &= c_0 + c_1 s + c_2 s^2 + c_3 s^3 \\ \theta &= \frac{dv(s)}{ds} = c_1 + 2c_2 s + 3c_3 s^2 \end{aligned} \qquad \ldots\ldots\ldots\ldots\ldots\ldots\ldots\ldots (5.31)$$

In a matrix form, the equation (5.31) can be represented for u and v:

$$\begin{bmatrix} u \\ v \end{bmatrix} = \begin{bmatrix} 1 & s & 0 & 0 & 0 & 0 \\ 0 & 0 & 1 & s & s^2 & s^3 \end{bmatrix} \begin{bmatrix} b_0 \\ b_1 \\ c_0 \\ c_1 \\ c_2 \\ c_3 \end{bmatrix} \qquad \ldots\ldots\ldots\ldots\ldots\ldots\ldots\ldots (5.32)$$

Solving for the constants and substituting into equation (5.32), to obtain:

$$\begin{bmatrix} u \\ v \\ \theta \end{bmatrix} = \begin{bmatrix} N_1 & 0 & N_2 & 0 & 0 & 0 \\ 0 & N_3 & 0 & N_4 & N_5 & N_6 \\ 0 & 0 & N_4 & & N_5 & N_6 \end{bmatrix} \begin{bmatrix} u_1 \\ v_1 \\ \theta_1 \\ u_2 \\ v_2 \\ \theta_2 \end{bmatrix} \quad \text{……..…… (5.33)}$$

The values the shape functions as given in equation (5.53) are defined as follows:

$$N_1 = \frac{1}{2}(1-\xi)$$

$$N_2 = \frac{1}{2}(1+\xi)$$

$$N_3 = \frac{1}{4}(2-3\xi+\xi^3)$$

$$N_4 = \frac{1}{4}(1-\xi-\xi^2-\xi^3)$$

$$N_5 = \frac{1}{4}(2+3\xi-\xi^3)$$

$$N_6 = \frac{1}{4}(-1-\xi+\xi^2+\xi^3)$$

Thus, the axial and transvers displacement can then be evaluated as:

$$u(s) = N_1 u_1 + N_2 u_2 \quad \text{……..…… (5.34a)}$$

$$v(s) = N_3 v_1 + N_4 \theta_1 + N_5 v_2 + N_6 \theta_2 \quad \text{……..…… (5.34b)}$$

Defining equation (5.32) in a compact form:

$$d = N d_i \quad \text{……..…… (5.35)}$$

From the compact form equation, defining the vector of the unknown values as *d*, and since we have three degrees of freedom per node, that is *v*, *u* and θ then the axial and bending strains can be define using equations (5.20) and (5.22) as

$$\varepsilon_A = \hat{N}_A d \quad \text{……..…… (5.36)}$$

Where

$$\hat{N}_A = \begin{bmatrix} N_1' & -\frac{N_3}{R} & -\frac{N_4}{R} & N_2' & -\frac{N_5}{R} & -\frac{N_6}{R} \end{bmatrix}$$

$$\varepsilon_B = \hat{N}_{B,EI}\, d + \hat{N}_{B,T} d \qquad \text{..... (5.37)}$$

Where

$$\hat{N}_{B,\,EI} = \left[-\frac{N_1'}{R} \;\; -N_3'' \;\; -N_4'' \;\; -\frac{N'}{R} \;\; -N_5'' \;\; -N_6'' \right]$$

$$\hat{N}_{B,\,T} = \left[-\frac{N_1}{R} \;\; -N_3' \;\; -N_4' \;\; -\frac{N}{R} \;\; -N_5' \;\; -N_6' \right]$$

The curved beam displacement due to kinetic energy can define as:

$$\left(\dot{u}^2 + \dot{v}^2\right) = N_A \dot{d}_A + N_B \dot{d}_B d\xi \qquad \text{..... (5.38)}$$

Where

$$N_A = \begin{bmatrix} N_1 & N_2 \end{bmatrix} \quad \dot{d}_A = \begin{bmatrix} u_1 & u_2 \end{bmatrix}$$

$$N_B = \begin{bmatrix} N_3 & N_4 & N_5 & N_6 \end{bmatrix} \quad \dot{d}_B = \begin{bmatrix} v_1 & \theta_1 & v_2 & \theta_2 \end{bmatrix}$$

5.7.1 The Matrix Formulation

Therefore, the element stiffness matrix is a contribution from the axial and bending stiffness, such that the expression for the strand stiffness is given as:

$$[K] = \left[\frac{d}{2} \int_{-1}^{+1} \hat{N}_A^T (EA) \hat{N}_A \frac{d}{2} d\xi \right] + \left[\frac{d}{2} \int_{-1}^{+1} \hat{N}_{B,EI}^T (EI) \hat{N}_{B,EI} \frac{d}{2} d\xi \right] + \left[\frac{d}{2} \int_{-1}^{+1} \hat{N}_{B,T}^T (T) \hat{N}_{B,T} \frac{d}{2} d\xi \right] \quad \text{.... (5.39)}$$

Substituting the displacement functions in equations (3.38 and 3.28) into the energy function (3.143) this gives expression for the mass matrix given as:

$$[M] = \frac{\dot{d}_A}{2} \int_{-1}^{+1} N_A{}^T \rho A N_A d\xi + \frac{\dot{d}_B}{2} \int_{-1}^{+1} N_B{}^T \rho A N_B \, d\xi \qquad \text{..... (5.40)}$$

The load vector expression is given as:

$$\delta W = \frac{1}{2} \int_{-1}^{1} F_y \delta u d\xi \qquad \text{..... (5.41)}$$

5.7.2 Finite Element Analysis of Straight versus Curve Beam Element

It was mention previously that curved beam is better suited to model conductors. This is because for the straight beams, the neutral axis of the section coincides with its centroidal axis and the stress distribution in the beam is linear. In case of curved beams, the neutral axis of the cross-section is shifted towards the centre of curvature of the beam causing a non-linear (hyperbolic) distribution of stress. Depending on the plane of bending and the direction of load, it could result in torsional moments and bi-axial bending which is more complicated than the regular single axis bending moment in straight beams, with loaded along the section axes, or in an added axial (normal to the cross section of the beam) force throughout its length. The torsional component in the curved beam gains importance compared to the same load situation on the straight beam. For the

application of the curved beam principle, it is imperative to illustrate its advantage by using the beam deformed under static loading as shown in figure (5.4)

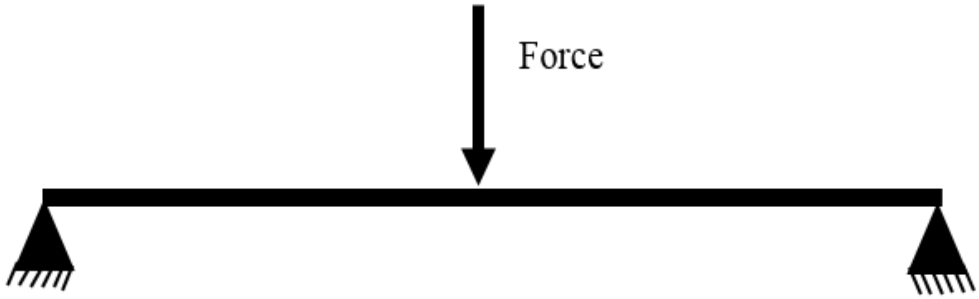

Figure 5.4: Deformed fixed supported Beam

The shown in figure (5.4) is simulated using the fixed (clamped) supported beam with the following Specifications:
Diameter – 0.03 m,
Transverse load at the center = 1 kN,
Length of the beam – 48 m,
Radius of the curvature – 1 m,
Linear elastic isotropic materials – steel

Base on FEM simulation, the results obtained for the circular cross-section for both beam type (straight and curved) are plotted in figure (5.5). The result showed that deflection parameters in curved beams is greater than that of the straight beam. Thus, this verified that there is a transfer of more loads in curve beam as compared to straight beam of the same cross-sectional area.

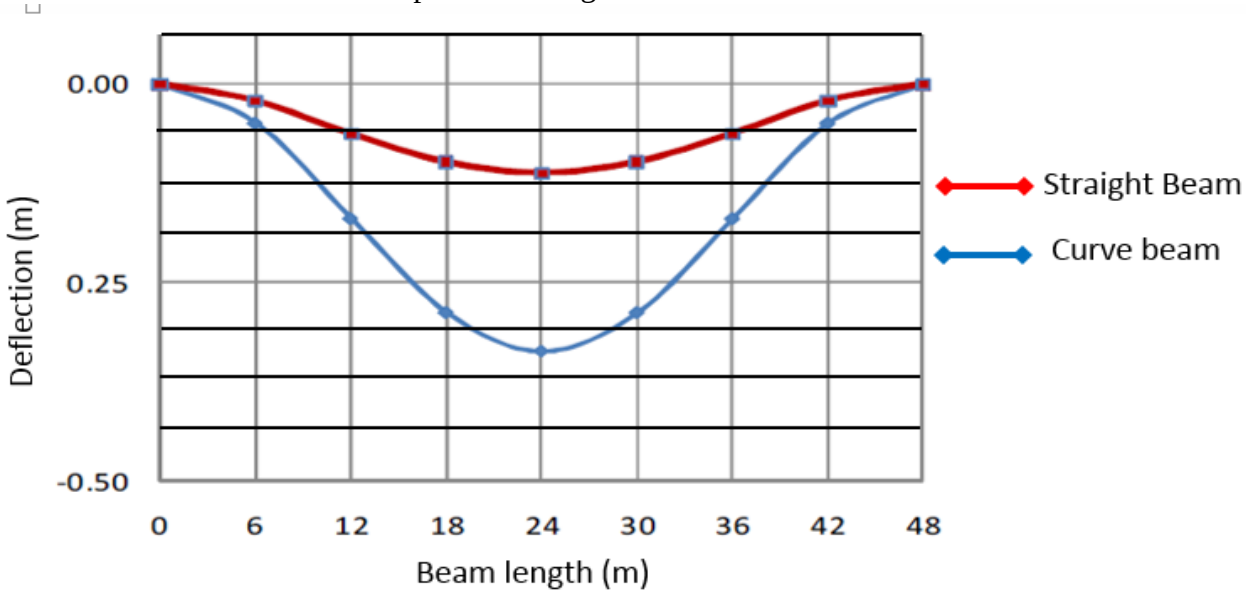

Figure 5.5: FEM comparison of Straight and Curve Beam under the same loading

5.7.3 Numerical Integration

In the iso-parametric formulation for the curved beam, the displacements were expressed in terms of natural coordinates. However, the equations of the finite elements that have been developed in the natural coordinate system have to be transformed into a new domain with respect to Cartesian coordinates (x; y; z). Correspondingly, the natural coordinates will be mapped into new curvilinear sets when assembling the global structure in the Cartesian space.

In each of these shape functions that is continuously differentiable, the iso-parametric mapping was implemented using the sampling points and weighting factors. This was accomplished through a transformation matrix and then using the Jacobean to perform the numerical integration. The numerical scheme that was employed for the integration was the Gauss-Legendre. This numerical integration for natural coordinates range from -1 to +1, for a function f(x) was obtain as a definite integral:

$$I = \int_{-1}^{+1} f(x)\,dx \qquad \text{..... (5.42)}$$

5.8 Formulation of Equation for the Un-Damped System

The stiffness and mass matrices and load vector can now be obtained using the energy expressions. Based on the energies equation for Euler-Bernoulli beam, used to model the strands, the stiffness, mass matrices and load vector are given by equations (5.36 - 5.37). The corresponding axial and bending displacements respectively are in the form:

$$u = \begin{bmatrix} u_1 & u_2 \end{bmatrix}$$

$$v = \begin{bmatrix} v_1 & \theta_1 & v_2 & \theta_2 \end{bmatrix}$$

By combining of the matrices and vector and using the concept of iso-parametric interpolation, the system matrices for the conductor system is obtained as:

$$\begin{bmatrix} M_{11} & M_{12} \\ M_{21} & M_{22} \end{bmatrix} \begin{pmatrix} \ddot{u} \\ \ddot{v} \end{pmatrix} + \begin{bmatrix} K_{11} & K_{12} \\ K_{21} & K_{22} \end{bmatrix} \begin{pmatrix} u \\ v \end{pmatrix} = \begin{pmatrix} F_1 \\ F_2 \end{pmatrix} \qquad \text{..... (5.43)}$$

The system equation formulated at this point is regarded as un-damped equation because; F_1 which is surface body force is zero. The formulation of this damping force is done later as external force acting at contact points

5.9 FEM Modelling of Conductor Damping

The conductor damping is mainly as a result of friction at the contact interface between the two contacting strands of different layers. To determine the energy dissipation at the contact points, the physics of these contact patches was used to formulate the equilibrium and conservative equation. The FEM characterization based on the contact mechanics was the modelling approach use to evaluate the internally damped energy of the vibrating conductor. This approach is in contrast to the method of adding the damping term into the governing conductor equation when done analytically. The addition of damping term does adequately account for process of variation of

conductor flexural rigidity that is directly related to the helical strands slip. The periodic slip causes frictional energy dissipation and damping of the conductor oscillations. Thus, a better representation of damping was obtained when the point of contacts area was characterized for energy dissipation. Model results obtained using this approach was compared with experimental tests performed on the conductors, as reported in the next chapter.

5.9.1 Inter-Strand Contact Patches

Contact problems generally exhibit nonlinearity that requires numerical simulation and using the finite element method has become a common approach recently. In contact mechanics, the major challenge has to do with the determination of contact boundary condition. As opposed to the classical solid mechanics problem where the boundary conditions can be classified either as Dirichlet or Neumann boundary or mixed. The fundamental laws of physics of solid mechanics, e.g., momentum balance and mass conservation laws also apply to contact mechanics. But contact mechanics problems, are the most difficult type of problems in mechanics. This is because it involves more conceptual, mathematical and computational efforts. As shown in figure (5.4), the point of contact between strands which is similar to two contacting inclined cylinders. Contact surface FEM of beam to beam point contact can be found in [87].

The contact FEM analysis in this study was modelled using the node-to-node contact configuration. The analysis of this form of contact entails parameter such as the displacement and velocity fields as a function of the contact traction. To generate a mesh for the contact patches motion, the formulation should allow the possibility that displacement was driven by the force under a prescribed motion scheme. To implement this approach, the nodes in the contact patches is set to have a motion that implement the node-to-node contact at each time step. This can be achieved by the use of the well-known Newton-Rapson iteration scheme. The formulation of inter-strand contact was modelled with the node-to-node approach for 2D contact problems subject to finite deformation.

The node-to-node contact is maintained throughout the contact point between strands. Figure (5.6) shows a 2D contact point of two contacting strands. The normal traction N_1 the compressive force always points inward and N_2 opposes to the relative sliding direction. The direction of N_2 implies that P^1 is moving to the right side of P^2. In the finite element approach to contact problems, the "tangent traction" or the frictional force is often set to be opposite to N_2. The normal traction N_1 is often expressed as the product of a non-negative scalar N_c and the outward unit normal **n**, as displayed in Figure (5.6).

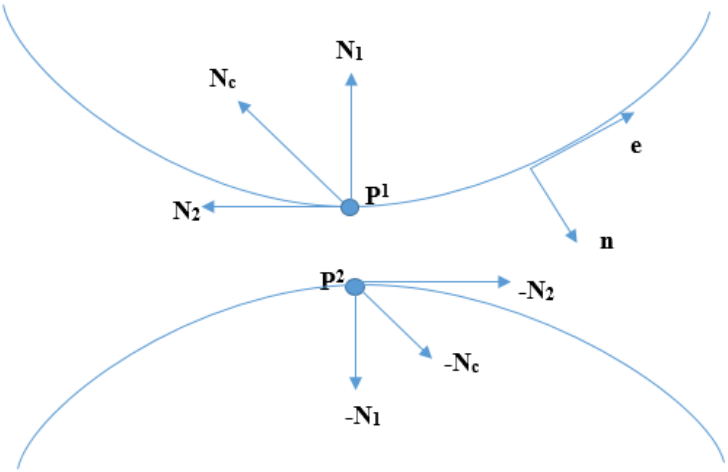

Figure 5.6: The forces at the inter-strand contact

5.9.2 The Friction Contact Model

The consideration of friction at area of contact makes the analysis of energy conservation much more complicated at the contact patches. This is because the tangent traction depends on the normal traction and the sliding between strands is path dependent. In the present analysis, the Coulomb model of the dry friction with a constant friction coefficient μ between the friction force F_T and the normal force F_N in the contact point between beams was used;

$$F_T = \mu F_N \qquad \text{..... (5.44)}$$

As explained earlier, the state of the interface of the contact pairs of strands at certain point can either be one of two categories: sticking or sliding. To obtain this condition, the analogy of a rigid-ideally plastic material was employed. This allows in distinguishing between two friction states: the stick state, which is characterized by no relative displacement between the bodies, and the slip state, where the relative displacement in the form of sliding was present. The stick state will occur when the frictional traction F_T is smaller than F_N, and the pair of strands is in a perfect sticking condition and therefore experiences no relative motion. Using the Coulomb friction law, motion is completely prevented due to friction force being greater than the shearing force. When the imposed bending load is greater than the friction force, relative motion between the strands occurs this signifies the slip condition. To optimize this constraint imposed by the friction force, the Lagrange multiplier is used.

5.9.3 The Lagrange multiplier

Generally, a system with two-body contact problems will have the strain energy part, the kinetic energy part which is the energy contributed by the external tractions and body forces, the energy

associated with contact forces. The balance of the global energy in a rate form can be expressed as [84]:

$$E^{Total} = E^{K.E} + E^{P.E} + E^{CONTACT} \quad \text{..... (5.45)}$$

For the contacting surface, the FEM formulation of the kinematics and constitutive relations concerning contact can be completely modelled based on the geometric surface used for the description of the contacting bodies. In [87] the solution of the contact problem using the theory of elasticity concerning the two bodies involved and a solution is obtained by finding the minimum of the potential energy functional Π as defined:

$$\min \Pi = \min(\Pi_1 + \Pi_2) \quad \text{..... (5.46)}$$

$$g_N = n \circ (x_1 + x_{2C})$$

Preserving the condition of non-penetrability requires that the penetration function remains non-negative

$$g_N \geq 0 \quad \text{..... (5.47)}$$

If the condition above is accompanied by the constraint of contact normal force, which can only be compressive:

$$F_N \geq 0 \quad \text{..... (5.48)}$$

$$F_N g_N = 0$$

As stated early, the contacting surface obeys the law of physics. The total energy in the two-body contact problem contains two parts wherein the first part comprises the kinetic energy and strain energy, and the second part comes from contribution of the contact tractions. The total energy with the imposed contact constrain is defined as:

$$\Pi^{Total} = \Pi^1 + \Pi^2 + \int_{\Gamma_C} \lambda_N g da \quad \text{..... (5.49)}$$

The frequently used method to include the equality constraints is known as the Lagrange multiplier method. In this approach, the saddle-point problem of the modified functional was encountered and this leads to the stationary point formulation. This can be expressed for the contact problem as:

$$stat\left(\Pi + \sum_{act} \lambda_N g_N \right) \quad \text{..... (5.50)}$$

Where λ is the Lagrange multiplier

Theoretically, g_N coincides with the normal contact traction N_1 in the Lagrange multiplier approach [88]. If the constrain condition is satisfied exactly, the last term on the right of equation (5.48) adds nothing to the total energy. Computing the directional derivative of equation (5.49) with respect to displacement yields the stationary condition.

$$\Pi = (\Pi_1 + \Pi_2) + \lambda^T (Au - b) = \frac{1}{2} u^T K u - u^T f + \lambda^T (Au - b) \quad \text{..... (5.51)}$$

The imposed constraint for the Lagrange multipliers, which constitute the set of extra unknowns obtained in the problem for the node-node contact is given as [87]:

$$\begin{bmatrix} K_A & K_{NAB} & K_{NA\lambda} \\ K_{NBA} & (K_B + K_{NBB}) & K_{NB\lambda} \\ K_{N\lambda A} & K_{N\lambda B} & 0 \end{bmatrix} \begin{bmatrix} \Delta q_A \\ \Delta q_B \\ \Delta \lambda \end{bmatrix} + \begin{bmatrix} R_A + R_{NA} \\ R_B + R_{NB} \\ R_{N\lambda} \end{bmatrix} = \begin{bmatrix} 0 \\ 0 \\ 0 \end{bmatrix} \quad \text{..... (5.52)}$$

5.10 Finite Element Modelling of Inter-Strands Contact

This form of node-to-node contact interactions was used to describe contacts between strands in different layers caused by the tensile load acting on the strand. Details of the node-to-node contact type method for the contacts between beams with friction effect can be found in [87]. For the FEM modelling, the influence of contact conditions between the strands and/or between strand and the core has been examined for two limit cases: stick and sliding with friction. These contact conditions have been applied for nodes situated on the area of contact between strands. This area of contact can be evaluated, as indicated in chapter 2 using the Hertz contact mechanics. These area of contact experiences high stress, therefore, for the surface patches of high stress concentration and the axial traction result to the contact nodes being densely meshed. However, it should be mentioned that the friction effect plays a role in developing the contact stiffness and the effect of friction on the response of the conductor structure under cyclic loading can be significant. The stiffness coefficients are computed in four successive steps corresponding to different response to loading conditions in tension and bending mode:

To adequately evaluate variables associated with these areas of contacts using the analysis of the beam to beam contact, the 2D, with four node element type was used. Beam contact was characterized by features, which demand a discretization of different approachs in which case the element type was defined between the surfaces of the individual adjacent strand. This concept is used in the contact patches discretization.

5.10.1 Discretization of Inter-Strand Contact Interface

The discretization of the contact inter-strand patches was done by the normalized two-dimensional bilinear element type. This is a typical of the four-node plane iso-parametric bilinear element, *Q*4 as shown figure (5.7).

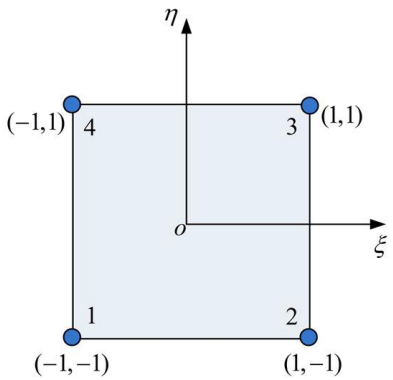

Figure 5.7: Bilinear two-dimension finite element

The coordinate of an internal point is interpolated from the corner coordinates as shown in figure (5.7).

The shape function for the nodes is defined as:

$$H_1 = \frac{1}{4}(\xi - 1)(\eta - 1)$$

$$H_2 = \frac{1}{4}(\xi + 1)(\eta - 1)$$

$$H_3 = \frac{1}{4}(\xi + 1)(\eta + 1)$$

$$H_4 = \frac{1}{4}(\xi - 1)(\eta + 1)$$

The displacement and the velocity are defined respectively as:

$$w = \sum_{i=1}^{4} H_i w_i \qquad \text{…….……. (5.53a)}$$

$$s = \sum_{i=1}^{4} H_i s_i \qquad \text{…….……. (5.53b)}$$

5.10.2 Finite Element Implementation for Inter-Strand Contact

The implementation of the element type for the contact surface follows the normal formulation of the FEM equation for the contacting surfaces as described by discretization of inter-strand contact interface. Analysis of the contact between conductor strands, due to their shape, allows the application of the beam-to-beam contact formulation with the additional frictional effects. One of

the simplest possibilities to treat such problems is a mechanical-mechanical coupling. As stated in section (2.5.1), besides, the contact between strands being point-wise, in order to implement the contact model between the strands, a line contact was assumed as shown in figure (5.8).

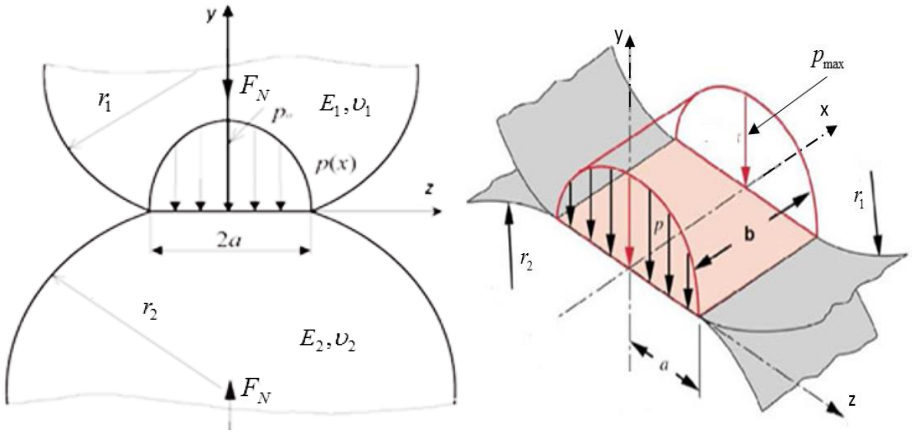

Figure 5.8: Equivalent line contact model for the two contacting strands [60]

Hence, the contact between two strands of a conductor with circular cross sections can be characterized by a rectangular contact area, as shown in figure (5.8).

The contact between two long conductors occurs at a small area and satisfies the condition:

$$g_N = u_2 - u_1 \qquad \text{..... (5.54)}$$

Where u_1 and u_2 denote displacement at the cross-sections of the strands 1 and 2, respectively, corresponding to the contact points. Their values can be expressed in terms of the local co-ordinates for these points as:

$$F = kg_N \qquad \text{..... (5.55)}$$

In such a situation to use the relation derive by the Hertz contact mechanics, there was a need to introduce the equivalent radius. This can be determined as a geometric mean value of the semi-axes of the resulting rectangle, the area of contacting surface and parameters regarding the Hertz's theory of contact between ideally elastic bodies are already defined in section (2.6)

The above formulation provides the necessary tools for the dynamic modelling of strands contacts mechanisms using the Hertz contact mechanics and Coulomb friction contact model. The Hertzian contact formulae describe the contact pressure distribution between two cylinders (line-contact). Surface energy, the higher the surface energy, the greater the area of contact.

Due to internal stresses at the area of contacts, friction is taken into account during the simulation. To take care of the incompressibility constraint a selective reduced integration method is applied, where the pressure is only integrated in the centre point of the bilinear element type.

To implement the FEM for the contact interface follows the procedure document in [88], with the imposition using the Lagrange multiplier. The explicit matrix formulation for the contact element with bilinear interpolation as described, for the displacement field and constant approximation of the contact pressure in the case of friction contact. In this case, it wise to approximate equation (5.52), which involves Lagrange multipliers and a regularization term. The weak form of the contact contributions is then formulated.

The usual approach in discretizing the contact area into FEM mesh is achieved by mapping the reference configuration into a collection of elements which form the approximation of the contact domain. An illustration of this form of meshing is given in figure (5.9). The left figure represents the physical shape and the right one is the mapped shape.

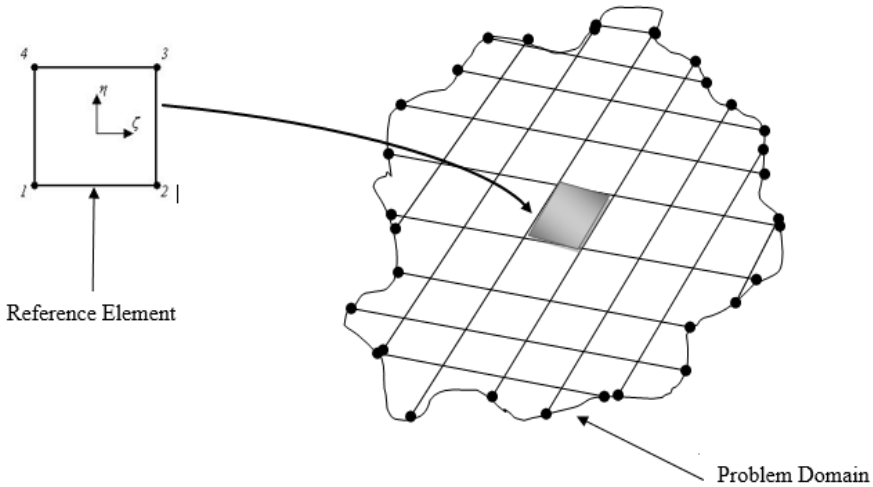

Figure 5.9: Bilinear mapping from the natural to the Cartesian coordinates

Assuming that the problem domain has *m* nodes, each node has 2 nodal degrees of freedom designated *q*, and v. It is now further assumed that the shape of each of the individual elements in the mesh is completely determined through a finite number of nodes. As an example, depicted in figure (3.9), the elements are quadrilaterals, whose shape is completely determined through the contact domain patches. Based on equation (5.53), analyzing the problem in two dimensions, the displacement vector, u_C, of an element will have two components. Such discretization is done in terms of displacement and the velocity will be in the form of:

$$u_C = \begin{pmatrix} w \\ v \end{pmatrix} = \sum_i^m \begin{pmatrix} x_1 H_1 & x_2 H_2 & x_3 H_3 & x_4 H_4 \\ q_1 H_1 & q_2 H_2 & q_3 H_3 & q_4 H_4 \end{pmatrix} = \sum_i^m H_i u_i \qquad \text{..... (5.56)}$$

where

$$H_i = \begin{bmatrix} N_1 & 0 & 0 & N_2 & 0 & 0 & \dots & N_m & 0 & 0 \\ 0 & N_1 & 0 & 0 & N_2 & 0 & \dots & 0 & N_m & 0 \\ 0 & 0 & N_1 & 0 & 0 & N_2 & & 0 & 0 & N_m \end{bmatrix}$$

5.11 FEM modelling of Stick-Slip regime

Figure (5.10) provides the illustration of the forces acting that tends to resist the shearing force between the conductor strands. Due to the bending load imposed on the tensile load, a critical point is reached where the strand experiences a slippage and enter into a slip mode. The critical point as it moves from stick to slip was determined as a function of the imposed radius of curvature, detailed explanation was given in chapter 4. The stick-slip motion between strands is a periodic motion which tends to alternating between static and dynamic friction at the contacting surface with a sliding velocity.

Tangential forces are attributed to surface friction between particles. Friction between the strands is modelled using Coulomb's Law of Friction defined as:

$$F_S = \begin{cases} Q & Q < \mu_S F_N \\ \mu_k F_N & Q \geq \mu_K F_N \end{cases} \qquad \text{..... (5.57)}$$

where μ_S is a static friction coefficient and μ_K is a kinetic or sliding friction coefficient

- For low shear forces, there is no relative motion (stick)
- For high shear forces, there is relative motion (slip)

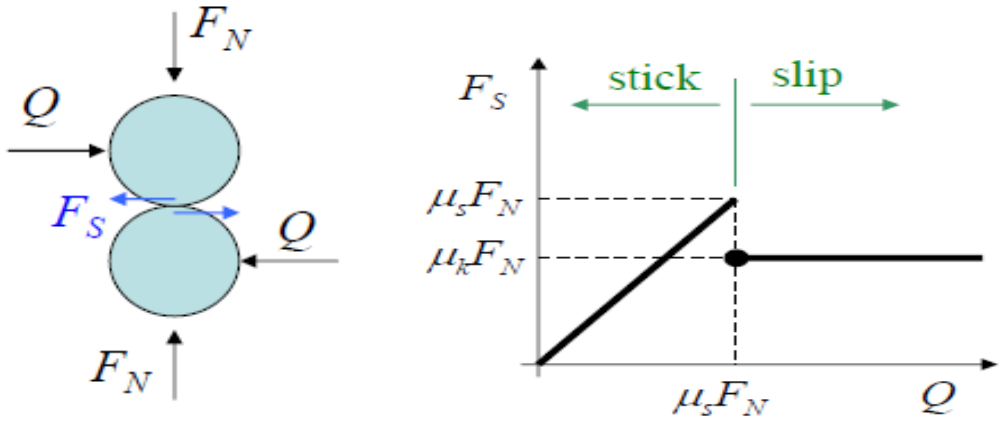

Figure 5.10: The analysis of the forces acting on and between strands

Where *k* denotes the tangential stiffness of the contact surface and according to hooks' law

$$F_S = 2E_{eq}A = q|p(x)| \qquad \text{..... (5.58)}$$

Where pressure distribution *p*(x) is over the contact width in a rectangular form with area $A = ab$, as shown in figure (5.8) and equivalent modulus is obtained as:

$$E_{eq} = \frac{E_1 E_2}{E_1 + E_2} \qquad \text{..... (5.59)}$$

In reference [81], the finite element analysis of inter-strand contact was used to establish the hysteresis loop due to the conductor alternate condition between the stick and the slip regimes. This was then used to evaluate conductor self-damping for a single-layered conductor. At the contact points, due to the shear force there is the tangential stiffness. These stiffness along the contact point are shown in figure (5.11). The evaluation of the compliance along the contact points are discussed in [89] and these tangential compliances can be used to determine the stiffness along the point's contacts.

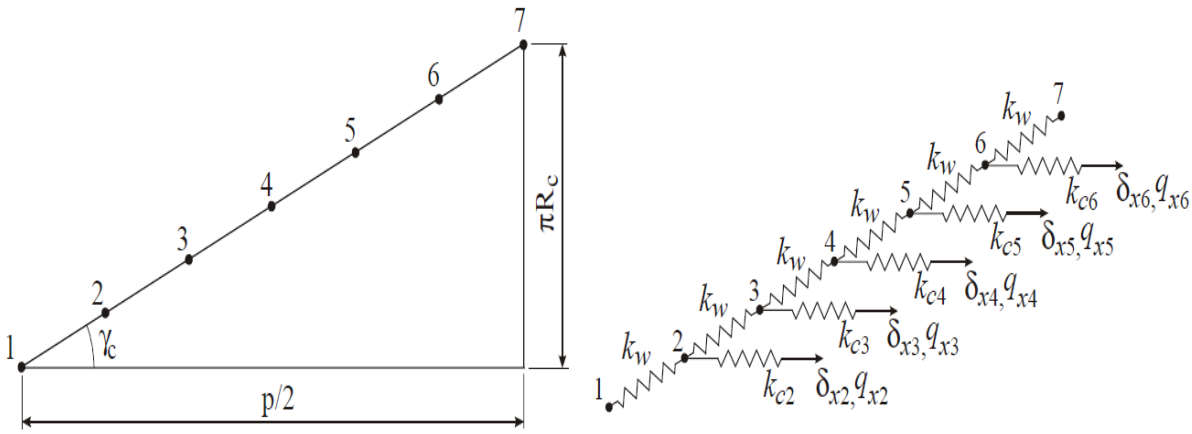

Figure 5.11: Contact points and its rheological representation [89]

Figure (5.11) indicates the number of point contacts between strands and the corresponding stiffness generated. In implementing this model as shown in figure (5.11) numerically can be very challenging and is not worth the effort of implementing as the equivalent line contact can produce relatively good results with very less effort. Therefore, the alternative means is to use an equivalent line contact model and the pressure is assumed to be constant along the line of contact between two strands.

Damping in the conductor is mainly due to hysteresis damping. This form of damping is caused by the axial displacement and the FEM formulation is similar to the finite element formulation for a bar element as shown in figure (5.12) where only the axial strain is considered. This implies that, the damping force is formulated by decoupling the axial parameters from the transverse parameters. Thus, using the bar element for the FEM formulation, taking into account the sinusoidal axial displacement for the two-node bar element. The strain ε_x can be related to the axial displacement u as

$$\varepsilon_x = \frac{\mathrm{d}u}{\mathrm{d}x} \qquad \text{..... (5.60)}$$

The axial displacement is interpolated by

$$u = N_1(\xi)u_1 + N_2(\xi)u_2 \qquad \text{..... (5.61)}$$

Where the shape functions are defined as

$$N_1(\xi)=\frac{1}{2}(1-\xi);\ N_2(\xi)=\frac{1}{2}(1+\xi) \qquad \text{..... (5.62)}$$

The resultant tensile on the strands can be evaluated as

$$\frac{1}{2}(T_2-T_1)=EA\frac{\Delta l}{l}=\frac{EA}{l}(u_2-u_1) \qquad \text{..... (5.63)}$$

The above equation can be written in matrix for as follows:

$$\begin{bmatrix} \frac{EA}{l} & -\frac{EA}{l} \\ -\frac{EA}{l} & \frac{EA}{l} \end{bmatrix}\begin{bmatrix} u_1 \\ u_2 \end{bmatrix}=\begin{bmatrix} T_1 \\ T_2 \end{bmatrix} \qquad \text{..... (5.64)}$$

Introducing the above equations in form of stiffness matrix for the contact surface is then obtained as:

$$K=\frac{EA}{l}\begin{bmatrix} 1 & -1 \\ -1 & 1 \end{bmatrix} \qquad \text{..... (5.65)}$$

Equation (5.60) provides the stiffness that tends to resist the shearing force between the conductor strands

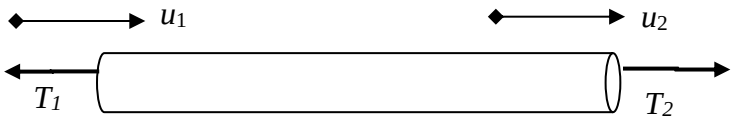

Figure 5.12: The bar element

The axial force acting on the strand can be determined by:

$$T_{i,j}(s)=EA\int_0^s \mu(s)\cdot q(s)ds \qquad \text{..... (5.66)}$$

Hence,

$$\frac{EA\cos^2\alpha}{l}[u_2-u_1]=qEA\mu(X)\cos^3\alpha$$

$$EA\cos^2\alpha\begin{bmatrix} 1 & -1 \\ -1 & 1 \end{bmatrix}\begin{bmatrix} u_1 \\ u_2 \end{bmatrix}=qEA\mu(X)\cos^3\alpha\begin{bmatrix} 1 \\ 1 \end{bmatrix} \qquad \text{..... (5.67)}$$

The finite element formulation is expressed on the basis of the finite element equilibrium equation and the force-displacement relation given in compact form as:

$$[K]\{u\}=\{f\} \qquad \text{..... (5.68)}$$

Where [K] the stiffness matrix, $\{u\}$ is the vector displacements and $\{f\}$ is the force vector and displacements $\{u\}$ are interpolated over the whole conductor strand as $\{u\} = [N]^{T} \{d\}$.

The system equation [K] $\{d\} = \{f\}$ was solved for by the system displacements $\{d\}$. In reference [16], the author drew the inference that the non-linearity in strand axial movement result in closed hysteresis loops.

To develop the stick-slip contact states, with the generation of hysteresis loop, is to combine the displacement with the developed traction stiffness and incorporating it into a bar model. A hysteresis loop [81] is shown in figure (5.12). and the explanation on how the loop can be use to determermine energy per cylce, see [16] for details. The finite element implementation of the stick-slip models for friction forces usually poses unexpected problems. The difficulty has to do with the implementation of both dynamic and static frictions in the numerical modelling of motion under the effect of friction.

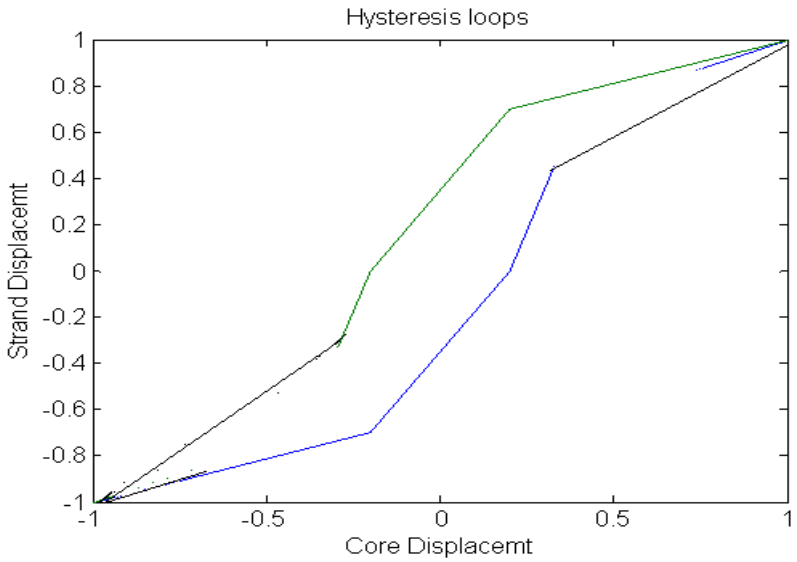

Figure 5.13: The hysteresis loop

This difficulty of modelling along contact arises from the existence of the imposed constraints to determine the state of the strands. This type of constraints can be represented by a set of inequality equations. The major challenge is determining the critical states of the load on the strands that conform the responses accordingly. To generate the hysteresis loop, the force model is implemented with the effect of the friction force f_S, determining *state* of the strands. The strands may be in sliding; still; or transitioning from sliding to still or from still to sliding. If the strands are sliding, the dynamic friction model is implemented. If the strands are still, the static friction model is used as shown in figure (5.10).

To model the inter-strand displacement as a function of friction and then simulates the displacement between strands with the surface stiffness K, the system is assumed to be massless

as shown in figure (5.14). The strands are pressed together underlying surface with a normal force F_N. This initial displacement is assumed to be $x0$, and oscillates as $x_0(t) = A \sin \omega t$ during the bending. However, there is a need to model the friction force F_S, but this depends on whether the strands are sliding or still.

The position of the strand by $x(t)$, its position relative to the bottom strands with the assumption that the strand starts from rest at $x(t) = 0$ at $t = 0$. According to Newton's second law, the force acting in the opposite direction to the surface friction forces, F_s are equal when the strand is in the sticking position and this will occur when the velocity is zero. In this case, the force will be the static friction force, Fs, which is equal to the other forces, $Fs = -\mu F_N$, so that the net force is zero. However, this is only true if the static friction force is less than the friction threshold before slip can take place.

$$F_S = -k\left(x - x_0(t)\right) > \mu_s F_N \qquad \text{..... (5.69)}$$

x = 0 and $x_0(t) = A\sin\omega t$

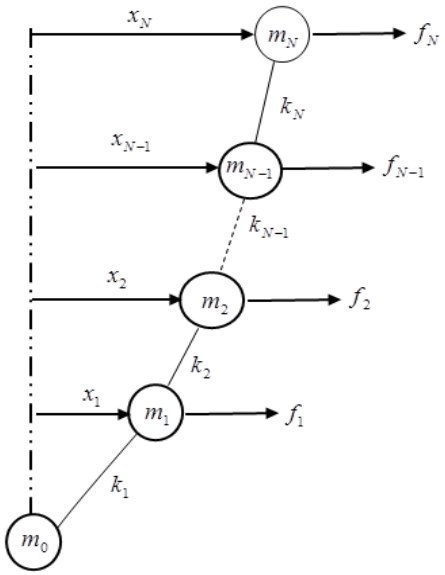

Figure 5.14: The slip pattern from the outermost towards the innermost layer

Initiation of sliding starts from rest and the strands will start to slip if the force f_i exceeds the maximum static friction force. The strands will start moving in a direction given by the force f_i, and the strands will then experience a dynamic friction.

Also in this model, it is assumed that the displacement of strands is equal in each layer. This allows the hysteretic behaviour to be treated in a unified manner by a single nonlinear differential equation with no need to distinguish different levels for the various Coulomb friction model but only the

values for the friction coefficient. The frictional hysteretic behaviour for the conductor in the dynamic state can be expressed as:

$$F_i \sin(\omega t) = \mu_i \operatorname{sgn}(\dot{x}) + \sum_{i=1}^{N} k_i x \qquad \text{..... (5.70)}$$

Changing the frictional state from sliding to static in equation (5.70), can only occur if the velocity is equal to zero, and this condition has to be constrain in the equation for this to occur during a simulation. However, when the velocity of the strand changes sign, the strand will actually stop and start sticking to the surface with a static friction force. Therefore, setting the velocity to be exactly zero when the velocity changes sign and enforces the constraint, indicating that strand is in a sliding or a sticking state.

To simulate these equations for the formation of the hysteresis loop, the same principle was used as employed in chapter 4 i.e. simulating the constraint using the Bouc-Wen. Also, the displacement pattern, follows a sequence in which the displacement in a given layer is completed before displacement can be initiated in the layer below and also the displacement starts from the outer layer of the conductor. Unlike, the loop formed in chapter 4 using the moment-curvature relation; here the loop was formed using the force-displacement relation.

5.12 The Formation of Conductor FEM Model

5.12.1 Dimensional Reduction from 3D solid element to 2D Line element

When carrying out a finite element analysis, the domain of the problem is divided (discretized) into some form of a mesh or finite element. Figure (5.15) shows the discretized model of a single span of conductor. Thus, figure (5.15), illustrates the global discretization of the conductor into n-nodes and *(n-1)*-elements.

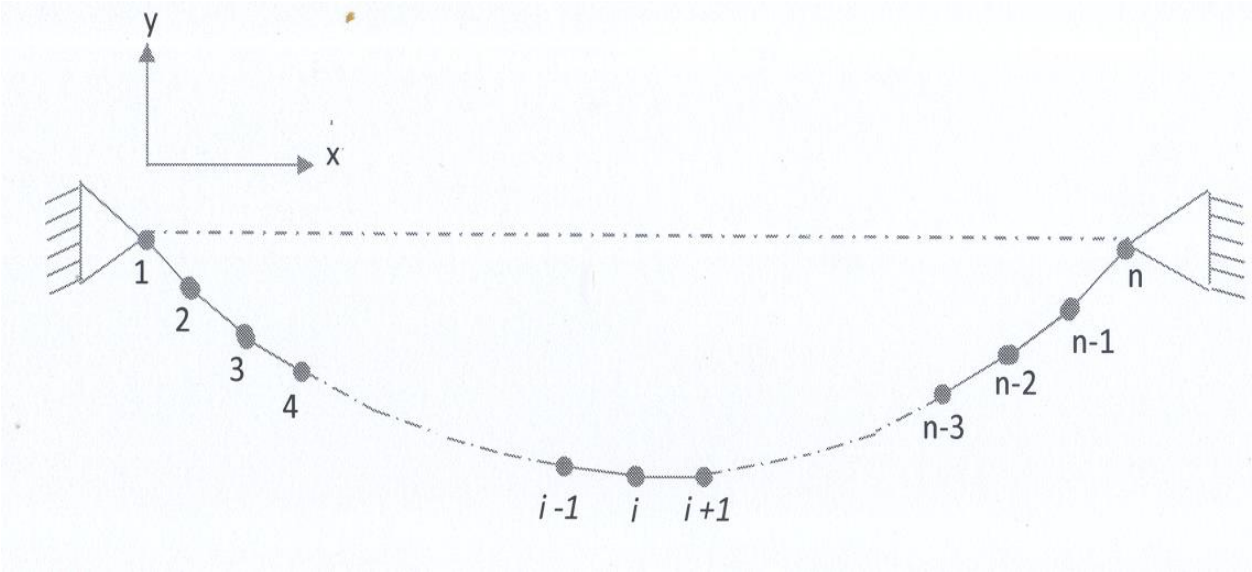

Figure 5.15: The global discretize Model of the Conductor

When a FEM problem is modelled using a 3D topology, the analysis is so large that the computation time will be long and expensive. This demands more physical memory of the computer and CPU time. For large structure simulation, there is a need to speed up numerical simulations, and reduce computational costs while keeping an optimal accuracy. For this reason, there is a need to employ a dimensional reduction technique which is used to transform the complex 3D to 2D or 1D problem or from lower order 2D to 1D system respectively. By doing so, computation times are significantly reduced, but this must be done not to compromise model accuracy thus, the use of element reduced dimension can be applied for the 3D beams element. Therefore, finite element analysis for beam structure that is long and slender, then it may be appropriate to use some sort of 1D or 2D element in place of the 3D space element. The finite element formulation for the conductor has been done with a curve beam finite elements: the 1 node-bar element and the 2-node plane beam element. Thus, to implement the dimension reduction, this 2 D line element for a curve beam was used in place of a 3D beam element. These elements which can now be regarded as the "strand element" can support tensile and bending loads, with the rotational degrees of freedom. This model is capable of modelling the strand cross-sectional profile in 2 D.

5.12.2 Iso-parametric Mapping

With the successful formulation of the finite element equation, and the generation of the discretized model in terms of local Cartesian coordinates, there follows the formulation of global model as function of the global Cartesian coordinates. The formation of the composite structure of the conductor was achieved by the iso-parametric mapping of its substructure. To obtain an adequate

representation of the conductor as a composite structure, iso-parametric mapping of the curved beam finite element was done for each strand including core. The formulation of this structure was developed using the already developed geometric formulation. Using the curved beam to model the deformed profile of each strand subjected to the axial load, has been restricted to the assumption that the longitudinal elements have the same length through the entire span. Based on the derivation of the curved beam model, the finite element modelling of the conductor as a composite structure is a new approach. This formulation entails mapping of the finite element into the discretized conductor helical layered structure and the finite analysis model was developed for the structural system on the basis of the mapping of the normalized single curved beam. For the material properties, each strand was assign the material and geometrical properties as given in the matrix form. This includes the Young's modulus for the material for individual strand, as well as the second moment of inertia of the cross section.

The overall mechanical properties of the composite conductor depend on the summation of the respective strand properties in various layers and their interactions. The stiffness matrix of a composite conductor element was formulated for the applied axial and bending loads, in which the interface slips at contact points can be taken into account. A structural analysis for the conductor as composite continuous beams was presented, and a structural computing program was compiled. The following process was used to develop the composite structure for the conductor.

5.12.3 Geometric Mapping for the Conductor

When strung under tension, the overhead transmission lines conductors support its weight thereby sagging and sag/span ratio depends on the axial tensions at both ends. When subjected to transverse vibration, each member of the conductor is subjected to both axial and bending loads.

In the development of the FEM either for the straight or for the conductor structure sagging due to its weight to form a centenary profile, some form of coordinated mapping is necessary. A reference curved beam finite element formulation was done using the natural coordinate system. This was done to take advantage of the iso-parametric interpolation as described by equation (5.42). The geometric equation in terms of x, y and z axis is already defined during the geometric formulation. For the formulation, the conductor geometry was defined in terms of global coordinate system. To implement the iso-parametric interpolation, the 3D geometric mapping is done. This is implemented using the 3D geometric equations (5.1-5.5). But the relation between the natural coordinate for the normalized curved beam was then transformed into global coordinates, the geometric transformation equations used for this mapping is defined in the next section. It is

imperative to emphasize that though the composite structure was done in 3D, the FEM equation implemented for element is that of 2D.

The configuration of the conductor is achieved by taking advantage of the geometric symmetry of the conductor sub-structures. To implement this, all mapping is done with respect to the conductor neutral axis which is assumed to coincide with the centre line of the core.

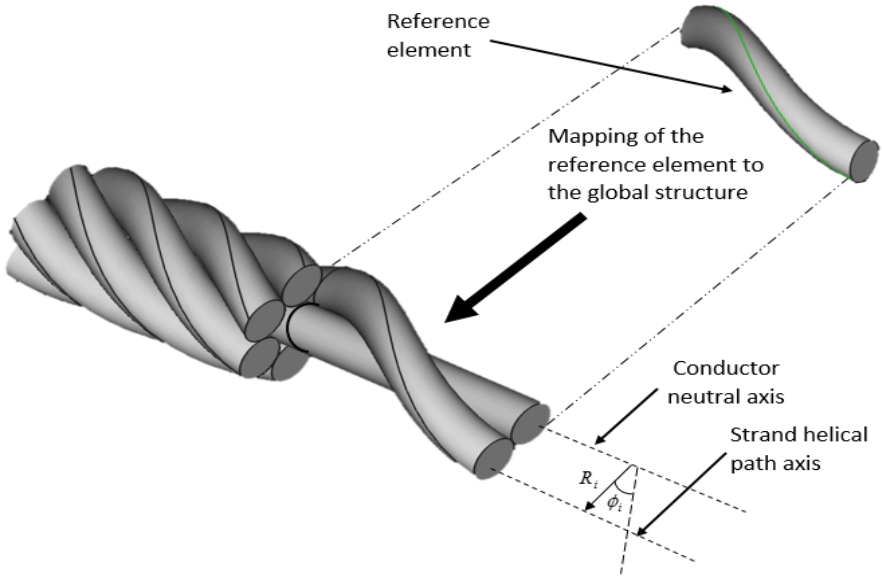

Figure 5.16: The illustration of iso-parametric mapping

Before mapping of the element is done, the line or the conductor neutral axis is first of all determined for the required stringing configuration i.e. iso-parametric element mapping along the helical path including the core.

Firstly, for the assumed configuration for a specific axial load, along the chord length path defined as the neutral axis, the finite elements for the core are mapped. The core strand coordinates are easily obtained as they are defined along the neutral axis.

The iso-parametric mapping for the strands in each layer, as illustrated (5.16) is done by co-ordinate mapping. It showed the mapping of the reference element into the conductor cross-section as defined by distance R_i, from the neutral axis and with helical angle ϕ_i with respect to z-axis in line with coordinate system defined in section (2.4.3) in chapter 2. The discrete functions nodal parameters at each element are expressed in terms of coordinates values that are defined at the centreline of the cross-section of the circular strands. This indicates that the coordinates of the strands in various layer are defined from the neutral axis with the helical radius R_i and the helical angle ϕ_i with i= 1, 2, 3,……n, i.e. the nodal discretization of the conductor as can be seen in figure (5.15). These values can be transformed into Cartesian coordinates by the conversion of the polar coordinate systems along the curvilinear helical path defined for each strand path.

To derive the geometric mapping, the process starts by defining each centre cross-section coordinates, for each strand as described in figure (5.15) along both core path and the strand helical path. The implementation of the mapping, i.e. conversion of the polar coordinates into the Cartesian coordinates can be illustrated. For example, the nodes conversion will take the form: R_1 and ϕ_1 = (x1; y1; z1); R_2 and ϕ_2 = (x2; y2; z2) and R_3 and ϕ_3 = (x3; y3; z3) and so on for other successive nodes. Using the interpolation process showed in figure (5.13), the reference strand element is then mapped into the successive finite elements as defined by the nodes points (xi; yi; zi) coordinates along both core and the helical path. The conversion of coordinates can be achieved by using equation (3.27). In the interpolation process only the x and the y coordinates are required. Finally, the composite structure is formed by the reference 2D curved beam, being geometrically mapped into the global structure of conductor.

The displacements and rotation at the nodes of the 2 D beam element as expressed into the global coordinate system for the conductor and the transformation matrix is defined as:

$$v = \begin{bmatrix} v_1 \\ \theta_1 \\ v_2 \\ \theta_2 \end{bmatrix} = \begin{bmatrix} \Delta x & \Delta y & 0 & 0 & 0 & 0 \\ \Delta x & \Delta y & 0 & 0 & 0 & 0 \\ 0 & 0 & 1 & 0 & 0 & 0 \\ 0 & 0 & 0 & \Delta x & \Delta y & 0 \\ 0 & 0 & 0 & \Delta x & \Delta y & 0 \\ 0 & 0 & 0 & 0 & 0 & 1 \end{bmatrix} \begin{bmatrix} u_{x1} \\ u_{y1} \\ \theta_1 \\ u_{x2} \\ u_{y2} \\ \theta_2 \end{bmatrix} \quad \text{..... (5.71)}$$

Where $\Delta x = \frac{x_2 - x_1}{L^e} = \cos\phi = c$ and $\Delta y = \frac{y_2 - y_1}{L^e} = -\sin\phi = -s$

Using the beam curved finite element as the reference element, employing the transformation matrix equation to the beam element, the stiffness matrix, mass matrices and load vector for the conductor are obtained as follows:

$$K_C^e = [T]^T [K_B^e][T] + [T]^T [K_A^C][T] \quad \text{..... (5.72a)}$$

$$K_C^e = [T]^T [M_B^e][T] \quad \text{..... (5.72b)}$$

$$f_C^e = [T]^T [f_B^e] \quad \text{..... (5.72c)}$$

Where $[T]$ is transformation matrix and is defined as

$$[T]=\begin{bmatrix} c & -s & 0 & 0 & 0 & 0 \\ c & -s & 0 & 0 & 0 & 0 \\ 0 & 0 & 1 & 0 & 0 & 0 \\ 0 & 0 & 0 & c & -s & 0 \\ 0 & 0 & 0 & c & -s & 0 \\ 0 & 0 & 0 & 0 & 0 & 1 \end{bmatrix}$$

The advantage of using this form of composite formulation to obtain the FEM model for the conductor was that the path of each strand including the core is defined first for the desired configuration catenary curve as a function of its axial loads before mapping the curved beam element along this path. The composite structure is then achieved by the use of the transformation equation to transform the reference element into the conductor structure at the desired configuration.

To implement this FEM model in computer program in terms of the element size was done as a function of the pitch length. Geometrically, the pitch length falls into two quadrants with each half in opposite path. For stress distribution, it is assumed that each quadrant carries equal and opposite stress. Based on this, discrete elements use should have the maximum length or size that is equal or less than half its pitch length. In the aspect of the implementation of global structure, the total length of the conductor used to assemble the finite element along deformed path, the initial conductor points or the point of suspension was made to coincide with the origin of global coordinate. This help defines the initial position of each strand and then the path each strand will follows with the reference to the neutral axis in the final formation of FEM composite model.

5.12.4 The System Equation

The geometric mapping and the coordinate transformation with the assembly of the element equations for mass, stiffness and load vector form the equation for the system. To find the global equation system for the whole solution region we must assemble all the element equations. In other words, we must combine local element equations for all elements used for discretization. The elements connectivities were used for the assembly process. The above transformation results in damped equation for the transverse vibration of conductor. Thus, the system matrix equation was obtained as:

$$\begin{bmatrix} M_{11} & M_{12} \\ M_{21} & M_{22} \end{bmatrix}\begin{pmatrix} \ddot{u} \\ \ddot{v} \end{pmatrix}+\begin{bmatrix} C_{11} & C_{12} \\ C_{21} & C_{22} \end{bmatrix}\begin{pmatrix} \dot{u} \\ \dot{v} \end{pmatrix}+\begin{bmatrix} K_{11} & K_{12} \\ K_{21} & K_{22} \end{bmatrix}\begin{pmatrix} u \\ v \end{pmatrix}=\begin{pmatrix} F_1 \\ F_2 \end{pmatrix} \qquad \text{..... (5.73)}$$

Before obtaining solution for equation (5,73), the boundary conditions must be imposed on the equation. However, the beam does not experience any bending moments, and was free to rotate; therefore, the bending moments were zero at both ends, assuming it was simply supported at both ends. Therefore, the assembled global equation must satisfy the boundaries conditions of simply supported beam for each strand path i.e.

$$u_1 = \theta_1 = u_n = \theta_n = 0$$

In the solution of the FEM equation for the system, direct and iterative method was used and the explanation for the numerical scheme used is given in the next section.

5.13 Numerical Computation for System Response

To carry-out the vibration analysis for the conductor, the direct integration method was used. This method employs a step-by step numerical integration method for the evaluation of the dynamics response and its algorithms usually assume continuity of displacements, velocities and acceleration. This form of analysis was done based on Newmark integration scheme [90]. To derive this scheme, representing the equation (5.73) in a more compact form, with this equation for the system expressed as:

$$[M]\{\ddot{y}\}+[C]\{\dot{y}\}+[K]\{y\}=[F] \qquad \text{…….……. (5.74)}$$

Where $[\hat{K}]_{s+1} = [K]_{s+1} + a_3[m]_{s+1}$

$$[\hat{F}]_{s,s+1} = \{F\}_{s+1} + [m]_{s+1}(a\{y\}_s + a\{\dot{y}\}_s + a\{\ddot{y}\}_s)$$

$$a_3 = \frac{2}{\gamma(\Delta t)^2} \qquad a_4 = \frac{2}{\gamma \Delta t} \qquad a_5 = \frac{1}{\gamma} - 1$$

Note: the calculation of the system response requires the knowledge of the initial conditions. Specifically, if this is not known, in this case the initial conditions for the analytical model defined in chapter 3 will then be used. It can be approximated from equation (5.74)

$$[\ddot{y}]_0 = [M]^{-1}[F]_0 - [K]^{-1}[y]_0 \qquad \text{…….……. (5.75)}$$

And acceleration vector $\{\ddot{y}\}_{s+1}$ are compute and

$$[\ddot{y}]_{s+1} = a_3(\{y\}_{s+1} - \{y\}_s) - a_4\{\dot{y}\} - a_5\{\ddot{y}\}_s$$

$$[\ddot{y}]_{s+1} = \{\ddot{y}\}_s + a_2\{\ddot{y}\}_s = a_1\{\ddot{y}\}_{s+1}$$

$a_1 = \alpha \Delta t$ and $a_2 = (1-\alpha)\Delta t$

The derivations for the central deference method and the various responses are presented in appendix C

Chapter 6

Experimental Set-up and Testing

6.1 Experimentation

The conductor self-damping capability is an important parameter for the conductor in designing overhead transmission lines. This is because the response of a conductor to the alternating forces induced by the wind is normally determined by the amount of damping present in the conductor. Despite its importance in evaluating the dynamic behaviour of conductors, its value is usually not specified by the conductor manufacturers. The conductor self-damping is generally determined through the measurements performed on a laboratory test span. Unfortunately, results from different laboratories all over the world have presented values with a very wide range of deviation. A "Guide on conductor self-damping measurements" had been prepared in the past, jointly by IEEE Task Force on Conductor Vibration and CIGRE SC22 WG01, to try and promote uniformity in the measuring procedures. The Guide has been published by IEEE as Std 563-1978 [91] and also published in Electra n°62-1979 by CIGRE [92].

In order to validate the two forms of models as discussed in chapter 3 and chapter 5 (the analytical and the numerical), the conductor responses from these models have to be compared with the measured response from the tests conducted either in an indoor-scale test line or at the outdoor test station. The experimental work conducted and presented in this chapter was used to simulate the Aeolian vibration in an indoor test span. For the experimentations, the test span was set-up using several aluminium-conductor-steel-reinforced (ACSR); these conductors were strung at different tensions. The experimental setup for testing the conductor self-damping was developed with the aim at highlighting the critical issue of determining its magnitude present in a conductor as a function of the axial tension. Several tests were conducted to reproduce the conductor vibration and they are reported in subsequent sections of this chapter. From these experiments, some important characteristics of conductor damping, with varying axial load were observed. Based on the analysis of the results obtained from these tests and the further analysis as presented in the next chapter, inferences were drawn.

6.2 Experimental Investigation of Wind-induced Vibration

There are wide range of measurements systems developed and used for measuring different aspect of vibration that occur on overhead power line conductors. These experiments can be used to investigate various areas of conductor vibrations ranging from fatigue test, damper test, and self-damping test. These experimental tests are being conducted in both the outdoor and indoor

laboratory stations in various parts of the world. The laboratory procedures for these tests have been developed in the form of standards that are being applied to design test rigs and also highlight how the experiments procedures can be conduct with the specifications for equipment required for the different type of test on the conductor.

Figure 6.1: The VRTC test span layout

The experiments for this study were conductor in an indoor laboratory. This indoor laboratory is the Vibration Research and Testing Centre (VRTC) which is situated at the University of KwaZulu-Natal, Westville campus. The laboratory test span at the VRTC is shown in figure (6.1). In this indoor laboratory, testing for conductor damping, the structural design for the span and the mechanical devices used, were set-up according to the IEEE standard for the vibration measurement in evaluating conductor self-damping [91]. To improve on the testing process, recent systems have been installed to accurately measure the deflection of the conductor close to fixed points of the span, near suspension clamps to measure the bending amplitude.

6.3 The Indoor Laboratory Testing Methods

The "Guide on conductor self-damping measurements" [92] highlights the three different methods for evaluating conductor self-damping in an indoor laboratory. The three main methods that are suggested are; the first is the "power method" in which the conductor is forced into resonant vibrations by a shaker and the power dissipated by the vibrating conductor is measured at the power input point.

The second method known as the "standing wave method", this is based on the measurement of the power flow through the conductor at the resonant conditions.

A third method referred to as "free vibration method" which derives the energy dissipated by the conductor from the rate of decay of the vibration after the disconnection of the driving force or the impart load.

Several laboratories around the world have performed conductor self-damping measurements. However, large disparities in self-damping predictions have been found among the results supplied by the various laboratories. The cause of these disparities has been identified and can be categorized into three main points [91]:

1. The different span end conditions adopted by the various researchers (fixed clamps, pivoted clamps, etc.)
2. The different types of connection between the shaker and the conductor (rigid or flexible) and the different location of the power input point along the test span.
3. The different conductor conditioning before the test (creep, running in, etc.).

The scope of the proposed Standard [93] is to provide test procedures based on the above-mentioned Guide, but more devoted to minimize the causes of discrepancy between test results. This can be achieved by taking into consideration the variety of test procedures used in these different laboratories and harmonize them into a test monograph which can then predict the outcomes of results depending on the particular procedure used. Moreover, this procedure would

be able to consider wide variety of conductors testing and suggest the most appropriate test method and procedure for each conductor type.

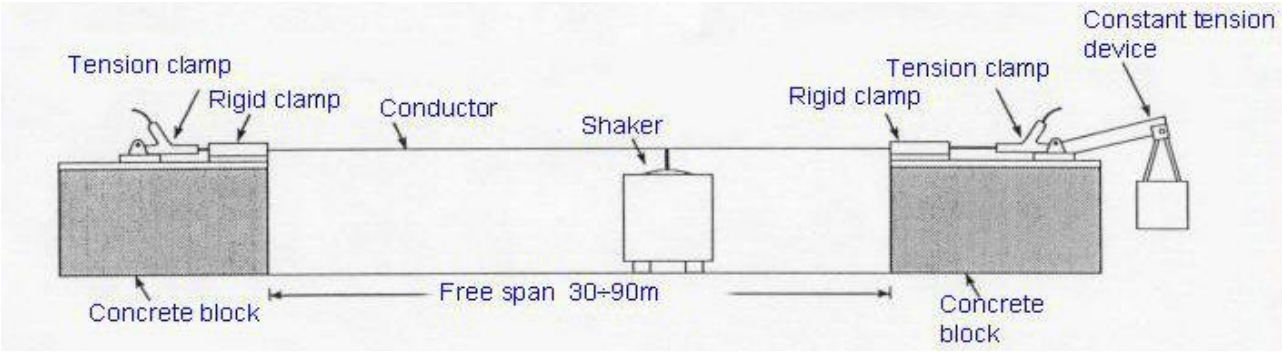

Figure 6.2: Experimental test set-up [2]

6.4 Description of Test Set-up

The laboratory test spans for conductor self-damping measurements at the VRTC comprises of apparatus similar to that shown in figure (6.2). This figure represents a schematic view of the actual experimental setup of the test span shown in figure (6.1), the experimental set-up layout at the VRTC. The conductor span length is about 86.4 m. The facilities at the VRTC was built in line with recommendations from the IEEE Std 563-1978 for the Measurement of conductor self-damping [1, 2, 91]. The laboratory equipment consists of a tension application device, shaker (the TIRAvib shaker type), conductor clamp system, and measurement system for data collection and processing. The free span length was preferably suited to produce a number of loop lengths longer than the longest loop length used in the tests. The test span is equipped with temperature controlling devices used to control its ambient temperature. Due to its relatively long length, the influence of the end termination losses, minimized by the rigid clamps, is further reduced and the distribution of the tensile load between the conductor strands is more homogeneous.

For the experimental setup as shown in figure (6.2), there is a device for applying tension known as the constant tension device. This device makes it possible to vary the applied tension by applying a specified load on the device. This helped to introduce different tensions to the test conductor by adding or removing loads weights at this device. This constant loading device cannot control the conductor tension after the conductor is camped, what does affect the tension is the temperature of laboratory at which the test is being conducted.

6.4.1 Shaker and Shaker Conductor Connection

Figure (6.3), shows the position of the shaker, which was used to provide the power input to the conductor. A vibration shaker is usually located near one end of the span i.e. loading arm part of the test set-up. This form of exciter used at the VRTC is the electro-dynamic shaker having a light

armature and linear bearings that was capable of exciting the conductor at its natural frequencies. The shaker induced a periodic function or a sinusoidal force on the test span. The alternating movement provided by the shaker produces a simple harmonic motion representing a specific mode of excitation. Vibration amplitudes and frequencies were controllable to the required accuracy and were done by the function generator through the power amplifier.

Figure 6.3: A flexible Connection used in connecting the Shaker to the Conductor

The location of the shaker along the test span was chosen to facilitate the required test frequency range in which the various modes can be produced. The 0.8 m distance from the end rigid clamp was used; this ensured that loop length at the highest test frequency was not produced between the shaker and the rigid clamp.

The connection between the conductor and the shaker was done using the flexible connection as shown in figure (6.3). The flexible connection between the shaker and the conductor guarantee that, at resonance, the conductor can vibrate at amplitudes higher that the amplitude imposed to the shaker table without driving the shaker armature. The power input from the shaker is adjusted to the resonant frequencies of the conductor to ensure that the displacement at the anti-node represents the speed of the wave travelling through it.

6.4.2 The Span End Conditions

The test span is strung between two massive blocks made of concrete which on top of it houses the clamp where the conductor is placed. This span end termination equipment has the capability of withstanding and maintaining a constant conductor tension. The span is terminated at the ends by two square clamps which are used to maintain the constant tension at the test span ends as shown

in figure (6.4). These heavy and rigid clamps end is inserted with groove diameters not exceeding more than 0.25 mm of the diameter of the conductor to hold the conductor in order to produce good results. A rigid clamp shown in figure (6.4) is used to minimize energy dissipation through the termination fixture, but they do not have any capacity in controlling the conductor tension. At VRTC test laboratory the conductor tension is kept constant by maintaining the ambient temperature.

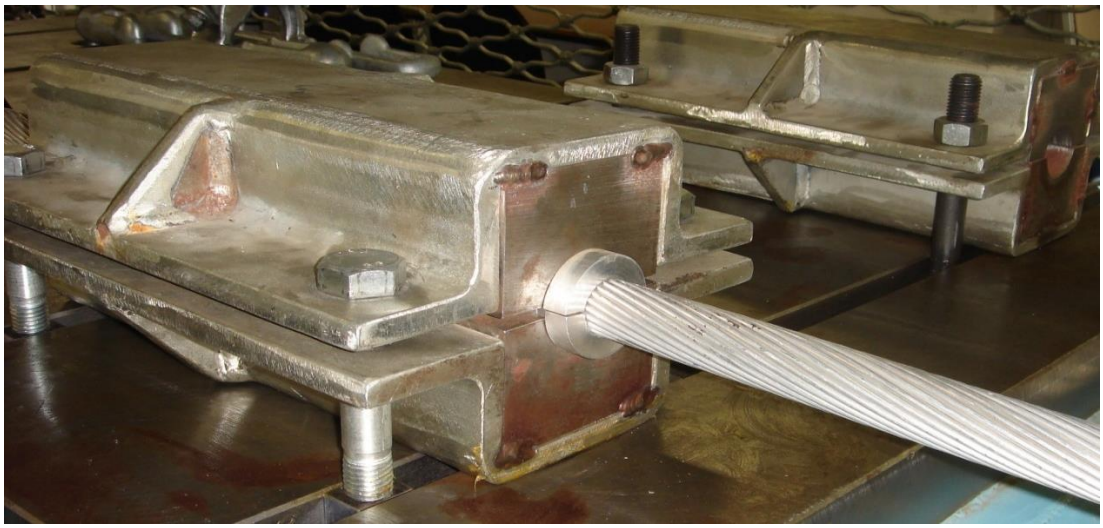

Figure 6.4: The span end termination

Between the clamp and the tension application device is the load cell measurement system and shackles as shown in figure 6.5. The shakes, the end sleeves threaded bars and pivotal balance beams are connected to the loading device. This arrangement was used to successfully achieve the constant tension applied to the conductor ends. For reliable results, the terminating fixtures and rigid clamps must have sufficient stiffness to ensure that energy losses do not occur beyond them i.e. not beyond the termination point of the conductor at the clamp.

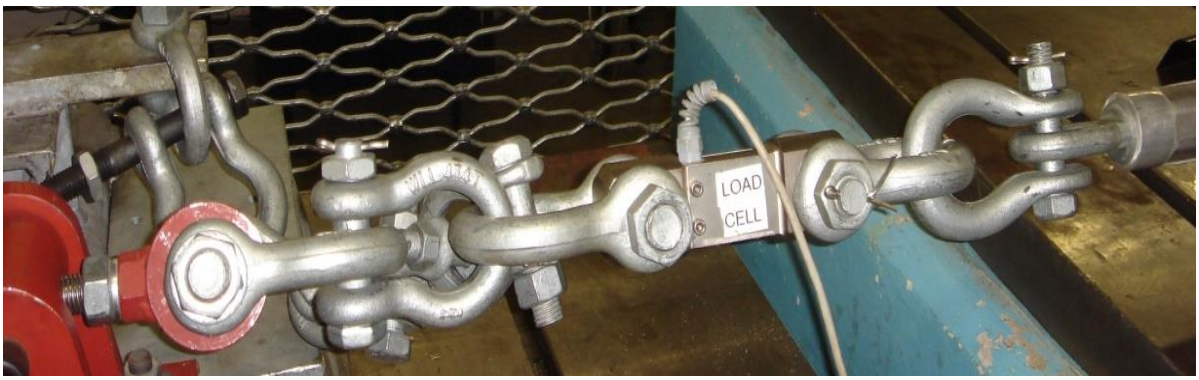

Figure 6.5: The connecting link between the clamp and the loading arm

6.4.3 Accelerometers and Force Transducers

In the collection of data from the conductor and also to feed control information to the shaker, the accelerometers and the force transducer was used. The accelerometers type used was the PCB Model 352A73, shown as figure (6.6). They were mounted to the conductor using wax at various positions along the span for the sweep test and by a clip during the hysteresis test. The clip was used for the hysteresis loop test because, the acceleration locations were chosen such that the vibration modes could be detected by placing it at the anti-nodes. The force transducer was placed at the Shaker-Conductor. The placement was also used to measure the node and the antinode amplitudes on the conductors.

The accelerometer and force transducer were expected to have a phase shift between the two signals because of the different response time of the two signals. This phase shift was frequency dependent and has taken into account in the determination of the phase angle between the measured quantities at each vibration mode. The computer controlled test system; the data acquisition software was set up to perform automatically the phase shift correction between the force transducer and accelerometers. In addition, load cell was used to determine the value of the axial tension.

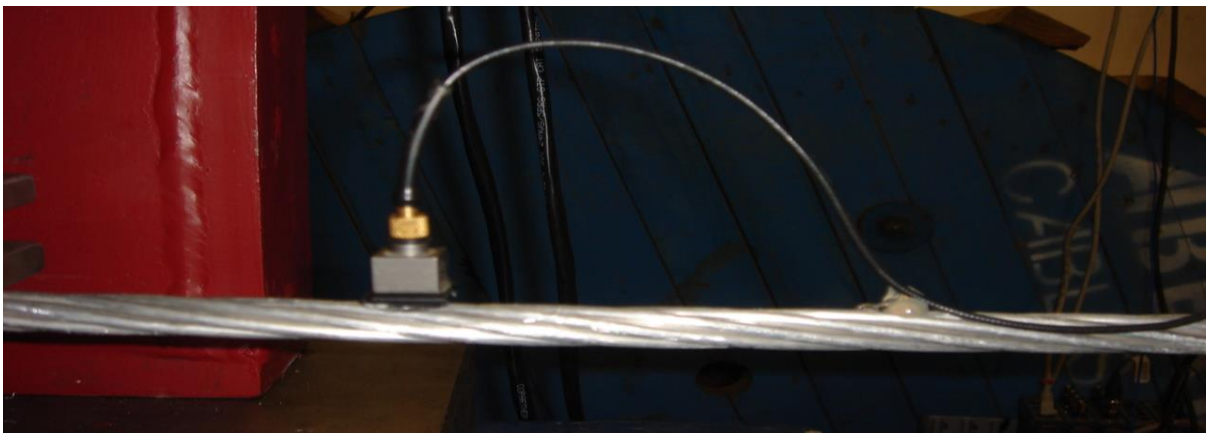

Figure 6.6: An accelerometer

6.5 Description of Experimental Methodology

The experiments conducted at the VRTC were in twofold. The first was the sweep test to produce the dynamic response of the conductors in order to determine the conductor natural frequencies. The second test was used, at a specified signal of a fixed frequency and amplitude sent from the function generator to drive and controlled excitation of the test span via the shaker. The frequency chosen was to coincide with one of the natural frequencies from the already conducted sweep test. For this test, the superposition of the force transducer and accelerometers positioned at various

positions on the conductors was used to generate a hysteresis loop. The area of the experimental obtained hysteresis loop is then used to calculate the conductor self-damping.

Both experiments consisted of applying a specified frequency to the line at a distance of 0.8 m from one end of the span. The horizontal tension applied at both ends was introduced as a percentage of the conductor ultimate tensile strength (UTS).

6.5.1 The Sweep Test

The measurements on the laboratory test span using the sweep test method was done to excite the conductor at its natural frequencies. As discussed in chapter 3, when modelling the conductor using the global analytical approach, the conductor was modelled as continuous distributed parameter system. The analytical equation for the conductor, using the beam model indicated that the conductor has a dense parameter of natural frequencies. The sweep test was made to resonant the conductor at these natural frequencies and then identify the dominant resonance frequencies as shown in figure (6.7) for Tern conductor at 15 % UTS.

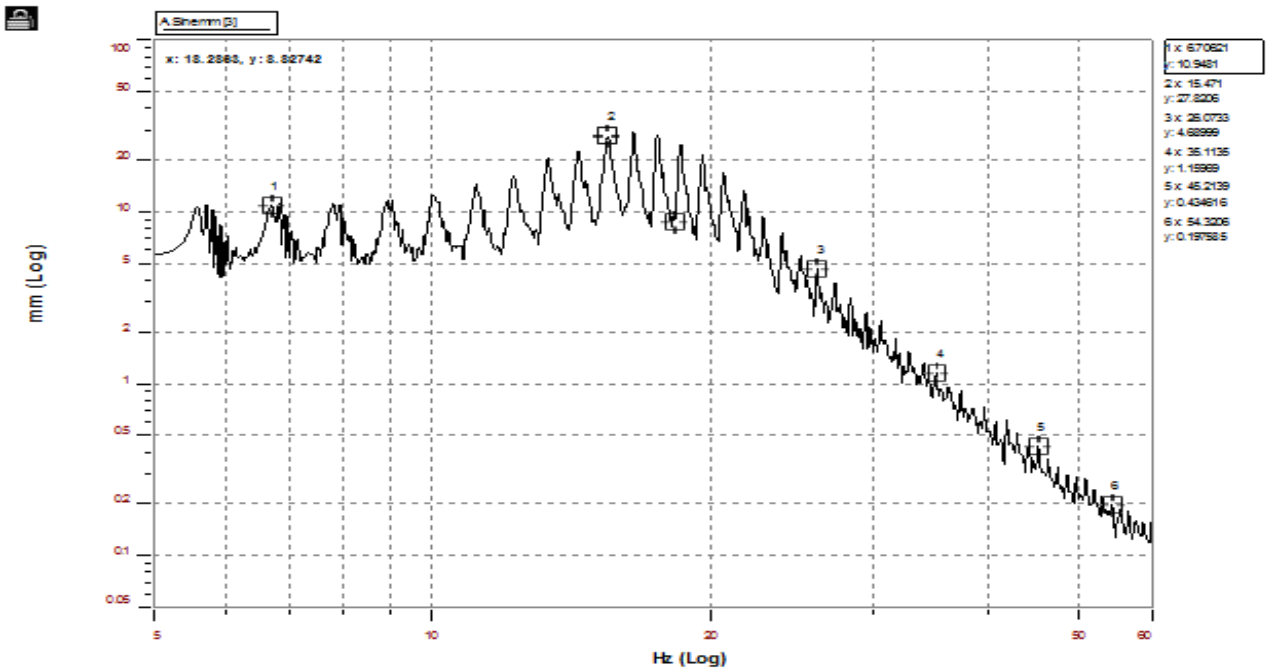

Figure 6.7: The resonance frequencies for Tern conductor at 15 % UTS

For each experiment performed on the conductor, the excitation frequency from the shaker is automatically tuned so as to correspond with one of the natural frequencies of vibration of the conductor. This was achieved by the PUMA software [85]. To ensure this condition was met, the shaker power was controlled automatically to adjust itself in order to provide the correct loop velocity at an antinode. Frequency was fine-tuned by the software to maximize loop amplitude. If necessary, the software which control the shaker was adjusted in order to provide the desired loop

amplitude corresponding to a particular mode. This process selects the system resonance at it various modes as the shaker sweep across the conductor. To determine the span resonance, the test method described was required to reach the conductor resonant conditions across a specified range of frequencies. In this regard, the determination of the conductor resonance, the shaker was operated at the frequency controlled range of between 5 Hz and 70 Hz. This provides various maximum displacement of the conductor at an antinode for different modes and this was repeated for different specified axial tensions.

6.6 Method for testing Conductor Self-damping

As indicated, the second form of testing that was conducted was the generation of the hysteresis loop. In [14] an extensive laboratory tests were carried out on the 84.6 m-length span. The tests documented in this work included that of using both the forced and free vibration testing method to determine the conductor self-damping. In this study, the form of testing method used, involved the determination of damping at a specified mode of vibration through the generation of hysteresis loop. It is unlike the test method done by the half power method, which is described in detail in Reference [14]. The next section explained the philosophy behind the measurement of self-damping using the hysteresis loop.

6.6.1 Experimental Design Philosophy for Generating Hysteresis Loop

In the article [44], the quasi-static behaviour of conductor was used to design a test rig to determine the conductor self-damping. The described methodology used to evaluate damping indicated that the experimental set-up used, was based on the relationship between the local bending moment and the curvature of the conductor centre line. This method assumed that conductor curvature is essentially a function of the bending moment. The local behaviour at a location on the conductor was described by the moment-curvature relation. The experimental set-up was used to measure the conductor damping using the moment-curvature relation at different locations of the conductor and the moment versus rotation angle curve. The moment was described by the following equation [48]:

$$M = \alpha N^{\frac{1}{2}}(\varphi + \beta N)^{(\frac{1}{2}-\delta)}[1-\exp(-\gamma N^{\delta}\varphi)] \quad \text{..... (6.1)}$$

The various constants in this equation can be found in [49]. The power dissipated per unit length P_E [W/m] was obtained as:

$$P_E \cong \frac{1024}{9}\gamma^2(C_* N)^{(\delta+\frac{1}{2})}c^2\pi^5\beta y_{\max}^3 m^3 f^7 \frac{EI}{N^4} \quad \text{..... (6.2)}$$

Although the test set-up as described in [49] produced good experimental results, the factor not taking into account was the flexibility of the conductor which is a function of its length. Taking into account this factor, using the 86.4 m span length at the VRTC, this test span considered the conductor to having a relatively high level of flexibility which is a function of its span length and the axial loading. The steady state vibration of the conductor is a function of the frequency of excitation and this directly determines the mode at which the conductor vibrates.

Based on this, there was a need to develop a testing methodology to evaluate the hysteresis phenomenon, during the conductor dynamic condition that was applicable to the relative long span as found at the VRTC. As documented in [57], where the explanation is given for the various phases leading to the formation of the hysteresis loop. Based on this, the experimental philosophy for generating hysteresis loop was developed. The design philosophy used to achieve this was also based on the moment-curvature relation for the conductor but it application was for the dynamic condition.

The travelling wave produces loops on the vibrating conductor at a specific frequency. The rate of formation of the loop length was used to determine the boundary condition for solving the moment-curvature equation. This vibrating conductor, the bending stiffness during periodic motion alternate between the maximum and the minimum bending stiffnesses. As the vibrating conductor alternating between these two bending stiffnesses, this results in the formation of a cyclic hysteresis loop. This concept was used to design a testing system as explained in the next section. Unlike the sweep test, were a range of frequencies are obtained, in this form of testing only one frequency is fed to the line for a specific test, thus only the steady state was instantly assumed by the test conductor.

6.7 Experimental Evaluation of Damping: Hysteresis Loop

The underlying objective for the work as described in this section was to outline the developed method of measuring vibrations with the aim to evaluate the self-damping in the form of a hysteresis loop. Firstly, the hysteresis loop formed represents the lagging between the loadings and displacements. Based on the concept that is explained in the previous section, a LabVIEW program was developed to generate the hysteresis loop. The LabVIEW program was developed in such a way to send signals to the conductor and also receive data from the test conductor.

6.7.1 Test Procedures and Data Acquisition using LabVIEW

In the experimental methodology, the tests conducted were done with the following procedures using the LabVIEW program. The LabVIEW program was developed and designed to send,

process and acquire signals between different hardware, the measuring instrument includes the computer, function generators, A/D converters, and power amplifier. The function generator was used to generate a signal with a given frequency and amplitude in the form of a sinusoidal signal. This signal was then amplified by the amplifier which is send to the shaker to excite the conductor. The output signals from the accelerometer was in a voltage form and was received by the NI USB-6210 (National Instruments data acquisition device with USB PC connection). The accelerometers were connected to the NI 9234 dynamic signal acquisition (DSA) module. The NI 9234 DSA module has a built-in antialiasing filter that automatically adjusts to the sampling rate. The DSA module was connected to a desktop computer, which houses the program that controls the function generator and the power amplifier that drives the shaker. A signal acquisition module with signal conditioning function, type NI USB 9234, was connected to a desktop and accelerometers. This digitizes the incoming signals to the analog output signals. The LabVIEW program was developed to work as both input and acquisition of data and also display the acquired data. Measurement of the hysteresis loop for the vibration conductor was done using the LabVIEW DAQ max.

For data input, acquisition, and display, the LabVIEW program that was developed was divided into three parts. For the purposes of these measurements, and the hysteresis loop formed, the graphical user interface (GUI) was created, see figures (6.8) to (6.10). The program was made to operate in any of these three GUI environments using the toggle buttons.

6.7.1.1 Data Input

The first part of the LabVIEW program was developed sending input signal to the conductor system. This program sends signal via the function generator to drive the shaker. The GUI for this aspect is shown in figure (6.8). The input data includes the frequency and amplitude at which the shaker was driven. This aspect was designed to send a specific frequency to drive the conductor. This specific frequency from the function generator can be changed without having to interfere with values in the program block diagram. This gives the ease during experiment to change the frequency while the shaker was still running. Also, this aspect of the program was also used to calibrate the accelerometers in order to verify the values that are being received from the accelerometers are reliable.

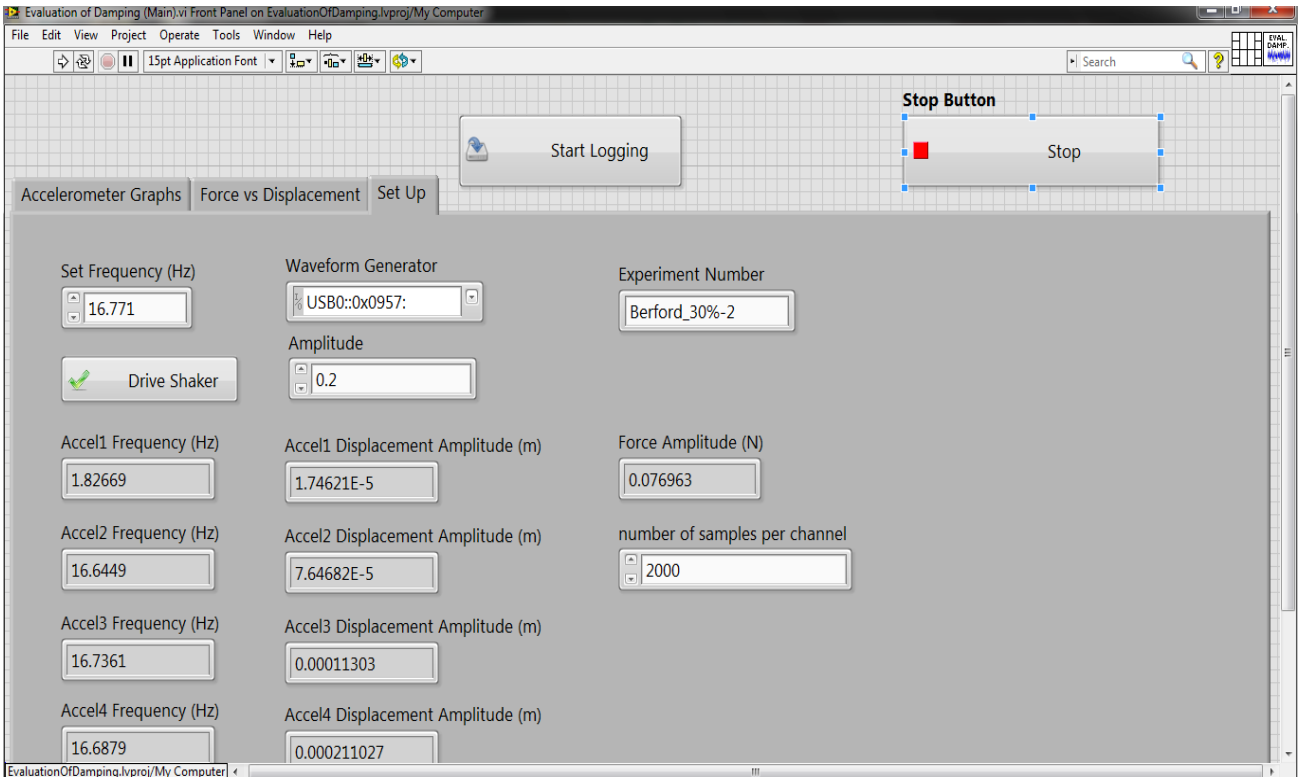

Figure 6.8: LabVIEW GUI for input signal

6.7.2 Data Acquisition and Display

For the aspect of data acquisition and display, two forms of data are received from the conductor. The first is the signal from the force transducer placed on the shaker. During measurement, a specific constant frequency value is fed to drive the shaker, while changing the position of the accelerometers using the clip to accelerometer is attached, to locate the position, which should coincide with the antinode of the vibration.

The second signal is obtained from the accelerometers. This outward signal is made to pass through a DAQ card whose function is to convert digital signals to analog signals by an A/D converter which is built inside it. The GUI for the program shown in figure (6.9), signals from the vibrating conductor were generated as sine waveforms, from the five different accelerometers placed on the line.

Each accelerometer was placed to coincide with an antinode. The experiments were conducted by continuously increasing the input frequency with the tension kept at constant value, the amplitude of the generated signal is then measured. Another experiment is done by changing the value for the axial tension, with another input frequencies.

The third aspect of this LabVIEW program was the generation of the hysteresis loop see figure (6.10). The program for the data acquisition, two forms of signal are received: one signal from force transducer placed between the shaker and the conductor. The second is the signals each from

the five accelerometers. The formation of the hysteresis loop was obtained by plotting the force transducers against any of the accelerometers signal. The hysteresis loop was obtained by plotting the signals from the force transducer with any of the accelerometer. This plot represents the force-displacement curve.

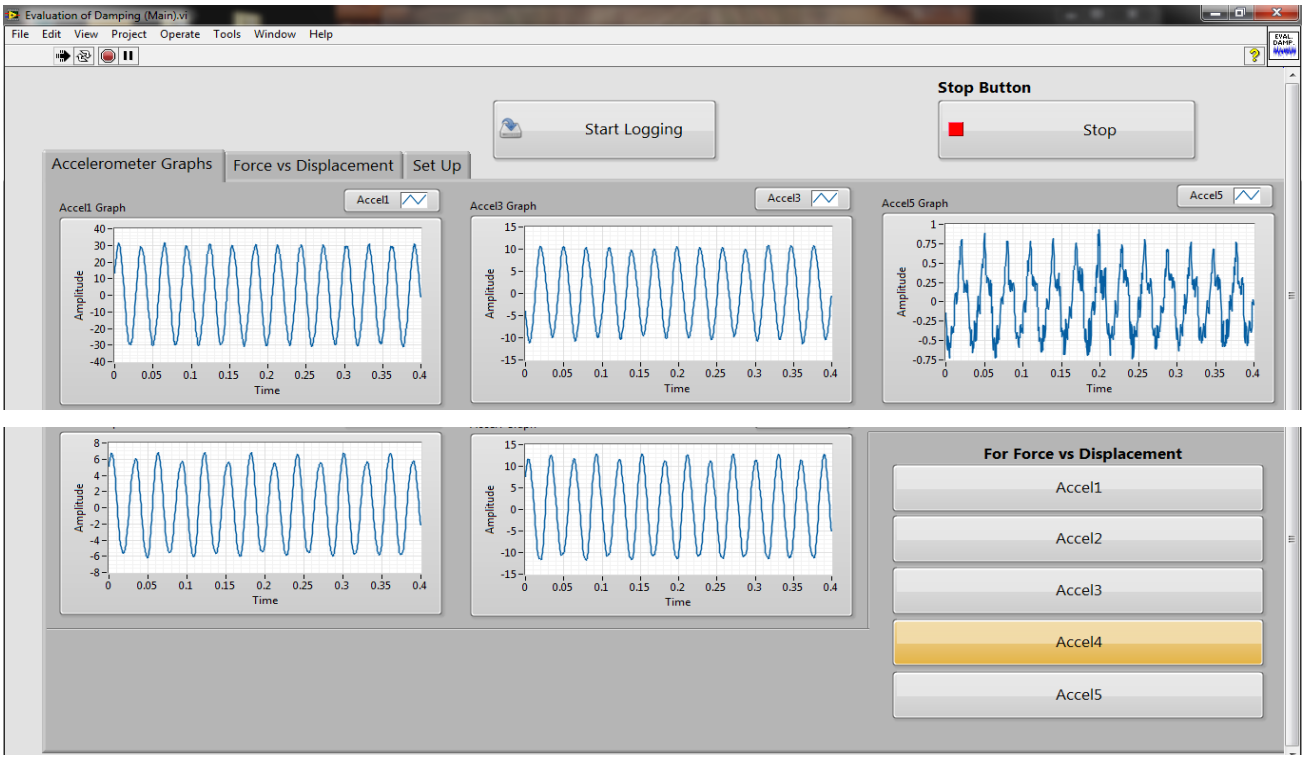

Figure 6.9: LabVIEW GUI for signal acquisition

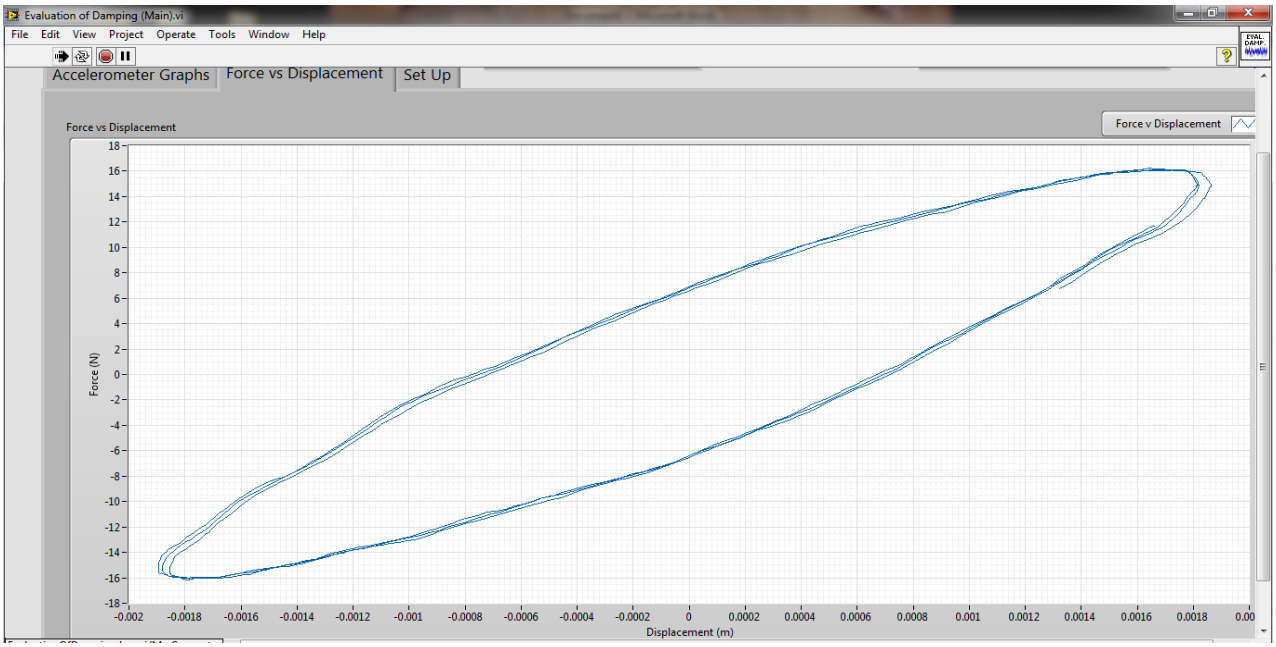

Figure 6.10: LabVIEW GUI for experimental formation of the hysteresis loop

All acquired data together with input variables were saved in a data file, from where they can be used for further analysis in the future. Matlab program was then developed to calculate the area for each loop obtained in order to determine the damping. Analysis of the experimental results is presented in the next chapter.

6.8 Test Conductors

Four conductors were tested for both experimental tests conducted. All the conductors were the Aluminium-Conductor-Steel-Reinforced (ACSR) with the code names Beresford, Tern, Pelican and Rabbit as shown in figure (6.11). The Rabbit has a centre core of steel and a single layer of strands made of aluminium. The Rabbit is a single layer conductor mostly used in the distribution aspect of power transmission. The Pelican has two layers, the centre core is made of steel and the two layers of strands made of aluminium. Tern has three layers, the centre core and the first layer is made of steel and other two layers is made of aluminium. The Beresford has four layers, the centre core and the first layer is made of steel and other three outer layers is made of aluminium. The cross-section views of these conductors are shown in appendix A. Table 6.1 reports the main physical characteristics of these conductors.

Table 6.1: Physical Properties of test Conductors

Conductors	Bersford	Tern	Pelican	Rabbit
Total area (mm^2)	746.9	403.77	255.77	52.9
Conductor diameter (mm)	35.56	27.00	20.70	10.1
Number of wires on each layer Steel	6-1	6-1	1	1
Number of wires on each layer Aluminium	22-16-10	21-15-9	6-12	6
Diameter of aluminium wires (mm)	4.27	3.38	4.14	3.35
Diameter of steel wires (mm)	3.32	2.25	4.14	3.35
Linear mass (kg/m)	2.375	1.340	0.771	0.210
Rated tensile strength (kN)	180	98.70	51.15	18.4

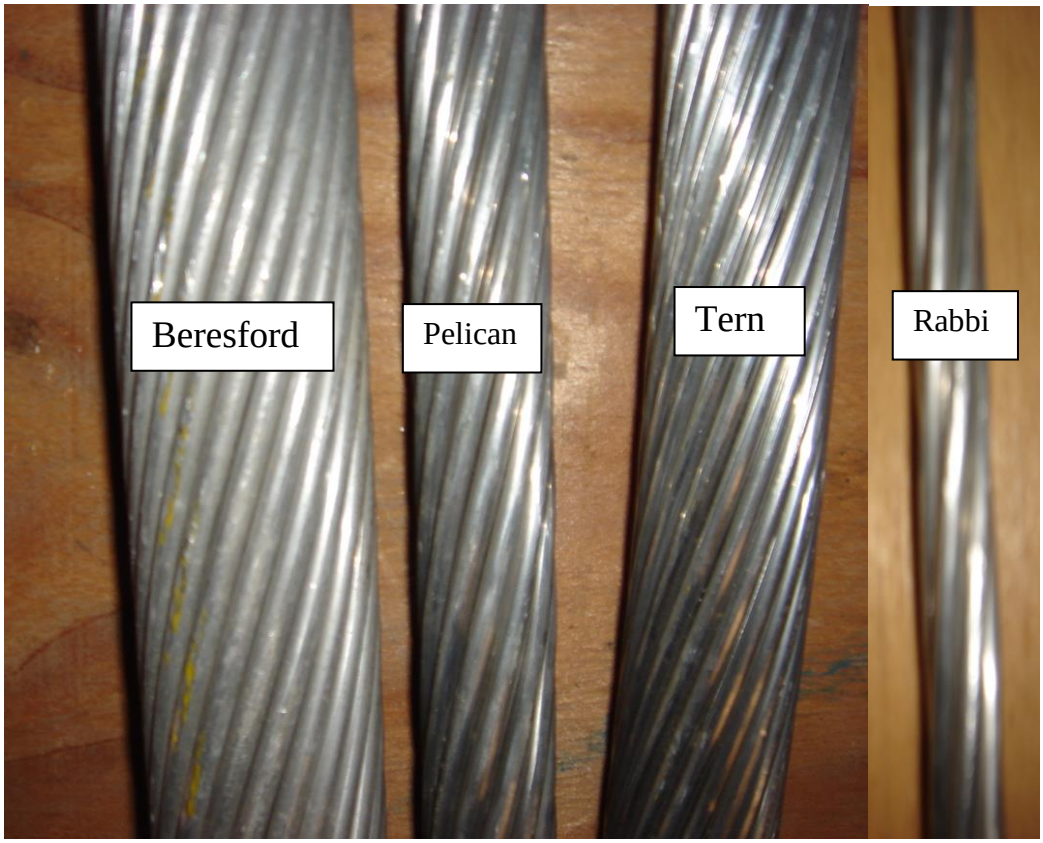

Figure 6.11: The test conductors

Chapter 7

Analysis and Discussion of Results

7.1 General Remarks

As discussed in chapter 1, besides this study seeking to gain more understanding into the phenomenon of wind-induced vibration, the main goal was the determination of the self-damping capability of the power line conductors. Three aspects of conductor vibration with respect to modelling and analysis, in terms of aeolian vibration were conducted in this study. These were the analytical, the numerical modelling and the experimental study.

In the analytical modelling of conductor, the conductor was modelled either as a distributed parameters structure or as a composite structure. Both models were used to predict the transverse vibration of the conductor either globally or used to investigate parameters associated with the internal structure. From these two analytical modelling, using the conductor physical properties and other input variables, the analytical results were obtained. Based on the results obtained, the fact still remains that precise analytical modelling of the dynamic behaviour of conductors remains a challenge. Obtaining the analytical model that adequately represents the conductor geometry is very difficult and this has differed mathematical equation such as the string or the beam equations. Also, another problem has to do with the fact that conductor vibration exhibits a non-linear response.

The second aspect that was investigated was the dynamic behaviour of the power line conductors using a numerical method i.e. the finite element analysis model. The FEM model was developed as a function of its geometry using the curved beam finite element type. Taking advantage of the concept of iso-parametric interpolation, the composite formulation of the global equation for the conductor was obtained. The FEM was also used to formulate and implement the inter-strand contact; the formulation was done as a function of stick-slip regime. This was used to evaluate damping as a result of the hysteresis loop formed from this process.

The third aspect of the investigation was the experimental study; the indoor laboratory experiments were conducted at the VRTC. The experiments conducted were used to determine the amount of damping from the conductor. There were two different tests that were conducted. The first was the sweep test that was used to obtain the conductor natural frequencies. The sweep test was used to determine the resonance frequencies for the conductors caused by the excitation from the sinusoidal force via the shaker. The second was the forced vibration tests. Based on these values obtained from the first test, this serves as input variable for the second test that was conducted and

this was used to generate the hysteresis loop. The area of the loop was used to determine the amount of damping for a chosen mode of vibration. The analysis of these results and the discussion are presented later in this chapter. It is of vital importance that for uniformity of results, the same parameters that were used for the conductors for the experimental study was also used to implement the analytical and the finite models. This was done for different configuration of the conductor system defined by the axial loads.

7.2 The Conductors Natural Frequencies

The three aspects of conductor modelling used to evaluate the dynamic, which was carried out in this study; all the three models have one parameter in common which is the conductor's natural frequencies. Generally, the number of natural frequencies of any system in vibration is equal to the number of degrees-of-freedom; thus, any system having distributed parameters such as conductors have an infinite number of natural frequencies. At a given time, such a system usually vibrates with appreciable amplitude at only a limited number of frequencies, often at only one frequency. The vibration amplitude at each natural frequency is associated with a particular shape, called the normal or natural mode. For example, for the conductor, any of its vibration modes is assumed to be simply supported beam. This implies that it vibrates laterally at its lowest or fundamental natural frequency, which assumed shape of a half sine wave. All possible vibration modes for the conductor are made up of superimposed vibrations of the mode shapes at the corresponding natural frequencies. This then indicates that, the total motion at any point of the conductor system is the sum of the motions resulting from the vibration in the respective modes. The complete solution of the vibration problem would require the determination of all the natural frequencies and the mode shape associated with each. In practice, it is often necessary to know only a few of the natural frequencies, usually the lowest frequencies are the most important.

The values for the natural frequencies from the three aspects of modelling is the most reliable platform for comparison of all the aspect investigated in this study. The comparison of the values for the natural frequencies indicate how well the two other models compared with experimental study, have adequately represented the conductor. The values for the natural frequencies are presented as function of the axial tension.

Figure (7.1) shows a sample diagram for experiment done for Pelican conductor at 20 % UTS and peaks indicate the natural (resonance) frequencies. Tables 7.1-7.4 showed the comparison between the natural frequencies obtained from the analytical, FEA models in comparison with experimental results for the four conductors used in this study.

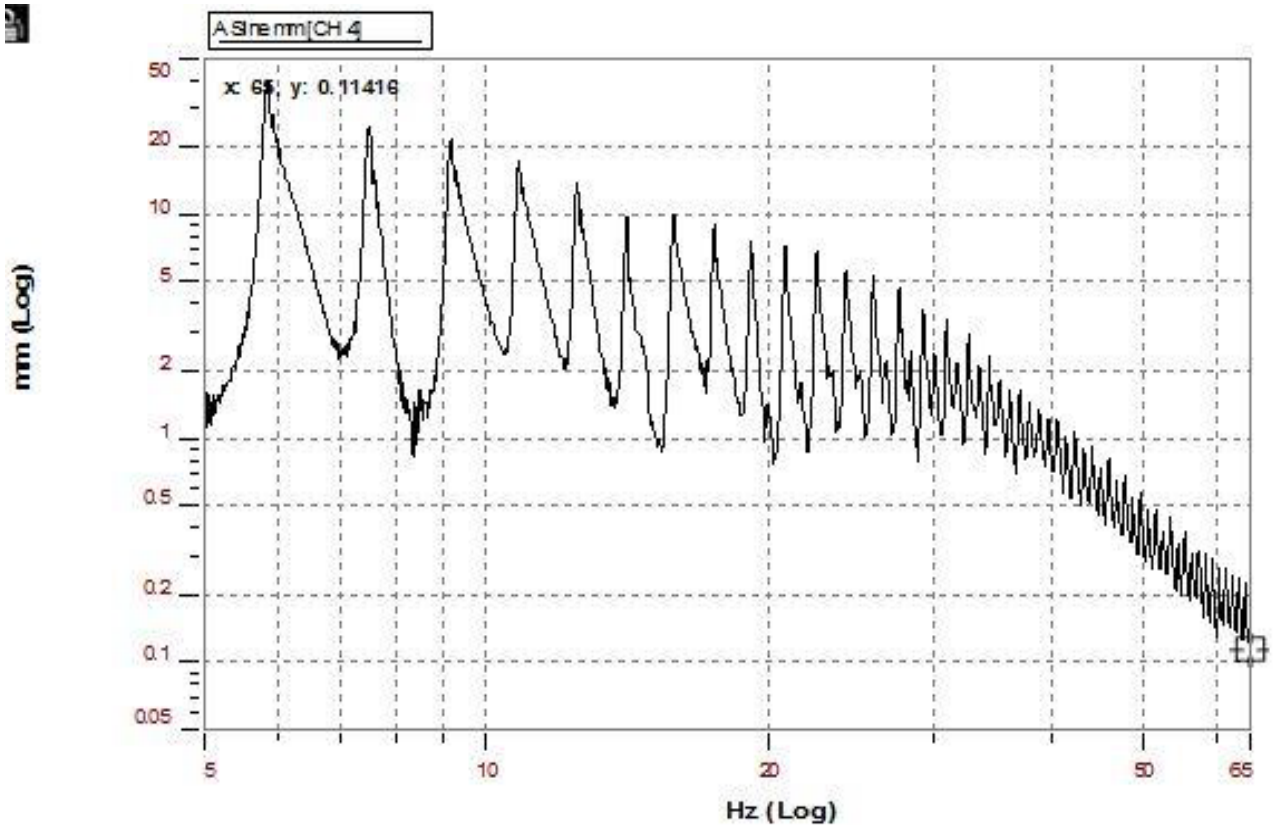

Figure 7.1: Sweep test graph done Pelican conductor at 20% UTS

Table 7.1: The comparison of natural frequencies values obtained from analytical, FEM and experimental result for Rabbit conductor

Natural Frequency (Hz) 25 % UTS				Natural Frequency (Hz) 30% UTS			Natural Frequency (Hz) 35% UTS			Natural Frequency (Hz) 40% UTS		
Mode	Analyt. Model	FEM	Exp. value	Analyt. Model	FEM	Exp. value	Analyt. Model	FEM	Exp. value	Analyt. Model	FEM	Exp. value
1	5.3815	5.982	6.058	5.8952	5.895	7.158	6.3675	6.911	7.692	6.8072	7.307	8.019
2	10.763	10.943	11.595	11.000	11.790	12.225	12.235	12.905	13.153	13.614	14.614	15.9338
3	16.145	16.934	17.193	17.686	18.100	18.451	19.103	20.244	21.308	22.422	23.334	25.869
4	21.527	22.007	22.792	23.582	24.712	25.680	25.471	26.231	27.465	27.23	28.112	30.806
5	26.910	27.922	29.396	29.478	30.112	31.912	31.839	32.840	34.625	34.038	35.638	38.747
6	32.293	33.456	34.005	35.375	36.357	37.150	38.208	39.631	41.789	40.846	41.111	43.693
7	37.677	38.679	39.622	41.272	42.003	43.394	44.578	46.921	48.959	47.655	49.346	52.645
8	43.062	44.234	46.247	47.117	48.672	50.646	50.948	51.950	53.135	54.465	55.667	57.604
9	48.447	49.451	52.882	53.069	54.073	57.908	57.319	58.323	60.320	61.275	63.280	65.573
10	53.834	54.891	56.530	58.968	60.006	62.181	63.691	64.699	66.515	67.086	68.195	71.553

Table 7.2: The comparison of natural frequencies values obtained from analytical, FEM and experimental results for Pelican conductor

Natural Frequency (Hz) 20 % UTS				Natural Frequency (Hz) 25% UTS			Natural Frequency (Hz) 30% UTS			Natural Frequency (Hz) 35% UTS		
Mode	Analyt. Model	FEM	Exp. value	Analyt. Model	FEM	Exp. value	Analyt. Model	FEM	Exp. value	Analyt. Model	FEM	Exp. value
1	4.1884	4.535	5.058	4.6828	4.683	5.058	5.1297	5.130	5.692	5.5407	5.541	5.948
2	8.3771	8.821	9.053	9.3658	9.366	10.924	10.206	10.646	11.014	11.082	11.581	12.898
3	12.166	12.643	13.320	14.049	15.322	16.067	15.390	16.790	17.734	16.623	16.983	17.848
4	15.247	16.756	17.717	18.733	19.890	20.373	20.521	21.690	22.934	21.165	22.344	23.801
5	20.947	21.547	22.183	23.418	24.821	25.622	25.652	26.442	27.110	27.707	28.790	29.756
6	25.138	26.542	28.111	28.104	29.772	31.349	30.785	31.222	33.283	33.25	34.045	35.714
7	29.331	30.490	31.123	32.791	35.101	37.167	35.918	36.919	39.000	38.794	39.346	41.677
8	33.526	34.109	35.965	37.479	39.480	40.976	41.053	42.155	44.987	44.34	45.342	47.646
9	37.722	38.625	39.893	42.169	43.661	44.789	46.189	47.193	49.895	49.887	50.691	53.620
10	41.92	42.126	43.103	45.247	46.867	47.789	51.327	52.334	53.089	55.435	56.442	58.603

Table 7.3: The comparison of natural frequencies values obtained from analytical, FEM and experimental result for Tern conductor

Natural Frequency (Hz) 15 % UTS				Natural Frequency (Hz) 20% UTS			Natural Frequency (Hz) 25% UTS			Natural Frequency (Hz) 30% UTS		
Mode	Analyt. Model	FEM	Exp. value	Analyt. Model	FEM	Exp. value	Analyt. Model	FEM	Exp. value	Analyt. Model	FEM	Exp. value
1	3.8322	3.832	4.193	4.425	4.850	5.937	4.9473	5.005	5.982	5.4194	5.483	6.546
2	7.6658	7.866	8.012	8.8512	9.900	10.212	9.8956	10.012	12.225	10.840	11.966	12.309
3	11.502	12.111	13.613	13.280	14.354	15.613	14.846	15.023	17.827	16.262	17.455	18.430
4	15.342	15.342	18.530	17.712	18.810	20.139	19.800	20.038	23.130	21.687	22.947	24.267
5	19.188	19.286	21.929	22.148	23.272	26.929	24.757	25.060	28.839	27.116	28.446	31.174
6	23.041	24.041	26.822	26.591	27.739	31.022	29.720	30.090	34.810	32.550	33.952	35.518
7	25.443	26.902	30.992	31.040	32.214	34.992	34.689	35.131	39.246	37.989	39.467	42.101
8	30.771	31.173	32.910	35.498	36.698	40.703	39.666	40.184	45.278	43.435	47.099	50.022
9	34.652	35.573	36.911	39.965	41.192	43.211	44.651	45.251	51.619	48.889	51.534	55.087
10	38.544	39.551	41.129	44.443	44.699	50.829	49.645	50.336	56.525	54.352	56.089	59.126

Table 7.4: The comparison of natural frequencies values obtained from analytical, FEM and experimental result for Bersford conductor

Mode	Natural Frequency (Hz) 15% UTS			Natural Frequency (Hz) 20% UTS			Natural Frequency (Hz) 25% UTS			Natural Frequency (Hz) 30 % UTS		
	Analyt. Model	FEM	Exp. Value	Analyt. Model	FEM	Exp. Value	Analyt. Model	FEM	Exp. Value	Analyt. Model	FEM	Exp. Value
1	3.8773	3.898	5.823	4.477	5.560	6.346	5.0054	5.216	5.921	5.483	6.516	7.146
2	7.7567	8.757	9.230	10.9558	11.121	12.323	10.012	12.433	14.916	14.968	15.833	16.240
3	11.640	11.940	12.850	15.438	16.684	17.309	16.023	18.653	19.157	20.455	21.953	22.462
4	15.530	16.888	17.526	21.926	22.251	23.541	23.038	24.875	26.121	30.947	32.275	34.088
5	19.429	20.212	21.288	26.422	27.822	29.283	30.060	31.101	32.624	37.445	39.501	42.918
6	23.338	24.319	26.063	32.927	33.400	34.970	36.090	37.333	40.391	43.951	44.733	45.153
7	27.261	29.561	31.221	37.443	38.984	40.112	42.130	43.571	45.782	48.466	49.971	52.795
8	32.198	34.211	38.239	42.971	44.576	47.649	50.182	52.816	55.947	52.991	53.116	55.218
9	38.151	39.156	41.100	49.515	50.179	51.943	55.247	57.671	60.643	61.529	62.971	65.201
10	42.124	43.133	44.204	54.075	55.794	57.730	61.326	63.937	65.247	66.208	67.537	72.368

As tabulated, the steady state frequency responses were obtained for the analytical, FEM and the experimental studies. To validate the FEM model, the root-mean-square error (RMSE) was used to measure of the differences between values from the FEM model and the values actually obtained from experiments. The formula for calculating the RMSE is given as

$$RMSE = \sqrt{\frac{\sum_{n=1}^{n}\left(f_{FEM} - f_{EXP}\right)^2}{n}} \quad \ldots\ldots\ldots\ldots\ldots\ldots\ldots\ldots (7.1)$$

The RMSE is concerned with deviations from the true value. The values for the four conductors showed a similar trend. For the sake of brevity, only the values for the Tern conductor will be used. RMSE calculation for Tern conductor gave the following values of 2.265, 3.069, 4.261 and 2.262 for the 15, 20, 25 and 30 % UTS respectively. These values are relative low, signifying a low deviation of the FEM model from the experimental values.

Based on the RMSE analysis, in comparison, the results showed of degree of agreement between the analytical and the FEM frequencies for the conductors used, for the three different tensions.

7.3 The Analytical Results

Wind-induced vibration of the conductors was investigated analytically to obtain the conductor dynamic behaviour. The analysis of the analytical model describing the transverse vibration of conductors was done depending on the parameters of interest, either on the basis of local or global. In terms of global analysis, the analytical modelling was used to obtain the global response of the conductor. The conductor was modelled using the partial differential equation; for this case, this form of modelling that was used, describes the conductor in terms of the linear response. The linear response was used because the aeolian vibration do vibrate with small displacement, which can be modelled analytically using the linear concepts. The analysis was done for the transverse vibration of the conductor as a simply supported beam. The conductor dynamic behaviour was used to obtain the natural frequencies and modes shapes as a function of the input power. This analytical modelling was very useful because on the global basis, the mode of vibration can be ascertained as a function of its natural frequencies and mode shapes. The mode shapes for the first ten resonance modes for the four different conductors as various axial tensions were recorded. Thus, the natural frequencies and mode shapes that were obtained in terms of the experimental studies for the conductors were already recorded in tables 7.1-7.4. The analysis indicated that there was a variation of the conductors' frequencies with respect to the variation to the axial loading on the conductors. As the axial load was being increased there was a corresponding increase in the natural (resonance) frequencies of the conductors.

To evaluate damping analytically, the amount of energy that was dissipated by the conductors, was obtained using the analytical expression for input power based on the power law. Analytically, the

power dissipated per unit length for the conductors was evaluated, as explained in chapter 4, empirically, using the Noiseux exponents (l = 2.44, m = 5.63 and n = 2.76). The reduced self-dissipation formula based on the Noiseux exponents was obtained as:

$$\frac{P_C}{f^3 d^4} = k \frac{1}{d^{1.56} T^{2.76}} f^{2.63} \left[\frac{y_{\max}}{D} \right]^{2.44} \quad \text{..... (7.1)}$$

The plot for the for Tern conductor at 15 - 30 % UTS is shown in figure (7.2)

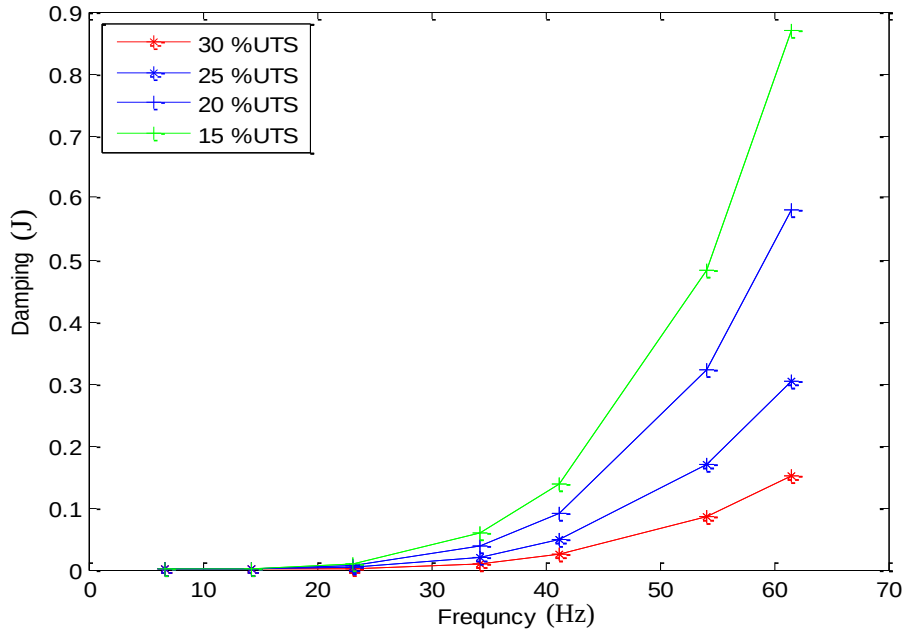

Figure 7.2: The analytical evaluation of damping for Tern

The expression used for wind power input, which is a function of reduced velocity V_r, dimensionless amplitude [Y_{max}/D], and reduced decrement, δ_r and these parameters was used to determine the amount input power. Document by C. B. Rawlins [31], in which he gave the various values for reduced decrement that relates to the turbulence effect with regards to the energy imparted on the conductor. The reduced wind input power expression was given by equation (2.89). For this analysis, the 1% turbulence was used. The analytical evaluation of self-damping was done for the four conductors and compared at several tensions, frequencies and amplitudes as shown in figure (7.2) for the tern conductor. The self-damping was deduced, as it can be seen in figure, there was a fairly good agreement between the curves, both in their trends and values.

Analytically, the composite model was also implemented. The conductor composite model was modelled and implemented using the curved thin rod model. The analysing of the damping for the conductor under the cyclic loading, the conductor was modelled as a bundle of equivalent rod representing the strands with amplitude dependent damping, and the inter-strand dry friction between the strands was considered. The relationship between the bending moment and curvature

was used as the parameters to evaluate the energy dissipation. Thus, the cyclical loading effect at the inter-strand contact was characterized, modelled and implemented as the function of the bending moment versus the curvature and the hysteretic phenomenon was implemented using the Bouc-Wen hysteresis model. An example of the loop obtained from this implementation of the smooth hysteresis model using the developed Matlab script is shown in figure (7.3). The value for the conductor damping was obtained as equal to the area of the loop.

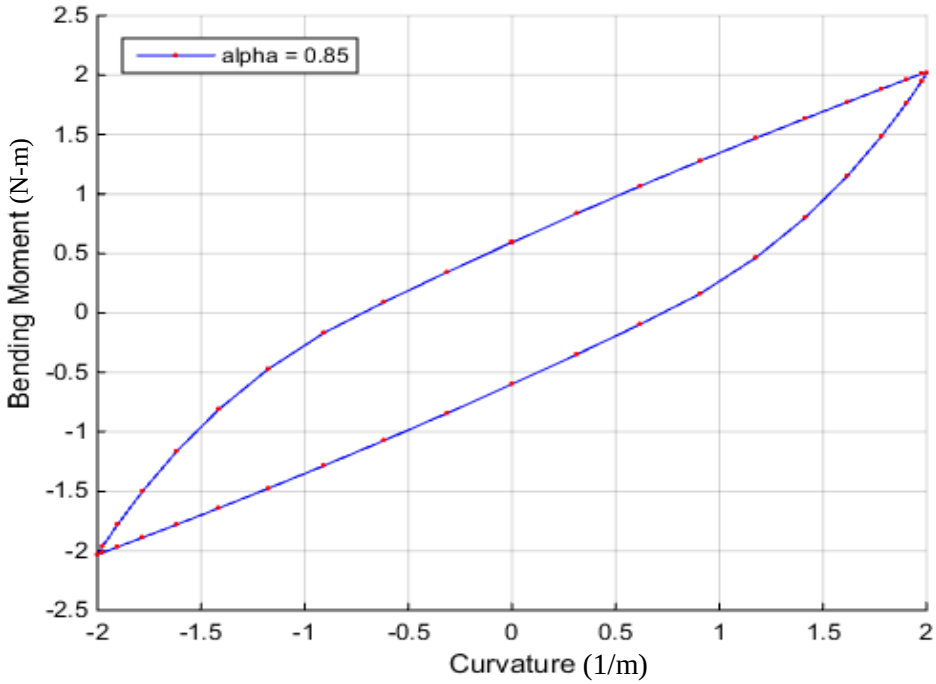

Figure 7.3: Matlab plot of Bouc-Wen hysteresis model

The analytical results showed that the energy losses are proportional to the axial tension, and inversely proportional to the inter-strand friction forces. The values obtained conclude that the damping in power line conductors was mainly caused by the dry friction between strands, while a small amount of energy is being dissipated through individual strands. This is illustrated by the graph shown in figure (7.4) for the Tern conductor, where the damping is plotted against the frequency. While as the conductor axial tension was being increase, there was a corresponding decrease in damping. The graph also showed that the damping was proportional to the frequency and the axial tension. This graph affirms that the conductor damping at a specific axial tension increase with the increase in frequency.

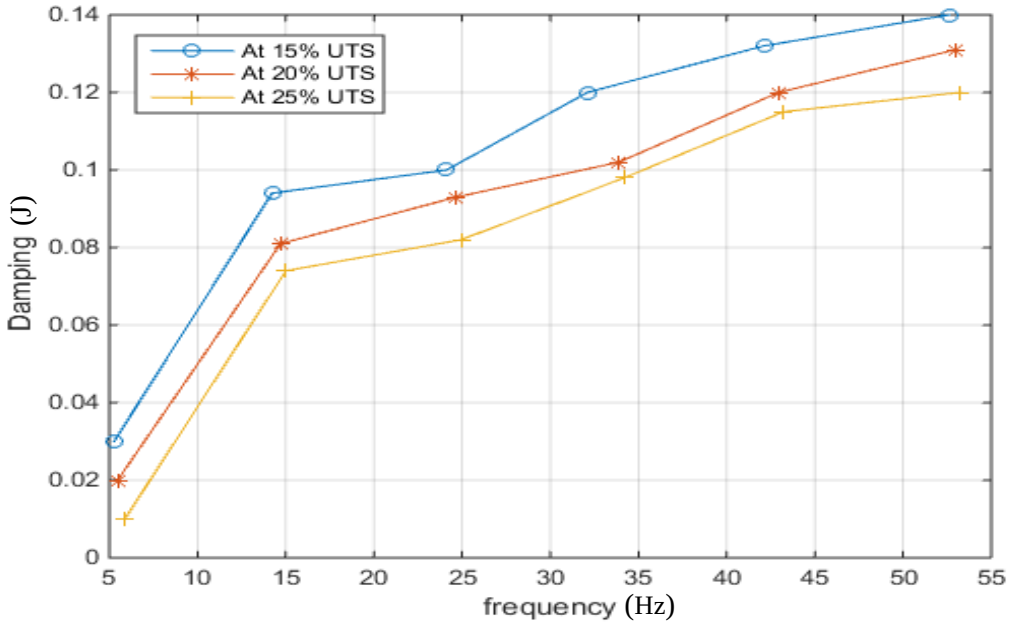

Figure 7.4: Plot of damping against frequency for Tern conductor

7.4 FEM Model

The central goal of this study was the development of FEM model for the conductor. The FEM model for the conductor was developed as a composite structure, in which each strand was model using the curved beam finite element type. In the formulation of the FEM, due to the helical structure, the axial tension was applied at both ends of the conductor, and this causes friction forces to be develop between the strands in the adjacent layer. As the axial force was being increased, there is increases of the stiffness of the conductor and results in higher stresses and strains at the contact region. The FEM was used to characterize the contact mechanics at the contact points as a function of the stiffness. As the conductor experiences bending and a critical curvature is reach, the strands start slipping over other strands, due to sinusoidal input, the slipping exhibits a periodic process. The dynamic simulation was used to model the periodic slippage and with the frictional effect at the contact point which leads to energy dissipation.

The FEM research on the effect of friction at the contact points provided a much better insight on what happens within the conductor. The magnitude of the friction between the strands in relation to curvature defined the transition between stick and slip states. This was directly related to the bending stiffness. In the modelling of the energy dissipation due to friction, the formulation of FEM using the contact mechanics was used to obtain the tangential stiffness for the inter-strands contact. The contact force and displacement resulting from the bending produced the hysteresis loop. The FEM results showed that the area of the loop produced was directly proportional to the axial tension. This furthers affirm the findings of the analytical model. Thus, the axial tension was

the major determining factor responsible for the amount of damping obtained from the vibration conductor.

In implementing the FEM for evaluating damping, the major challenge was to ascertain the exact value for coefficient of friction for both the stick and slip conditions. Making use of the actual static and dynamic friction coefficients would improve the FEM composite model.

7.4.1 The FEM Computer Implementation

The successful development of FEM model used to describe the transverse vibration of the conductor as a composite structure; a computer code was written and implemented. This FEM code was implemented using the Matlab environment. The development of the composite structure FEM Matlab code was challenging and also rewarding. The advantage of using the Matlab code was based on the fact that all the FEM code was explicitly setup and calculations are completely accessible as opposed to commercial FEM programs which function as a black box. To correctly use and, more importantly write, a successful Matlab FEM code, such as the one developed in this study, there was a need to have adequate knowledge of the entire FEM modelling process from the start to the finish. This tends to enhance understanding of FEM's application in modelling the conductor physical world problems. This process provided the opportunity to further gain an insight into the FEM concepts, as researched upon in this study for the dynamic behaviour of conductors.

To achieve the bundle structure of the conductor, the idea was to take advantage of the iso-parametric element type mapping, taking advantage of the symmetrical nature of the strands and then assembled into the composite system. This process involves developing functions for the various aspects of the finite element formulation as well as the geometric parameters to implement the mapping process. Although, this was a complicated and time-consuming process in its formulation, it ended up adding to the overall value and experience in embarking on the project in a very significant way.

The development of the code used to implement the conductor FEM model involved the derivation and implementation of a number of functions in Matlab. The following function were developed and implemented to simulate the conductor dynamic behaviour and evaluate damping:

- The function used to discretization the conductor as a composite structure in terms of its geometry
- The function used to define the equations for finite element using shape functions using the concept of iso-parametric interpolation

- The function for the generation of the finite element equation in term of stiffness, mass matrices and load vector
- The functions to calculate the cross-section properties such as axial and bending stiffness
- The function for the formation of the system equation
- The function used to define the corresponding boundary elements
- The function for the Newmark numerical scheme to simulate the conductor dynamic response
- The function to generate the hysteresis loop using the Bouc-Wen model
- The function to evaluate the area of the hysteresis loop formed in order to determine damping

7.4.2 FEM Dynamic Response

Based on the Matlab code developed above, the FEM model was simulated in the Matlab environments. In implementing the Matlab code, the dynamic simulation of the conductor was done with a forced harmonic excitation at a specific frequency and the response was obtained by using the Newmark numerical scheme, documented in appendix C. For reliability of results, the frequencies of excitation were introduced into the FEM system at the same location as that used in the laboratory tests. The response of particular modes as a function of time can be seen in figure (7.5) for Pelican conductor.

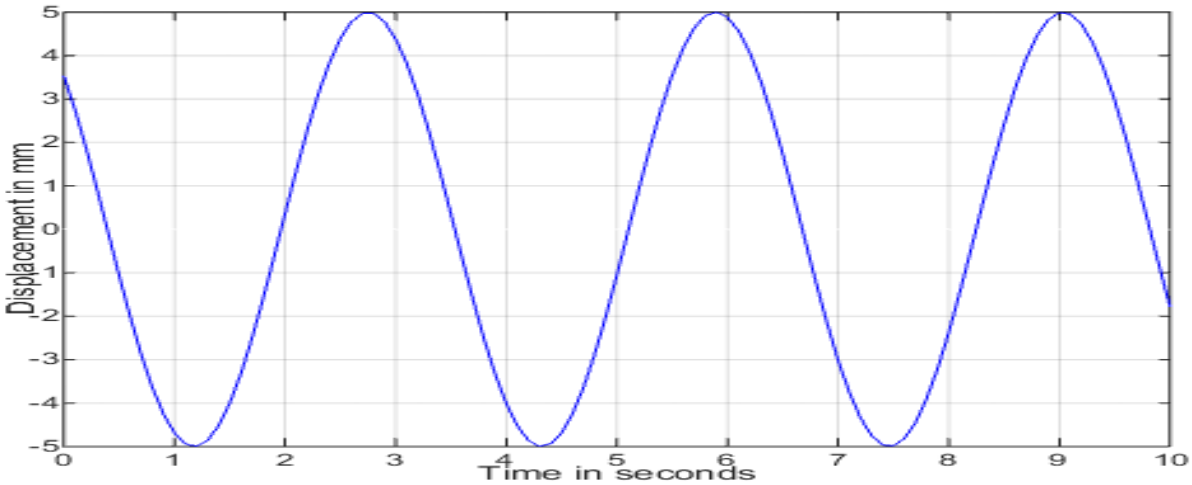

Figure 7.5: The conductor steady state response

Various eigen frequencies were computed by the FEM analysis for the composite model. The energy dissipation over one axial load cycle was obtained with more detail explanation in the next section. The analysis also showed that the damping is inversely proportional to the conductor axial tension. To obtain the load-elongation relationship, the total elongation of the conductor was

assumed to be comprised of two parts, one from the section without inter-strand slippage, and the other is when there is slippage at inter-strand. The FEM results demonstrated that the conductor axial stiffness increased as the axial tension increases, and also the damping is inversely proportional to the conductor tension. However, the analysis might underestimate the conductor elongation caused by vibration as a function of imposed curvature. This is because of the difficulty to accurately determine the curvature as function of the stiffness. Based on the FEM, similar to analytical model using the Bouc-Wen model the hysteresis loop was also developed similar to that shown in figure (7.3).

7.4.3 FEM Damping Results

Conductor self-damping is a non-linear phenomenon because the energy loss depends on the conductor vibration amplitude. Consequently, the energy dissipated cannot be easily determined by the superposition principle when several modes are excited in the conductor. To overcome this difficulty, a single frequency excitation was employed. Based on this concept, the FEM model was used to evaluate the energy dissipated by the conductor undergoing a single sinusoidal response as opposed to the multi-modal vibration response.

The hysteresis loop which was formed by the helical structure of conductor are expressed with a resonance frequency approach, where the damping in each helical strand for each layer was calculated as a function of the frequency in the helical strand from the outer strand to the strand last layer before the core. Together with the geometrical formulation, the effect of the friction between components was taken into account. This model enables the introduction of a variable bending stiffness for the conductor taking into consideration the sticking and slipping regime of strands into account. This model based on the results obtained can be used to find the appropriate configuration for the string profile for the power line as a function of the possible dynamic loading conditions. This helps achieves the optimum sag required for clearance between the ground and the conductor.

The FEM method was able to relate the forcing function with the inter-strand deformations which was influenced by the local stiffness for both the single and multi-level helical conductor structure. The applied deformation is expressed as combination of tension and bending. The resultant force versus displacement was also modelled using the Bouc-Wen smooth hysteresis model as shown in figure (7.6).

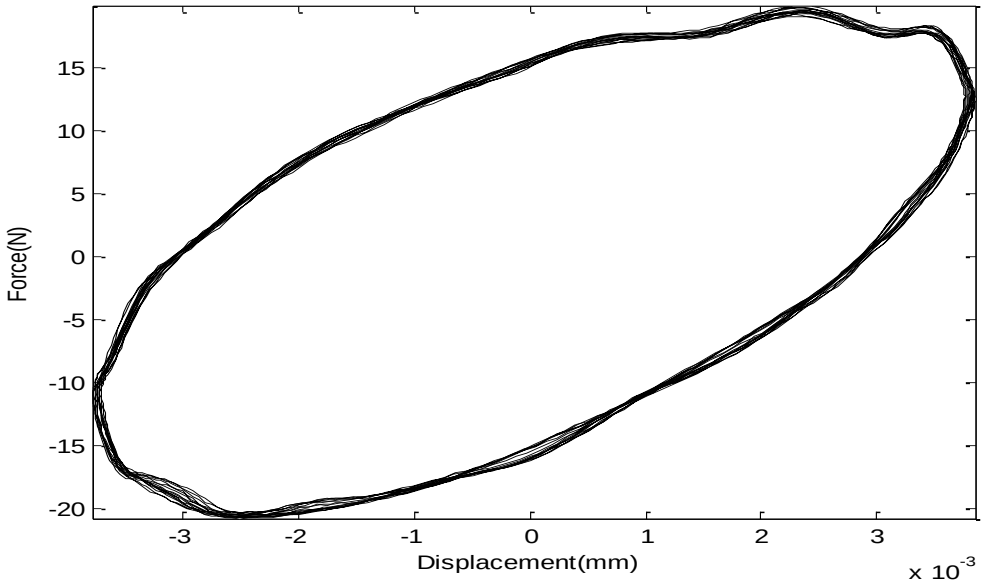

Figure 7.6: FEM Bouc-Wen model formulation of a hysteresis loop

The tables (7.5-7.8) show the values of FEM damping results for the four test conductors and accompany each table is the plot of damping against frequency.

Table 7.5: FEM damping value for Rabbit conductor

Rabbit Conductor							
25 % UTS		30 % UTS		35 % UTS		40 % UTS	
Frequency (Hz)	Damping (J)	Frequency (Hz)	Damping (J)	Frequency (Hz)	Damping (J)	Frequency (Hz)	Damping (J)
10.943	0.0131	11.790	0.0113	12.905	0.0090	14.614	0.0074
22.007	0.0530	24.712	0.0456	26.231	0.0365	28.112	0.0299
33.456	0.1390	36.357	0.1195	39.631	0.0956	41.111	0.0784
44.234	0.1460	48.672	0.1256	51.950	0.1004	55.667	0.0824
49.451	0.2381	54.073	0.2048	58.323	0.1638	63.280	0.1343
54.891	0.2610	60.006	0.2245	64.699	0.1796	68.195	0.1472

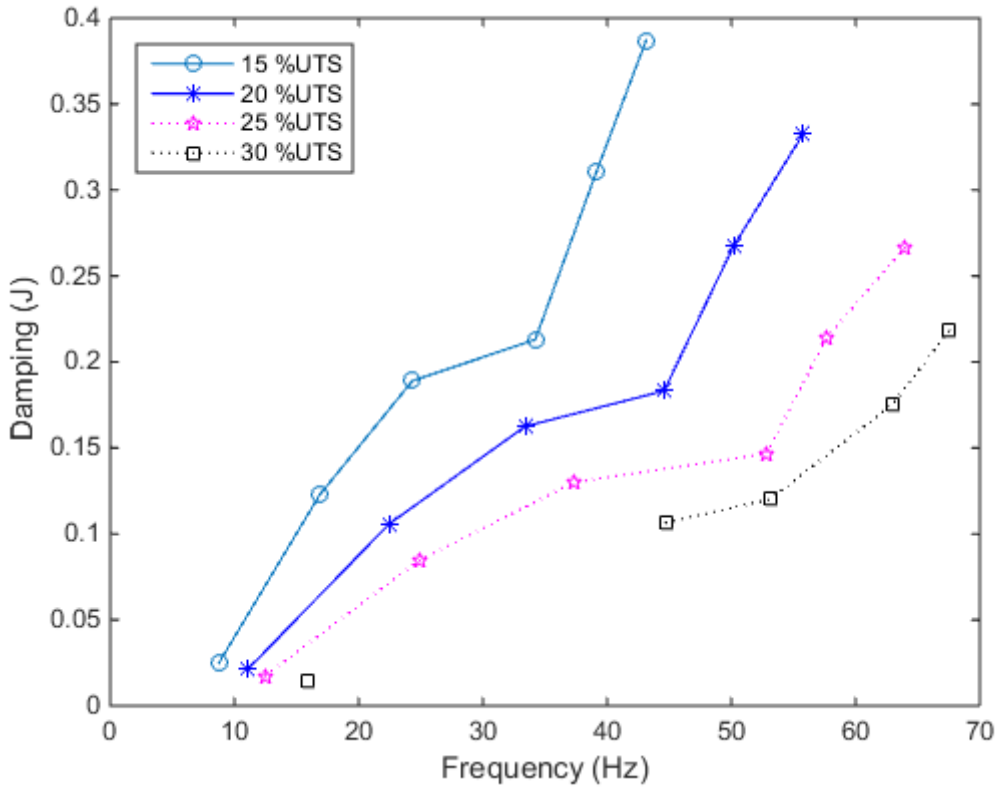

Figure 7.7: The damping versus frequency for Rabbit conductor

Table 7.6: FEM damping value for Pelican conductor

Pelican Conductor							
20 % UTS		25 % UTS		30 % UTS		35 % UTS	
Frequency (Hz)	Damping (J)	Frequency (Hz)	Damping (J)	Frequency (Hz)	Damping (J)	Frequency (Hz)	Damping (J)
8.821	0.0160	9.366	0.0138	10.646	0.0110	11.581	0.0090
16.756	0.0790	19.890	0.0679	21.690	0.0544	22.344	0.0446
26.542	0.1530	29.772	0.1316	31.222	0.1053	34.045	0.0863
34.109	0.1810	39.480	0.1557	42.155	0.1245	45.342	0.1021
38.625	0.2640	43.661	0.2270	47.193	0.1816	50.691	0.1489
42.126	0.2920	46.867	0.2511	52.334	0.2009	56.442	0.1647

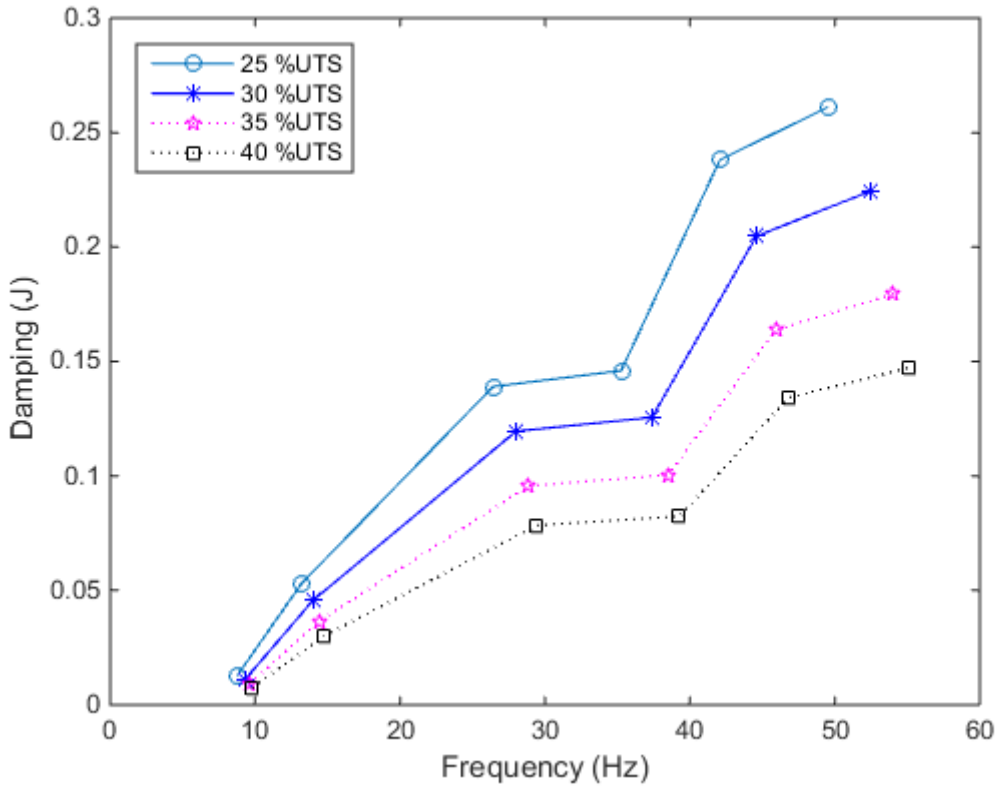

Figure 7.8: The damping versus frequency for Pelican conductor

Table 7.7: FEM damping value for Tern conductor

Tern Conductor							
15 % UTS		20 % UTS		25 % UTS		30 % UTS	
Frequency (Hz)	Damping (J)	Frequency (Hz)	Damping (J)	Frequency (Hz)	Damping (J)	Frequency (Hz)	Damping (J)
7.866	0.0210	9.900	0.0181	10.012	0.0144	11.966	0.0118
15.342	0.0690	18.810	0.0593	20.038	0.0475	22.947	0.0389
24.041	0.1250	27.739	0.1075	30.090	0.0860	33.952	0.0705
31.173	0.1920	36.698	0.1651	40.184	0.1321	47.099	0.1083
35.573	0.3140	41.192	0.2700	45.251	0.2160	51.534	0.1771
39.551	0.4730	44.699	0.4068	50.336	0.3254	56.089	0.2668

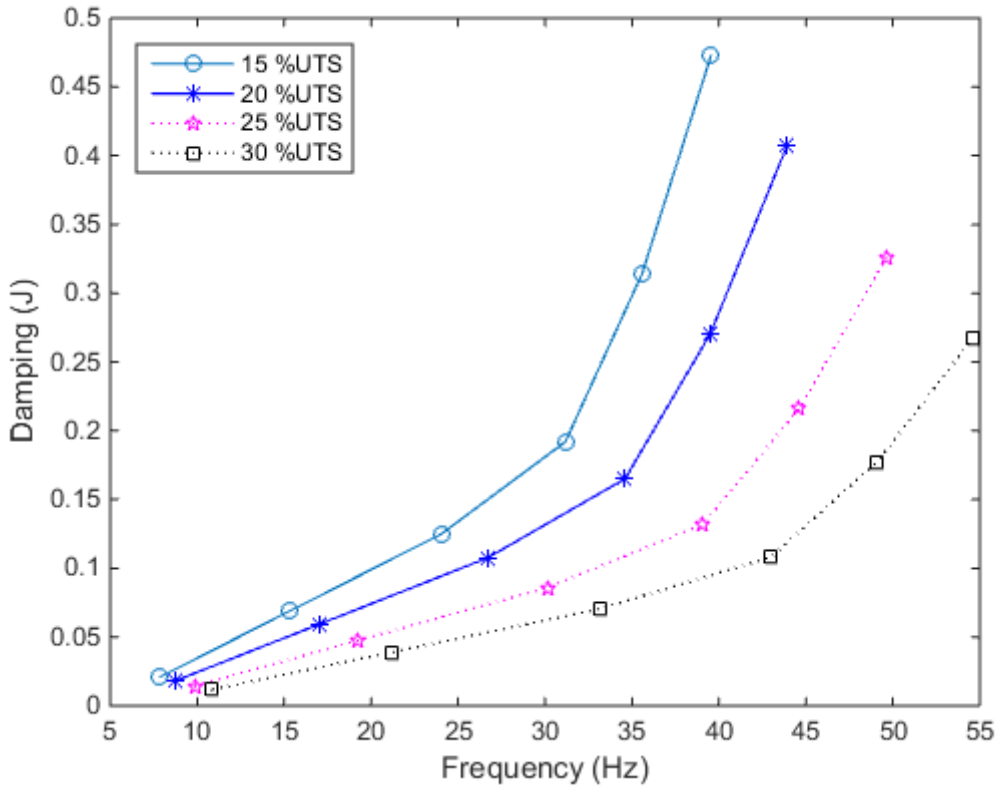

Figure 7.9: The damping versus frequency for Tern conductor

Table 7.8: FEM damping value for Bersford conductor

Bersford Conductor							
15 % UTS		20 % UTS		25 % UTS		30 % UTS	
Frequency (Hz)	Damping (J)	Frequency (Hz)	Damping (J)	Frequency (Hz)	Damping (J)	Frequency (Hz)	Damping (J)
8.757	0.0251	11.121	0.0216	12.433	0.0173	15.833	0.0142
16.888	0.1230	22.251	0.1058	24.875	0.0846	32.275	0.0694
24.319	0.1890	33.400	0.1625	37.333	0.1300	44.733	0.1066
34.211	0.2130	44.576	0.1832	52.816	0.1465	53.116	0.1202
39.156	0.3110	50.179	0.2675	57.671	0.2140	62.971	0.1755
43.133	0.3870	55.794	0.3328	63.937	0.2663	67.537	0.2183

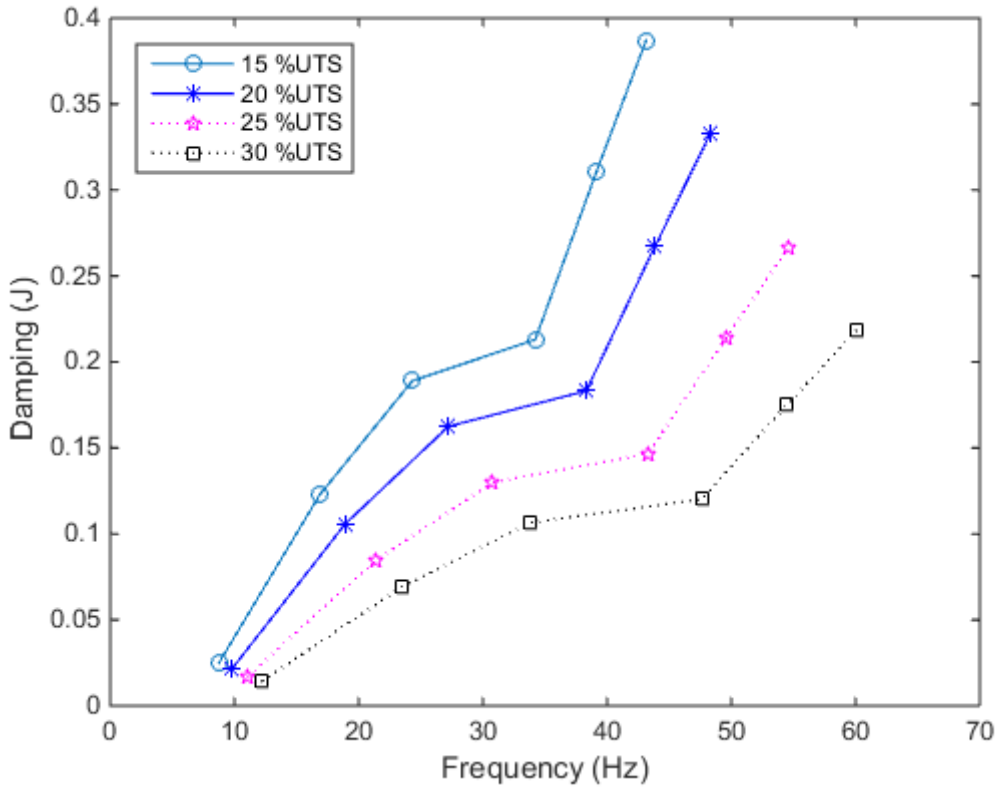

Figure 7.10: The damping versus frequency for Bersford conductor

7.5 Experimental results

As hinted earlier, in the indoor laboratory, a series of tests were carried out at the VRTC to determine the conductor self- damping. Laboratory tests are usually performed to validate results from other forms of conductor modelling. The laboratory simulations of aeolian vibration on overhead conductors, conducted at VRTC have provided useful data in determining the amount of self-damping in the conductors when exposed to this form of oscillation. These tests were done for four conductors (see chapter 5 for description), the range of values used for the test were deduced as a function of the axial tension. A series of dynamic tests were carried out to try and reproduce the phenomenon of wind induced vibration. In all the laboratory tests conducted, reproducing such phenomenon is very difficult. This means, it was impossible to reproduce the same condition each time the conductor test was performed. The response of the conductor was conducted for a limited number of experimental studies, due to the time consuming process of setting up the test rig and for the duration for conducting the experiments itself.

The test span at the VRTC due to its relatively long span was able to produce reliable results for this study. However, there are limitations and restrictions regarding the experimental investigation of this problem as there are several aspects which make the investigation difficult. This includes setting the loading arm to the exact required value, controlling the temperature of the indoor test span and placement of the sensors at the exact antinodes during testing. The test conducted at the VRTC was in two parts. For both parts of the experiments, the tests were done for the steady-state amplitude of vibration as shown in figure (7.11).

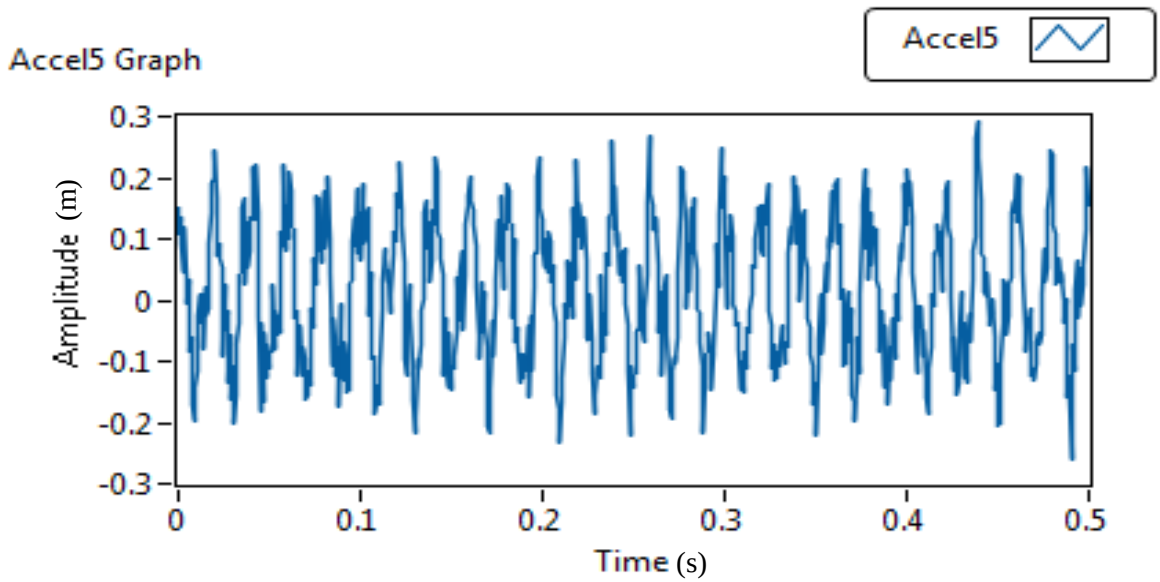

Figure 7.11: The experimentally measured conductor steady state response

The first part of the experiment was the sweep test to obtain the resonance condition of the conductors. This helps to obtain the resonance frequencies with the associated vibration modes as function of its axial tension. The sweep tests were carried out between a certain range of measurement, as shown in figure (7.12) for pelican for which the displacement was plotted against frequency.

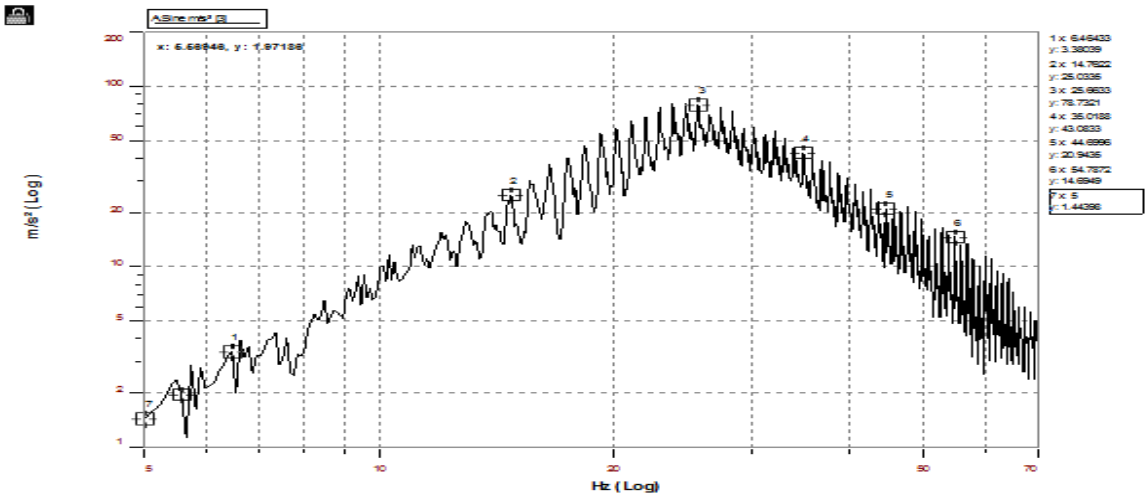

Figure 7.12: The experientially measured displacement against frequency

The second part of the experimental procedure is the generation of hysteresis loop as shown in figure (7.13) using the developed LabVIEW program. During the test, to get the desired condition to measure the damping, there was the use of the measurements/monitoring process of the force transducer and accelerometers in terms of their relative phase angle. The phase angle between the force and the acceleration signals should be stable at or near 90° to indicate resonance.

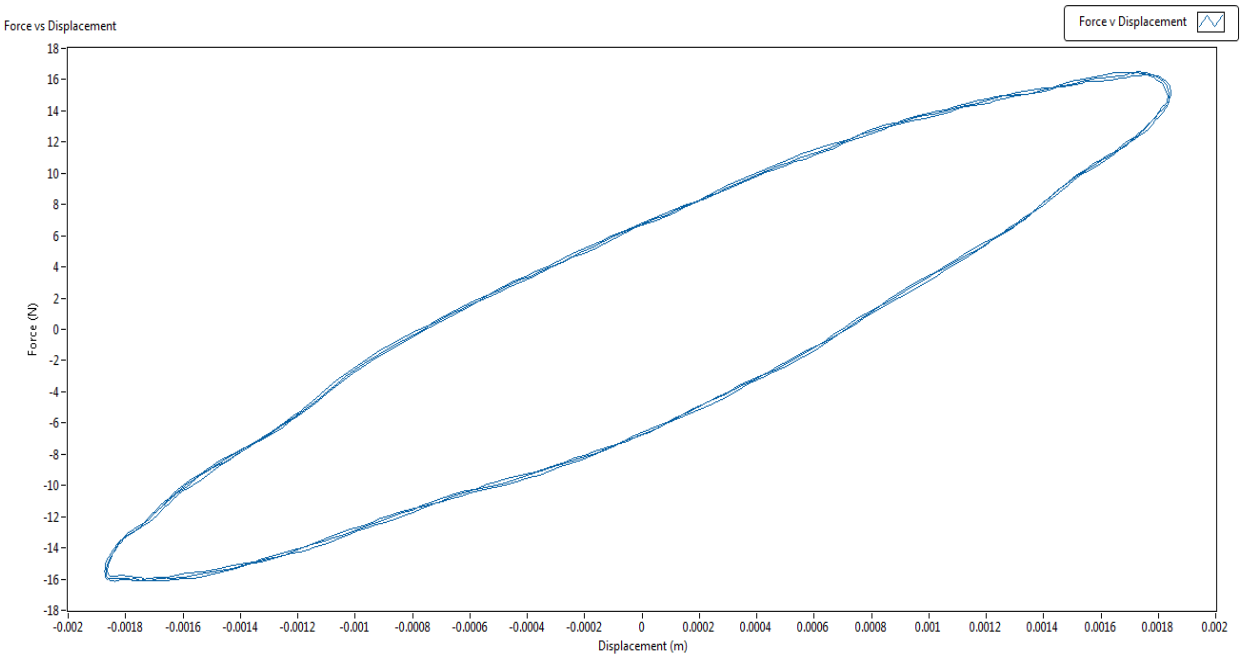

Figure 7.13: The experientially measured hysteresis loop

To achieve this, during each experiment the accelerometers was moved periodically along the span to coincide with the point of antinode displacement. Using a clip, the accelerometer is monitored and moved to the position to ensure their positions were at the antinode of vibration. The various frequencies from the first test serve as input variable into this LabVIEW program. The idea behind using hysteresis loop method was to measure, during vibration the change in bending strain or force with the displacement or curvature. The bending strain is proportional to the local curvature of the line and this determines the force imposed at the contact points.

The four conductors used for these tests were subjected to the sinusoidal input force as function of frequency for the different configuration of the system. For each conductor, the configuration assumed by the conductor was a function of the axial load and this was done for four different axial loads as a percentage of its UTS. The five frequencies were specifically chosen, in order to test the specimens under the most severe conditions. Each frequency corresponds to a particular natural frequency, produced by each of the motion of the excitation that was superimposed to cause resonance in one of the natural frequency of the conductor.

The laboratory experiments with the four conductors; with different layers, provided an interesting information on ascertaining the conductor self-damping behaviour.

For the laboratory tests performed to simulate aeolian vibration, four distinct sample constructions of conductors were used to determine the self-damping characteristics. Three of which are used as overhead transmission conductors and one for the distribution network. These four conductor constructions each having a steel core, these are ACSR conductors with code names: Bersford, Tern, Pelican, Rabbit.

The tests for the Bersford conductor was done at 15%, 20%, 25% and 30% of its Rated Tensile Strength (RTS). For that of Tern conductor was also done 15%, 20% 25% and 30% of its Rated Tensile Strength (RTS).

For each test, to determine damping, a minimum of five different modes per tension level was tested for each conductor. The approximate modes of 2, 4, 8, 9 and 10, as recorded in tables (7.1-7.4), were chosen to be tested since they were within the ranges of the frequencies and wind speeds generated as classified that can cause the aeolian vibration on power line conductors.

Table 7.9 to table 7.12 represent the power dissipation for the four test conductors, for four configurations of the different axial loads, with the various frequencies for the sinusoidal input power.

Table 7.9: Experimental self-damping results for Rabbit conductor

Rabbit Conductor							
25 % UTS		30 % UTS		35 % UTS		40 % UTS	
Frequency (Hz)	Damping (mWatt)	Frequency (Hz)	Damping (mWatt)	Frequency (Hz)	Damping (mWatt)	Frequency (Hz)	Damping (mWatt)
11.595	23	12.225	18	13.153	13	14.614	9
22.792	53	25.680	43	27.465	34	28.112	29
34.005	133	37.150	131	41.789	121	41.111	115
46.247	289	50.646	245	53.135	211	55.667	191
52.882	875	57.908	893	60.320	568	63.280	468
56.530	20156	62.181	1674	66.515	590	68.195	558

Table 7.10: Experimental self-damping results for Pelican conductor

Pelican Conductor							
20 % UTS		25 % UTS		30 % UTS		35 % UTS	
Frequency (Hz)	Damping (mWatt)	Frequency (Hz)	Damping (mWatt)	Frequency (Hz)	Damping (mWatt)	Frequency (Hz)	Damping (mWatt)
9.053	21.910	10.924	16.30	11.014	15.90	12.898	12.32
17.717	45.901	20.373	39.40	22.934	31.80	23.801	27.224
28.111	121.000	31.349	116.20	33.283	108.50	35.714	102.901
35.965	234.003	40.976	222.60	44.987	189.50	47.646	170.125
39.893	788.056	44.789	712.00	49.895	567.00	53.620	534.682
43.103	1930.320	47.789	1600.10	53.089	1335.50	58.603	1257.899

Table 7.11: Experimental self-damping results for Tern conductor

Tern Conductor							
15 % UTS		20 % UTS		25 % UTS		30 % UTS	
Frequency (Hz)	Damping (mWatt)	Frequency (Hz)	Damping (mWatt)	Frequency (Hz)	Damping (mWatt)	Frequency (Hz)	Damping (mWatt)
8.012	23	10.212	18	12.225	13	13.309	9
18.530	53	20.139	43	23.130	34	24.267	29
26.822	133	31.022	131	34.810	121	35.518	115
32.910	289	40.703	245	45.278	211	50.022	191
36.911	875	43.211	893	51.619	568	55.087	468
41.129	20156	50.829	1674	56.525	590	59.126	558

Table 7.12: Experimental self-damping results for Bersford conductor

Bersford Conductor							
15 % UTS		20 % UTS		25 % UTS		30 % UTS	
Frequency (Hz)	Damping (mWatt)	Frequency (Hz)	Damping (mWatt)	Frequency (Hz)	Damping (mWatt)	Frequency (Hz)	Damping (mWatt)
9.230	33.23	12.323	29.34	14.916	21	16.240	17
17.526	78.34	23.541	60.9	26.121	54	34.088	45
26.063	183.34	34.970	167.2	40.391	144	45.153	121
38.239	401.54	47.649	347.5	55.947	311	55.218	278
41.100	1600.29	51.943	1000.5	60.643	790	65.201	659
44.204	2900.22	57.730	2671.4	65.247	2215.6	72.368	1856

Based on the values of the frequencies chosen as an input variable for the second experiments, the damping energies obtained as shown in tables (7.9) – (7.12), the following conclusions were drawn from these tests for the four different types of conductors used for this study. The graphs drawn for damping versus frequency for the four test conductors illustrated that damping has a relation to the overall diameter, strand sizes, number of layers and number of strands in a given layer. The graphs illustrated that damping is directly proportional to the diameter of the conductor, the number of strands, number of layer, the conductor twist or lay, and inversely proportional to the axial tension. The comparison with experimental results showed that the results for the analytical model in terms of damping was found to underestimate the experimental test result. This finding requires further investigation.

7.6 Comparison of Self-Damping Results and the Effects of Variable Tension

All of the aforementioned investigations in this study focuses on the damping of a single span conductors with different diameters. However, the knowledge of the dynamic characteristics of individual conductor is not sufficient for the prediction of dynamic characteristics of a conductor structural system. To accomplish the prediction of conductor dynamic behaviour, comparison with other conductors with different physical properties is necessary in order to determine the interaction between the structural components (strands). This was done in order to know the consequence of varying the axial tension on the conductor damping and the comparison was done for three different axial tensions. This was achieved by identifying the parameters of the experimental study and comparing to other models using the same parameters. These comparisons

can be inferred from the tables for natural frequencies and later with graphs already drawn showing the variation of damping with frequencies.

The main criterion for having a suitable FEM model for the power line is to show an agreement between the measured and simulated global response for the applied load. Simulations of the response of the power line conductor after applying a point load were done for the transverse displacement and was compared with the measured displacement from the analytical model and the experimental studies. The finite element model seems to be a good representation of the power line, and the initial response seems to correspond well to the measured response. Some level of discrepancies was observed at higher frequencies which are due to the effects of the surrounding structure like the mass connecting shaker to the conductor.

The three models presented in this study have been used to evaluate the conductor self-damping. Since the damping of the conductor was mainly due to bending, the bending behaviour of a conductor was examined at different configuration as already documented in previous sections. This energy dissipation was identified to be mainly caused by the inter-strand friction and this established the fact that friction is the origin of energy dissipation for a vibrating conductor. Damping of energy as related to changes in the dynamic behaviour with the variation of the vibration amplitude and this parameter can be used to determine the conductor response at the specified axial load.

For each model presented, the amplitude and frequency was observed to produce a similar mode of vibration. The results from the three models have clearly shown, by comparing behaviour of the conductors, that the axial tension determines the amount of conductor self-damping. Although, the damping can also be a function of the number of layer present, number of stands in each layer and strands diameter. The dependence of the conductors' energy dissipation on the stringing tension was almost the same for all the models. With respect to the span/sag ratio, the tension on the conductor has to be high enough to determine the minimum UTS in which the conductor can adequately damped out the imposed energy. All other things being equal, determining this critical tension, will induce an optimal energy dissipation capacity for the conductors.

The energy dissipation is very much influenced by the frequency of vibration which is a function of the modal shape and the radius of curvature of the vibration for a given amplitude and by the conductor tension, which has a huge effect on the inter-layer contact pressure.

7.7 Conductors Self-Damping Characteristic

Structural vibration testing and analysis of power line conductors contributes to the power industries identification and suppression of unwanted vibration in order to improve the power line

reliability. The most common form of vibration suppression is within the conductor itself (self-damping) and the addition of external dampers to the conductor structural elements because it is lightly damped. The conventional types of conductors like ACSR inherently have some degree of capability for damping aeolian vibration imposed on them. As previously discussed, the ability to damp out this energy due to aeolian vibration is dependent on factors like the number of layers, the strand configuration, conductor construction, internal friction, frequency of vibration and the axial tension. This is evident in the results from all aspect of this study. The most dominant factor is the axial loads. This is because the lower the normal compressive forces between conductor's strand layers leads to increased strand movement and higher self-damping capability. At lower axial tension, the conductor exhibits lower compressive forces between the aluminum strand layers and the steel core. At this state, the self-damping capability of the conductors' construction is well beyond that of input loading that external dampers are not required. As the tension was increased the damping capability was reduced, beyond a certain limit the conductor became incapable of mitigating, within safety limits, the energy, and external energy absorbers were required.

7.7.1 Retrospect on the Study Hypotheses

Achieved, the main objective of this study, presented was a unified FEM model as compared to some analytical models. The developed FEM model in this study, which was basically to simulate the stick-slip model, is based on Coulomb's laws of friction. This FEM model has provided a more realistic model that is very useful in the interpretation of experimental data. Using a viscoelastic material with adequate parameter values, the moment versus curvature hysteresis curves was observed experimentally and was able to accurately reproduce the conductor hysteresis behaviour, the area within the hysteresis represents the conductor self-damping. Basically, the analysis of these experimental tests has validated the developed finite element model for overhead power line conductors. All the non-linear effects due to changes in tension are verified with the finite element simulation and analysis. This FEM model served as the basis to interpret and discuss the experimental results. This model has helped in the evaluation of the energy balances that serves as the basis to quantify the different contributions of the energies between the imposed and that damped by the conductor.

Based on the FEM model, a new formulation for conductor self-damping was proposed, which unlike others is based on the physics behind the phenomenon itself as explored in this study and because it was dimensionally correct, an algorithm was then developed.

7.7.2 The Developed Algorithm to Evaluate Self-Damping

Generally, for any power line conductor, it is expected that there will be a violent oscillation imposed on the structure because of the little damping as compared to other structures whose rate of energy dissipation is high. Although, the conductor damping maybe small, the intention of this research was to achieve a FEM model that can quantify its values and then establish a methodology for its determination. The concepts established in this study were used to determine, as a function of specific stringing tension, the conductor self-damping capability. This can help to ascertain whether the value for the damping at that particular tension is enough to curtail the effect of the wind loading. These investigations form the basis for the development of a computational model that can provide a method to analyse the motion of a conductor under a range of inputs force. The developed FEM model is capable of determining damping using, the input force, and physical parameters of a conductor as the model inputs variables. The FEM model can, for a chosen span length as well as at various applied external tension produce an adequate approximation of the conductor's response to different wind loading.

To apply the FEM aspects of this study with regards to self-damping, an algorithm was developed. The following steps were used to implement the algorithm as shown in figure (7.14).

Step 1: The physical parameters of the conductors as defined in terms of geometry and the axial load and used to determine the line centenary profile. Also defined at this stage is the input power.

Step 2: This entails defining the shape functions thereby initialling the FEM for the dynamic analysis.

Step 3: Discretization of the conductor domain into its finite element.

Step 4: Formulation of the finite element equations for the stiffness, mass matrices and load vector,

Step 5: The above step is followed by assembly finite element equations into the system equation using iso-parametric interpolation.

Step 6: Imposing boundary conditions on system equation, the computer simulation can be done for either for as an Eigen value problem in order to obtain the natural frequencies or numerical simulation using the Newmark numerical scheme in order to obtain the conductor response.

Step 7: The results for the conductors' vibration for variables such as natural frequencies, modes shapes, damping, and dynamic responses are determined using FEM. The result obtained depends on the decision of the variable required as function of step 6.

Step 8: This was specifically used for the evaluation of the conductor self-damping and this was done as a form of the hysteresis loop and the conductor damping capability was defined per unit area length.

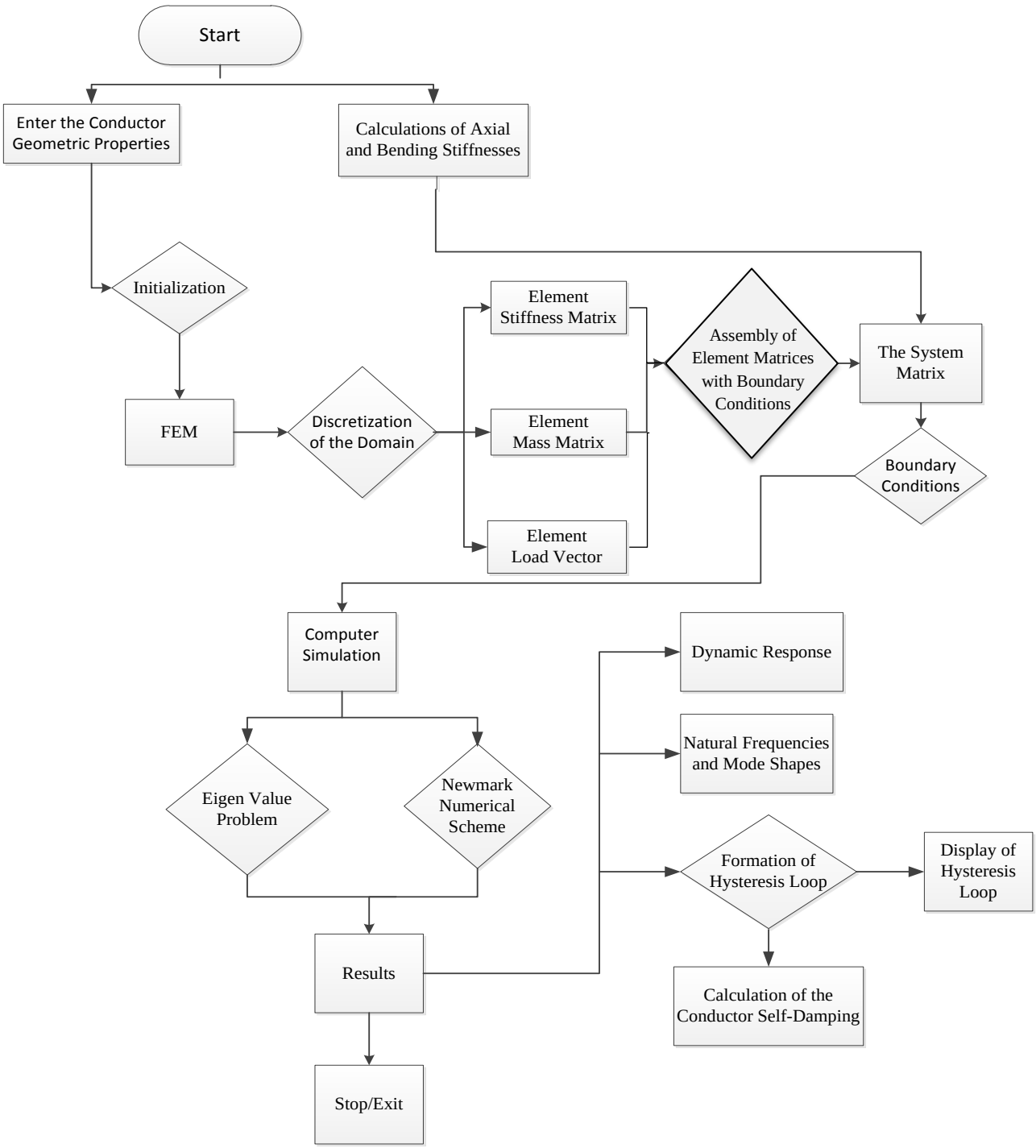

Figure 7.14: The developed FEM algorithm to evaluate the Conductor dynamic response and self-damping

Chapter 8

Conclusion and Recommendation

8.1 Conclusion

The evaluation of conductor self-damping was carried out in this study. This was done using three models: analytical, FEA, and experimental. The analytical modeling for the conductor was done as continuous or as a composite structure. The FEM formulation and implementation was done using a more realistic model for the conductor as composite structure using the iso-parametric interpolation. The conductor self-damping was mainly due to frictional effects at the inter-strand contacts, the energy dissipation was based on the contact mechanics characterized by Hertzian contact mechanics and the energy dissipation by Coulomb friction model. The developed damping force as function of geometry was used to obtain the damped equation of motion and system response simulated using the Newmark numerical scheme.

In this study, the method of hysteresis loop was used to evaluate damping at different tensions. The data obtained from this method clearly demonstrate the dependence of damping on the axial tension. This indicated that damping decreases as the axial tension increases. Also, the results from these methods also illustrated the dependence of damping on the number of layers conductors in the conductor. Therefore, there was a direct relationship between self-damping and the numbers of layers. This proved that the higher the number of layers in the conductor the higher the damping. The dependence of damping on the frequency of vibration at a constant tension was also investigated. This also revealed the direct relation between damping and frequency at a constant tension, i.e. increase in frequency also leads to increase in damping.

In the experimental study, the conductor was excited at a constant tension at different frequencies. The experimental data showed that self-damping increase with the increase in frequency. This validated the empirical expression and FEM results for damping where there is direct relation between energy dissipation and frequency. Results showed that the value for the self-damping of the transmission lines at high tension was small and not adequate to control aeolian vibration within safety limits.

Finally, the successful modelling and implementation of the FEM model greatly reduces the too much dependence on experimental testing to evaluate damping. Experiments conducted in the laboratory are very expensive and a time consuming process. Setting up the conductors, the placement of the shaker, calibration of instrument and data capture and analysis are cumbersome task to achieve. Experimental task can now be greatly minimized with the use of the FEM model.

It is very important to note that experiment studies cannot be eliminated. This is because experiments are very important to verify the model used in the simulation, thus, simulation alone is not sufficient.

The determination of conductor damping can now be achieved by the use of the FEM thus validating the hypothesis of the research carried out in this study.

8.2 Recommendation

The study undergone in this thesis was by no means complete but a means that open other concepts that can be investigated in the area of the dynamic behaviour of power line conductors. The successful development of the FEM model as a composite structure can be employed to investigate the coupling effect of axial, torsion and bending phenomenon as associated with the strands. Also, this FEM model can be used to specifically investigate the implementation of variable bending stiffness of conductor. The FEM model was developed as a more representation of the conductor. From the geometry formulation with the FEM equation for the power line, the variable bending stiffness can be implemented for the bundle structure and also as a function of deformation history along the conductor.

In addition, the FEM that was developed in this study for conductor vibration can be used for future research related to fatigue failure. Damping was assumed to occurs along the entire span of the conductor in the development of FEM for conductor. In a similar manner, using the geometric properties, fatigue failure that occur at the areas where conductor motion is constrained can be investigated.

For future investigation, the concept of the 2D FEM for each strand superimposed into the 3D bundle geometry used in this study may be improved upon by using the 3 D curved beam elements to represent the conductor strands. This may come at a high computational cost, but this can be alleviated with the advent of fast computer with high processors. This will increase the accuracy of modelling local phenomena such as damping, fretting and fatigue. This process can help determine the types and amount of damper needed on the line in order to prevent damage caused by conductor oscillation.

Further study could also be done to develop a FEM method that can be used to obtain the variable values for the bending stiffness as it varies along the conductor length. This can then be used to formulate a computer programme that can be used as a design parameter for bending stiffness for transmission lines.

In the experimental study, there was a problem of synchronising the sweet test and the hysteresis loop test. This was because there were two different programs used; sweet test done by Puma

software and hysteresis test done by LabVIEW. This a need to develop a program using LabVIEW to excite the conductor with a manually fed frequencies via the function to determine when the conductor is at resonance. But if the two programs were developed in LabVIEW, this will have ease the process of sending the signal to the hysteresis program thereby making the whole testing process to become a one complete process. Finally, because the experimental data available was used for the verification of the analytical and FEM models for aeolian vibration only, this can be extended to other types of conductor vibration. Typically, due to its close relation, these three concepts covered in this study can also be extended to the analysis of wake-induced vibration. As a product of this study, the author has developed a FEM toolbox in Matlab environments as shown in figure (D1) in appendix D used for both static and dynamic analysis of power line conductors

References

[1] EPRI Transmission Line Reference Book. *Wind-Induced Conductor Motion. EPRI Palo Alto CA*. 1979.

[2] EPRI Transmission Line Reference Book. *Wind-Induced Conductor Motion. EPRI Palo Alto CA*, Second edition 2006.

[3] I. Páczelt and R. Beleznai, "Nonlinear contact-theory for analysis of wire rope strand using high-order approximation in the FEM," *Computers & Structures*, vol. 89, pp. 1004-1025, 2011.

[4] F. Foti and L. Martinelli, "A model for the friction controlled bending behaviour of cables," in *Proceedings of 9th International Symposium on Cable Dynamics, Shanghai, China*, 2011.

[5] R. Claren and G. Diana, "Mathematical analysis of transmission line vibration," *IEEE Transactions on power apparatus and systems*, vol. 12, pp. 1741-1771, 1969.

[6] L. Möcks and J. Schmidt, "Survey on measurements of mechanical self-damping of ACSR conductors," *CIGRESC22-89 (WG-11) TF1-2*, 1989.

[7] J. Vecchiarelli, I. Currie, and D. Havard, "Computational analysis of aeolian conductor vibration with a stockbridge-type damper," *Journal of Fluids and Structures*, vol. 14, pp. 489-509, 2000.

[8] N. Barbieri, O. H. de Souza Júnior, and R. Barbieri, "Dynamical analysis of transmission line cables. Part 1—linear theory," *Mechanical Systems and Signal Processing*, vol. 18, pp. 659-669, 2004.

[9] G. A. Costello, *Theory of wire rope*: Springer Science & Business Media, 1997.

[10] A. Cardou and C. Jolicoeur, "Mechanical models of helical strands," *Applied Mechanics Reviews*, vol. 50, pp. 1-14, 1997.

[11] R. Knapp, "Helical wire stresses in bent cables," *Journal of Offshore Mechanics and Arctic Engineering*, vol. 110, pp. 55-61, 1988.

[12] R. Hobbs and M. Raoof, "Behaviour of cables under dynamic or repeated loading," *Journal of Constructional Steel Research*, vol. 39, pp. 31-50, 1996.

[13] K.-J. Hong, A. Der Kiureghian, and J. L. Sackman, "Bending behavior of helically wrapped cables," *Journal of engineering mechanics*, 2005.

[14] E. E. Ojo, "Dynamic Characteristics of Bare Conductors," University of KwaZulu-Natal, Durban, 2011.

[15] T. Seppa, "Self-damping measurements and energy balance of ACSR Drake," in *IEEE winter power meeting*, 1971.

[16] C. Hardy, "Analysis of self-damping characteristics of stranded cables in transverse vibration," in *Proc Can Soc Mech Eng Forum*, 1990, pp. 117-122.

[17] F. Tavano, "Results of self-damping measurements on conductor for overhead lines and on earth wires with optical fibres," Cigre Report, SC22-88(WG11)18, 1988.

[18] S. Goudreau, F. Charette, C. Hardy, and L. Cloutier, "Bending energy dissipation of simplified single-layer stranded cable," *Journal of engineering mechanics*, vol. 124, pp. 811-817, 1998.

[19] C. B. Rawlins, "Flexural self-damping in overhead electrical transmission conductors," *Journal of Sound and Vibration*, vol. 323, pp. 232-256, 2009.

[20] R. Bouc, "Forced vibration of mechanical systems with hysteresis," in *Proceedings of the fourth conference on non-linear oscillation, Prague, Czechoslovakia*, 1967.

[21] Y.-K. Wen, "Method for random vibration of hysteretic systems," *Journal of the engineering mechanics division*, vol. 102, pp. 249-263, 1976.

[22] http://www.skm-eleksys.com. (2011/01). *transmission-line-accessories.html*.

[23] T. Varney, "The Vibration of Transmission-Line Conductors," *American Institute of Electrical Engineers, Transactions of the*, vol. 47, pp. 799-807, 1926.

[24] R. Monroe and R. Templin, "Vibration of overhead transmission lines," *Electrical Engineering*, vol. 51, pp. 413-413, 1932.

[25] R. Sturm, "Vibration of cables and dampers-I," *American Institute of Electrical Engineers, Transactions of the*, vol. 55, pp. 455-465, 1936.

[26] R. Sturm, "Vibration of cables and dampers-II," *American Institute of Electrical Engineers, Transactions of the*, vol. 55, pp. 673-688, 1936.

[27] J. Tompkins, L. Merrill, and B. Jones, "Quantitative Relationships in Conductor Vibration Damping [includes discussion]," *Power Apparatus and Systems, Part III. Transactions of the American Institute of Electrical Engineers*, vol. 75, 1956.

[28] T. Slethei and J. Huse, "Conductor vibration—theoretical and experimental investigations on a laboratory test span," in *Proceedings of the Institution of Electrical Engineers*, 1965, pp. 1173-1179.
[29] F. B. Farquharson and R. E. McHugh, "Wind tunnel investigation of conductor vibration with use of rigid models," *Transactions of the American Institute of Electrical Engineers. Part III: Power Apparatus and Systems*, vol. 3, pp. 871-878, 1956.
[30] G. Diana and M. Falco, "On the forces transmitted to a vibrating cylinder by a blowing fluid," *Meccanica*, vol. 6, pp. 9-22, 1971.
[31] C. Rawlins, "Model of power imparted to a vibrating conductor by turbulent wind," *Alcoa Conductor Products Company*, 1983.
[32] M. Lutchansky, "Axial stresses in armor wires of bent submarine cables," *Journal of Manufacturing Science and Engineering*, vol. 91, pp. 687-691, 1969.
[33] J. W. Phillips and G. A. Costello, "Contact stresses in twisted wire cables," *Journal of the Engineering Mechanics Division*, vol. 99, pp. 331-341, 1973.
[34] A. E. H. Love, *A treatise on the mathematical theory of elasticity* vol. 1: Cambridge University Press, 1944.
[35] S. Machida and A. Durelli, "Response of a strand to axial and torsional displacements," *Journal of Mechanical Engineering Science*, vol. 15, pp. 241-251, 1973.
[36] R. Knapp, "Derivation of a new stiffness matrix for helically armoured cables considering tension and torsion," *International Journal for Numerical Methods in Engineering*, vol. 14, pp. 515-529, 1979.
[37] F. Hruska, "Calculation of stresses in wire ropes," *Wire and wire products*, vol. 26, pp. 766-767,799-801, 1951.
[38] K. McConnell and W. Zemke, "A model to predict the coupled axial torsion properties of ACSR electrical conductors," *Experimental Mechanics*, vol. 22, pp. 237-244, 1982.
[39] J. Lanteigne and A. Akhtar, "Evaluation of Tensile Strength of Multistrand Conductors—Part I: Theoretical Basis," *Journal of engineering materials and technology*, vol. 120, pp. 33-38, 1998.
[40] A. Akhtar and J. Lanteigne, "Evaluation of Tensile Strength of Multistrand Conductors—Part II: Experimental Results," *Journal of engineering materials and technology*, vol. 120, pp. 39-47, 1998.
[41] X. Huang and O. G. Vinogradov, "Dry friction losses in axially loaded cables," *Structural Engineering and Mechanics*, vol. 4, p. 330, 1996.
[42] W. Jiang, "A general formulation of the theory of wire ropes," *Journal of applied mechanics*, vol. 62, pp. 747-755, 1995.
[43] H. Ramsey, "Analysis of interwire friction in multilayered cables under uniform extension and twisting," *International Journal of Mechanical Sciences*, vol. 32, pp. 709-716, 1990.
[44] S. Sathikh and N. Parthasarathy, "Effect of contact friction on bending stiffness and slip damping of stranded cable," in *Proc Natl Conf lndust Trib*, 1989, pp. 11.1-11.6.
[45] M. Labrosse, A. Nawrocki, and T. Conway, "Frictional dissipation in axially loaded simple straight strands," *Journal of Engineering Mechanics*, vol. 126, pp. 641-646, 2000.
[46] F. Foti and L. Martinelli, "A Model for the Friction Controlled Bending Behaviour of Cables," presented at the 9th International Symposium on Cable Dynamics - ISCD Shanghai, China, 2011.
[47] A.-t. Yu, "Vibration damping of stranded cable," Lehigh University, 1949.
[48] S. Guérard and J.-L. Lilien, "Evaluation of power line cable fatigue parameters based on measurements on a laboratory cable test span," in *ISCD'09 International symposium on CABLE DYNAMICS*, 2009.
[49] A. Godinas and G. Fonder, "Experimental measurements of bending and damping properties of conductors for overhead transmission lines," in *Third Cable Dynamics Conf. proceedings*, 1999, pp. 13-19.
[50] D. Noiseux, "Similarity laws of the internal damping of stranded cables in transverse vibrations," *IEEE Transactions on Power Delivery*, vol. 7, pp. 1574-1581, 1992.
[51] R. Claren, G. Diana, and and F. Tavano, "Proposal for calculating, on the basis of experimental results, the conductor self-damping," Cigre SC22-91 (WG-11 - TF1)-8 September, 1991.
[52] K. Papailiou, "On the bending stiffness of transmission line conductors," *IEEE Transactions on Power Delivery*, vol. 12, pp. 1576-1588, 1997.

[53] S. R. Ghoreishi, T. Messager, P. Cartraud, and P. Davies, "Validity and limitations of linear analytical models for steel wire strands under axial loading, using a 3D FE model," *International Journal of Mechanical Sciences*, vol. 49, pp. 1251-1261, 2007.
[54] W. Jiang, M. Yao, and J. M. Walton, "A concise finite element model for simple straight wire rope strand," *International Journal of Mechanical Sciences*, vol. 41, pp. 143-161, 1999.
[55] A. Nawrocki and M. Labrosse, "A finite element model for simple straight wire rope strands," *Computers & Structures*, vol. 77, pp. 345-359, 2000.
[56] C. B. Rawlins, *Analytical Elements of Overhead Conductor Fabrication*: Fultus Corporation, 2005.
[57] K. O. Papailiou, "Bending of helically twisted cables under variable bending stiffness due to internal friction, tensile force and cable curvature," *Doctor of technical sciences Thesis, ETH, Athens*, 1995.
[58] A. Cardou, *Stick-Slip Mechanical Models for Electrical Conductors in Bending with Matlab® applications*. GREMCA, Université Laval, Québec, , 2013.
[59] H. Hertz, "On the contact of elastic solids," *J. reine angew. Math*, vol. 92, p. 110, 1881.
[60] K. L. Johnson, *Contact mechanics*: Cambridge university press, 1987.
[61] F. H. Hruska, "Radial forces in wire ropes," *Wire and wire products*, vol. 27, pp. 459-463, 1952.
[62] F. Hruska, "Tangential forces in wire ropes," *Wire and wire products*, vol. 28, pp. 455-460, 1953.
[63] C. Jolicoeur and A. Cardou, "A numerical comparison of current mathematical models of twisted wire cables under axisymmetric loads," *Journal of Energy Resources Technology*, vol. 113, pp. 241-249, 1991.
[64] M. Raoof and T. Davies, "Determination of the bending stiffness for a spiral strand," *The Journal of Strain Analysis for Engineering Design*, vol. 39, pp. 1-13, 2004.
[65] K. McConnell and W. Zemke, "The measurement of flexural stiffness of multistranded electrical conductors while under tension," *Experimental Mechanics*, vol. 20, pp. 198-204, 1980.
[66] J.-B. Dastous, "Nonlinear finite-element analysis of stranded conductors with variable bending stiffness using the tangent stiffness method," *IEEE Transactions on Power Delivery*, vol. 20, pp. 328-338, 2005.
[67] K.-J. Hong, C. Yi, and Y.-k. Lee, "Geometry and friction of helically wrapped wires in a cable subjected to tension and bending," *International Journal of Steel Structures*, vol. 12, pp. 233-242, 2012.
[68] T. Von Kármán, *Aerodynamics*: Cornell University press: Mc Graw-Hill company, 1963.
[69] L. Rayleigh, "On the dynamics of revolving fluids," *Proceedings of the Royal Society of London. Series A, Containing Papers of a Mathematical and Physical Character*, pp. 148-154, 1917.
[70] Y. Tsui, "Recent advances in engineering science as applied to aeolian vibration: an alternative approach," *Electric Power Systems Research*, vol. 5, pp. 73-85, 1982.
[71] J. Lilien, S. Guérard, and B. Godard, "Power Line Aeolian Vibrations," *Department of Electronics, Electricity and Computer Sciences. Transmission and Distribution of Electrical Energy. Liège, Belgium*, Novenber, 2013.
[72] M. Lu and J. Chan, "An Efficient Algorithm for Aeolian Vibration of Single Conductor with Multiple Dampers," *IEEE Transactions on Power Delivery*, vol. 22, pp. 1822-1829, 2007.
[73] P. Hagedorn, "On the computation of damped wind-excited vibrations of overhead transmission lines," *Journal of Sound and Vibration*, vol. 83, pp. 253-271, 1982.
[74] H. Dwight, "Sag calculations for transmission lines," *Transactions of the American Institute of Electrical Engineers*, vol. 45, pp. 796-805, 1926.
[75] J. Bradbury, G. Kuska, and D. Tarr, "Sag and tension calculations for mountainous terrain," in *IEE Proceedings C (Generation, Transmission and Distribution)*, 1982, pp. 213-220.
[76] R. Hobbs and M. Raoof, "Interwire slippage and fatigue prediction in stranded cables for TLP tethers," *Hemisphere Publishing Corp*, pp. 77-99, 1983.
[77] F. Blouin and A. Cardou, "A study of helically reinforced cylinders under axially symmetric loads and application to strand mathematical modelling," *International journal of solids and structures*, vol. 25, pp. 189-200, 1989.
[78] C. Jolicoeur and A. Cardou, "Semicontinuous mathematical model for bending of multilayered wire strands," *Journal of engineering Mechanics*, vol. 122, pp. 643-650, 1996.
[79] W. Jiang, T. Wang, and W. Jones, "Forced vibration of coupled extensional-torsional systems," *Journal of engineering mechanics*, vol. 117, pp. 1171-1190, 1991.

[80] J. Lanteigne, "Theoretical estimation of the response of helically armored cables to tension, torsion, and bending," *Journal of applied mechanics*, vol. 52, pp. 423-432, 1985.
[81] E. E. Ojo and S. Shindin, "Finite Element Analysis of the Dynamic Behaviour of Transmission Line Conductors Using MATLAB," *Journal of Mechanics Engineering and Automation*, vol. 4, 2014.
[82] M. Ismail, F. Ikhouane, and J. Rodellar, "The hysteresis Bouc-Wen model, a survey," *Archives of Computational Methods in Engineering*, vol. 16, pp. 161-188, 2009.
[83] I. Pivovarov and O. Vinogradov, "One application of Bouc's model for non-linear hysteresis," *Journal of sound and vibration*, vol. 118, pp. 209-216, 1987.
[84] M. Petyt, *Introduction to finite element vibration analysis*: Cambridge university press, 2010.
[85] J. N. Reddy, *An introduction to the finite element method* vol. 2: McGraw-Hill New York, 1993.
[86] O. C. Zienkiewicz, R. L. Taylor, O. C. Zienkiewicz, and R. L. Taylor, *The finite element method* vol. 3: McGraw-hill London, 1977.
[87] P. Litewka, *Finite element analysis of beam-to-beam contact* vol. 53: Springer Science & Business Media, 2010.
[88] P. Wriggers, *Computational contact mechanics*: Springer Science & Business Media, 2006.
[89] C. Hardy and A. Leblond, "On the dynamic flexural rigidity of taut stranded cables," in *Proceedings of the Fourth International Symposium on Cable Dynamics*, 2003, pp. 45-52.
[90] K.-J. Bathe and E. L. Wilson, "Numerical methods in finite element analysis," 1976.
[91] IEEE Standard 563–1978, May 1978, Guide on conductor self-damping measurements
[92] S. Cigré, I. P. T, and D. Committee, "Guide on conductor self damping measurement," *Electra*, pp. 79-90, 1979.
[93] IEC 62567 Standard, Overhead Lines, "Methods for testing self-damping characteristics of conductors ", Edition1.0, 2013-09.

Appendix A: Physical and Geometric Parameters for Test Conductors

To calculate the conductor bending stiffness (maximum and minimum), the following equations developed by K. O. Papillion [56] was used:

$$EI_{\min} = E_0 I_0 + \sum_{i=1}^{N} n_i E_i I_i \cos\alpha_i \quad \text{..... (A1)}$$

$$EI_{\max} = EI_{\min} + EI_{compl} \quad \text{..... (A2)}$$

$$EI_{compl} = \sum_{i=1}^{N} \frac{n_i}{2} A_i E_i R_i^2 \cos^3\alpha_i \quad \text{..... (A3)}$$

1. Physical Parameters for Rabbit Conductor

Conductor diameter (mm): 10.1
Ultimate tensile strength (kN): 18.4

layer	Material	Diameter (mm)	No of strands	Pitch Length (cm)	Lay angle	Lay Direction
Layer 0	Steel	3.35	1	N/A	0	N/A
Layer 1	Aluminium	3.35	6	12.40	9.56	Right hand Lay

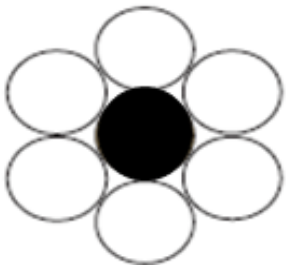

Minimum Bending Stiffness (EI_{min}): 3.859

Maximum Bending Stiffness (EI_{max}): 23.78

2. Physical Parameters for Pelican

Conductor diameter (mm): 15.77
Ultimate tensile strength (kN): 51.15

layer	Material	Diameter (mm)	No of strands	Pitch Length (cm)	Lay angle	Lay Direction
Layer 0	Steel	2.25	1	N/A	0	N/A
Layer 1	Aluminium	3.38	6	16.12	6.26	left hand Lay
Layer 2	Aluminium	3.38	12	22.25	9.95	Right hand Lay

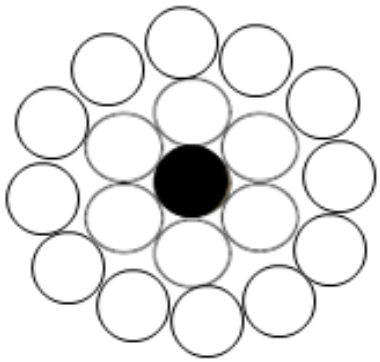

Minimum Bending Stiffness (EI_{min}): 7.32 N. m^2

Maximum Bending Stiffness (EI_{max}): 135.22 N. m^2

3 Physical Parameters for Tern Conductor

Conductor diameter (mm): 27.00
Ultimate tensile strength (kN): 98.7

layer	Material	Diameter (mm)	No of strands	Pitch Length (cm)	Lay angle	Lay direction
Layer 0	Steel	2.25	1	N/A	0	N/A
Layer 1	steel	2.25	6	12.25	- 6.58	left hand Lay
Layer 2	Aluminium	3.38	9	22.20	8.16	Right hand Lay
Layer 3	Aluminium	3.38	15	26.50	-11.32	left hand Lay
Layer 4	Aluminium	3.38	21	30.45	13.70	Right hand Lay

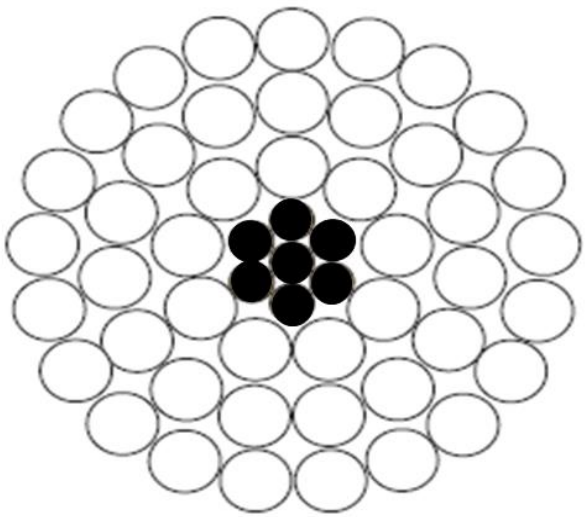

Minimum Bending Stiffness (EI_{min}): 29.074 N. m^2

Maximum Bending Stiffness (EI_{max}): 1311 N. m^2

4 Physical Parameters for Bersford Conductor

Conductor diameter (mm): 35.56
Ultimate tensile strength (kN): 180

layer	Material	Diameter (mm)	No of strands	Pitch Length (cm)	Lay angle	Lay Direction
Layer 0	Steel	3.32	1	N/A	0	N/A
Layer 1	steel	3.32	6	17.14	- 6.94	left hand Lay
Layer 2	Aluminium	4.27	10	30.29	8.44	Right hand Lay
Layer 3	Aluminium	4.27	16	31.89	-12.64	left hand Lay
Layer 4	Aluminium	4.27	22	38.04	14.40	Right hand Lay

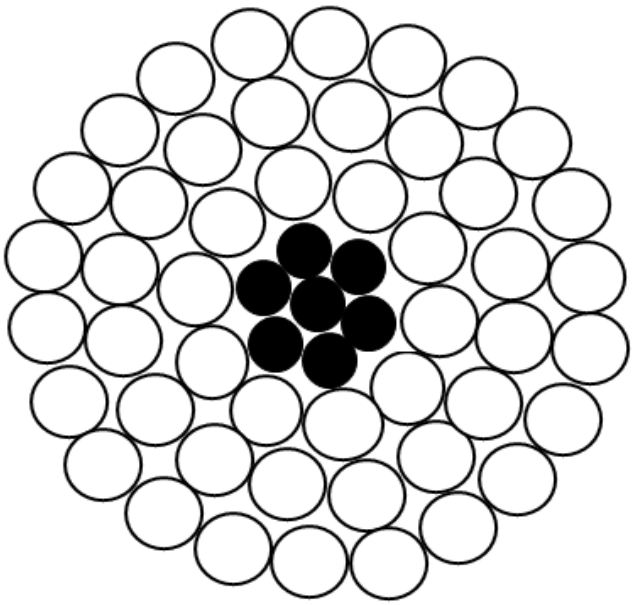

Minimum Bending Stiffness (EI_{min}): 63.4 N. m^2

Maximum Bending Stiffness (EI_{max}): 3760.1 N. m^2

Appendix B: Cost/Benefit Analysis of the Conductor Static Profile

The cost-benefit analysis of conductor strung on towers is achieved by determined the slack at different configuration. This analysis revealed the benefit of using a more tensioned conductor for both for new installations and those that are being refurbished. As for both the aspect of technical and economic interests has been validated, achieved in this study by employing the FEM. The installation of conductors can now be done on the South African transmission network to take advantage of this study. The geometric specifications have been drawn up as shown in figure (B1). Using the Tern conductor out of the four test conductors used in this study with an average of 360 m span length.

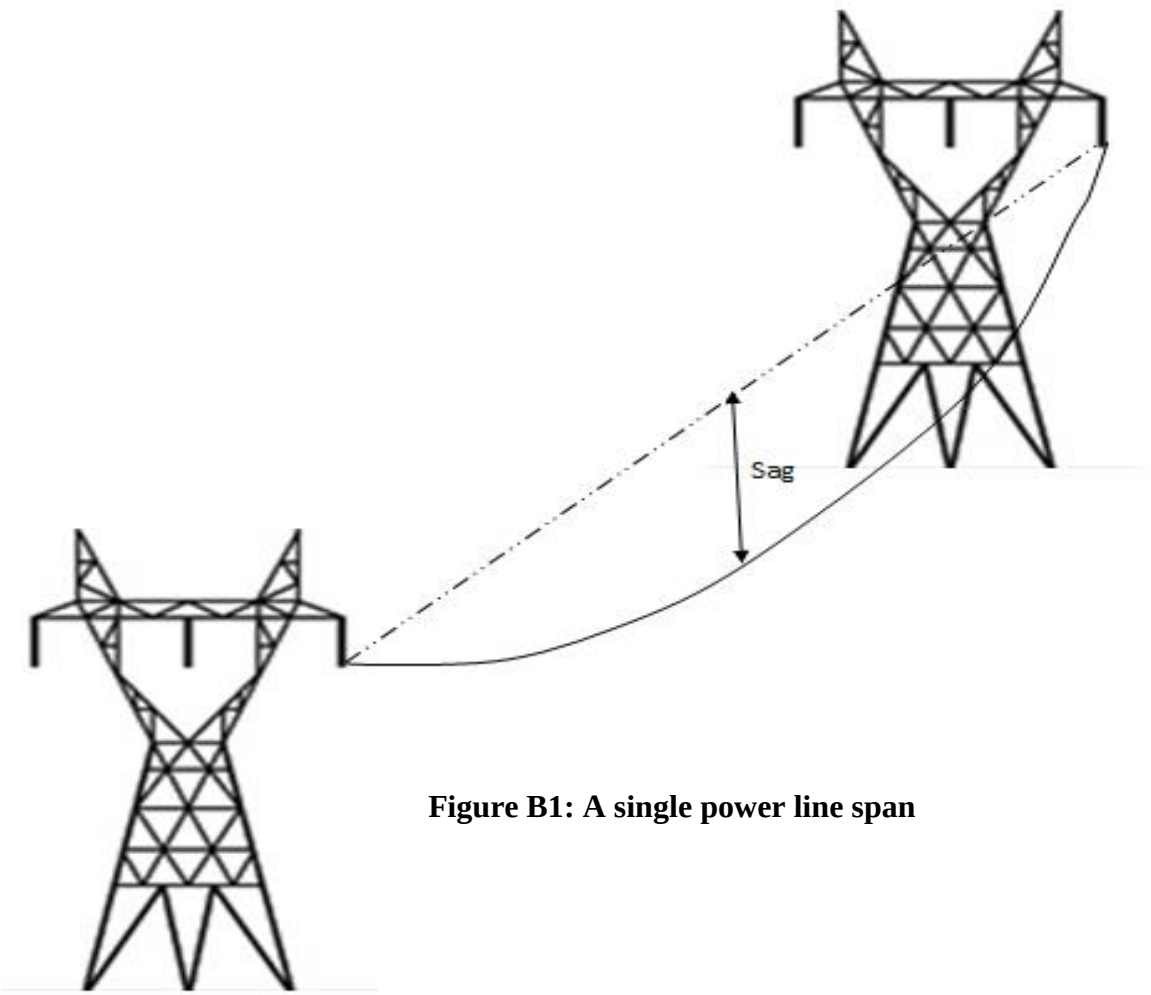

Figure B1: A single power line span

Table B1: Sag values at a specified axial loading

UTS	Sag (m)
15 %UTS	1.4597
20 % UTS	1.0948
25 % UTS	0.8758
30 % UTS	0.7299

Appendix C: The Newmark Numerical Scheme

In order to illustrate the use of this family of numerical integration methods, consider the solution of the linear dynamic equilibrium equations written in the following form

$$M\ddot{u}_t + C\dot{u}_t + Ku_t = F_t \quad \text{..... (C1)}$$

The direct use of Taylor's series provides a rigorous approach to obtain the following two additional equations

$$u_t = u_{t-\Delta t} + \Delta t\dot{u}_{t-\Delta t} + \frac{\Delta t^2}{2}\ddot{u}_{t-\Delta t} + \frac{\Delta t^3}{6}u_{t-\Delta t} + ... \quad \text{..... (C2)}$$

$$\dot{u}_t = \dot{u}_{t-\Delta t} + \Delta t\ddot{u}_{t-\Delta t} + \frac{\Delta t^2}{2}\dddot{u}_{t-\Delta t} + ... \quad \text{..... (C3)}$$

Newmark truncated these equations and expressed them in the following form:

$$u_t = u_{t-\Delta t} + \Delta t\dot{u}_{t-\Delta t} + \frac{\Delta t^2}{2}\ddot{u}_{t-\Delta t} + \beta\dddot{u} \quad \text{..... (C4)}$$

$$\dot{u}_t = \dot{u}_{t-\Delta t} + \Delta t\ddot{u}_{t-\Delta t} + \gamma\dddot{u} \quad \text{..... (C5)}$$

If the acceleration is assumed to be linear within the time step, the following equation can be written:

$$\dddot{u} = \frac{(\ddot{u}_t - \ddot{u}_{t-\Delta t})}{\Delta t} \quad \text{..... (C6)}$$

The substitution of Equation (C5) into Equations (C3 and C4) produce Newmark's equations in standard form as

$$u_t = u_{t-\Delta t} + \Delta t\dot{u}_{t-\Delta t} + \left(\frac{1}{2} - \beta\right)\Delta t^2\ddot{u}_{t-\Delta t} + \beta\Delta t^2\dddot{u} \quad \text{..... (C7)}$$

$$\dot{u}_t = \dot{u}_{t-\Delta t} + (1-\gamma)\Delta t\ddot{u}_{t-\Delta t} + \gamma\,\Delta t\,\dddot{u} \quad \text{..... (C8)}$$

Newmark used Equations (C6, C7 and C8) iteratively, for each time step, is solve for each displacement of the structural system. The term u_t was obtained from Equation (C1) by dividing the equation by the mass associated with the displacement.

In 1962 Wilson [2] formulated Newmark's method in matrix notation, added stiffness and mass proportional damping, and eliminated the need for iteration by introducing the direct solution of the equations at each time step. This requires that Equations (C4 and C5) be rewritten in the following form:

$$u_t = b_1(u - u_{t-\Delta t}) + b_2\dot{u}_{t-\Delta t} + b_3\ddot{u}_{t-\Delta t} \quad \text{..... (C9)}$$

$$\dot{u}_t = b_4(u - u_{t-\Delta t}) + b_5\dot{u}_{t-\Delta t} + b_6\ddot{u}_{t-\Delta t} \quad \text{..... (C10)}$$

Where the constants b_1 to b_6 are defined as follows:

$$b_1 = \frac{1}{\beta\Delta t^2},\ b_2 = \frac{1}{\beta\Delta t},\ b_3 = \beta - \frac{1}{2},\ b_4 = \gamma\,\Delta t\,b_1,\ b_5 = 1 + \gamma\Delta t b_2 \text{ and } b_6 = \Delta t(1 + \gamma\,b_3 - \gamma)$$

The substitution of Equations (C9 and C10) into Equation C1 allows the dynamic equilibrium of the system at time "t" to be written in terms of the unknown node displacements $\mathbf{u}_t$ and can be expressed:

$$\left(b_1 M + b_4 C + K\right)u_t = F_t + M\left(b_1 u_{t-\Delta t} - b_2 \dot{u}_{t-\Delta t} - b_3 \ddot{u}_{t-\Delta t}\right) + C\left(b_4 u_{t-\Delta t} - b_5 \dot{u}_{t-\Delta t} - b_6 \ddot{u}_{t-\Delta t}\right) \ldots\ldots \text{(C11)}$$

The Newmark direct integration algorithm is summarized in Table C1. Note that the constants b_i need be calculated only once and for the effective dynamic stiffness matrix $\boldsymbol{K}$.

Table C1: The summary of the Newmark time-integration schemes

Algorithm	γ	β	Stability limit $\omega\Delta t$
Purely explicit	0	0	0
Central difference	$1/2$	0	2
Fox and Goodwin	$1/2$	$1/12$	2.45
Linear acceleration	$1/2$	$1/6$	3.46
Average constant acceleration	$1/2$	$1/4$	∞

Appendix D: The FEM Toolbox

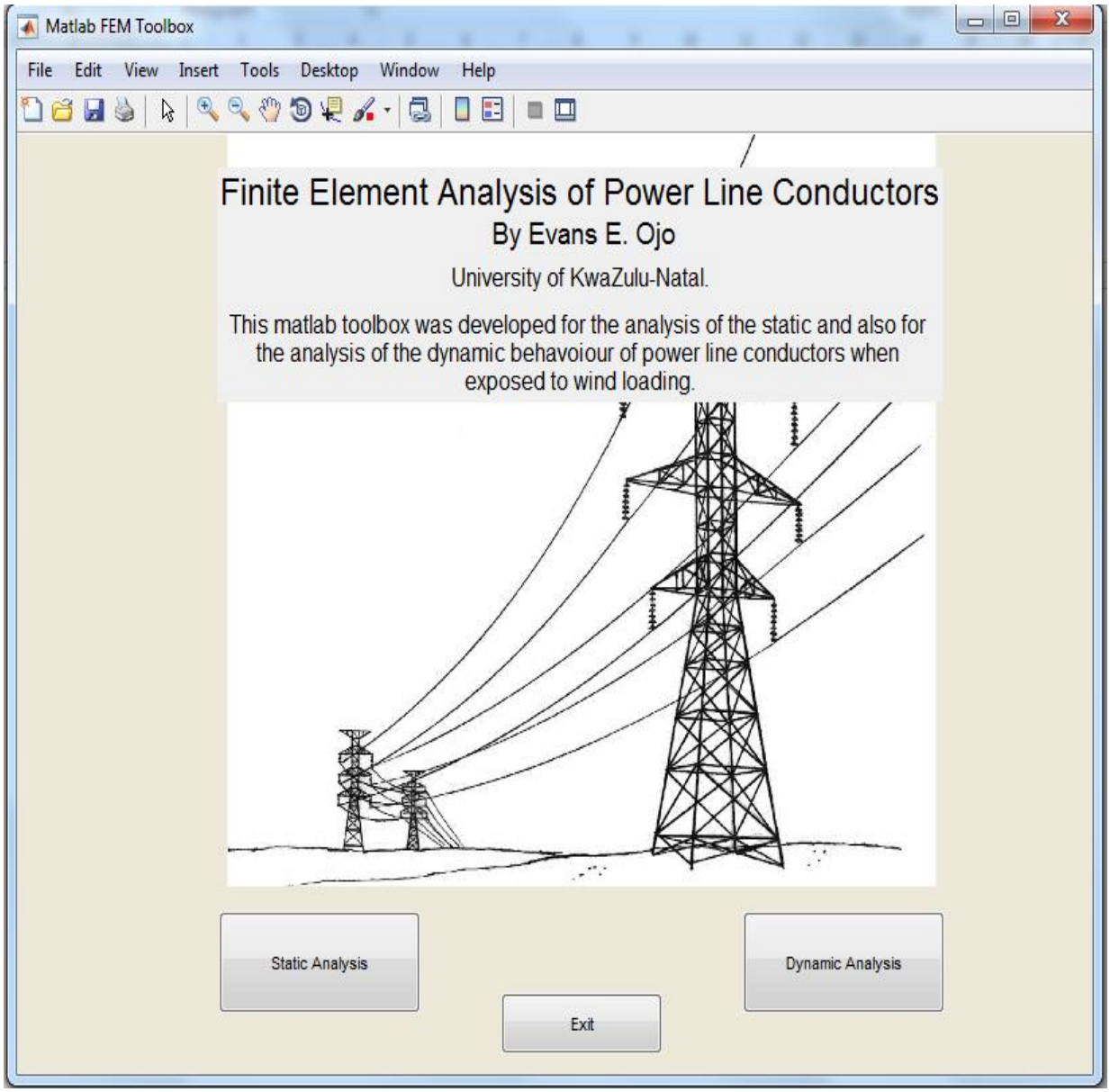

Figure D1: GUI for the FEM Toolbox

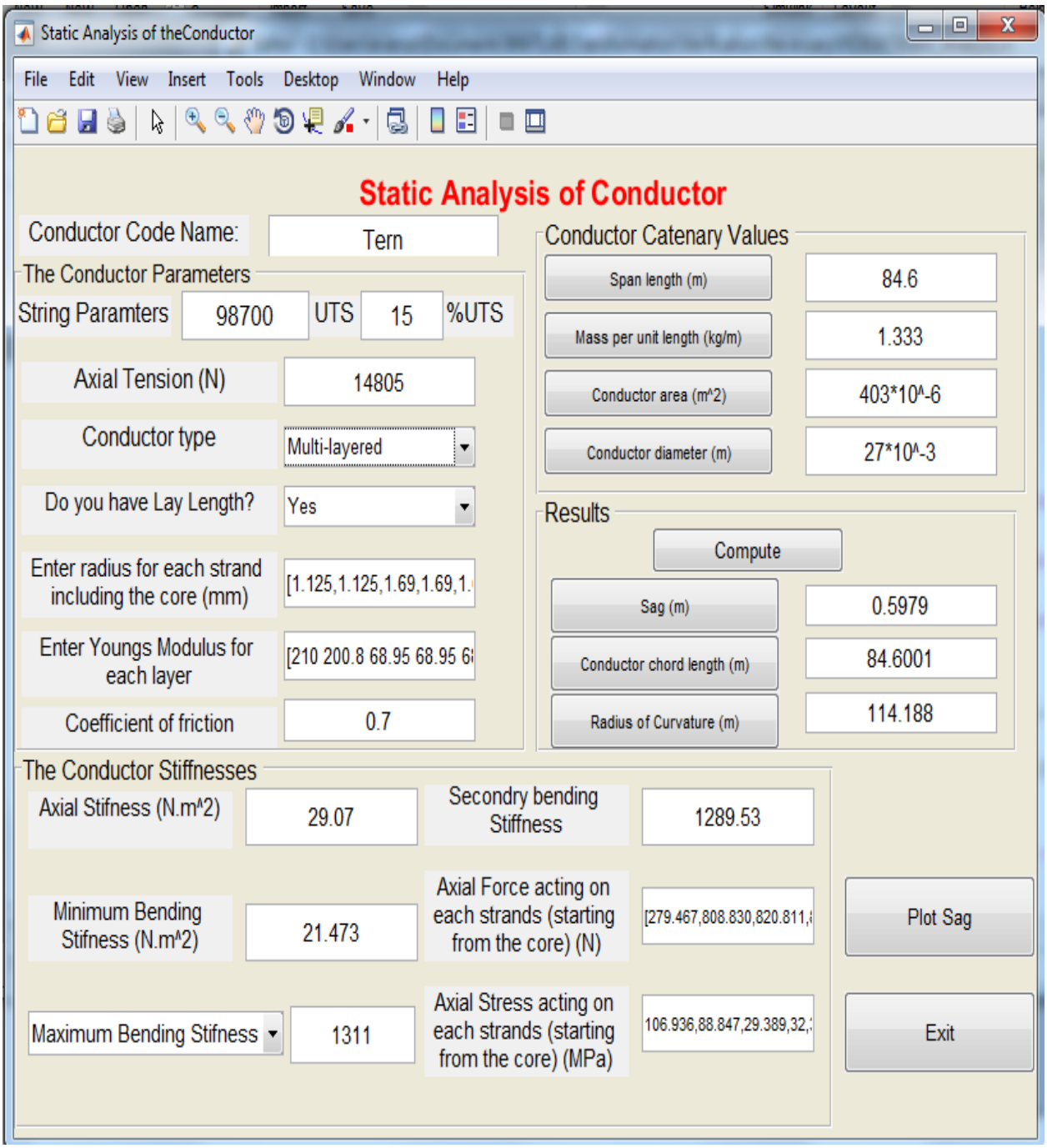

Figure D2: GUI for the static analysis of conductor

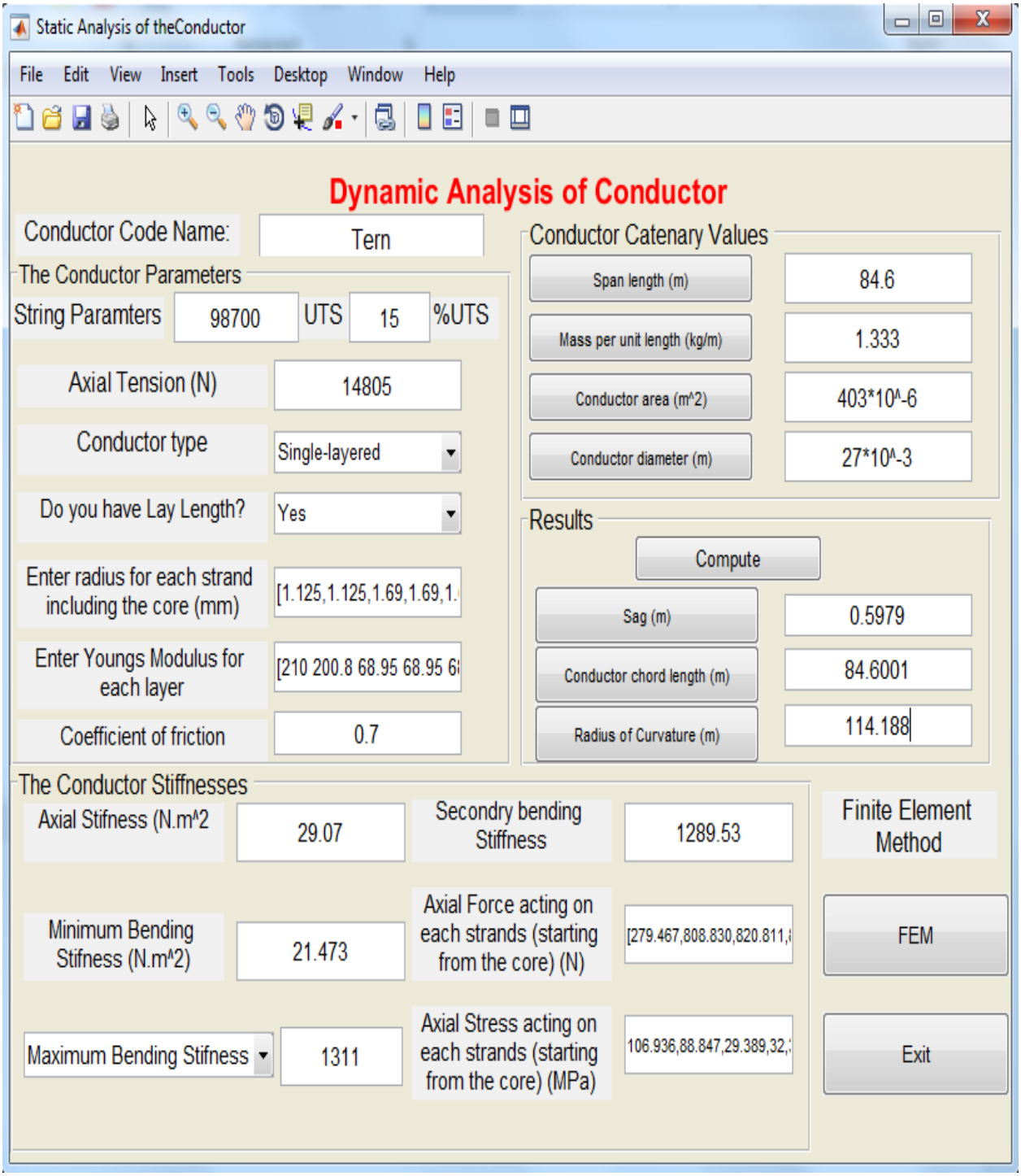

Figure D3: GUI for the dynamic analysis of conductor

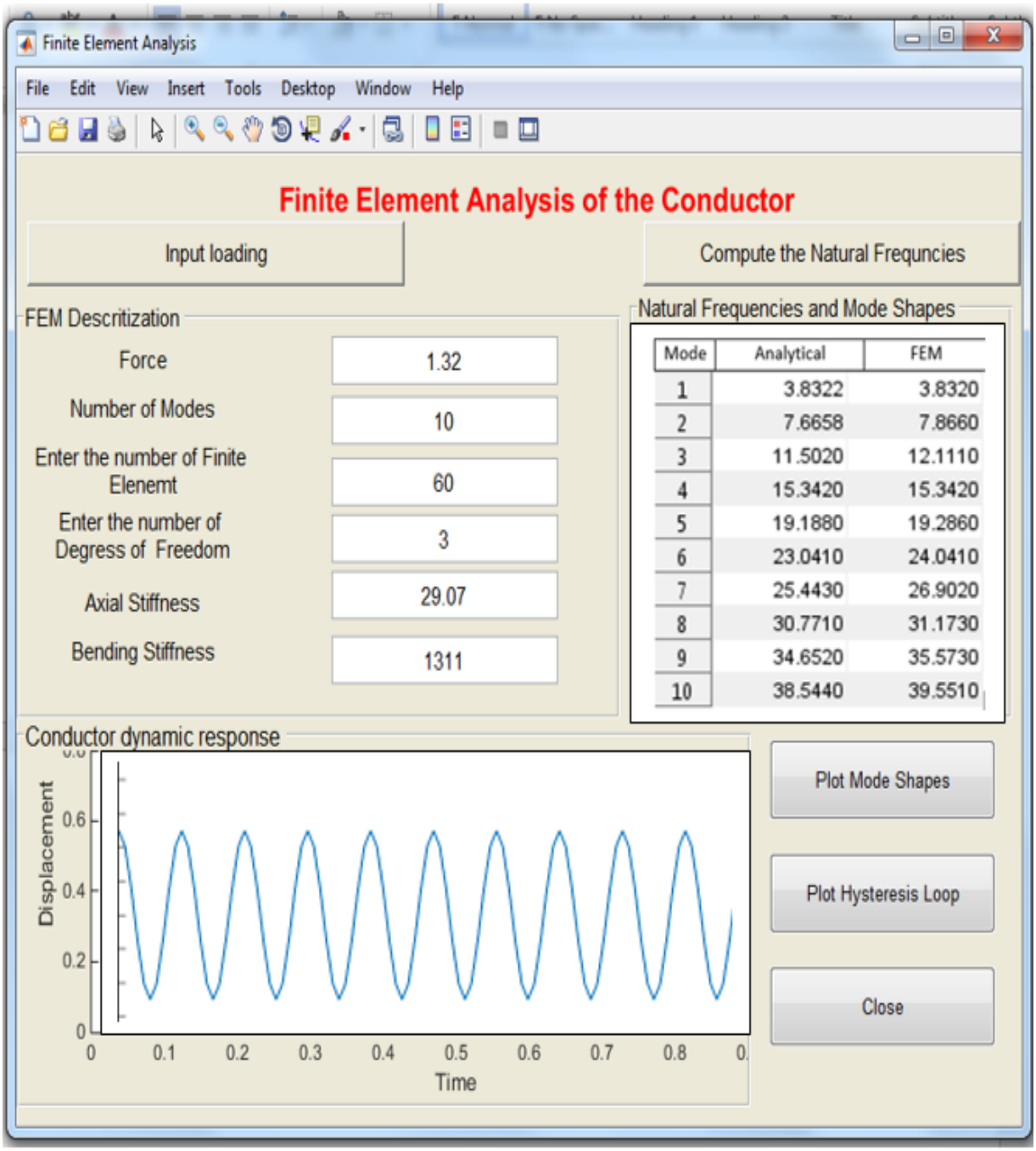

Figure D4: GUI for the FEM of conductor

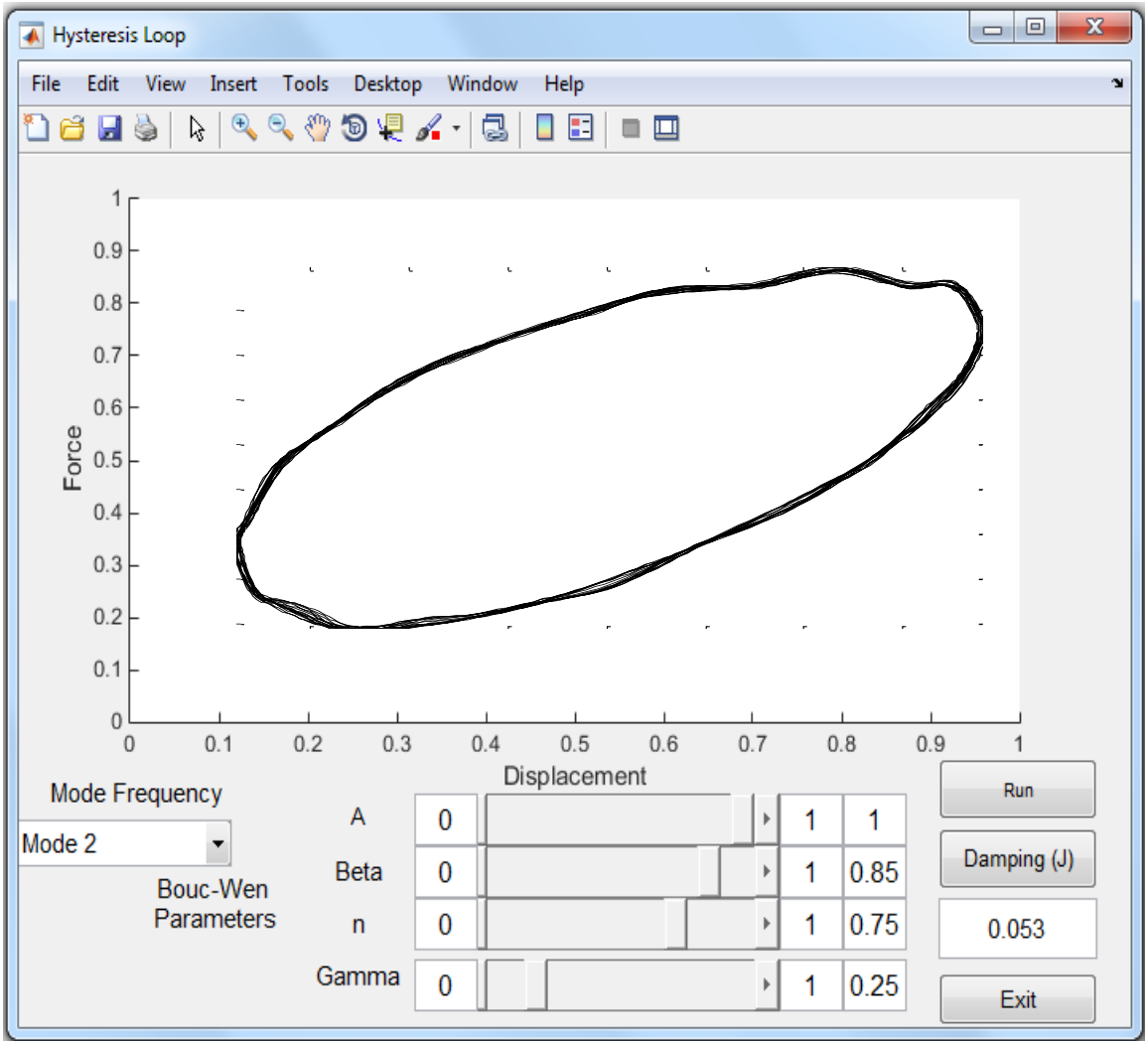

Figure D5: GUI for plotting the hysteresis loop for the conductor